Finite amplitude propagation of focused ultrasonic waves in water

Baker, Andrew C.

Award date:
1989

Awarding institution:
University of Bath

FINITE AMPLITUDE PROPAGATION OF FOCUSED ULTRASONIC WAVES IN WATER.

submitted by Andrew C. Baker

for the degree of Ph.D.
of the University of Bath.

1989

A C Baker

ProQuest LLC
789 East Eisenhower Parkway
P.O. Box 1346
Ann Arbor, MI 48106-1346

ABSTRACT

Ultrasound is widely used in medical imaging and therapy at pressure levels that are high enough to generate finite amplitude distortion. This thesis examines the acoustics of such systems through a study of the propagation of finite amplitude ultrasound from focused circular apertures. Extensive comparisons are made between experimental measurements and numerical solutions of the nonlinear parabolic wave equation. A 2.25 MHz plane piston transducer (38 mm diameter) was used as a source of finite amplitude ultrasound and the resulting pressure field was monitored with a 1 mm diameter membrane hydrophone mounted on a computer controlled translation stage. The acoustic beam was focused by the addition of plano-concave perspex lenses to the transducer to give focal lengths of 147, 216 and 440 mm, corresponding to gains of 11.9, 7.6 and 3.7 respectively. Drive levels between 10 kPa and 300 kPa were used. The theoretical model was based on a numerical solution to the parabolic nonlinear wave equation (sometimes known as the KZK equation), which is valid for large circular apertures when the angle subtended by the field point is small (less than 20 degrees). It is shown that accurate predictions can be made for the harmonic amplitudes and phases up to the fifth harmonic for focusing gains between 0 (i.e. a plane piston) and 11.9. Initial work on pulsed ultrasonic fields is also reported and shows good agreement between experiment and theory.

Table of Contents

LIST OF SYMBOLS 1

Chapter 1: INTRODUCTION 3
1.1 BACKGROUND 3
1.2 AIMS OF THE PROJECT 4
1.3 THESIS CONTENT 5
1.4 MEDICAL ULTRASOUND SYSTEMS 5
1.5 IMPLICATIONS OF FINITE AMPLITUDE PROPAGATION 7
1.6 INTRODUCTION TO FINITE AMPLITUDE PROPAGATION 11

Chapter 2: REVIEW OF LITERATURE 22
2.1 INFINITESIMAL ACOUSTICS 22
2.1.1 Plane piston source 22
2.1.2 Focused source 23
2.1.3 Pulsed fields 24
2.2 FINITE AMPLITUDE ACOUSTICS 26
2.2.1 Finite amplitude plane waves 26
2.2.2 Plane piston source at finite amplitudes 26
2.2.3 Focused source at finite amplitudes 29
2.2.4 Gaussian source 30

Chapter 3: THEORY 32
3.1 INTRODUCTION 32
3.2 GENERAL WAVE EQUATION 32
3.3 PARABOLIC APPROXIMATION 32
3.4 NUMERICAL SOLUTION 34
3.4.1 Plane piston - continuous wave 34
3.4.2 Initial and boundary conditions 36
3.4.3 Limitations 38
3.5 EXAMPLE CALCULATION 43
3.5.1 Harmonic amplitudes 43
3.5.2 Harmonic phases 45
3.6 FOCUSED FIELDS 48
3.7 PULSE EXCITATION 48
3.7.1 Pulse shape 49
3.7.2 Extension to tissue-like media 51

Chapter 4: EXPERIMENTAL CONFIGURATION 53
4.1 GENERAL 53
4.2 TRANSDUCER 55
4.2.1 Quasi-continuous wave drive 55
4.2.2 Shock excited drive 56
4.2.3 Lenses 57
4.2.4 Transducer alignment 58
4.2.5 Determination of transducer parameters 59
4.3 HYDROPHONE 61
4.3.1 Sensitivity and calibration 62
4.3.2 Diffraction loss 68
4.4 DIGITAL STORAGE OSCILLOSCOPE 71
4.5 TRANSLATION STAGE 71
4.6 IBM COMPUTER 72
4.6.1 Note on using FFT subroutine 72
4.6.2 Measurement schemes 73
4.7 ACCURACY 76
4.7.1 Pressure 76
4.7.2 Time 78
4.7.3 Positional 78

4.7.4 Properties of the medium 78
4.7.5 Transducer parameters 79

Chapter 5: RESULTS AND DISCUSSION 80
5.1 SMALL SIGNAL FIELDS 81
5.2 FINITE AMPLITUDE FIELDS 86
5.3 RADIAL FIELD 110
5.4 EFFECT OF DRIVE LEVEL 125
5.5 TIME DOMAIN MEASUREMENTS 128
5.6 PULSED FIELDS 135

Chapter 6: CONCLUSIONS 140

ACKNOWLEDGEMENTS 143

REFERENCES 144

Appendix A: SMALL SIGNAL THEORY FOR FOCUSED RADIATORS ... A-1
1.1 AXIAL FIELD A-2
1.1.1 Fresnel approximation A-5
1.1.2 Plane piston A-6
1.1.3 Validity of Fresnel approximation A-6
1.2 RADIAL FIELD A-7
1.3 CORRECTION FOR FINITE HYDROPHONE SIZE A-7
1.4 DISCUSSION A-8

Appendix B: USER GUIDE FOR PROGRAM pulse.f B-1
1.1 GENERAL B-1
1.2 INPUT FILES IN DETAIL B-3
1.2.1 *param.dat* B-3
1.2.2 *init.dat* B-5
1.2.3 *pgrid.dat* B-6
1.3 OUTPUT FILES IN DETAIL B-7
1.3.1 *ax.out* B-7
1.3.2 *rad1.out, rad2.out* and *rad3.out* B-8
1.3.3 Graphical output B-9
1.4 REFERENCES B-9

Appendix C: PUBLISHED PAPERS C-1

1 FOCUSED FIELDS C-2

2 PLANE PISTON C-3

3 PULSED FIELDS C-4

LIST OF SYMBOLS

a - aperture radius.

b - diffusivity of sound ($= 2\alpha ck^2$).

C - capacitance.

c - speed of sound (1486 m/s for water at 20°C).

D - effective radius of curvature of lens.

f - frequency. (f_o - fundamental frequency).

G - focusing gain ($= R_o/D$).

g - Fourier coefficient in solution.

h - Fourier coefficient in solution.

J_1 - Bessel function of first kind, order 1.

j - $\sqrt{-1}$.

k - wavenumber ($= 2\pi/\lambda$).

l_D - shock distance ($= 1/\beta\varepsilon k$).

n - harmonic number.

p - acoustic pressure ($= P - P_o$).

p_o - acoustic pressure at the source.

P - total pressure (static + acoustic).

P_o - static pressure.

q - Fourier solution amplitude.

R_o - Rayleigh distance ($= ka^2/2$).

R_1 - reflection coefficient.

r - radial coordinate.

S - hydrophone sensitivity.

s - condensation ($= (\rho - \rho_o)/\rho_o$).

T - absolute temperature.

T_1 - transmission coefficient.

t - time.

u - particle velocity.

u_o - particle velocity at the source.

Z - acosutic impedance.

z - axial coordinate.

α - absorption coefficient (2.5×10^{-15} Np $m^{-1}Hz^{-2}$ for water).

β - parameter of nonlinearity (3.5 for water at 20°C).

Γ - shock parameter ($= \beta \varepsilon k/\alpha$).

ε - acoustic Mach number ($= u/c$).

ζ - normalised radial coordinate ($= r/a$).

θ - harmonic phase.

λ - wavelength ($= c/f$).

ρ - instantaneous density.

ρ_o - unperturbed (or static) density.

σ - normalised axial coordinate ($= z/R_o$).

σ_s - shock parameter ($= \beta \varepsilon k x$).

τ - retarded time ($= \omega t - kz$).

ω - angular frequency ($= 2\pi f$).

Φ - scalar velocity potential.

Ψ - Fourier solution phase.

∇ - gradient operator.

∇_1 - transverse gradient operator.

Chapter 1: INTRODUCTION

1.1 BACKGROUND

Acoustics can be defined as the study of the generation, propagation and reception of vibrational waves; it is usually assumed that the vibrations are of infinitesimal amplitude since this allows the theoretical treatment to be simplified. The resulting linearised wave equation is applicable to most everyday situations and provides a useful basis for analysis since the methods of linear systems theory, such as the superposition theorem, can be applied. There are circumstances however when the wave amplitude can no longer be treated as infinitesimal. Such finite amplitude waves are solutions of nonlinear wave equations and pose special problems in both theoretical analysis and experimental measurement. Probably the most noticeable effect of finite amplitude propagation is that an initially sinusoidal waveform will distort until it resembles a sawtooth waveform; as the waveform distorts energy is transferred to higher frequencies and subsequently lost as heat.

The ideas of finite amplitude waves and nonlinear effects are not new; eminent 19th Century scientists like Rayleigh, Poisson, Faraday and Helmholtz were all involved in the study of nonlinear acoustics.[1] It was many years before the practical applications were explored in the field of underwater acoustics, for example the parametric array [Westervelt, 1963]. It was later still before it was generally accepted that nonlinear effects were of significance in medical ultrasound systems [Muir and Carstensen, 1980]. Since then the existence of finite amplitude effects in imaging systems has been demonstrated for water paths [Duck and Starritt, 1984 and Parker, 1985] and in tissue, both in vitro [Starritt et al, 1986] and in vivo [Starritt et al, 1985]. A survey of the output of ultrasonic imaging equipment [Duck et al, 1985] indicated that most imaging systems would be subject to finite amplitude effects and a more recent study

---

1 See for example Beyer [1974] for a historical perspective

[Duck, 1989] suggested that drive levels had increased still further. One of the keys to the widespread acceptance of the existence of finite amplitude effects in medical systems was the availability of broadband hydrophones such as the polyvinylidene difluoride (PVdF) membrane hydrophone; typically these have a smooth frequency response from 1 MHz up to at least 20 MHz and do not greatly perturb the field under measurement [Bacon, 1982]. These devices make observation of finite amplitude distortion a relatively simple task.

1.2 AIMS OF THE PROJECT

The widespread use of medical ultrasound and the small amount of published work on finite amplitude effects in such pressure fields provides the motivation for this project which attempts to approach the complexity of medical ultrasound systems from a starting point based on the physics of a simple geometry (the circular piston radiator) in a relatively simple medium (water). The justification for only looking at water (and not tissue) was threefold; first, water occurs commonly in real situations such as obstetric scans where the acoustic path usually includes the urine in the bladder and the amniotic fluid. Second, it is easy to produce and maintain a water path in the laboratory and to make measurements in it. Third, finite amplitude propagation in fluids appeared to be a problem that had a realistic chance of a theoretical solution. The transducer used in this study was chosen to be slightly larger than typical medical systems in order to simplify field measurements and lenses were used to focus the ultrasonic beam since this gave a wide choice of focal gains ranging from 0 to 12[(2)]. The main part of the work concentrated on continuous wave pressure fields as this simplified both experimental measurements and theoretical predictions; some work on pulsed fields was also performed. The project was part of a larger venture within the

---

2 The definition of gain (G) used here is: $G = R_o/D$, where R_o is the Rayleigh distance ($R_o = ka^2/2$) and D is the focal length. It should be noted that many authors use the ratio of the peak axial pressure to the average pressure at the transducer which would give a gain of 2 for the plane piston transducer as opposed to a gain of 0 from the above definition.

Acoustics Group (in collaboration with the Medical Physics Department of the Royal United Hospital, Bath) to model fully the interactions of finite amplitude ultrasound in tissue under the conditions encountered in medical ultrasonics.

1.3 THESIS CONTENT

The remainder of this chapter describes the types of system currently in use in medical ultrasound and outlines some of the implications of finite amplitude effects in such systems. Some of the key concepts of finite amplitude propagation are also introduced. In Chapter 2 a review of published work is presented in two parts: firstly the infinitesimal pressure fields due to plane and focused circular sources, secondly the finite amplitude pressure fields are considered. Chapter 3 presents the theoretical background to the problem with the emphasis on the finite difference model used in this study and Chapter 4 contains details of the experimental configuration. The main results and discussion are given in Chapter 5, the main part of which consists of comparisons between experimental measurements and theoretical predictions. Chapter 6 contains the conclusions and ideas for future work. In addition there are three appendices: the first contains some small signal results relating to circular apertures, the second is a brief user guide for the finite difference program and finally copies of a number of published papers arising from the research are attached.

1.4 MEDICAL ULTRASOUND SYSTEMS

Many medical ultrasound sets share a number of basic similarities. They all tend to use high acoustic drive levels (between say 200 kPa and 50 MPa), high drive frequencies (usually between 500 kHz and 10 MHz), large apertures (typically in excess of 20 wavelengths across) and some form of focusing. Although the systems differ in detail they can be conveniently grouped under three broad headings:

a. Diagnostic scanners

Diagnostic scanners usually operate in a pulse-echo mode to form real time images and are widely used to monitor foetal development as well as imaging

organs such as the liver and heart in adults. The transmitted pulse is usually short (of the order of micro-seconds) to give good spatial resolution and the pulse repetition rate is low (of the order of kHz) to allow time for the pulse to propagate the required distances. The transducer may be a single element but more commonly a linear array is used and the electrical drive is either by shock excitation or a short tone burst to enable Doppler analysis on the return signal. The transducers generally have low focusing gains (say 3 to 6) and operate in the frequency range 2 to 10 MHz at peak pressures of around 1 to 5 MPa. Focusing is usually achieved either by electronic phasing of array elements or by acoustic lenses. Duck et al [1985] provides details of a number of medical ultrasound scanners.

b. Hyperthermia systems

Hyperthermia systems are driven with longer tone bursts and are used in physiotherapy to cause localised heating to ease discomfort and to assist the healing process. Hyperthermia is also being considered as an adjunct to chemotherapy and as a method of directly killing cancerous cells. Most of these systems employ focusing and operate at higher time average intensities than imaging systems.

c. Extra-corporeal lithotripters

Lithotripters are used to break up stones that form in kidneys and produce blockages. Extra-corporeal lithotripters use an ultrasonic transducer acoustically coupled to the patient's abdomen to focus a series of short high pressure pulses onto the stone in order to break it up. A number of techniques are used to generate the pulse including a spark discharge in an elliptical focusing bowl, a single electromagnetic transducer focused with a lens and a hemispherical bowl populated with piezo-electric elements. The pressures generated at the focus of

lithotripters have been shown to be in the region of 30 - 40 MPa [Coleman et al, 1987], although the zero crossing frequencies are lower than imaging systems (about 0.5 MHz).

1.5 IMPLICATIONS OF FINITE AMPLITUDE PROPAGATION

The existence of finite amplitude distortion in medical ultrasound fields is now generally accepted and it has many implications. Some of the potential problems and benefits are listed below.

a. Calibration and safety standards

Ultrasound systems are normally calibrated in water since it is readily available and has well known acoustic properties. The main disadvantage is that water is not an ideal calibration medium at finite amplitudes as it has a low absorption coefficient which allows nonlinear effects such as distortion of the waveform to build up relatively rapidly and to an extent that would not necessarily occur in tissue. Thus a calibration performed in water will not always reflect the nature of the acoustic field of a system used in a clinical situation. Various tissue mimicking gels are available but they lack the convenience of water and it has yet to be shown that the scattering effects in the mimics are comparable with those in tissues.

Current ultrasound safety standards (FDA, 1985) are based on intensity measurements and as such do not take explicit account of nonlinear effects although measurements are derated to in-situ levels to take some account of the difference between water and tissue. Current measurement standards (IEC, 1988) use a single nonlinearity parameter known as σ_m to establish the importance of nonlinearity when making measurements. The inclusion of nonlinear effects in safety standards is not a trivial problem. Firstly, there are a large number of acoustic parameters that could be used to

characterise a system[3]. Secondly there is the difficulty that arises in relating acoustic parameters to biological effects as it is still not clear which parameters should be minimised to reduce their probability. Finally, a problem arises in the implementation of any safety standard since there are so many different ultrasound equipments on the market and their complexity and the number of available options and operating modes increases steadily. A better understanding of the finite amplitude propagation process will aid the selection of the parameters which best describe an ultrasound system both in terms of acoustic output and any biological effects.

b. Complexity of theoretical models

The nature of finite amplitude propagation in the fields of real transducers ensures that any accurate theoretical model will necessarily be complicated. The pressure at a point in a finite amplitude sound field is not only dependent on the pressure distribution at the source but on interactions that occur between the source and the field point. In addition other factors need to be considered, namely:

(i) The high amplitudes and frequencies used in medical ultrasound can generate highly distorted waveforms, i.e. the system is highly nonlinear, which puts the analysis beyond the reach of simple perturbation models so a full nonlinear solution is needed if all the interactions between different frequency components are to be included.

(ii) As the waveform distorts energy is transferred to higher harmonics giving a very broad frequency spectrum (sometimes in excess of 100 harmonics). Under these conditions attenuation effects must be included to dissipate the energy at the top end of the spectrum.

---

3 For example, peak positive pressure, peak negative pressure, various temporal and spatial average intensities, fundamental amplitude, relative harmonic levels and their phases and the pressure gradient across the shock front.

(iii) Diffraction due to the large apertures generates complex near-field structures with rapid phase changes that affect the build up of harmonic levels.

(iv) Focusing needs to be included but it increases the complexity of the near-field structure and leads to higher levels of nonlinear distortion.

(v) Pulsed fields need to be considered if the full range of medical equipment is to be included.

(vi) Tissue characteristics such as scattering will affect the propagation process and will need statistical treatment.

Because of the complexity of a full theoretical solution there is also a need for a simple model that will approximately predict the pressure at certain points in the field (on the acoustic axis for example). This would allow quick checks to be made on ultrasound equipment in service. However, this simple model would still require the existence of the full model in order to check its validity.

c. System design and exploitation

Nonlinear effects have significant implications for the design of most types of medical ultrasound equipment. For example, acoustic saturation[4] could limit the output of an imaging system so that increasing the drive level may simply increase the risk of biological damage without improving the performance. It may be possible to use the harmonics generated to improve lateral resolution [Rugar, 1984] or to give quantitative measurements of tissue parameters [Bjørnø, 1986]. The design of hyperthermia systems could benefit from an accurate theoretical model for finite amplitude propagation in tissue since it would then be possible to predict the

---

4 An acoustic beam is said to be saturated when an increase in drive level fails to cause an increase in received pressure at some distant field point because the energy is being transferred to higher harmonics and lost as heat.

temperature rises generated in specific regions of the pressure field. The efficiency of lithotripters could also be improved if nonlinear effects can be maximised to give the best chance of breaking up stones.

d. Biological effects[5]

The effects of high intensity ultrasound on living tissue are not altogether clear and the complex and dynamic nature of biological systems makes it difficult to perform experiments or make theoretical predictions. However on a macroscopic scale, it is known that ultrasound can cause heating and a relatively small increase in temperature (6 °C) can cause damage in normal tissue particularly if the exposure is prolonged. The mammalian foetus is thought to be even more sensitive to elevated temperatures [Williams, 1983]. On a microscopic scale cavitation[6] is probably an important effect since it can cause mechanical damage due to the violent collapse of cavitation bubbles and can also generate the highly reactive OH^- groups that may cause cell damage. In addition the high tensile stresses that exist across a shocked wavefront could cause some mechanical damage.

The absence of clear mechanisms for biological damage at diagnostic levels of ultrasound and the difficulty in characterising finite amplitude pressure fields pose problems in defining a safe dose level for ultrasound since it is necessary to relate the level of the acoustic field to the biological effects. The problem of biological effects was examined from an epidemiological view-point [Ziskin and Petitti, 1988] and it was concluded that there was no evidence for adverse effects of ultrasound over a period of 25 years, although they did not preclude the possibility of subtle, long term or certain genetic defects which had so far escaped detection.

---

5 Williams [1983] provides a useful review of biological effects of ultrasound.

6 The generation of vapour bubbles in the medium due to high negative pressures.

1.6 INTRODUCTION TO FINITE AMPLITUDE PROPAGATION

Some of the concepts needed in a discussion of finite amplitude propagation can be introduced by considering the propagation of a plane wave. It should be stressed however, that although effects like nonlinear distortion, diffraction and attenuation can all be examined separately it is not necessarily a simple problem to combine all three effects in a single model.

Finite amplitude plane waves

Simple linear theories of acoustic propagation assume that the acoustic disturbance is infinitesimally small, that is the changes in pressure and density associated with the wave are negligible in comparison with the static values, in addition the particle velocity is small when compared with the propagation velocity. This simplifies the algebra and the methods of linear systems theory can be employed to solve many problems of practical interest. Medical ultrasound systems however generally operate under conditions where the amplitude of the acoustic disturbance is sufficiently large to violate the linear assumptions and analysis has to be based on nonlinear methods that account for finite amplitudes. Under these finite amplitude conditions it can be shown that an initially sinusoidal finite amplitude plane wave will distort progressively as it propagates and in the case of maximum distortion will resemble a sawtooth waveform. There are two main sources of nonlinearity, one is due the nonlinear nature of the medium and the other is due to the finite particle velocity of the wave (sometimes referred to as convective nonlinearity). The two types of nonlinear behaviour are described below but it should be noted that both sources of nonlinearity cause the same type of effects on the waveform.

Nonlinearity in the medium

In deriving the equations for acoustic waves in fluids one of the factors considered is the equation of state for the medium, this relates changes in density to changes in pressure. In general we can write $P = P(\rho)$ where P is the total pressure (static +

acoustic) and ρ is the instantaneous density. If the function is expanded as a Taylor series about the equilibrium (or static) density ρ_o we can write:

$$P = P_o + \left(\frac{\partial P}{\partial \rho}\right)_{\rho_o} (\rho - \rho_o) + \frac{1}{2}\left(\frac{\partial^2 P}{\partial \rho^2}\right)_{\rho_o} (\rho - \rho_o)^2 + \ldots$$

This expression is based on two assumptions, firstly that the changes caused by the acoustic wave occur rapidly so that the process is adiabatic, i.e. there is no heat transfer between adjacent regions of the medium. Secondly, that the process is reversible, i.e. there is no change in entropy.

The acoustic pressure ($p = P - P_o$) can be written as:

$$p = P - P_o = As + \frac{Bs^2}{2!} + \frac{Cs^3}{3!} + \ldots$$

where $s = (\rho - \rho_o)/\rho$ and is known as the condensation and:

$$A = \rho_o\left(\frac{\partial P}{\partial \rho}\right)_{\rho_o} \qquad B = \rho_o^2\left(\frac{\partial^2 P}{\partial \rho^2}\right)_{\rho_o} \quad \text{etc}$$

Often the changes in density ($\rho - \rho_o$) caused by the acoustic excitation are small so the series can be truncated and the acoustic pressure (p) can be related to the change in density by:

$$p = P - P_o \approx \left(\frac{\partial P}{\partial \rho}\right)_{\rho_o} (\rho - \rho_o)$$

and it transpires that the speed of propagation (c) for infinitesimal waves is given by the linear relationship:

$$c^2 = \left(\frac{\partial P}{\partial \rho}\right)_{\rho_o}$$

hence the speed of sound is given by the slope of the equation of state at the static density (ρ_o). If the wave has a large amplitude (i.e. ρ_- to ρ_+ in Figure 1.1) then the excursions in density are great enough that the slope of the equation of state, and hence the propagation velocity have changed. It is then necessary to include the second derivative in the Taylor's series.

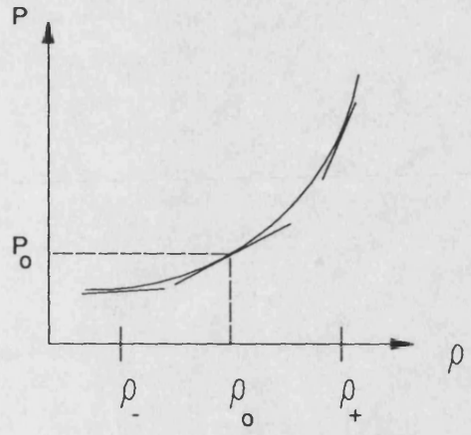

$c^2 = \left(\frac{\partial P}{\partial \rho}\right)$ and varies with density

Thus $\left(\frac{\partial^2 P}{\partial \rho^2}\right)$ is the rate of change of c^2 with density.

Figure 1.1 Equation of state.

It is then usual to use the ratio B/A as a measure of the nonlinearity with:

$$\frac{c^2}{\rho_o}\frac{B}{A} = \left(\frac{\partial^2 P}{\partial \rho^2}\right)_{\rho_o}$$

B/A is often expressed in terms of the nonlinearity parameter $\beta = 1 + B/2A$. β is then related to the rate of change of the propagation velocity with amplitude and has a value of 3.5 for water at 20 °C.

Finite particle velocity

The second source of nonlinearity can be seen by considering the wave motion in terms of the particle velocity (u), in the linear case the particle velocity is very much smaller than the propagation velocity and the entire waveform propagates at the same speed. In the finite amplitude case, since sound waves are longitudinal, a high particle velocity will add to the propagation velocity in a compressional half cycle and subtract from it during the rarefaction. The result is that the wave peaks travel faster than the troughs, eventually the peaks catch up with the troughs and a shock front is formed since the wave cannot become multi-valued. (See Figure 1.2). The shock front then moves at the average propagation speed. The resultant waveform is a sawtooth. This effect is sometimes referred to convective nonlinearity because the motion of the fluid due to the particle velocity gives rise to a local flow field. The ratio of the

particle velocity (u) to the infinitesimal sound speed (c) is known as the acoustic Mach number ($\varepsilon = u/c$). Mach numbers as low as 1/1000 can lead to significant distortion if the waveform is allowed to propagate far enough since the effect accumulates with range.

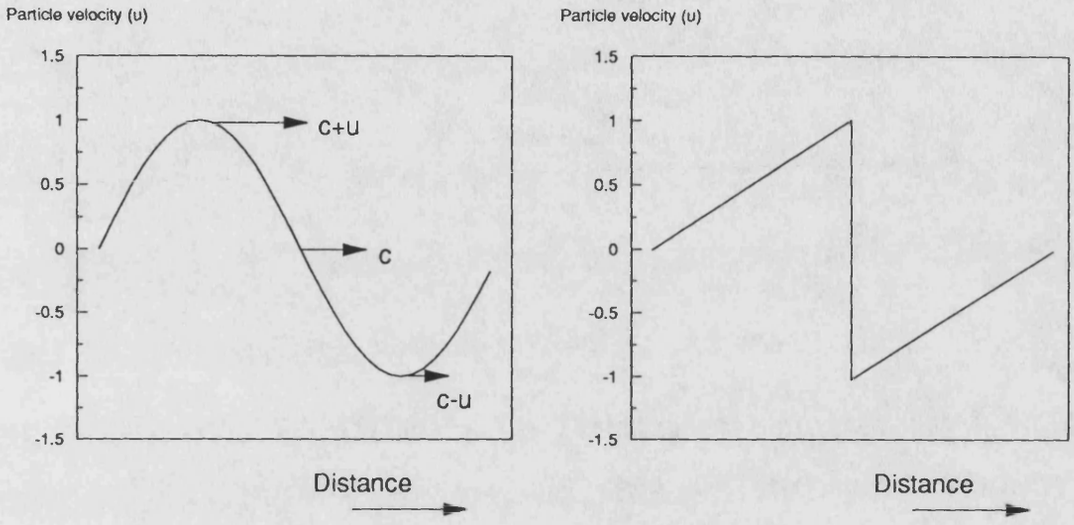

Figure 1.2 Effect of finite particle velocity.

The combination of convective nonlinearity with the nonlinearity due to the medium gives rise to a wave similar to that shown in Figure 1.2 but with the peaks travelling with velocity $c + \beta u$ and troughs travelling with velocity $c - \beta u$. Note that the two effects are independent, even if the medium is perfectly linear, i.e. B (the second derivative) is zero then β will be unity. In the case of very small particle velocity (u) it is still possible to generate distortion if the medium is sufficiently nonlinear.

Burgers equation

The combined effect of the two sources of nonlinearity can be expressed in a one dimensional nonlinear wave equation known as Burgers equation. Blackstock [1962] derived the following Burgers equation for a lossless medium:

$$\frac{du}{dt} + c\left(1 + \beta\frac{u}{c}\right)\frac{du}{dx} = 0$$

where x is the spatial co-ordinate in the propagation direction. The term $\beta u/c (= \beta\varepsilon)$ governs the amount of nonlinearity and in the limit of infinitesimal waves, i.e. $\beta\varepsilon$ tends toward zero, we have a simple linear wave equation:

$$\frac{du}{dt} + c\frac{du}{dx} = 0$$

which will admit solutions of the form,

$$u = f(\omega t - kx)$$

where f is an arbitrary function and the velocity of propagation $c = \omega/k$. The inclusion of nonlinear effects then gives rise to a waveform that travels with velocity $c(1 + \beta\varepsilon)$, i.e. the propagation velocity is a function of particle velocity and nonlinearity parameter. The quantity $\beta\varepsilon$ can be regarded as the shift in the peak positive pressure per cycle and it is common to define a shock parameter;

$$\sigma_s = \beta\varepsilon kx$$

which is the total shift in peak positive pressure in propagating a wave (with wavenumber k) over a distance x. The effect of different values of σ_s is shown in Figure 1.3.

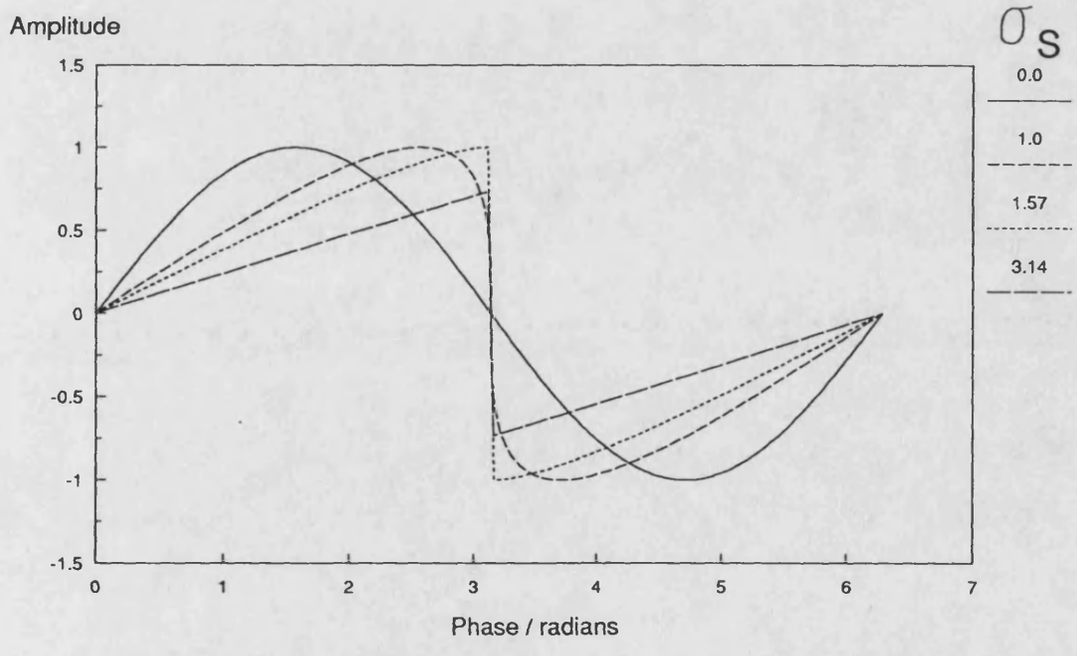

Figure 1.3 Effect of shock parameter (σ_s) on a sinusoidal waveform.

The initial undistorted wave is represented by the curve $\sigma_s = 0$, a value of $\sigma_s = 1$ corresponds to a wave that has just started to form a shock, that is there is a small vertical region in the waveform at the zero crossing point. A fully shocked wave occurs when $\sigma_s = \pi/2$ since the peak positive pressure will have moved forward (by $\pi/2$ radians) to the zero crossing point of the wave and similarly the peak negative pressure will have receded to the same point. The distance at which this occurs is known as the shock distance (l_D) and is given by:

$$l_D = \frac{1}{\beta \varepsilon k}$$

At this distance the wave also reaches its maximum distorted amplitude since further propagation (e.g. $\sigma_s = \pi$ leads to a reduction in amplitude as more of the shock wave moves into the shock region.

If the effect of attenuation is to be included it is usual to combine the absorption coefficient (α) with the shock distance to obtain the Goldberg number:

$$\Gamma = \frac{1}{\alpha l_D} = \frac{\beta \varepsilon k}{\alpha}$$

which indicates the relative importance of nonlinearity and absorption. The effect of absorption is to oppose nonlinear distortion since it dissipates the energy pumped into the higher harmonics by the distortion. Thus a low Goldberg number suggests that it will be difficult to generate nonlinear distortion.

Frequency domain representation

The progressive distortion of a finite amplitude waveform in the time domain corresponds to the generation of harmonics in the frequency domain with a loss of energy from the fundamental frequency to the harmonics. A frequency domain representation of nonlinear distortion is illustrated in Figure 1.4 for the case of plane wave that is initially sinusoidal, i.e.

At $z = 0$, $u(t) = \sin(\omega t)$

As the wave propagates the higher harmonics are generated and the distortion builds up so that at ranges much greater than the shock distance (z = 0.66 m) the harmonic amplitudes vary as the reciprocal of the harmonic number, i.e the time waveform is a sawtooth with:

$$u(t) \propto \sum_{n=1}^{\infty} \frac{\sin(n\omega t)}{n}$$

The loss of energy from the fundamental can also be seen as the harmonics increase in amplitude.

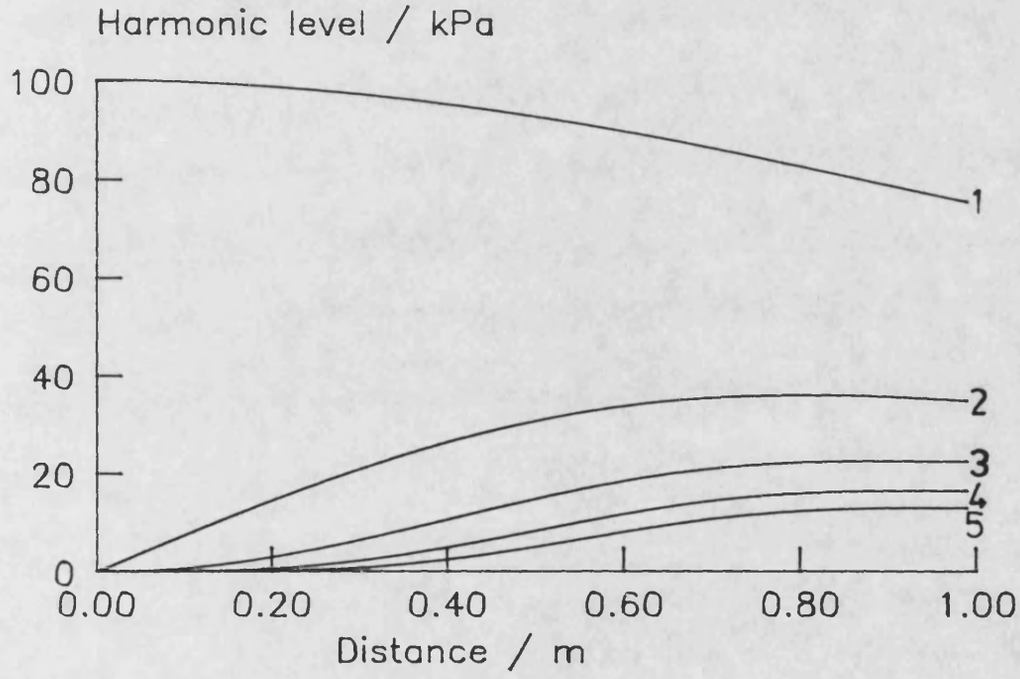

Figure 1.4 Calculated amplitudes (up to 5th harmonic) for plane wave distortion in water, p_o = 100 kPa, f_o = 2.25 MHz.

Effect of phase shifts [7]

In practice the symmetrical waveforms of Figure 1.3 are not usually observed since diffraction effects, due to the finite source size, will cause phase shifts between the harmonics which leads to asymmetry in the waveform. This effect can be illustrated by evaluation of the Fourier series

$$y(t) = \sum_{n=1}^{40} \frac{\sin(n\omega t - \theta_n)}{n}$$

for different values of phase shift (θ_n). In Figure 1.5 the effect of three different phase shifts is shown.

In all three cases the harmonics have all been shifted the same amount i.e. $\theta_n = \theta$. In the case of zero phase shift we have the usual sawtooth waveform although there is some ripple caused by truncating the Fourier series at the 40th harmonic. A phase shift of 0.785 radians ($\pi/4$) generates a waveform that has a higher positive peak than the sawtooth and a lower negative peak. The ratio of peak positive to peak negative pressure is about 4:1. The negative peak also shows a much smoother variation than the positive peak. Waveforms like this are commonly observed in medical ultrasound systems. A further shift in the harmonic phases to 1.57 radians ($\pi/2$) increases further the top-bottom asymmetry to produce a bowl shaped waveform with even symmetry.

---

7 Note that the Fourier sine series representation of time waveforms is used throughout this thesis with the phases of harmonics expressed relative to the fundamental phase and in radians of the fundamental. Thus if we have a signal $y_1(t) = \sin(\omega_1 t - \theta_1)$ and its nth harmonic $y_n(t) = \sin(n\omega_1 t - \theta_n)$ then the phase angle between them would be expressed as $(\theta_n/n - \theta_1)$

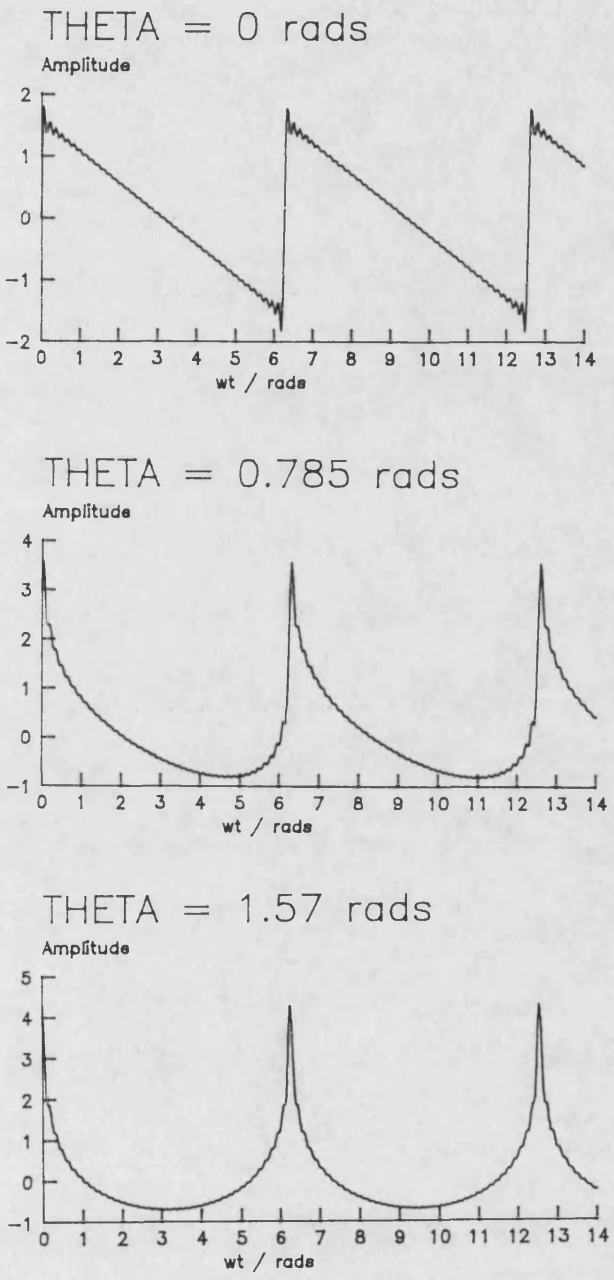

Figure 1.5 Effect of phase shifting the harmonics of a sawtooth waveform.

Figure 1.6 shows a "real" time waveform that fairly typical of many observed in this study. The waveform shows some ripple which is due to a resonance in the hydrophone but otherwise is very similar to the middle waveform of Figure 1.5. Fourier analysis of the waveform (Figure 1.7) shows that the harmonic amplitudes have a reciprocal dependence on frequency although the hydrophone resonance causes some deviation above about 20 MHz and the harmonic phases are proportional to harmonic number, again with some deviation due to the hydrophone resonance. Note that the phase has been plotted within the range $\pm\pi$ hence the apparent jumps at around 15 and 40 MHz.

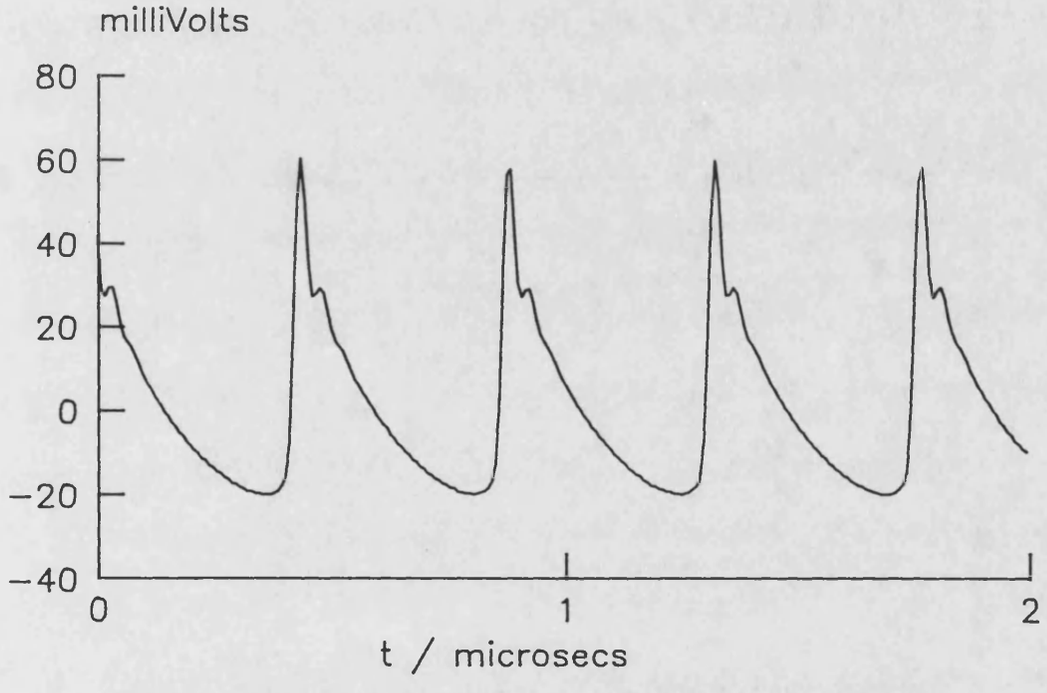

Figure 1.6 Typical observed waveform.

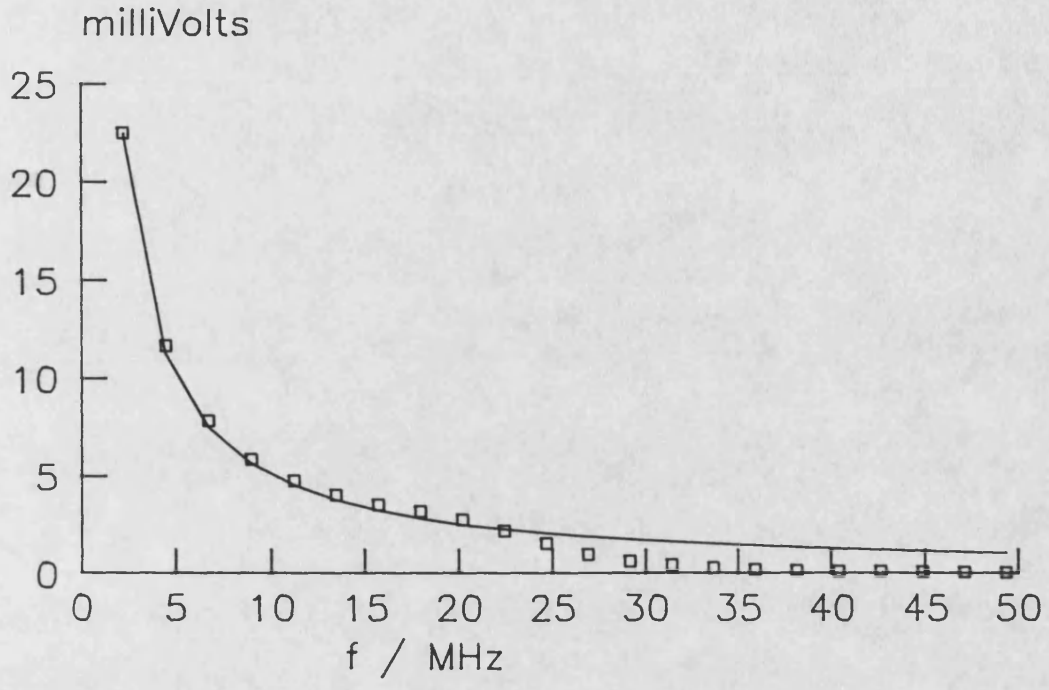

Observed harmonic amplitudes (Solid line fitted as 1/f from fundamental)

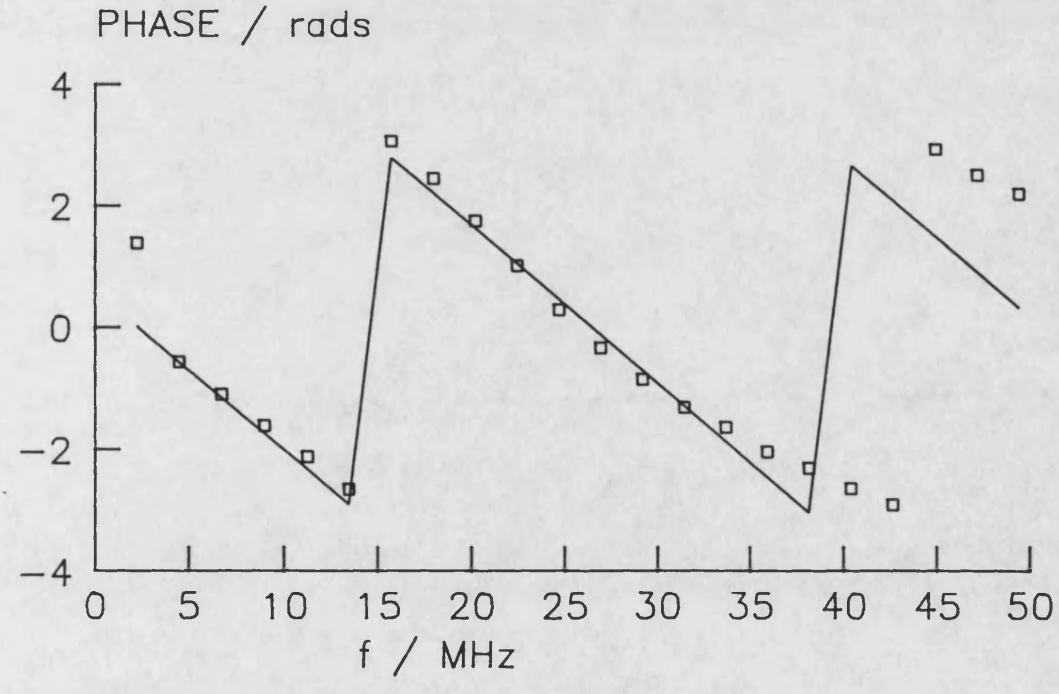

Observed harmonic phases (Solid line fitted as constant slope from second harmonic)
Figure 1.7

Chapter 2: REVIEW OF LITERATURE

This chapter reviews some of the published literature in areas related to this study. The first part of the chapter covers infinitesimal acoustics applied to plane and focused circular radiators. The second part covers finite amplitude acoustics starting with one dimensional solutions and progressing through plane piston fields to focused fields.

2.1 INFINITESIMAL ACOUSTICS

At infinitesimal source levels the pressure field due to an aperture can be calculated as the integrated effect of point sources over the aperture[8]. This is known as the diffraction integral (or Rayleigh integral) and is based on the superposition theorem of linear systems theory. One of the difficulties of this method is expressing the distance from the source point to the field point in a form that makes the integration straightforward. There are only a few special cases when the solution can be expressed in closed form and in general the integral has to be evaluated numerically or approximations introduced to reduce the complexity.

2.1.1 Plane piston source

Plane circular apertures of various dimensions (a/λ between 1 and 20) were examined theoretically by Zemanek [1970], he presented contour plots and three dimensional plots based on the exact form of the diffraction integral with the resulting double integral being evaluated numerically. Although Zemanek was not the first to calculate such results his plots showed clearly the near-field oscillations and their increased complexity for apertures that were large with respect to the wavelength.

A more efficient method was presented by Lockwood and Willette [1973]. They showed that a time domain Green's function approach could be used to reduce the problem to a single integral in the case of a plane piston, since the impulse response

---

8 See, for example, Kinsler et al [1982]

of the piston could be expressed in closed form. They went on to reproduce Zemanek's results and showed that the method is equivalent to, but computationally more efficient than, the exact double integral method.

Experimental measurements were compared with theoretical predictions by Hutchins et al [1986]. They demonstrated good agreement for plane and annular circular sources at low amplitudes.

2.1.2 Focused source

One of the earliest theoretical papers on focused fields was that of O'Neil [1949]; he evaluated the infinitesimal pressure field of a concave spherical shell by evaluating the diffraction integral as a double numerical integral. The calculation used the exact form of the diffraction integral but, in common with all the approaches described here, ignored the effect of secondary diffraction, i.e. the individual point sources are assumed to radiate freely into half space. This assumption is unlikely to be of importance for weakly focused systems. O'Neil noted several points of interest:

1. The point of greatest pressure occurs on the source side of the centre of curvature, i.e. not in the true focal plane.

2. The relative pressure in the focal plane has the same form as the far-field directivity pattern of a plane piston radiator.

3. The axial pressure field can be expressed in closed form, see Appendix A.

More recently, Madsen et al [1981] derived an exact solution for continuous wave focused apertures that can be expressed as a single integral. They also demonstrated good agreement between experiment and theory with extensive comparisons for a focused transducer (19 mm diameter and 110 mm focal length, i.e. gain (G) = 4.3).

Penttinen and Luukkala demonstrated the application of the impulse response method to a curved circular radiator [1976a] and a focusing lens [1976b]. This corresponds to the technique of Lockwood and Willette [1973] for the plane case.

The parabolic approximation[9] of Tjøtta and Tjøtta [1980] was used by Lucas and Muir [1982] to investigate the small signal field of focused sources and they obtained good agreement with experimental measurements for a focused circular array. Their general solution has the advantage that it requires only a single numerical integration that reduces to an analytic expression on the acoustic axis. An equivalent but more general expression was derived by Thompson et al [1987] for the pressure fields of elliptical apertures with focusing under the parabolic approximation. Their general expression reduces to that of Lucas and Muir [1982] in the case of a circular aperture with the lens adjacent to the radiator.

An exact expression for the pressure field of a focused piston at infinitesimal amplitudes is that of Hasegawa et al [1986 and 1987]. Their solution eliminates the need for integration but is in the form of an infinite series involving Legendre polynomials and Bessel, Hankel and spherical Neumann functions.

2.1.3 Pulsed fields

The main effect of pulsing the drive to the transducer is on the near-field structure and the side-lobes in the farfield directivity pattern. Consider for example a plane piston transducer driven with a continuous wave; the pressure fluctuations in the near-field are caused by interference between the edge wave and the central plane wave. If the drive is only switched on for a single cycle then the edge wave and central plane wave do not overlap until the last axial minimum of the continuous field (where the path difference is sufficiently small); thus the pressure field in the preceding region will be devoid of interference effects. If the pulse is lengthened then the two waves meet closer to the transducer and interference effects are seen over a larger region (see

---

9 See Chapter 3: Theory

Appendix A). The high order side-lobes in the diffraction pattern are also due to interference of the central and edge waves so these are diminished in the pulsed case. These effects were demonstrated by Weyns [1980a and 1980b] who presented theoretical predictions for pulsed transducers, both planar and focused. He used a simple, but time consuming, double numerical integration of a time varying function, based on the diffraction integral.

An alternative approach when modelling pulsed fields at low amplitudes is to calculate the separate continuous wave solutions due to each of the Fourier components in the initial drive waveform and then to superimpose these solutions at the appropriate field point. This was shown by Goodsit et al [1982] who extended their previous work on continuous wave fields [Madsen et al, 1981] and obtained good agreement with experimental measurements on pulsed fields from medical ultrasound transducers at 2.25 MHz and 3.5 MHz.

The continuous wave solution of Lucas and Muir [1982] was reduced by Cobb [1984] from a single integral to a series of Lommel functions, which were in turn are evaluated in terms of Bessel functions. The pulsed field solutions were then obtained by superposition of a number of these simplified continuous wave solutions.

The time domain Green's function approach has also been applied to the pulsed problem, see for example Stephanishen [1971], Beaver [1974], Tjøtta and Tjøtta [1982] and Hutchins et al [1987].

2.2 FINITE AMPLITUDE ACOUSTICS

2.2.1 Finite amplitude plane waves

Poisson [1808] put forward a general solution for the finite amplitude plane wave problem. His solution had the form:

$$u = f\left(t - \frac{z}{c + \beta u}\right)$$

but it was some time later that Stokes [1848] produced the first sketches of this solution to illustrate that waveform distortion would occur. In 1931 Fay published an analytical solution for the finite amplitude plane wave problem that was valid for highly shocked waves ($\sigma_s > 1$) with viscous losses; another solution due to Fubini [1935] applied to weak shocks ($\sigma_s < 1$) in a lossless fluid. It was Blackstock [1966] who connected the Fay and Fubini solutions and was responsible for much work on finite amplitude plane waves using Burger's equation[10] [Blackstock, 1962, 1964a].

Blackstock [1964b] also produced a one dimensional solution based on Burger's equation that was applicable to finite amplitude cylindrical and spherical waves. An early numerical solution of Burger's equation by Fox and Wallace [1954] applied distortion in the time domain and attenuation in the frequency domain necessitating repeated application of Fourier transforms. The later numerical solution of Trivett and Van Buren [1981] had the advantage that all the calculations were carried out in the frequency domain, thus reducing the computational requirements.

2.2.2 Plane piston source at finite amplitudes

There are a number of different approaches to the problem of finite amplitude propagation in diffractive fields; some of them are outlined below.

(a) Perturbation methods

The second harmonic can be calculated as a perturbation of the fundamental pressure

---

10 See Chapter 1, Introduction to finite amplitude propagation

field; in its most basic form the second harmonic at a point in space is proportional to the integral of the fundamental pressure squared along the path from the source to the field point. The chief advantage of such a method is that the reduced complexity of the problem leads to a simple numerical solution but there are a number of drawbacks. Firstly, the method is only applicable to relatively low levels of nonlinearity and does not account for loss from the fundamental. Secondly, diffraction effects in the second harmonic beam are not included. A perturbation approach was used by Ingenito and Williams [1969] to examine second harmonic generation in the near-field of a plane piston and they obtained reasonable agreement with experimental measurements. It was also shown that the most important contribution to the integral came from the region immediately preceding the field point.

(b) Full solutions

Full solutions take a nonlinear, three dimensional wave equation and attempt to solve it for all the harmonics generated. This has the advantage that the entire pressure field is calculated and interactions between harmonics and the fundamental can be seen. The disadvantage of this method is its complexity and heavy computational requirements. The theoretical approach used in this thesis falls in this category and some of the background to the method follows.

Kuznetsov [1971] derived a second order approximation to the nonlinear wave equation which included diffraction, absorption and nonlinearity terms (all correct to the second order). Kuznetsov's equation was derived by considering the equations of fluid mechanics for a viscous, heat-conducting fluid and followed the derivation of Zabolotskaya and Khokhlov [1969] which was correct to second order in the diffraction and nonlinear terms but took no account of absorption. It was shown that some simplification is possible if it is assumed that the solution has the form of a quasi-plane wave. This quasi-plane wave form is generally known as the parabolic approximation to the nonlinear wave equation; it is also sometimes referred to as the KZK equation after Khokhlov, Zabolotskaya and Kuznetsov. The parabolic

approximation is applicable in the case of a circular aperture that is many wavelengths across and can be shown to be equivalent to the Fresnel approximation sometimes used in the diffraction integral for near-field calculations. The theoretical background is outlined in Chapter 3.

Tjøtta and Tjøtta [1981] derived the same parabolic equation and showed its application to circular apertures and parametric arrays. The work was extended to circular apertures with time periodic, but otherwise arbitrary, source conditions [Aanonsen, Barkve, Tjøtta and Tjøtta, 1984]. They presented theoretical results for the first few harmonics in the near-field a plane piston with uniform excitation and with Gaussian shading. Later work by Hamilton, Tjøtta and Tjøtta [1985] extended the analysis to the far-field and showed good agreement between their theoretical solution and some existing experimental results for the far-field. The approach used by Tjøtta and Tjøtta was to cast the finite amplitude parabolic equation in non-dimensional form and then insert a trial solution in the form of a Fourier series for the time waveform. The Fourier coefficients (amplitude and phase) were assumed to be functions of the spatial co-ordinates; this yielded an infinite set of coupled differential equations which were truncated and solved using a finite difference numerical method. The solution has a some limitations although none too severe to preclude its use for several real systems of interest (See Chapter 3).

(c) Other methods based on the one dimensional solution.

Lockwood et al [1973] suggested that in the far-field of a source, waves at different angles propagate independently and can therefore be treated using a one dimensional wave solution. They made measurements of far-field distortion for a fundamental frequency of 450 kHz and compared them with a weak shock theory, corrected for absorption. The relatively low fundamental frequency and the need to work get in the far-field of the source meant the experiment had to be conducted in a lake. Good agreement was obtained at observation distances of 41 and 117 yards and it was concluded that the results supported their hypothesis. However an experimentally

observed splitting of the second harmonic side-lobe which had not been predicted theoretically was attributed to second harmonic generation at the source. Subsequent work has shown that, in fact, it was a feature of the nonlinear propagation. They also showed that near the acoustic axis the directivity pattern for the n^{th} harmonic could be approximated by:

$$D_n(\Theta) \approx [D_1(\Theta)]^n$$

where D_1 is the directivity pattern at the fundamental frequency.

Lancaster's approach [1983] to solution of the near-field problem was to take the one dimensional solution of Burger's equation by Trivett and Van Buren [1981] and force the fundamental component to follow the small signal pressure field of the plane piston. This gave reasonably good agreement with experimental results on the acoustic axis but because of the lack of interaction of the harmonics with the fundamental, effects such as saturation of the fundamental could not be modelled.

2.2.3 Focused source at finite amplitudes

In 1968, Smith and Beyer presented measurements made on a spherical cap (30 cm radius of curvature and outer radius of 1 inch) over a range of drive levels. They compared experimental measurements with the model proposed by Naugolnykh et al [1963] and obtained some agreement at short ranges for the lower drive levels.

Lucas and Muir [1983] extended their earlier work [1982] to finite amplitudes using a perturbation of their small signal solution to obtain predictions for the second harmonic amplitude and phase. They again showed agreement with experimental results although the solution was necessarily limited to weak shock since it was a perturbation of the small signal case. It does however provide a relatively simple method (a triple numerical integral) for predicting the second harmonic and thus the degree of distortion present. Humphrey et al [1986] provided further experimental measurements confirming the accuracy of Lucas and Muir's result. The results showed similar discrepancies in the second harmonic level to those observed by

Lucas and Muir in the post focal region. Saito et al [1987] compared a modified form of Lucas and Muir's result with experimental measurements made on a focused radiator with amplitude shading across the aperture, with some success.

The finite difference method of solution for the nonlinear parabolic equation was extended by Hart and Hamilton [1987] to allow high focusing gains and high initial amplitudes similar to those encountered in acoustic microscopy. This was done by introducing a transformation to tighten the finite difference grid near the focal plane thus improving the efficiency of the calculation.

2.2.4 Gaussian source

A number of studies have involved apertures with a Gaussian shading. This has the advantage that diffraction effects become less important and theoretical modelling is simplified. The Gaussian beam has none of the rapid near-field oscillations of the plane circular aperture and there are no side-lobes; thus the Gaussian beam approximates quite well to the pulsed aperture.

A method of producing Gaussian amplitude shading in transducers has been demonstrated by Martin and Breazeale [1971] and Du and Breazeale [1985]. They used partially electroded piezo-electric transducers and relied on fringing of the electric field to reduce the amplitude of vibration across the aperture. Du and Breazeale [1986] also compared a perturbation theory for finite amplitude distortion in the field of a circular Gaussian source with experimental measurements and obtained good agreement at low amplitudes (the second harmonic level was about 1% of the fundamental).

Bacon [1986] developed a model for predicting the harmonic content of Gaussian beams at higher drive levels. The model is valid in the main axial lobe of the pressure field and he showed agreement in this region with experimental measurements on a focused transducer. Bacon's model was compared with the finite difference model used in this study and with experimental measurements on a focused transducer

[Bacon and Baker, 1989]. Both models agreed with the experiment to within about 10% but it seems likely that the transducer in question had a source distribution that lay somewhere between a Gaussian and a top hat; thus the finite difference model could probably have been made more accurate if the aperture excitation had been determined more precisely. Bacon also extended his model for predictions in tissue mimicking gels with some success.b

Chapter 3: THEORY

3.1 INTRODUCTION

There are many theoretical approaches to the problem of nonlinear propagation; this chapter follows one particular route from the parabolic wave equation to a numerical solution programmed in FORTRAN. The small signal case is considered in Appendix A which summarises some results for a focused field under conditions of infinitesimal amplitudes.

3.2 GENERAL WAVE EQUATION

Kuznetsov [1971] derived a nonlinear wave equation for a scalar potential, Φ, by considering the dynamics of a viscous, heat conducting fluid. The equation was correct to the second order with terms for diffraction, absorption and nonlinearity:

$$\frac{\partial^2\Phi}{\partial t^2} - c^2\nabla^2\Phi = \frac{\partial}{\partial t}\left[2\alpha c k^2\nabla^2\Phi + (\nabla\Phi)^2 + \frac{B}{2A}\frac{1}{c^2}\left(\frac{\partial\Phi}{\partial t}\right)^2\right] \qquad 3.1$$

The left-hand side of equation 3.1 is simply the three dimensional linear wave equation, of the three terms on the right-hand side the first term is a linear term and accounts for absorption, the second term is due to convective nonlinearity and the third is due to nonlinearity in the equation of state.

3.3 PARABOLIC APPROXIMATION

Kuznetsov also showed that the equation (3.1) could be simplified, by approximation, in the case of a quasi-plane wave field. A circular aperture that is many wavelengths in diameter (i.e ka is large) falls in this category since most of the energy is confined to a beam in the axial direction. This is known as the parabolic (or paraxial) approximation and is equivalent to the Fresnel approximation that is sometimes used in the diffraction integral for near-field calculations. Kuznetsov's parabolic approximation can be expressed in a normalised form [Hamilton et al, 1985]:

$$\left(4\frac{\partial^2}{\partial\tau\partial\sigma}-\nabla_1^2-4\alpha R_o\frac{\partial^3}{\partial\tau^3}\right)\overline{p}=2\frac{R_o}{l_D}\frac{\partial^2}{\partial\tau^2}\overline{p}^2 \qquad 3.2$$

where $\overline{p}$ (= p/p_o) is the acoustic pressure normalised by the source pressure and $\tau(=\omega t-kz)$ is the retarded time, i.e. includes a phase term for a plane wave travelling in the z direction. σ is the axial coordinate normalised by the Rayleigh distance and ζ is the radial coordinate normalised by the aperture radius, i.e.

$$\sigma=\frac{2z}{ka^2} \text{ and } \zeta=r/a$$

A trial solution was then assumed in the form of a Fourier series (for the time waveform) with amplitude and phase that were functions of the spatial coordinates, i.e.

$$p(\sigma,\zeta,\tau)=\sum_{n=1}^{\infty}q_n(\sigma,\zeta,\tau)\sin(n\tau+\psi_n(\sigma,\zeta,\tau)) \quad \text{or}$$

$$p(\sigma,\zeta,\tau)=\sum_{n=1}^{\infty}g_n(\sigma,\zeta,\tau)\sin(n\tau)+h_n(\sigma,\zeta,\tau)\cos(n\tau) \qquad 3.3$$

where $g_n=q_n\cos\psi_n$, $\quad h_n=q_n\sin\psi_n$

and n is the harmonic number, with n=1 representing the fundamental frequency. Substituting the trial solution (3.3) into equation 3.2 and collecting terms in $\sin(n\tau)$ and $\cos(n\tau)$ gives a set of coupled differential equations for g_n and h_n:

$$\frac{\partial g_n}{\partial\sigma}=-n^2\alpha R_o g_n+\frac{1}{4n}\nabla_1^2 h_n+$$

$$\frac{nR_o}{2l_D}\left(\frac{1}{2}\sum_{k=1}^{n-1}(g_k g_{n-k}-h_k h_{n-k})-\sum_{p=n+1}^{\infty}(g_{p-n}g_p+h_{p-n}h_p)\right) \qquad 3.4$$

$$\frac{\partial h_n}{\partial\sigma}=-n^2\alpha R_o h_n+\frac{1}{4n}\nabla_1^2 g_n+$$

$$\frac{nR_o}{2l_D}\left(\frac{1}{2}\sum_{k=1}^{n-1}(h_k g_{n-k}+g_k h_{n-k})+\sum_{p=n+1}^{\infty}(h_{p-n}g_p-g_{p-n}h_p)\right) \qquad 3.5$$

These equations were then solved numerically.

3.4 NUMERICAL SOLUTION

3.4.1 Plane piston - continuous wave

Equations 3.4 and 3.5 form the basis of the numerical solution which was implemented by Aanonsen in a FORTRAN program called FOCAB [1983]. Standard numerical approximations were used for the derivatives and the pressure field was calculated using a finite difference technique. The harmonic coefficients (g_n and h_n) were represented by pairs of two-dimensional grids, one such grid is shown in Figure 3.1.

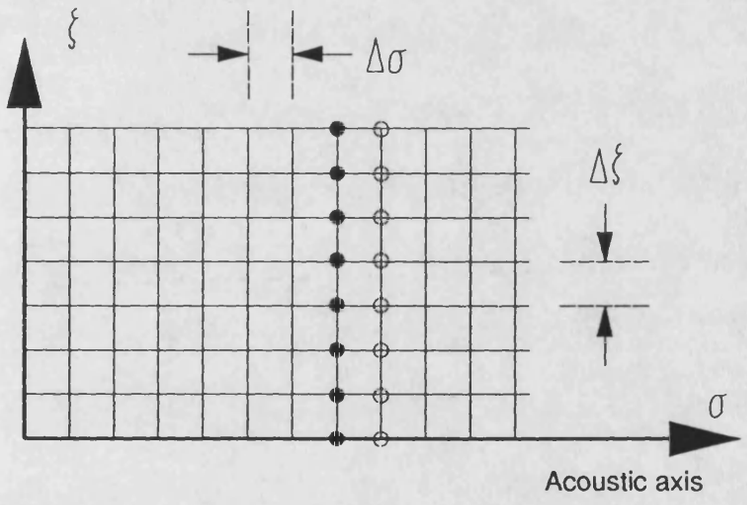

Figure 3.1
Simplified finite difference grid.

Thus if the filled circles of Figure 3.1 represented known values of g_n in the radial direction, then equation 3.4 relates them to the next set of values along the acoustic axis (denoted by the empty circles). The numerical scheme replaces the partial derivatives of equation 3.4 with small increments, e.g.

$$\frac{\partial g_n}{\partial \sigma} \text{ becomes } \frac{g'_n - g_n}{\Delta\sigma}$$

where g'_n is the new value of g_n. Similar numerical approximations were used to replace the transverse gradient operator and the resulting equations were solved to give the change in the harmonic component $(g'_n - g_n)$ for a small step $(\Delta\sigma)$ in the axial

direction. The initial conditions were given by the radial pressure distribution across the piston face and baffle. The physical meaning of the scheme described by equations 3.4 and 3.5 can be seen more clearly if the equations are written in a slightly different form. If we take equation 3.4 and express it in terms of the original z coordinate we get an expression for the change in g_n with axial range (z):

$$\frac{\partial g_n}{\partial z} = -n^2 \alpha g_n + \frac{1}{4nR_o}\nabla_1^2 h_n +$$

$$\frac{n}{2l_D}\left(\frac{1}{2}\sum_{k=1}^{n-1}(g_k g_{n-k} - h_k h_{n-k}) - \sum_{p=n+1}^{\infty}(g_{p-n}g_p + h_{p-n}h_p)\right) \qquad 3.6$$

This shows that the change in the field g_n with distance along the z axis is due to three terms:

a. Attenuation.

This term has an n^2 dependence (i.e. it varies with the square of the frequency) and is proportional to α (the absorption coefficient); thus we have the classic frequency squared dependence of absorption in a fluid.

b. Diffraction.

This term has a reciprocal dependence on nR_o; thus diffraction becomes less important as the frequency (or harmonic number) increases and as the aperture radius increases. In other words, the more wavelengths across the aperture the more the beam looks like a plane wave travelling in the z direction. Diffraction also depends on the transverse gradient, with rapid changes in the field in the radial direction giving rise to large diffraction terms, such as occur at the piston edge. It was implicit in the initial assumptions that the field would be quasi-plane wave; hence the absence of the longitudinal term in the gradient operator.

c. Nonlinearity.

The nonlinear term is proportional to n, hence nonlinearity becomes more important

with increasing frequency. It also depends on the reciprocal of l_D, the shock distance. The shock distance is defined for a plane wave as:

$$l_D = \frac{1}{\beta \varepsilon k}$$

that is a plane wave goes into shock more quickly with increasing parameter of nonlinearity, increasing acoustic Mach number and increasing fundamental frequency. The shock distance must be treated with some caution because in a diffractive field it does not have the same meaning as it does for a plane wave since the definition takes no account of the rapid spatial fluctuations that occur in highly diffractive fields. However, it is still a useful indicator of the strength of nonlinear effects present.

The nonlinear term is the only coupling term in the equation, i.e. it intermixes terms of different harmonic number. If the products under the summations are evaluated it is found that they pick out all combinations of harmonics that have sum or difference equal to the harmonic (n) in question. For example in evaluating the fourth harmonic the nonlinear term involves products of the following harmonics: 1 and 3, 2 and 2, 1 and 5, 2 and 6, 3 and 7 ... etc. This term is also the only one with any connection with the drive level (p_o) so small signal runs were achieved by reducing the pressure across the piston face, and hence the Mach number so that nonlinear generation became insignificant.

A similar result to equation 3.6 is obtained from equation 3.5 for the change in h_n along the axis.

3.4.2 Initial and boundary conditions

The initial conditions are specified by the amplitude and phase of each harmonic at each radial point in the plane of the aperture. In the simplified diagram of the finite difference grid (Figure 3.2) the grid points in the plane of the aperture are indicated by a series of small squares. The aperture in the diagram occupies four grid points hence four 1's and the rest of the column set to 0's. (i.e. a top hat distribution) In

practice at least 20 grid points would be used across the aperture. The figure shows the grid for the fundamental, in the case of a continuous wave excitation all the other harmonics are initialised as 0's for all points in the radial section. It can be seen at this stage that it is a simple matter to include focusing by advancing the initial phase of the fundamental across the aperture and amplitude shading can be included by changing the initial amplitudes across the aperture.

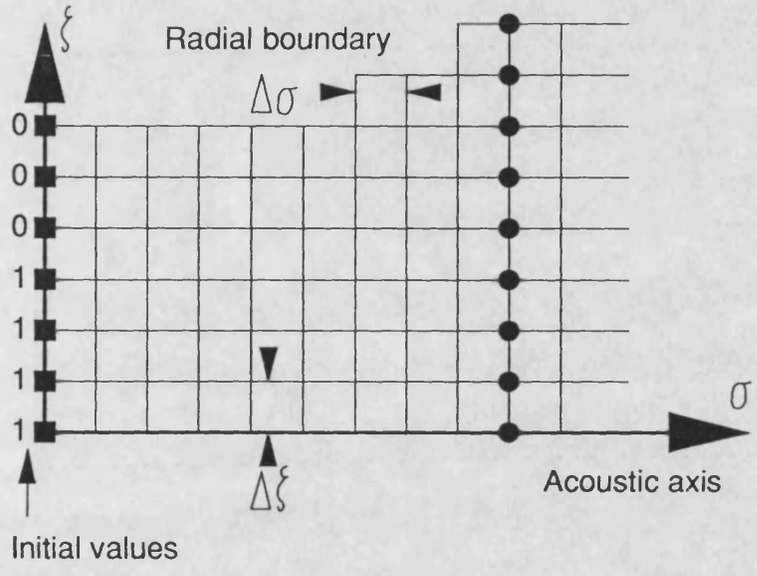

Figure 3.2
Simplified finite difference grid.

Figure 3.2 also shows the increased radial boundary used to reduce the effect of "reflections" from the edge of the grid. In this simplified example only seven grid points are used initially but as the calculation progresses (indicated by the row of circular points) and the beam spreads the radial boundary is increased accordingly. In practice the initial number of radial points might be 80 and increase to say 300 by the end of the run. In order to reduce the computer run-time separate radial boundaries are maintained for each harmonic since the higher harmonics are mainly generated near the acoustic axis. The row of circular points also indicate that although it is necessary to maintain radial arrays for all the harmonics it is not necessary to retain all the previous radial arrays since the calculation relies only on the most recent previous set of radial points.

The model can be initialised using any radial plane in the field. So, for example, if the field is known accurately through the focal plane then this can be used as the starting point and the calculation continued for the post-focal region.

3.4.3 Limitations

There are a number of constraints imposed by the assumptions implicit in the model:

a. Parabolic approximation.

The parabolic approximation requires that the aperture is several wavelengths across, i.e. ka >> 1. It also puts a limit on the maximum angle that a vector from the origin to the field point can subtend to the acoustic axis, hence positions close to the aperture or far off axis must be avoided. On axis of radiators such as those studied here the error starts to become important at ranges of less than 4 piston radii. Off axis, the error is acceptable for aperture angles of less than 20°. Outside these limits the model still gives results but the approximations will be in error and the positions of maxima and minima will become less accurate as the source is approached. In practice these restrictions do not pose great problems since many geometries of practical importance can be studied within these constraints.

b. Grid step size.

(i) Axial step size.

The finite difference technique calculates the field for an array of equally spaced radial points and in equally spaced increments in the axial direction. If the spatial frequency of the field variations is greater than the grid spacing then the variations are "over-looked". In the case of the plane piston the fundamental pressure field fluctuates rapidly between 0 and $2p_o$ near the piston face with the fluctuations becoming less rapid as the far-field is approached. If large axial steps are used the calculated solution close to the piston is almost constant at unity, i.e. the average value. Further from the piston the solution starts to show the expected oscillations. The effect on the axial field of reducing the axial step size can be seen in Figure 3.3.

The finer step size picks out more of the near-field detail than the coarser step but at the cost of increased computer run-time. However, there is no advantage in reducing the step size to show all of the near-field detail since the parabolic approximation limits the accuracy of the results at short axial ranges, in the case of Figure 3.3 at normalised ranges less than 0.04.

(ii) Radial step size.

The radial step size can affect the solution in a similar manner to the axial step size, since coarse radial steps will cause small detail to be overlooked, but there is a more serious problem that relates to the calculated positions of the axial maxima and minima. These positions depend on the Rayleigh distance, which is proportional to the square of the aperture radius; thus a small change (or error) in the aperture diameter will have a significant effect on the axial geometry which becomes greater close to the piston. Since the aperture excitation is described by a series of discrete radial points there will always be some error due to this effect. Figure 3.4 shows that reducing the radial step size causes the locations of the maxima and minima to shift towards their true positions but has little effect on their amplitudes.

The technique used for solving the equations imposes a further constraint on the axial and radial step sizes as it is required that the square of the axial step size be greater than twice the radial step, i.e.

$$\frac{\Delta\sigma}{(\Delta\zeta)^2} < 0.5$$

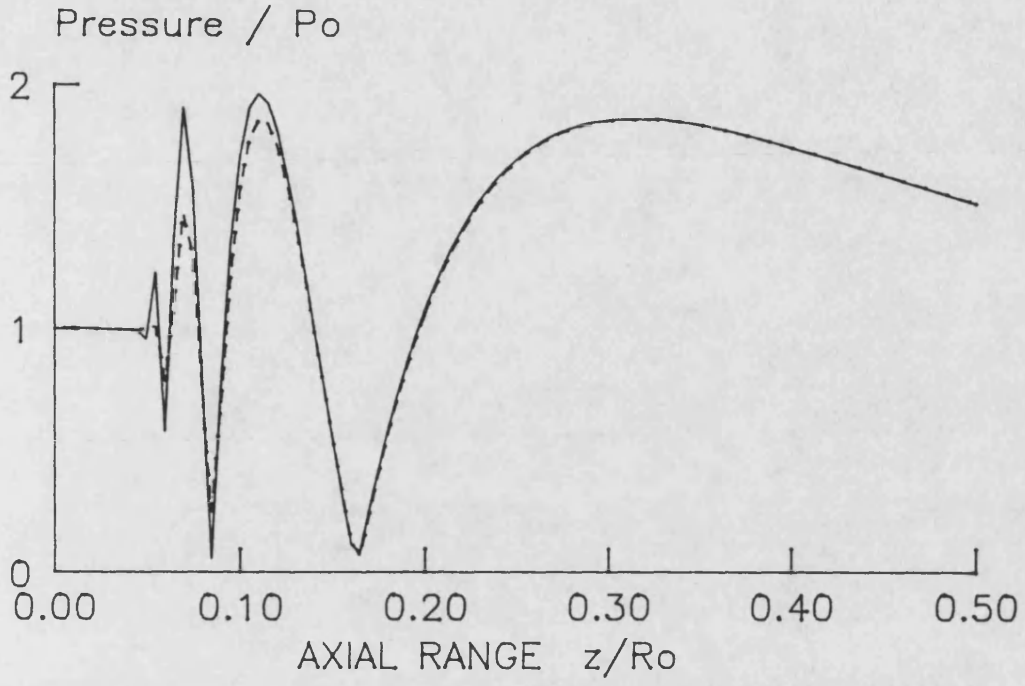

Figure 3.3 Effect of axial step size on axial fundamental pressure field of a plane piston radiator. Axial step = 0.00036 R_o (- -) and 0.00012 R_o (—).

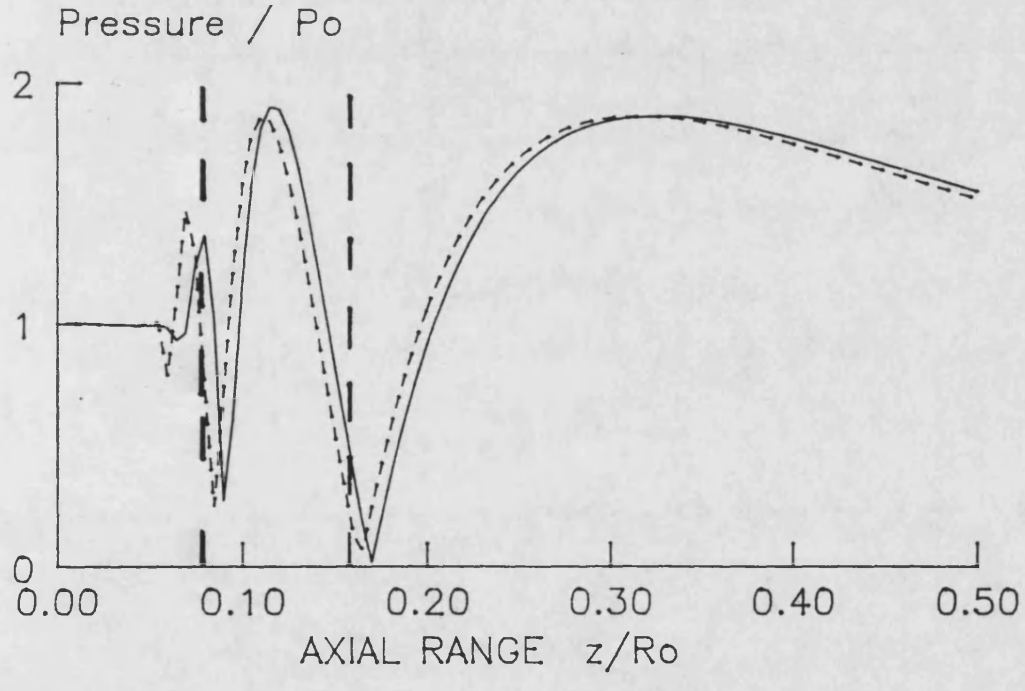

Figure 3.4 Effect of radial step size on axial fundamental pressure field of a plane piston radiator. Radial step = 0.03 a (- -) and 0.04 a (—). Vertical dashed lines indicate correct positions for minima.

c. Radial boundary.

The finite difference grid is of limited size and it is inevitable that eventually some of the energy from the piston will reach the boundary of the calculation. When this happens some energy is reflected back, in much the same way that a physical boundary would cause a reflected wave. The reflected wave will eventually return to the axial position where it is manifest as ripple in the axial field. Anastasiadis [1987] looked at a number of different ways of eliminating this reflection and concluded that the simplest method of reducing the effect of the reflection was to increase the radial boundary as required. This is preferable to starting the calculation with a massive boundary since computer run-time is conserved at short axial ranges. The ultimate limit on the radial boundary was dependent on the radial step size and the number of harmonics included in the calculation since these determined the overall memory requirement of the program.

d. Number of harmonics.

Ideally an infinite number of harmonics should be included in the solution; however at relatively low drive levels only a small amount of energy is transferred to higher harmonics so the solution was truncated in order to reduce the computer run-time. If the drive level is too high for the maximum number of harmonics in use then energy builds up in the last few harmonics and eventually starts to feed back down the spectrum. The number of harmonics in the calculation was varied within the program by monitoring the last few harmonics; if they exceeded a specified limit then the total number of harmonics was increased. The ultimate limit on the number of harmonics was determined by the computer memory size; in the case of the IBM PC-AT with 512 Kbytes of memory the program could be run with 100 harmonics and 400 radial steps before problems were encountered. The Gould NP1 main-frame computer could run with 200 harmonics and 1000 radial points without any difficulty although the run-time became several hours in such a case.

e. Computing requirements.

The finite difference model is costly in terms of computer memory and run-time. The model calculates a single axial section at each step and the real and imaginary parts of the field are stored in two separate arrays. These arrays have two dimensions, the radial steps being held in one dimension and the harmonics in the other. Typically, using the IBM PC-AT, the radial field was calculated across a grid of 400 points with up to 100 harmonics in the pulsed case. This required a minimum of storage requirement of 80,000 real numbers (320 Kbytes assuming 4 bytes per real number). In the case of continuous wave fields the maximum number of harmonics could be reduced to 5 for lower drive levels, with a significant advantage in run-time. A typical, fairly coarse, run (i.e. 1400 axial steps, a maximum of 300 radial steps and 5 harmonics) took about 50 minutes to run on the IBM PC-AT. Mainframe computers offered a speed advantage, a factor of about 5 in the case of the Honeywell Multics system and a factor of about 60 for the Gould NP1 system. This had to be weighed against the poorer accessibility of the main-frame machines. The Gould machine also allowed substantial increases in the array sizes in comparison with the IBM.

3.5 EXAMPLE CALCULATION

The axial field of a plane piston source is used here as an example with which to illustrate some of the above points. Its relatively simple axial field readily shows any deviation from the ideal case. The following parameters were used in the calculation:

aperture radius, a = 19 mm, (R_o = 1725 mm),

fundamental frequency, f_o = 2.25 MHz,

pressure amplitude at piston face, p_o = 100 kPa,

axial step size = 0.00015R_o,

radial step size = 0.02a,

radial boundary = 2a (increasing to 4a),

maximum number of harmonics = 5.

Note: The model does not use the drive level and aperture radius directly but instead they are taken into account by two parameters, Γ and A where,

$$\Gamma = \frac{1}{\alpha l_D} \text{ and } A = 2\frac{R_o}{l_D}$$

or

$$\Gamma = \frac{\beta p_o 2\pi f}{\alpha \rho_o c^3} \text{ and } A = \frac{4\pi^2 \beta p_o f^2 a^2}{c^4 \rho_o}$$

3.5.1 Harmonic amplitudes

The amplitudes of the first five harmonics on the acoustic axis are shown in Figure 3.5. This shows that the near-field oscillations of the fundamental become less pronounced as the axial range decreases. This is due to the axial step size, which at short ranges is greater than the length scale of the pressure variations caused by diffraction, the result being that the model ignores the diffraction effects and on axis the wave propagates as a plane wave.

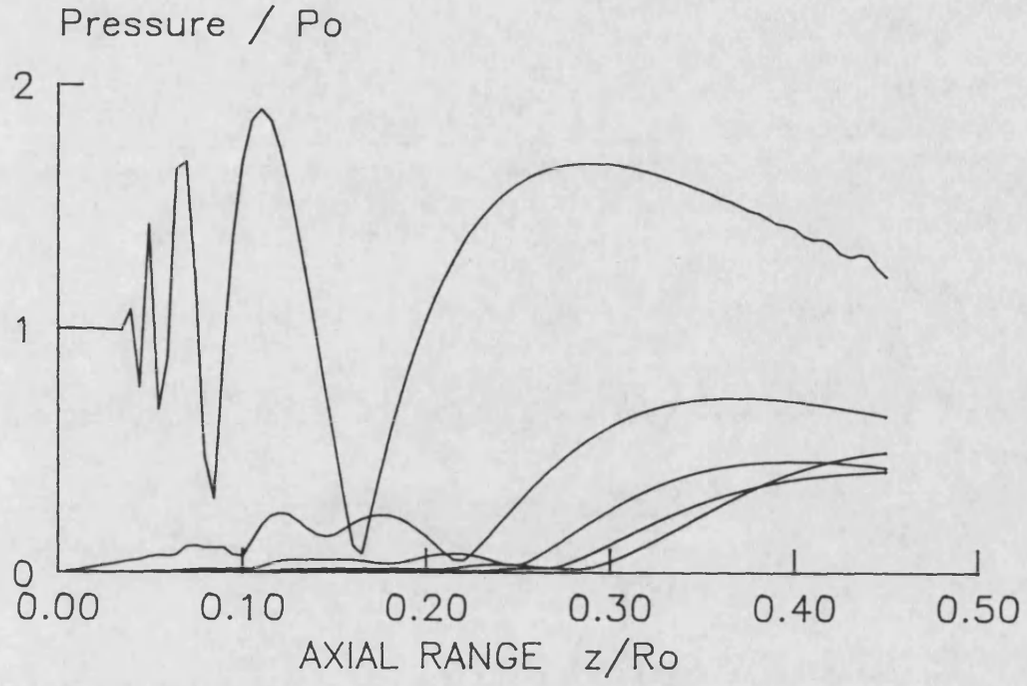

Figure 3.5
First five harmonics of the axial pressure field of a plane circular piston as calculated by finite difference model. ka = 181, p_o = 100 kPa.

This effect is similar to the diffraction loss caused by the finite size of the hydrophone which records the average pressure over its active area rather than the pressure at a point in space. The phase plots showed similar behaviour in this region with a reduction in the extreme values close to the transducer.

Another effect that is purely an artefact of the model is the way that the fourth and fifth harmonics exceed the third at long ranges, due to the truncation of the Fourier series which stops energy propagating beyond the fifth harmonic. This only becomes important when the waveform becomes heavily distorted, but the higher drive levels need more harmonics to remedy this effect. In this case re-running the model with 10 harmonics showed the fourth and fifth harmonics behaving normally although the ninth and tenth harmonics were still a little higher than they should have been.

The fundamental shows the effect of reflections from the radial boundary at normalised ranges greater than about 0.4 where a ripple can be seen in the amplitude on axis.

A real (physical) effect that is demonstrated by Figure 3.5 is the onset of acoustic saturation. The model accounts for all the interactions between the harmonics in the calculation and thus the peak in the fundamental that occurs around $z/R_0 = 0.3$ is reduced in amplitude compared to the previous peak ($z/R_0 = 0.11$) since a significant amount of energy has been lost to the harmonics. This effect is not seen in perturbation models since they assume that energy is lost to the harmonics without significant effect on the fundamental.

3.5.2 Harmonic phases

Figures 3.6 and 3.7 show the harmonic phases up to the fourth harmonic. Here a larger radial boundary than Figure 3.5 has been used to eliminate the ripple caused by reflections from the boundary. Unlike the other phase plots in this thesis, the phases in these two figures are plotted relative to the excitation at the piston face and the phase angles are given in radians of the harmonic.[11]

All four harmonic phases show a reduction in the phase variation as the aperture is approached due to the step size used in the model. The fundamental phase shows a fairly smooth variation between the phase jumps that occur at the minima in the pressure field and is starting to approach its far-field value of $\pi/2$. The other harmonics have similar behaviour with rather more detail in the near-field due to the effect of the fundamental on nonlinear generation. In order to compare these values with experimental measurements it is necessary to calculate the relative phases (θ_n) which are obtained from these values (Ψ_n) by dividing by the harmonic number (n) and then subtracting the fundamental phase (Ψ_1); this gives phases relative to the fundamental in radians of the fundamental, i.e.

$$\theta_n = \frac{\Psi_n}{n} - \Psi_1$$

---

11 In general in this thesis phase angles are plotted relative to the fundamental in radians of the fundamental.

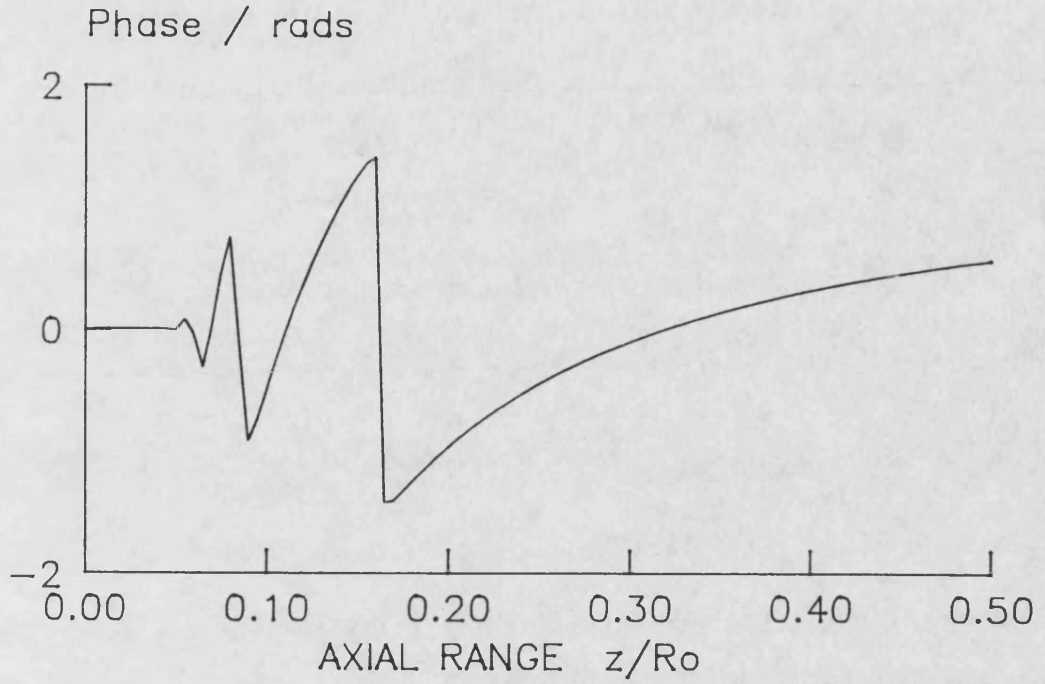

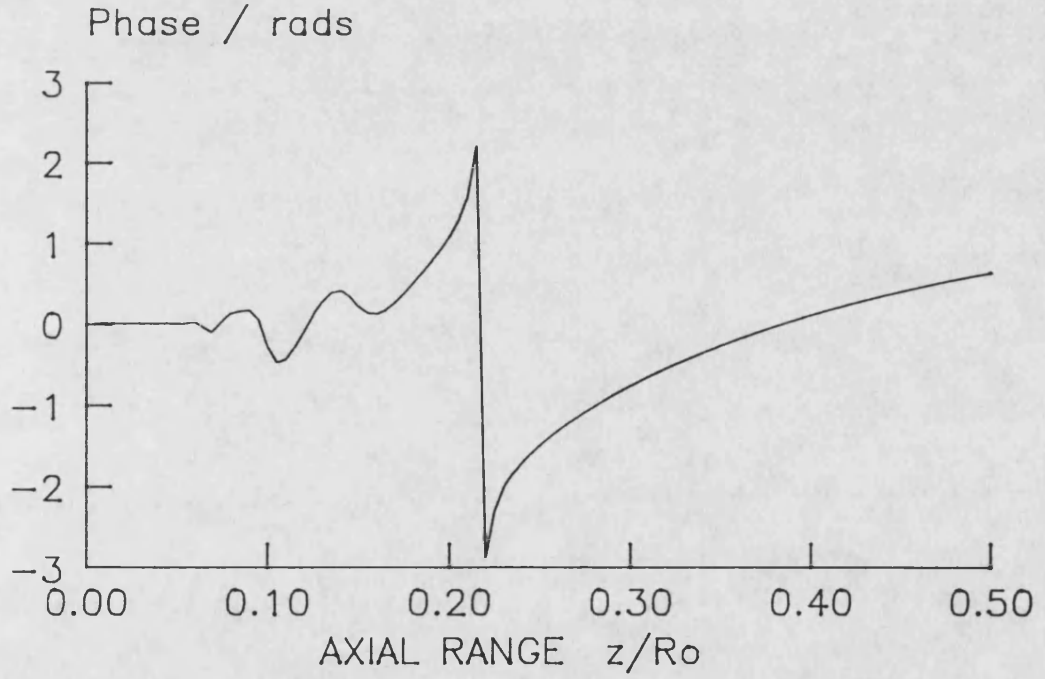

Figure 3.6
Fundamental (top) and second harmonic (bottom) phases for the axial pressure field of a plane circular piston as calculated by the finite difference model, ka = 181, p_o = 100 kPa. Phase angles are in radians of the harmonic relative to the excitation at the piston.

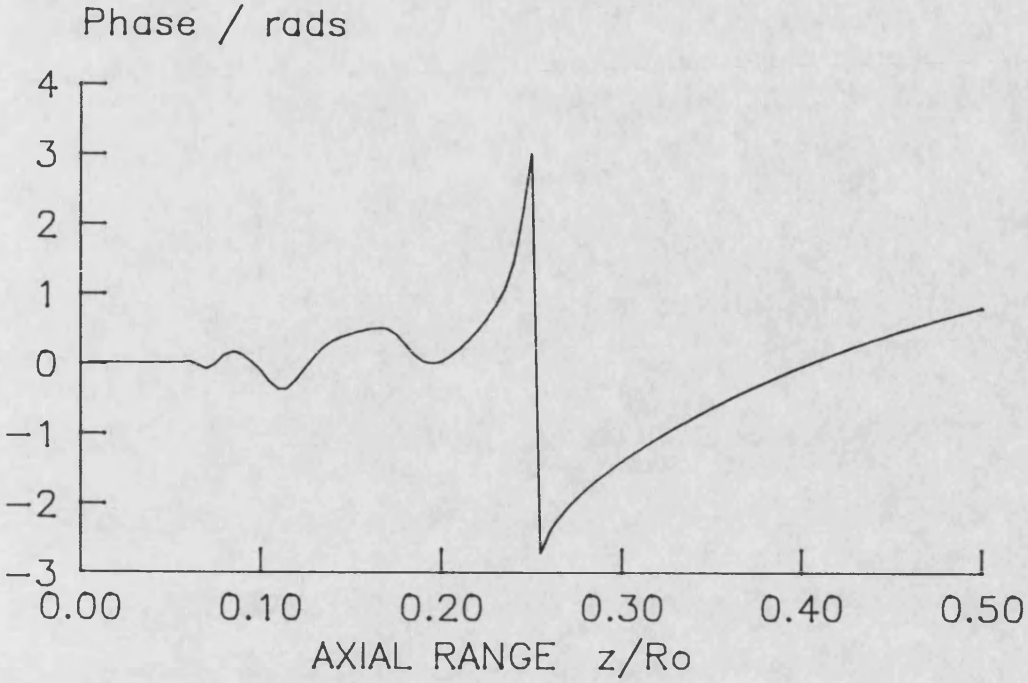

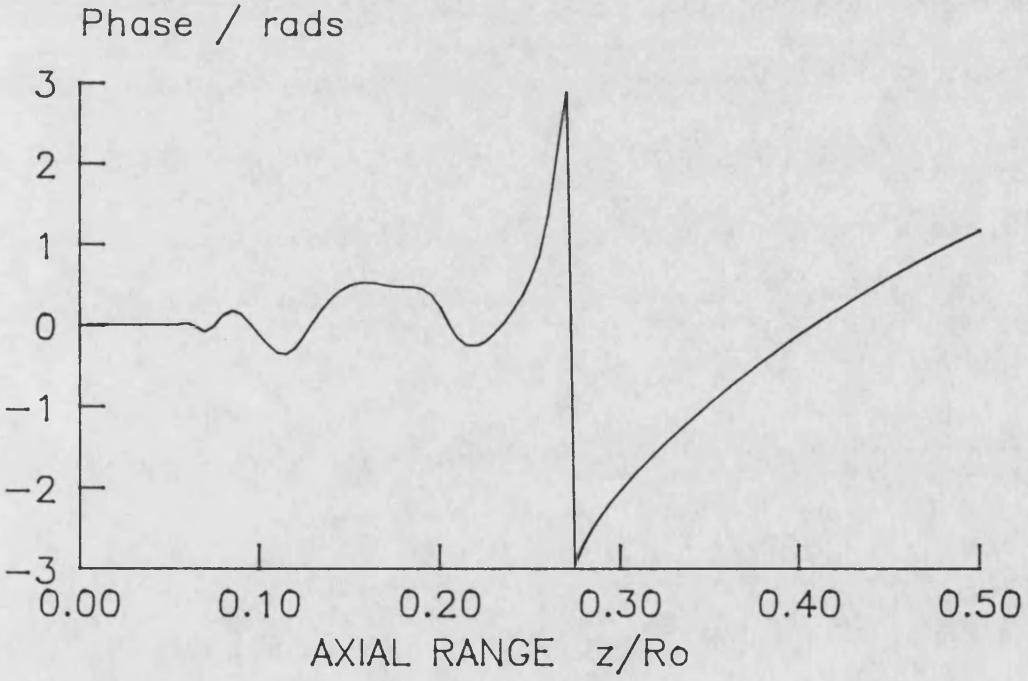

Figure 3.7
Third (top) and fourth (bottom) harmonic phases for the axial pressure field of a plane circular piston as calculated by the finite difference model, ka = 181, p_o = 100 kPa. Phase angles are in radians of the harmonic relative to the excitation at the piston.

3.6 FOCUSED FIELDS

Focusing was included in the model by adding an appropriate phase shift to the initial conditions. If the focal length (D) is greater than three times the aperture radius (a) then the phase advance due to focusing ($\Delta\Psi$) across the aperture can be approximated by the expression:

$$\Delta\Psi \approx \frac{\zeta^2}{2D^2}$$

where ζ is the normalised radial coordinate (= r/a).

3.7 PULSE EXCITATION

Pulsed fields[12] were studied by initialising the frequency components of the model to correspond with the spectrum (amplitude and phase) of the required time signal at the piston face. This meant that the centre frequency of the initial pulse would typically be the fourth or sixth Fourier component of the model; hence for a given centre frequency the pulsed case had its first component four to six times lower in frequency, thus more Fourier components were used than in the continuous wave case and the run-time increased accordingly. The Fourier amplitudes of the initial pulse were also scaled, this was done by taking the amplitude of the largest component of the input spectrum as p_o and then the whole input spectrum was normalised by this value.

The model was tested initially by re-running the continuous wave case with the fundamental frequency shifted up to the fourth component of the model. Figure 3.8 compares the results of the scaled case with the normal CW case and shows that the results are the same except for the more pronounced variations in the fundamental near the source. This is caused by the reduction in the frequency of the first component of the model which leads to a shorter Rayleigh distance and since the axial step size is normalised by the Rayleigh distance more steps are needed to reach the same point in space.

---

12 See also Baker and Humphrey [1989], a copy is appended to this thesis.

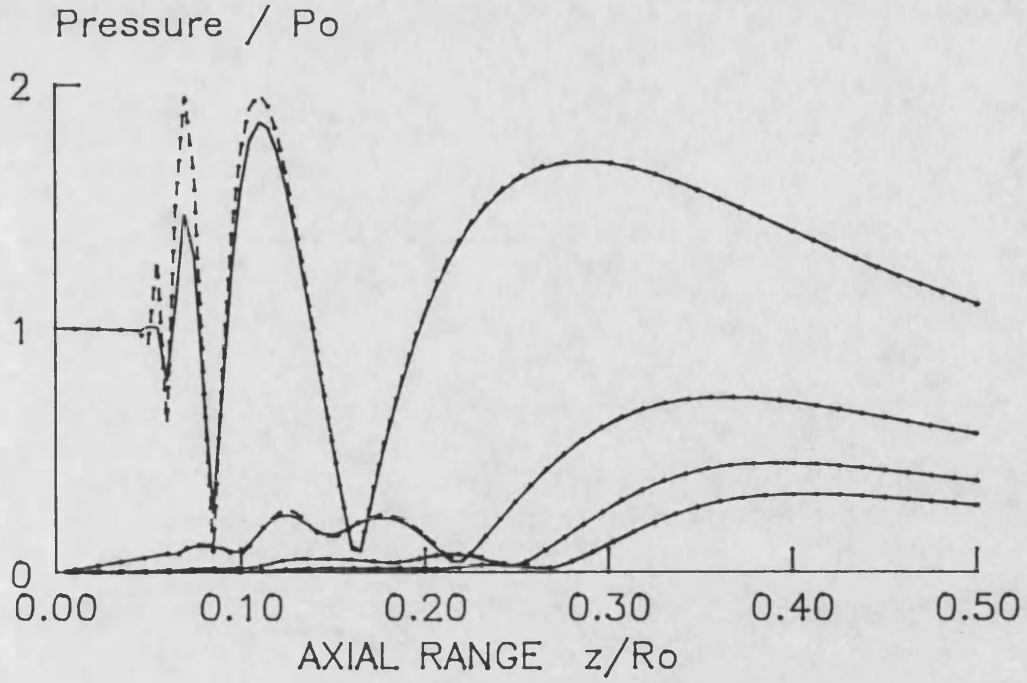

Figure 3.8
Comparison of finite difference model using different components for the fundamental. First component = fundamental (—), fourth component = fundamental (- -).

The focused case also requires the gain to be recalculated for the new first component since the Rayleigh distance has been reduced.

3.7.1 Pulse shape

Typical diagnostic ultrasound pulses are between four and six cycles long although the bulk of the energy is in the central cycle or two. Thus to capture a pulse of given centre frequency the time window required is at least four to six times that of the fundamental (or zero crossing) period. The length of this time window determines the lowest frequency component necessary in the model and the centre frequency of the pulse becomes a harmonic of this component. There is another consideration in determining the component that will represent the centre frequency of the pulse namely the diffractive field of the aperture. The circular aperture can be considered in terms of the interaction between a plane central wave and another plane wave emanating from the edge of the aperture and for a given field point there is a path difference (or time delay) between the two components. In the case of a very short

pulse (of the order of a single cycle) the two components do not meet until the path difference is comparable with the pulse length which will occur near the last axial minimum. The finite difference model is basically a continuous wave system; therefore if the pulse is modelled with its centre frequency as the fourth component then the resultant excitation at the aperture will be an infinite series of identical pulses four cycles apart. Thus interactions may occur between adjacent pulses in time and unwanted nonlinear effects will occur in the near-field close to the piston face. This can be eliminated in two ways:

1. The centre frequency could be located at a higher component in the model, i.e. the pulse is taken with more zeros either side so that there is no interference between adjacent pulses in time. The drawback of this method is that strictly the time window would have to be equivalent to the aperture diameter (approximately 60 wavelengths in this case) which would require a substantial increase in the number of harmonics.

2. The axial step size could be kept deliberately coarse so that the near-field interactions are overlooked (or averaged out). Figure 3.3 shows the effect of coarser axial steps and if the step size is coarse enough then the axial field will only show the last maximum and minimum.

In practice the second of these two methods was used.

Initial conditions for pulsed field

The initial condition for the model is the pulse spectrum as measured at or very close to the aperture. Two methods were considered for obtaining this spectrum:

1. At short ranges the central plane wave and the edge wave are resolved due to the difference in path length. This allowed direct measurement of the initial waveform

using the hydrophone. The finite hydrophone size was unimportant in this case since the measured waveform was effectively a plane wave. The Fourier amplitudes and phases of this waveform were then used to initialise the finite difference model.

2. In the far-field of a plane piston the time waveform is the derivative of the driving function [Morse and Ingard, 1968] since it can be represented as the sum of the plane central wave and the slightly delayed and inverted edge wave. Thus the time waveform has the form f(t) - f(t+dt), which is proportional to the derivative of f(t), the driving function. A similar situation arises in the focal plane for a focused piston (see Appendix A) thus f(t) can be found from the axial waveform in the focal plane by integrating it with respect to time. The Fourier transform of the integral of f(t) can then be used to initialise the model.

In practice both methods gave similar results so the direct plane wave measurement was used as it was simpler than the pulse integral method.

3.7.2 Extension to tissue-like media

Propagation of ultrasound through tissue differs from fluids in a number of ways these are summarised with typical values in the table below:

Factor	Water	Tissue
Absorption / dB.cm^{-1}	0.01	1.0
Frequency dependence of absorption	f^2	f to $f^{1.5}$
Scattering	None	Weak
Sound speed / m.s^{-1}	1486	1500
Density / kg.m^{-3}	1000	1060
Nonlinearity parameter B/A	5.0	5.2

The most significant factor as far as nonlinear effects are concerned is likely to be the higher absorption coefficient since this will reduce the fundamental level and hence reduce nonlinear interactions. It would be relatively easy to modify the theoretical

model to account for the different absorption coefficient and frequency dependence and this should reduce the computational requirements since fewer harmonics harmonics would be required.

Chapter 4: EXPERIMENTAL CONFIGURATION

4.1 GENERAL

The general layout used for the experimental measurements is shown in Figure 4.1. An ultrasonic transducer was mounted at one end of a water filled tank and the resulting acoustic pressure field was probed using a broadband hydrophone. The hydrophone was mounted on a computer controlled, two dimensional translation stage and its output was recorded on a digital storage oscilloscope (DSO) prior to transfer to a microcomputer for analysis. The transmit block of Figure 4.1 was used to generate a quasi-continuous wave signal and was replaced by a Philips clinical ultrasound scanner for the measurements on pulsed fields.

The tank was filled with tap water since large quantities of distilled water were not available. The water was left for a few days after filling to allow the entrained gas to diffuse out. The water temperature was not regulated but was fairly constant at room temperature, about 20 degrees centigrade. Typically the temperature would vary by one or two degrees during the course of the day and was noted at intervals as necessary. The speed of sound in the tank at a temperature of 21 °C was calculated from the difference in the arrival times of a single pulse at two different hydrophone locations. It was found to be 1486 ± 60 m/s, compared with the expected value of 1481 m/s [Kinsler et al, 1982].

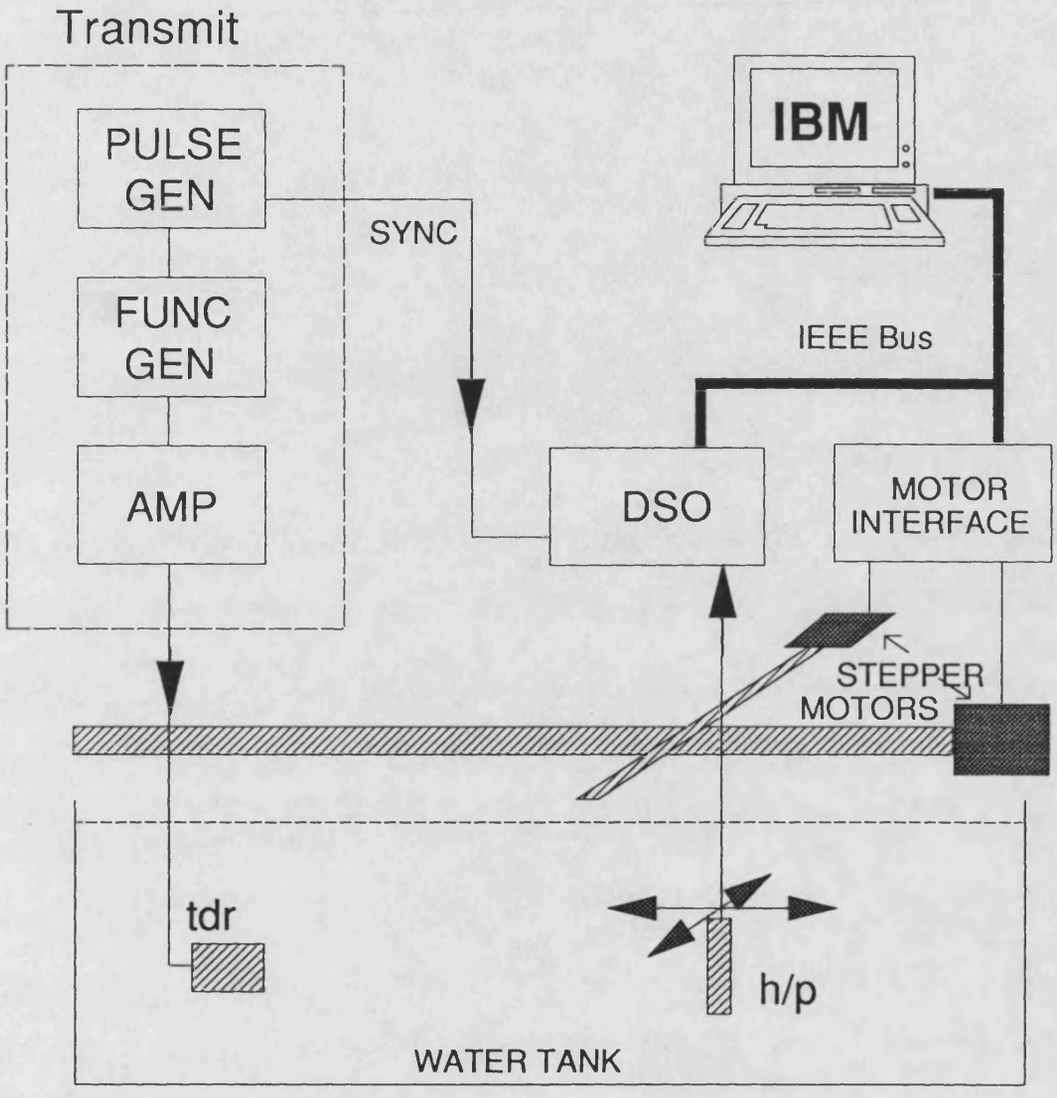

Figure 4.1.
Experimental configuration.

KEY:
DSO - digital storage oscilloscope
h/p - hydrophone
IBM - IBM Personal Computer (PC-AT)
tdr - transducer
sync - synchronising pulse to DSO trigger input

4.2 TRANSDUCER

The transducer used for most of the measurements was a 38 mm diameter, 2.25 MHz, plane circular transducer manufactured by Panametrics. Focusing was achieved by the addition of a plano-concave perspex lens to the front face of the transducer as discussed later in this chapter. The transducer was driven either with a quasi-continuous wave signal or in a shock excited pulsed mode.

4.2.1 Quasi-continuous wave drive

The transducer was driven, at its centre frequency, with a tone burst of about 80 cycles duration, at a pulse repetition frequency (prf) of about 100 Hz. This eliminated any problems with standing waves in the tank that would be obtained with a true continuous wave field. It also allowed higher drive levels to be achieved since the time average power dissipated in the power amplifier and the transducer was reduced. The transducer was driven, via a 50Ω matching transformer, by a radio frequency power amplifier (E.N.I. 2100L) which gave 50 dB gain over the frequency range 10 kHz to 12 MHz. The signal for the power amplifier was produced by a function generator (Krohn-Hite KH1400 triggered by a Lyons PG 71N pulse generator). Measurements were made over a range of drive levels; the maximum electrical drive at the transducer was 240 V (peak to peak) corresponding to 300 kPa at the transducer face. The lowest drive level used was 8 V (peak to peak) corresponding to 10 kPa at the transducer face. The majority of nonlinear results were obtained with 80 V (peak to peak) at the transducer (about 100 kPa at the transducer face). At this drive level the harmonic levels present in the electrical drive signal and in the acoustic field close to the transducer were low (see table below).

Harmonic content of drive signal and pressure waveform close to transducer (z=20 mm).		
Harmonic number	Electrical drive / dB	Pressure signal / dB
1	0	0
2	-38	-36
3	-46	-42
4	-58	-48
5	-45	-58

The occurrence of harmonic levels greater than these in the acoustic field can be attributed to nonlinear effects occurring in the medium.

4.2.2 Shock excited drive

A medical ultrasound scanner (Philips sono DIAGNOST B) was used to drive the transducer via a variable attenuator. The system, typical of many in current clinical use, drives the transducer directly with a single high voltage pulse that causes the transducer to ring at its natural frequency. The transducers are always heavily damped so the resultant pulse is short. Figure 4.2 shows the pressure field near a shock excited transducer. The waveform was measured on-axis, 35 mm distant from the 38 mm diameter plane transducer and at this range the edge wave and the plane central wave are resolved to such an extent that the edge wave does not appear in this figure. The waveform thus represents the excitation at the transducer since there are no diffraction effects at this position.

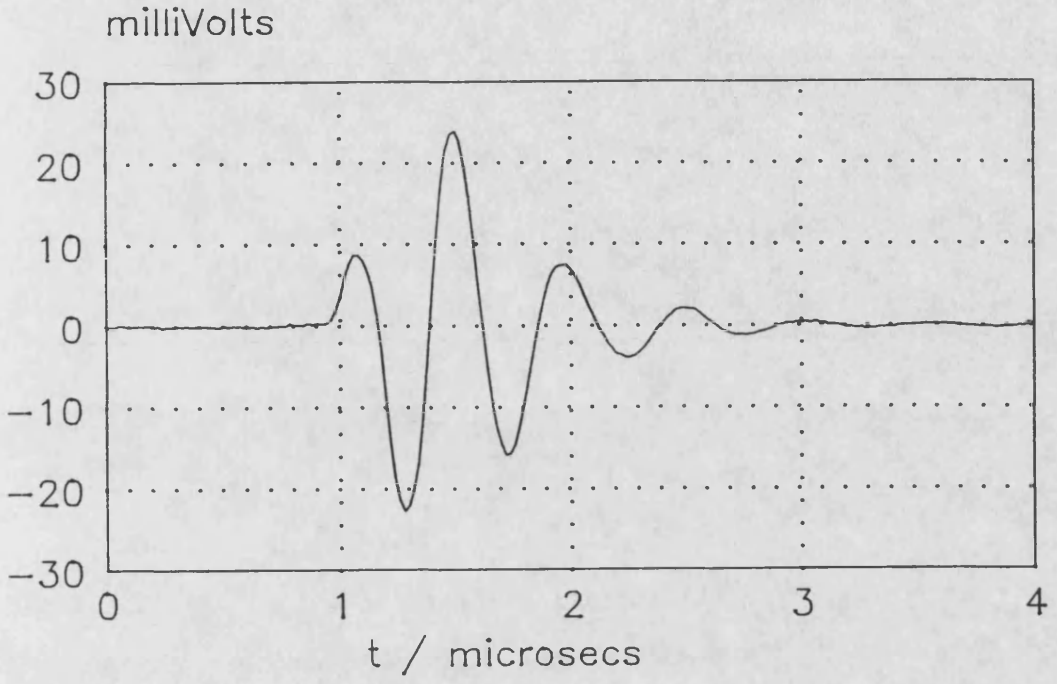

Figure 4.2
Typical pressure waveform close to a shock excited transducer.

4.2.3 Lenses

Focused fields were obtained using a plano-concave Perspex acoustic lens in front of the plane transducer. The thin lens formula [Papoulis, 1981] relates the radii of curvature (R_1 and R_2) of a lens to the distance to the focal plane (D):

$$\frac{1}{D} = (n-1)\left(\frac{1}{R_1} + \frac{1}{R_2}\right)$$

where n is the refractive index, given in this case by $n = c/c_L$ where c is the speed of sound in water and c_L is the speed of sound in the lens. In the case of a plano-concave lens one radius of curvature is infinite and the other is negative (due to the geometry used to define the initial problem) and the resulting expression is:

$$\frac{1}{D} = \left(\frac{c}{c_L} - 1\right)\left(-\frac{1}{R_1}\right)$$

Using c = 1486 m/s and c_L = 2700 m/s gives a refractive index (n) of 0.55; thus for a

plano-concave Perspex lens in water:

$$D = 2.2R_1$$

The lenses were machined on a lathe using a tool mounted in a radius arm that pivoted on the tool post. The slight marks left from the turning process were polished out with fine abrasive paper followed by metal polish. Three lenses were used, their radii of curvature being 199, 98 and 67 mm. These gave focal lengths of 438, 216 and 147 mm assuming the speed of sound in perspex to be 2700 m/s. The lenses were of slightly greater diameter than the transducer element (42 mm as compared with 38 mm) since they clipped to the outside rim of the transducer. This gave rise to some uncertainty in determining the actual aperture size when the lenses were used. The increased lens thickness towards the outer edge also gave rise to uncertainty in the amplitude of the initial excitation since the attenuation increases as the lens gets thicker. In the worst case the lens was 4 mm thicker at the edge than the centre; assuming an attenuation of 1 dB/cm in perspex this would lead to a 5% reduction of amplitude at the edge of the transducer. Comparisons with theoretical linear models showed good agreement assuming the calculated value for focal length, an effective diameter of 38 mm and a uniform amplitude distribution across the lens face. See Figures 5.1 - 5.4 in Chapter 5.

The lenses were held in place by three small plastic strips trapped under an elastic band around the circumference of the lens and were acoustically coupled to the transducer using a commercial ultrasonic coupling gel.

4.2.4 Transducer alignment

The transducer was fixed at one end of the tank but had a small amount of movement available for alignment to the axes of the translation stage. The translation stage had two degrees of freedom, in the horizontal plane, so it was important to ensure that the acoustic axis of the transducer lay parallel to the plane of movement. The alignment

was checked by identifying the acoustic axis. This was done by noting the transverse position that gave maximum distortion at the far end of the tank and comparing it with the transverse position of one of the axial pressure minima in the transducer near-field.

4.2.5 Determination of transducer parameters

A number of parameters were required as input to the theoretical models; these parameters were aperture radius (a), distance to the focal plane (D) and the drive pressure at the transducer face (p_o). None of these parameters could be determined directly so indirect methods were used.

(i) Aperture radius (a)

The importance of the aperture radius and excitation (amplitude and phase) lies in the fact that they are the starting point for any theoretical prediction. The simplest plane piston model assumes a circular aperture excited with a plane wave; if the aperture size and excitation are not known then further calculations are difficult if not impossible. A number of factors can affect the effective aperture radius and the velocity distribution at the piston face. The construction of the transducer may be such that the edges of the element are clamped and are not free to vibrate with the rest of the element, or alternatively poor damping may lead to additional modes of vibration in the element. Both of these effects will lead to non-uniform excitation of the aperture which in turn will cause the piston field to become non-ideal. In the case of the Panametrics transducer used here the excellent agreement of the axial pressure field with small signal models lead to the conclusion that the excitation at the piston face was uniform and the effective radius matched exactly the active element radius. In the case of the focused systems it was not possible to get quite such good agreement with theoretical predictions and there are a number of possible explanations for this:

1. The lenses were made from Perspex which has a high absorption coefficient in comparison with water. Thus the edge of the lenses, where the Perspex was thicker, attenuated the wave field more heavily, giving rise to a slight shading across the aperture, particularly in the highly focused case.

2. The lenses were slightly larger in diameter than the active element to allow attachment to the transducer. Thus further uncertainty arose in determination of the effective aperture radius.

3. The lenses were coupled to the transducer face using a proprietary ultrasonic coupling gel. However, it was evident from observation of short pulses close to the transducer that there were some reflections occurring in the lenses which may have contributed to the deviations from the ideal.

In practice, once the focal plane had been located, the positions of the first zeros off-axis were used to determine the aperture radius. The field in the focal plane should follow the function $2J_1(x)/x$, where $x = ka\sin(\theta)$ (k is the wavenumber, a is the aperture radius and θ is the angle off axis to the field point.) θ was determined from the hydrophone-transducer geometry, k was known and the first zero of $J_1(x)/x$ occurs for an x value of 3.8; thus a was determined.

(ii) Focal length (D)

The focal plane does not necessarily occur at the range where the axial pressure has its maximum value (see Appendix A); however, as mentioned earlier, the pressure field across the focal plane (assuming uniform excitation) should follow $2J_1(x)/x$. Either side of the focal plane the pressure field deviates from this pattern and probably the most noticeable feature is that the first zeros either side of the axis become minima. An example of this is shown in Chapter 5. Focal lengths determined by this method agreed with the expected values from the lens formula.

(iii) Drive level (p_o)

The presence of nonlinear effects causes problems in determination of the drive level at the aperture. It should be possible in the case of a plane piston to measure the pressure level at any one of the axial pressure peaks and halve it to get p_o. The problem is that at high drive levels the waveform is distorted so it is necessary to take its Fourier transform and use the level of the fundamental. This, however, is still likely to be in error since saturation reduces the fundamental amplitude due to the energy loss to higher harmonics. At short ranges the nonlinear effects have not had time to build up but the hydrophone is subject to diffraction loss due to the closeness to the transducer. To overcome these problems a calibrated attenuator was used in the transducer drive circuit. The attenuator setting was increased until nonlinear effects were reduced to a negligible level; the pressure at the penultimate axial maximum was then measured and scaled by the attenuator setting to reach the drive pressure for the nonlinear case. The focused cases were additionally complicated by the fact that the axial pressure had to be further scaled to allow for the focusing envelope, D/(D-z), in order to obtain the drive pressure at the transducer face.

4.3 HYDROPHONE

The hydrophone used for most of the measurements presented here was a GEC polyvinylidene difluoride (PVdF) membrane device (Type Y-33-7611, number MRQ IP018) with a standard 65 cm, 75 Ω cable. It was a bilaminar device consisting of two 25 micron thick sheets of PVdF mounted on a circular frame of about 13 cm diameter. The central active area was 1 mm in diameter and gave an open circuit sensitivity of 0.175 V/MPa at 1 MHz[13]. The hydrophone was mounted on a two dimensional translation stage with movement in the horizontal plane driven by stepper motors controlled by the computer. Manual adjustments were available to vary the angle of

13 See Bacon [1982] and Galantree [1987] for further details.

the hydrophone relative to the vertical, its vertical position and the hydrophone azimuth. The hydrophone was connected directly to the input of a digital storage oscilloscope (DSO).

4.3.1 Sensitivity and calibration

The frequency response of the hydrophone was dominated by a thickness resonance at about 24 MHz; below this frequency the response was relatively flat and above this frequency it rolled off fairly rapidly (Figure 4.3). The effect of the resonance was noticeable in the measurement of heavily shocked waveforms where there was sufficient energy in the higher harmonics to excite the resonance. This made time domain measurements on such waveforms rather difficult (see also Smith [1986]). The problem was eliminated by deconvolving the hydrophone response from the measured time waveform; this was done in the frequency domain by taking the Fourier transform of the time waveform, dividing by the complex hydrophone sensitivity and then taking the inverse Fourier transform to get the "true" acoustic waveform. This typically results in a 20 to 30 % reduction in the measured peak positive pressure when dealing with heavily shocked waveforms [Smith, 1986].

The hydrophone sensitivity was also corrected to account for the loading caused by the DSO input impedance. The hydrophone impedance was mainly capacitive (about 90 pF) and the calibration figures referred to an open circuit voltage at the hydrophone terminals. Thus the connection of the DSO with an input capacitance C_i across the hydrophone capacitance C_h led to a reduction of the output voltage by a factor of $C_h/(C_h + C_i)$.

The hydrophone was compared with two other nominally identical devices that had been calibrated at the National Physical Laboratory (NPL). The NPL calibrations covered the amplitude response from 1 MHz to 15 MHz in steps of 1 MHz. Some of the measurements described in this thesis required some knowledge of the frequency response, magnitude and phase up to higher frequencies, typically 50 MHz. It was

therefore necessary to arrive at some estimate for the hydrophone response in this region. It was not obvious how this could be achieved directly so a number of different but approximate approaches were tried, and the results considered acceptable so long as all gave the same general frequency response. It should be stressed that the following methods were only used to extend the hydrophone response to higher frequencies and to infer phase information. At low frequencies direct comparison with the NPL calibration was used.

(i) Theoretical model.

The frequency response of such hydrophones was modelled by Bacon [1986] by considering the mean pressure through the membrane. This gave rise to a thickness resonance when the incident radiation had a frequency corresponding to half a wavelength in the membrane. The sensitivity (S) was the expressed as:

$$S = \frac{T_1 \sin(\Theta)}{\Theta(\exp(-j\Theta) - R_2 \exp(j\Theta))} \qquad 4.1$$

where: $\Theta = \frac{kx}{2}$, $T_1 = \frac{2}{1+Z}$, $R_2 = \frac{Z-1}{Z+1}$,

k is the wavenumber in the film, x is the film thickness and Z is the ratio of the acoustic impedance of water (Z_{water}) over the acoustic impedance of the film (Z_{film}). The expression ignores electrode effects and losses in the film and gives a frequency response as shown in Figure 4.3 assuming the following parameters which are representative of the hydrophone used:

x = 50 microns

$Z_{film} = \rho_{film} . c_{film} =$ 1780 x 2400 Rayl

$Z_{water} = \rho_{water} . c_{water} =$ 1000 x 1486 Rayl

$k = 2\pi \frac{f}{c_{film}}$.

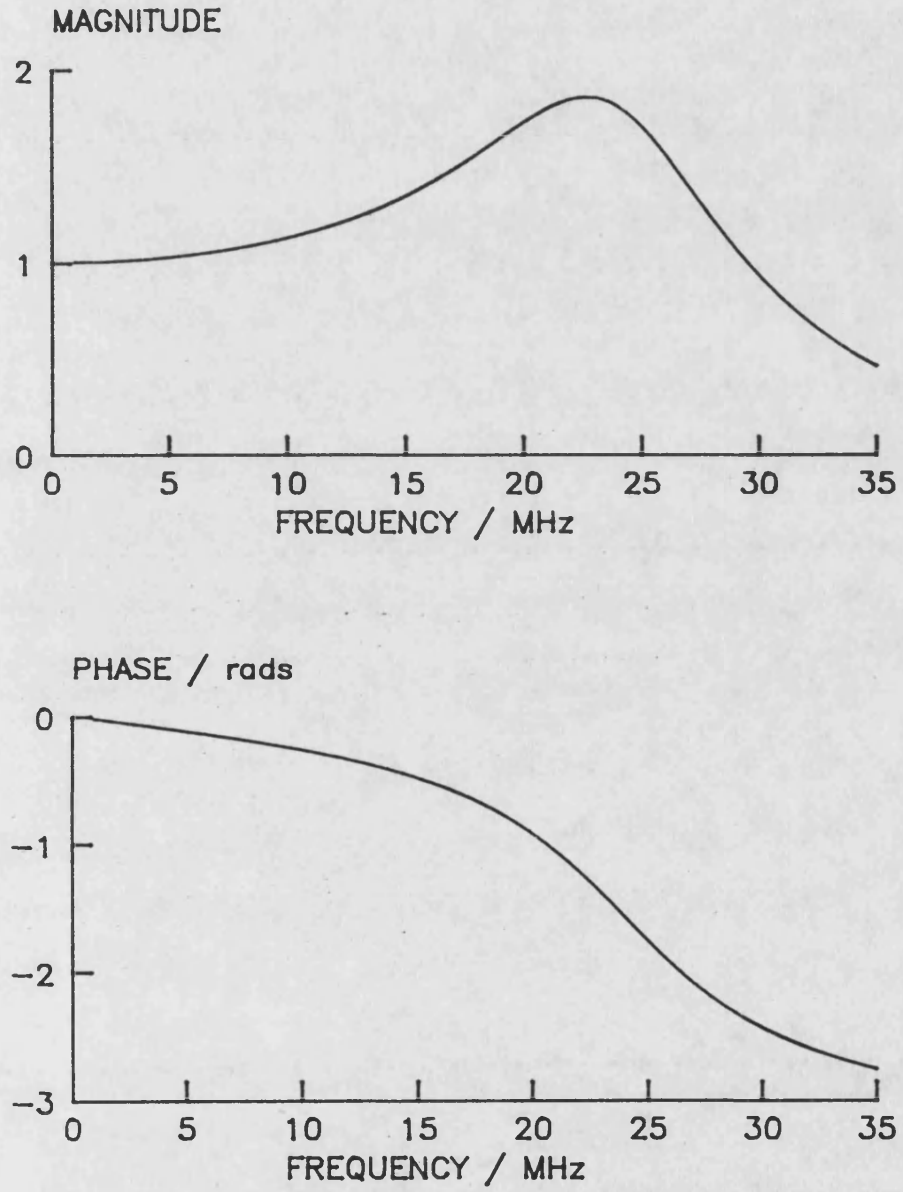

Figure 4.3.
Theoretical frequency response of a thin film. (See equation 4.1)

(ii) Inter-comparison with coplanar hydrophone.

In addition to the low frequency comparison with two NPL calibrated hydrophones, a further comparison was made with a 9 micron coplanar film device. The theoretical model showed that this device would have a much higher resonant frequency (100 MHz for a 9 micron film). The problem with the coplanar device was that it could only be used in de-ionised water which was not practical in the tank used for field measurements. However, it was possible to make an inter-comparison in a smaller tank and use the coplanar hydrophone as a reference. Here it was assumed that the coplanar hydrophone had a flat frequency response up to 40 MHz and it was then used to record a moderately distorted waveform in the small tank. The bilaminar hydrophone was then put in place of the coplanar hydrophone and the waveform again recorded. Taking the FFTs of both waveforms and then dividing the coplanar spectrum by the bilaminar spectrum gave an estimate of the hydrophone frequency response in amplitude and phase. This frequency response was then compared with the theoretical model (Figure 4.4) and found to be in reasonable agreement if a film thickness of 53.5 microns was used, so the expression above (Eqn 4.1) was used for the deconvolution of time waveforms. The discrepancy in the film thickness needed to match the two results was probably due to the electrode effects and losses that are ignored in equation 4.1.

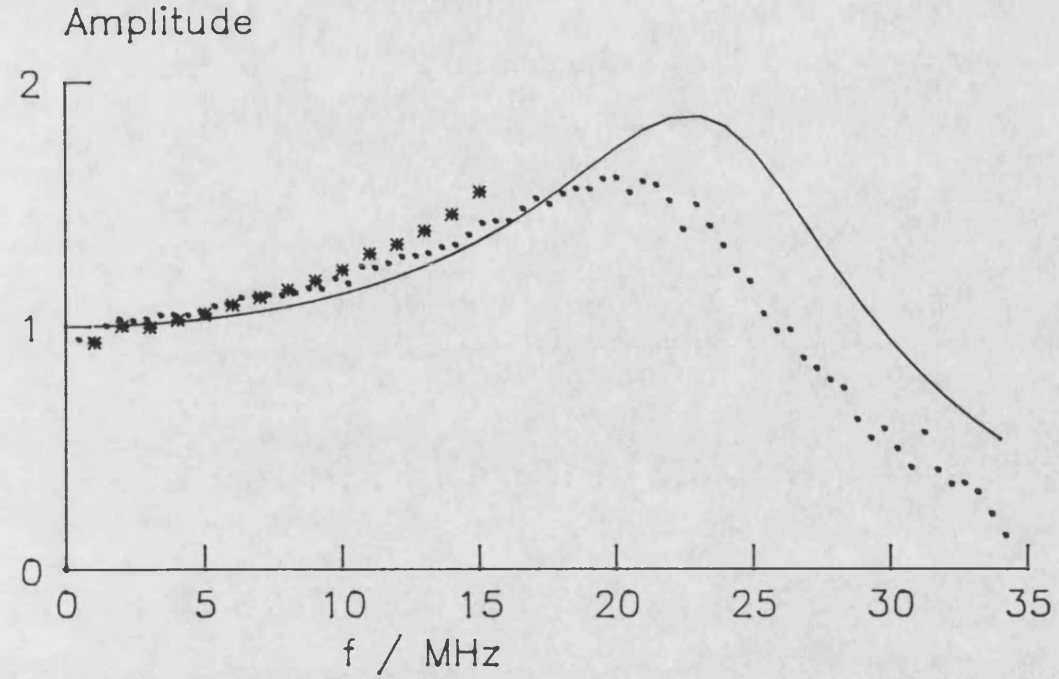

Figure 4.4.
Normalised hydrophone response: Theory and inter-comparison with other hydrophones. Thin film model (Eqn 4.1) (—), comparison with bilaminar (*), comparison with coplanar (.).

(iii) Use of nonlinear effects

The accuracy with which the finite difference model predicted the pressure field at high levels of nonlinearity, especially on the axis of the plane piston at longer ranges, indicated that a good estimate of the hydrophone response could be obtained by simply comparing the experimental measurements with the results from the finite difference model. At first sight this was not very satisfactory since nonlinear effects were the main subject of the study and to calibrate the hydrophone in this manner would lead to perfect agreement between experiment and theory since any difference could be attributed to the hydrophone response.

However, an argument in favour of using this method was that the transducer under test showed near perfect piston-like behaviour over a range of amplitudes which allowed comparison of the pressure field with exact small signal models as well as the

finite difference model. Thus some confidence could be placed in measurements obtained, particularly at moderate distances from the transducer where the finite hydrophone size was negligible. In the absence of any more rigourous methods, the finite difference model could be taken to represent the "true" acoustic field in certain regions of relatively simple nonlinear fields in order to allow better estimates of hydrophone response to be made.

A simple variant on this method is to find a point in a nonlinear pressure field where the waveform is strongly shocked and varying slowly; according to plane wave nonlinear theory, in such a region the Fourier components of the time waveform should vary as the reciprocal of the harmonic number. Thus, if a single cycle from a strongly shocked time waveform was the subject of an FFT and each component was multiplied by its harmonic number then an estimate of the hydrophone response could be obtained. This method is demonstrated in Figure 4.5 which shows such an estimate plotted against the thin film model of equation 4.1. It can be seen that frequencies below 30 MHz good agreement is obtained but at higher frequencies the estimated response exceeds the thin film prediction. The estimate shows marked deviation at the second and third harmonics of the film resonance (22 MHz); this may be attributable to the level of approximation used in equation 4.1 or to inadequacies in the approximate nonlinear analysis. Whatever the cause, these deviations at high frequencies indicate the need for further investigation in this area.

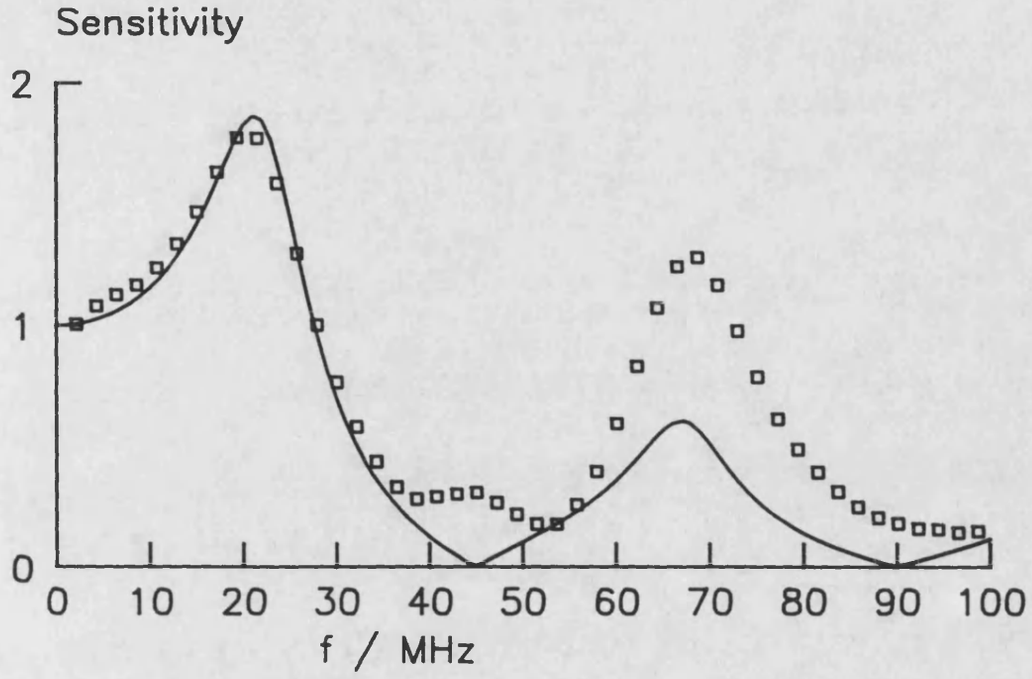

Figure 4.5.
Normalised hydrophone response: Estimated response from strongly shocked waveform (o) and thin film model of Eqn. 4.1 (—).

4.3.2 Diffraction loss

In an ideal system the hydrophone would produce a voltage proportional to the pressure at a point in space but the finite diameter and thickness of real hydrophones means that the output voltage is proportional to the integrated pressure over the volume of the hydrophone. In a pressure field that has a rapid spatial variation this means that small features will be overlooked since the hydrophone will average over them.[14] In this study the hydrophone thickness (25 micron) was ignored since it was much less than the diameter (1 mm), and Beissner's expression [1981] for the measured pressure field of a circular source when observed with a circular receiver of finite size was used to estimate the diffraction loss. Comparison of measurements

---

14 The effect can also be considered in terms of the directivity function of the hydrophone since a large hydrophone is less sensitive to waves coming from larger off axis angles.

made on the plane piston source at low drive levels with Beissner's expression (Figure 4.6) show good agreement. Figure 4.6 also illustrates the high spatial frequency of the experimental measurements, each point representing a single measurement.

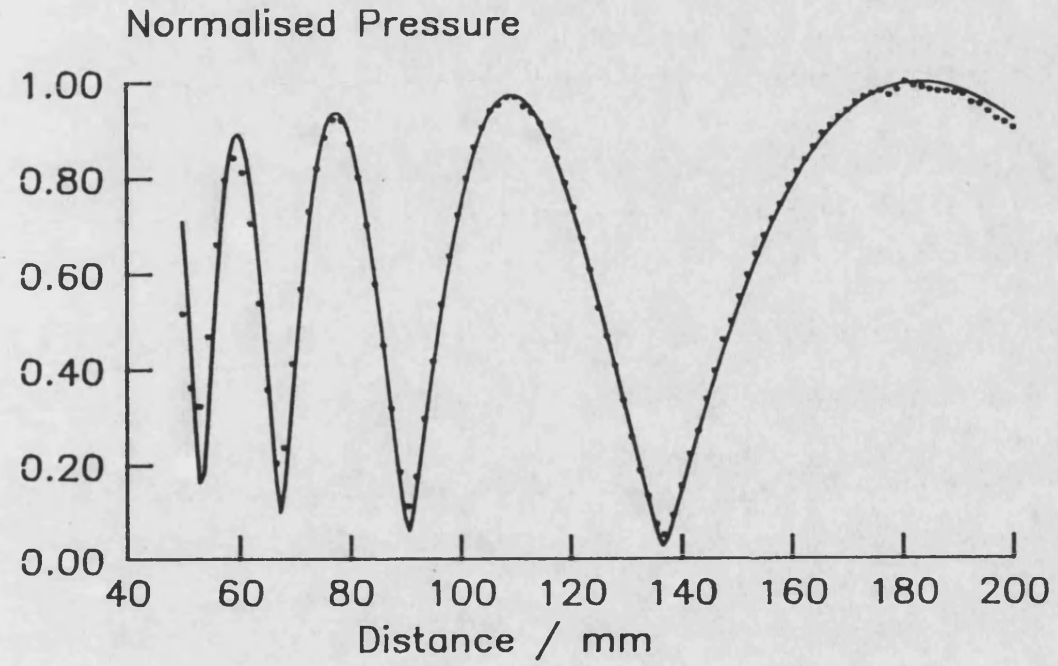

Figure 4.6.
Measured near field (.) of a plane transducer (a = 19 mm) compared with small signal theory (—) allowing for the finite (b = 0.5 mm) hydrophone size at 2.25 MHz.

A further complication of the finite hydrophone size is that in finite amplitude fields the harmonics have narrower beams so that the effect of spatial averaging becomes more important at higher harmonics. An estimate of the effect of increasing hydrophone size on the harmonic levels in the focal plane of a finite amplitude beam is shown in Figure 4.7. It was assumed that the fundamental beam followed a $2J_1(x)/x$ pattern and that the harmonic amplitudes varied as the fundamental beam pattern raised to the harmonic order so that the n^{th} harmonic beam pattern followed $(2J_1(x)/x)^n/n$.

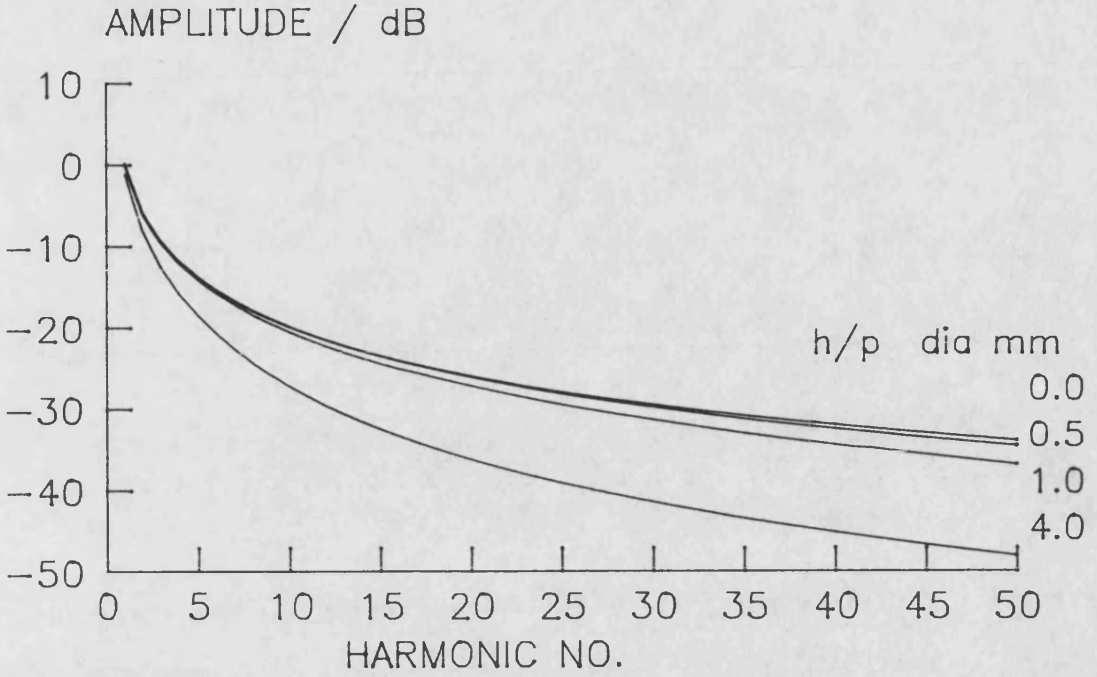

Figure 4.7.
Effect of increasing hydrophone size on the measured harmonic levels on the axis of a finite amplitude beam. Transducer radius = 19 mm, focal length = 200 mm, fundamental frequency = 2.25 MHz, gain = 8.5.

In Figure 4.7 the curve for a hydrophone diameter of 0 mm represents the true acoustic pressure. It can be seen that for this geometry, the 1 mm diameter hydrophone leads to about a 3 dB reduction in level of the 50th harmonic whereas the 4 mm hydrophone gives a 10 dB reduction at the 20th harmonic.

It should be emphasised that all of the continuous wave measurements presented here show only the first five harmonics; thus they fall inside the region for which the amplitude response of the hydrophone was known. It was assumed that the phase shift of the hydrophone over this frequency range was constant since the amplitude response was relatively flat. The pulsed field measurements relied on the extrapolated response of the hydrophone but it could be argued that the accuracy of the calibration at the higher frequencies was less important since the amplitude of the higher harmonics was small.

4.4 DIGITAL STORAGE OSCILLOSCOPE

A Philips PM3315 digital storage oscilloscope (DSO) was used to monitor and capture the time waveform at the hydrophone. This instrument is based on a relatively slow analogue to digital converter but uses a charge coupled delay line to achieve a maximum direct sampling rate of 125 MHz (8 ns between samples). Repetitive signals could be sampled at an effective rate of 5 GHz (0.2 ns between samples). The input amplifiers had a -3 dB bandwidth of 60 MHz and an input impedance of 1 MΩ in parallel with 25 pF. The input capacitance (C_i) was significant since it was comparable with the hydrophone capacitance (C_h) of about 90 pF. It was necessary to correct the open circuit hydrophone sensitivity by a factor of $C_h/(C_h+C_i)$ to account for the loading effect of the DSO. The digitised signal was held in the DSO as 256 bytes with 8 bits per byte, thus at the maximum direct sampling rate (125 MHz) the maximum time slice that could be captured was 2 μs. The relatively short record length of the instrument was compensated for by a trigger delay that could be varied from -10 to 9999 divisions of time-base; this allowed the position of the time window to be set around the required portion of the time waveform [Philips, 1985].

The DSO could be controlled from its front panel or from the computer via the IEEE bus. Computer control allowed auto-ranging to be carried out for the attenuators and the trigger delay could be determined by the computer and set automatically each time the hydrophone was moved, thus allowing a highly automated data capture sequence. The captured waveforms were transferred via the IEEE bus to the computer for analysis.

4.5 TRANSLATION STAGE

The translation stage comprised two Time and Precision Uni-slides mounted in the horizontal plane at 90 degrees to each other. The hydrophone support was mounted on the cross slide and incorporated manual adjustment vertically and in azimuth. The Uni-slides had a resolution of about 6 microns and were driven by the computer via the IEEE bus and a Digiplan stepper motor drive. The translation stage was mounted

over a water-filled tank 1.2 m long, 0.3 m wide and 0.3 m deep. Measurements were typically made at intervals of 1 to 10 mm along the acoustic axis and 0.3 to 1.0 mm intervals across the axis.

4.6 IBM COMPUTER

An IBM Personal Computer, PC-AT, was used to control the translation stage and the DSO via an IEEE bus. This could be done either in an interactive manner or the system could be set up to carry out a series of measurements and move the hydrophone between measurements. This allowed measurements to be made on pressure fields in a fraction of the time that it would take if the operation were carried out manually and at much closer spatial intervals than would normally be practical. The data from such measurements were stored by the computer.

The finite difference model was implemented on the IBM and was used on a number of occasions; however the speed of execution and the limited memory size did pose some problems. The use of a Gould NP1 main-frame system simplified theoretical runs considerably and the results were transferred back to the IBM for comparison with the experimental data held there.

A number of programs were written for the IBM, mostly in FORTRAN, and where possible they used "purpose built" subroutines held in a library on the fixed disk. A number of subroutines from commercially available packages were also used, in particular the IBM Plotting System, the IBM General Purpose Interface Bus routines and the Numerical Algorithm Group's PC-50 numerical subroutines.

4.6.1 Note on using FFT subroutine

The Fourier analysis of the time domain signals was performed with the NAG subroutine C06EAF, this takes the time series data and returns the FFT as a series of real (X_n) and imaginary (Y_n) values. The Fourier magnitudes (A_n) and phases (ψ_n) were calculated in the usual way, i.e.

$$A_n = \sqrt{X_n^2 + Y_n^2} \quad \text{and} \quad \psi_n = \tan^{-1}\left(\frac{Y_n}{X_n}\right).$$

The phases however represent the Fourier cosine series phases so $\pi/2$ radians were added to each value to convert to sine series phases. Then the phases were divided by their harmonic number and the fundamental phase subtracted from them to give θ_n the harmonic phase angle relative to the fundamental in radians of the fundamental, i.e.

$$\theta_n = \left(\frac{\psi_n + \pi/2}{n}\right) - (\psi_1 + \pi/2).$$

4.6.2 Measurement schemes

(i) Quasi-continuous wave mode.

Initially measurements were with a quasi-continuous wave excitation and in order to eliminate standing waves it was necessary to drive the transducer with a moderately long tone burst, typically 80 cycles long. The pulse length was chosen so that the number of cycles in the pulse was greater than $ka/2\pi$ (the aperture radius in cycles); this ensured that interference effects close to the aperture were not lost.

A typical set of measurements for the pressure field along the acoustic axis was obtained in the following manner:

The transducer drive level and frequency were set and the hydrophone positioned manually at the first required measurement point. The DSO was set to trigger externally from the 'SYNC' pulse and the trigger delay adjusted until the required part of the pulse was in view on the DSO, usually the central portion of the pulse. The FORTRAN control program AXM.FOR was set running and the number of measurements along the axis and their spacing in millimetres entered as parameters. The trigger delay was also entered. The program then took control of the hydrophone position and the DSO, according to the algorithm of Figure 4.8, and dumped the first time waveform to the IBM. The time series data comprised 256 bytes of 8 bits each. Each time a waveform was dumped the program checked that the data did not reach

the upper and lower limits of the digitiser. If clipping had occurred then the program increased the oscilloscope attenuator setting and repeated the capture alternatively if the data occupied less than half the dynamic range of the digitiser then the attenuator setting was decreased. A software flag interlocked the attenuator setting changes to avoid "hunting". If the data was within the required amplitude limits a single cycle was extracted between zero crossings and re-sampled back to 256 points to simplify the FFT. The single cycle was then subject of an FFT and the amplitudes and phases of the first five harmonics were stored on the hard disk. The stepper motors were then activated to move to the next measurement position and the data capture repeated. The end product was a file with amplitudes and phases for the first five harmonics at a number of axial positions. A typical axial run might comprise 200 measurements at spacings between 1 and 10 mm. The spacing was set at the start of the run and remained constant throughout although typically a set of axial measurements would be made from three consecutive runs spliced together. The first run, closest to the transducer would be, say, 1 mm spacing, the next set at 5 mm spacing and the most distant run, where the field varied less slowly, at 10 mm intervals. It would be feasible to alter the scheme to amend the spacing during the run, so if for example the fundamental level changed by more than 10% between two adjacent measurements the interval would be halved.

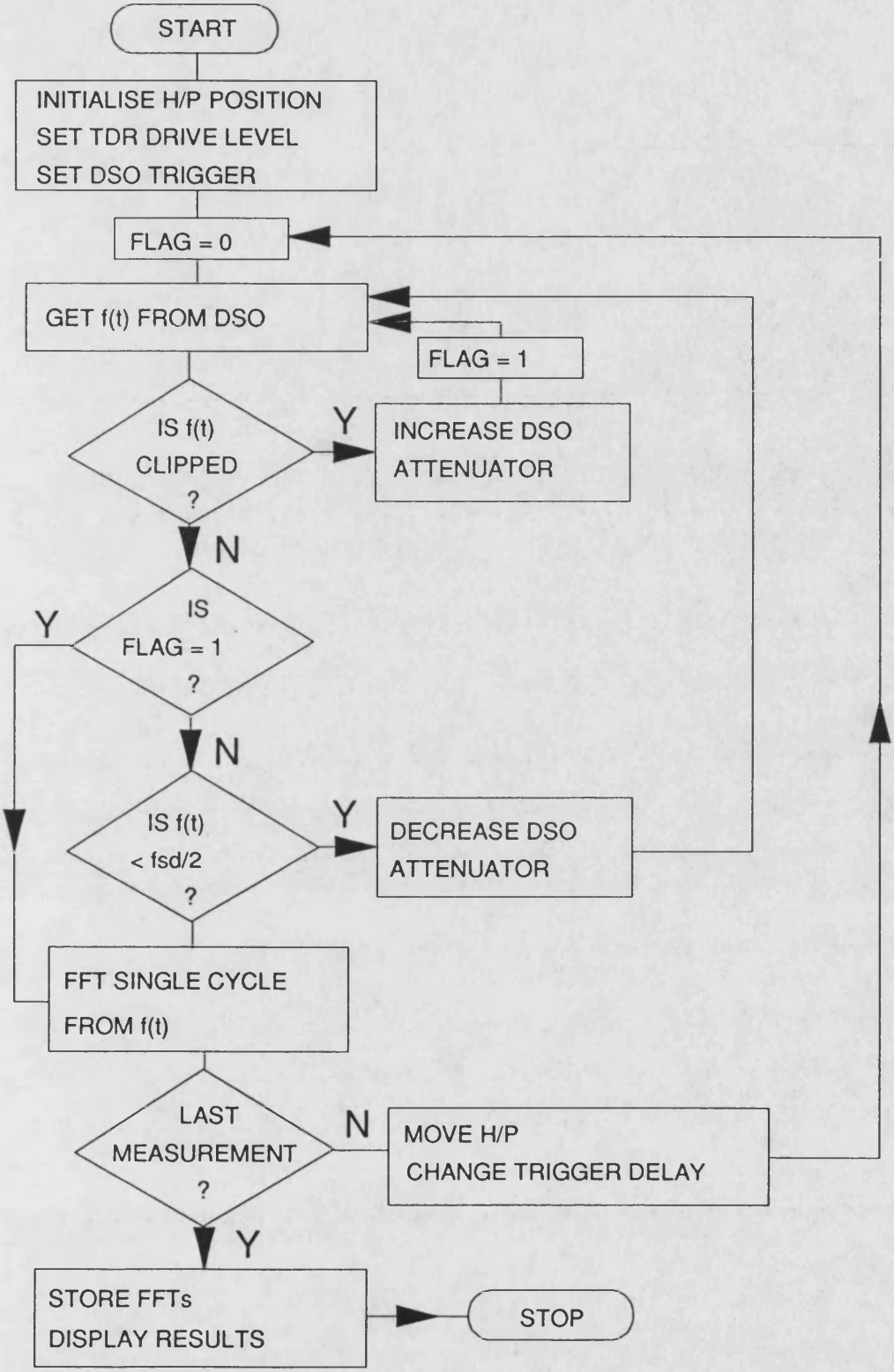

Figure 4.8. Measurement algorithm for CW measurements.
Key: DSO digital storage oscilloscope; f(t) - time series data; h/p - hydrophone; fsd - full scale deflection.

(ii) Pulsed mode

The wider bandwidth required for analysis of pulsed waveforms meant that the above method was not really suited to measurements on pulsed fields. Instead a program (AVEREG.FOR) that simply dumped the time waveform from the DSO to a file on the computer was used. This program assumed the user would position the hydrophone at the correct point in the field. Averaging was also implemented in the program but the data transfer rate and the conversion from ASCII data to real numbers took some 5 seconds per average.

Auxiliary programs (PLOTREG.FOR and PROCREG.FOR) allowed the data to be analysed and plotted as required.

4.7 ACCURACY

The main sources of uncertainty in the experimental measurements are now described.

4.7.1 Pressure

(i) Hydrophone

The reference hydrophone, used to cross calibrate the 1 mm diameter bilaminar hydrophone used in this study, had been calibrated, in amplitude only, at the National Physical Laboratory and had uncertainty, at the 95% confidence level, certified as 6% over the frequency range 1 to 4 MHz, rising to 10% over the range 13 to 15 MHz. Additional errors of similar magnitude could have affected the cross calibration. The phase response of the hydrophone was inferred from a theoretical model that gave good agreement with the calibrated range of amplitudes. The phase uncertainty is difficult to estimate and all that can be said with confidence is that the phase error increases as the signal level decreases. The level of agreement with the theoretical model of the nonlinear piston field suggested however that the phase model of the

hydrophone was a good approximation. The foregoing assumes that the hydrophone was properly aligned and was not being used in a pressure field where the finite hydrophone size was important.

It seems likely that the uncertainty in the hydrophone calibration dominated any other sources of uncertainty for the experimental measurements.

(ii) Digital storage oscilloscope

(a) Amplitude

The oscilloscope (Philips PM3315) used for the capture of time waveforms in this study was quoted by the manufacturers as having a vertical accuracy of better than 3%. It was assumed that this figure referred to 3% of full scale deflection; on this basis a signal that just clips on one range and occupies just over half the range on the next higher attenuator setting will be subject to 6% uncertainty. The digitisation of the signal also left 1 bit of jitter on the 8 bit signal, i.e. 1 in 256. This corresponded to a noise level at -48 dB of the full scale deflection which can be seen in some of the spectral plots. The relatively low level of the higher harmonics was a problem for waveform capture since the maximum sensitivity of the DSO for signal capture was in general determined by the level of the fundamental signal. This was not a very severe problem for the lower harmonics since at these levels of nonlinearity they were comparable in amplitude with the fundamental.

(b) Phase

The input amplifiers of the DSO had a -3 dB bandwidth of 60 MHz; thus the phase shift at frequencies below 30 MHz should be negligible.

Assuming that the above sources of error were independent the overall error in pressure measurement was unlikely to exceed 10%.

4.7.2 Time

The uncertainty in the time-base of the DSO was guaranteed to less than 2% [Philips, 1985]; thus frequency measurements inferred from the zero crossing frequency of the time waveform could be expected to have similar uncertainty.

The frequency of the continuous wave signal was set by monitoring the output of the function generator, in continuous mode, with a frequency meter (uncertainty about 5%) and then switching the function generator to tone burst mode prior to use in the experiment. The frequency was then checked using the zero crossing period of the time waveform on the DSO.

4.7.3 Positional

The translation stage had 4000 steps to the inch (about 160 to the millimetre) and manual check measurements were made periodically to ensure the accuracy of the translation stage but in general the precision of the stage was far in excess of that required particularly when using a 1 mm diameter hydrophone.

The initial alignment of the transducer proved a time consuming problem. The measurements relied on the acoustic axis of the transducer being parallel to the motion plane of the translation stage. Accurate alignment was however simplified by the almost perfect piston behaviour of the transducer which gave symmetrical beam patterns; hence by moving the hydrophone by a fixed amount on either side of the assumed position of the acoustic axis, usually to a minimum in the field, good alignment could be achieved.

4.7.4 Properties of the medium

Kinsler et al [1982] gives an empirical expression for the speed of sound in water:

$$c(P,t) = 1402.7 + 488t - 482t^2 + 135t^3 + (15.9 + 2.8t + 2.4t^2)(P/100) \text{ m/s}$$

where t = T/100, T is the temperature in degrees centigrade and P is the pressure in bars (1 bar = 10^5 Pa). The expression is accurate to 0.05% for temperatures (T) between 0 and 100 °C and pressures in the range 0 to 200 bar. The water temperature was typically steady to within +/- 1 °C which on the basis of the above equation would cause a variation in sound speed of ± 3 m/s.

The speed of sound in freshwater was measured experimentally with the largest contribution to its uncertainty coming from the time-base of the DSO (2%) increased to 4% by using the difference between two readings. Thus the experimental value was 1486 ± 60 m/s which compares favourably with the expected value of 1482 m/s at 20 °C.

The parameter of nonlinearity B/A was taken as 5.0 after Beyer [1974].

4.7.5 Transducer parameters

Errors in determining the transducer parameters had no direct effect on the experimental measurements but as the parameters were input to the theoretical models good agreement relied on accurate values for the transducer radius (a) and its focal length (D). The radius was particularly important since the positions of the axial maxima and minima are proportional to the square of the transducer radius. The determination of a and D was achieved to a large extent by comparison of experimental data with small signal theory and in general this gave rise to an uncertainty of about 5% in a and D. It was assumed that the transducer behaved as a perfect plane piston on the basis of the good agreement of the small signal measurements with theory. It was also assumed that the lenses affected only the phasing across the aperture although it seems likely that some amplitude shading must have occurred.

Chapter 5: RESULTS AND DISCUSSION

This chapter presents a number of results, mostly in the form of comparisons between experimental measurements and theoretical predictions. Four basic geometries were considered, namely the plane piston and focused fields with gains of 3.7, 7.6 and 11.9.

A large quantity of data was available for inclusion; however, in an attempt to make the thesis more readable only a limited selection is included. The plane piston has a gain of zero and is treated fairly comprehensively since it represents the starting point of the thesis and, by virtue of its simpler axial pressure field, is best suited to demonstrate limitations of the theoretical model. Of the focused systems, the lowest gain (3.7) is closely examined since it is most representative of diagnostic ultrasound scanners and is similar to many physiotherapy sets. The highest gain (11.9) is of interest due to additional features such as the post focal minima and its similarity to some lithotripsy systems. The focused system of intermediate gain (7.6) has a limited number of results presented but it was felt important to include these as they provide a bridge from the low gain systems to the highly focused systems. The range of drive levels shown has likewise been restricted, in the main, to two cases, "small signal", corresponding to a few kPa at the piston face, and "moderately nonlinear" (70 to 100 kPa at the piston face). The intermediate range and higher drive levels (up to 300 kPa) are covered in the investigation into the effect of drive level for the plane piston case.

The relevant parameters for each system are tabulated below.

Focusing gain ($G = R_o/D$)	0	3.7	7.6	11.9
Fundamental frequency (f_o) / Mhz	2.25			
Effective aperture radius (a) / mm	19.0	18.5	18.6	19.1
Rayleigh distance (R_o) / mm	1730	1630	1640	1750
Effective radius of curvature (D) / mm	∞	440	216	147
Source pressure for finite amplitude measurements (p_o) / kPa	100	68	72	75

Table 5.1: Parameters of systems considered.

The first part of this chapter examines the small signal pressure fields along the acoustic axis for each of the four systems. Next the finite amplitude axial fields of the four systems are considered followed by the finite amplitude radial field of the low gain system (G = 3.7). The variation of harmonic amplitudes and phases with drive level is studied for a single axial position in the plane piston field and finally some time domain measurements are presented along with the preliminary results for the pulsed pressure field.

In general the experimental results are plotted as continuous lines since the data points are so closely spaced that individual markers would be impractical. The use of solid lines shows any fluctuations due to experimental error and noise, no error bars are shown but in general the experimental measurements were subject to an error of about 10% (See Chapter 4). The theoretical curves are plotted as dashed lines since they vary more smoothly in the absence of noise.

5.1 SMALL SIGNAL FIELDS

It was important to establish the small signal behaviour of the systems under consideration so that parameters such as focal length, effective aperture radius and

drive levels could be determined. Some results of small signal theory for focused circular apertures from Appendix A are compared with experimental measurements below.

Figures 5.1 to 5.4 show comparisons for the axial pressure fields for the four systems under consideration and it can be seen that in general the agreement between experiment and theory is good. The main deviation seen for all four systems occurs at short axial ranges where the measured field shows a diffraction loss, caused by spatial averaging due to the finite hydrophone size and hence the reduced amplitude of the experimental measurements close to the transducer. It is relatively easy to observe the diffraction loss in the plane piston case since all maxima are expected to be at the same level ($2p_o$) and all minima should be zeros but the diffraction loss is seen as the tapering off of these maxima and minima. In the case of the focused fields the diffraction loss is partially masked since the axial maxima diminish in any case as the piston is approached but the minima still become progressively less pronounced with decreasing range.

The good agreement between experiment and theory for the plane transducer (Figure 5.1) shows that the Panametrics transducer was rather unusual in that it displayed perfect piston behaviour; hence the closeness of the measured small signal field with theoretical predictions. This is an important result since the finite difference model requires the aperture excitation as part of the initial conditions and if the transducer had not behaved as a plane piston it would have been difficult to deduce the actual aperture excitation and hence the initial conditions for the theoretical model would have been uncertain.

The focused cases deviated slightly from the ideal since the addition of the lens had some undesirable side effects. The varying thickness of the lens across the aperture combined with the relatively high absorption coefficient of perspex (about 1 dB/cm) lead to uncertainty in aperture shading function. In addition, the impedance mismatch at the transducer-lens interface and at the lens-water interface reduced the

transmission coefficient of the lens. Hence the same basic transducer radius and electrical drive level produce slightly different source pressures and effective aperture radii for the three focused systems (see Table 5.1).

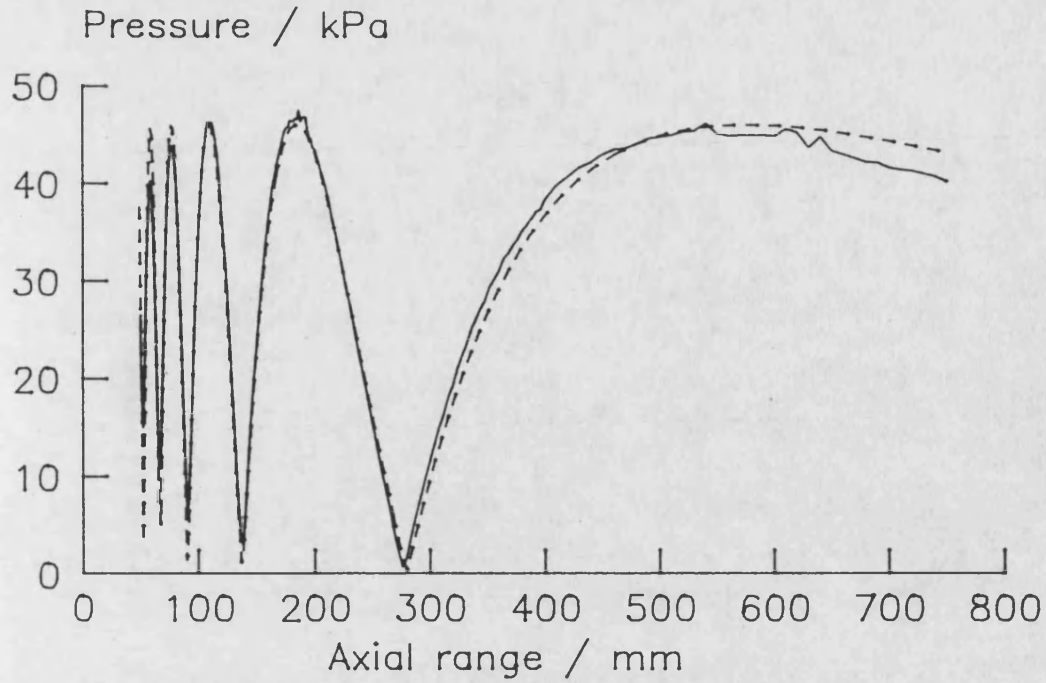

Figure 5.1. Small signal, axial pressure field for a plane piston, experiment (—) and theory (- -).

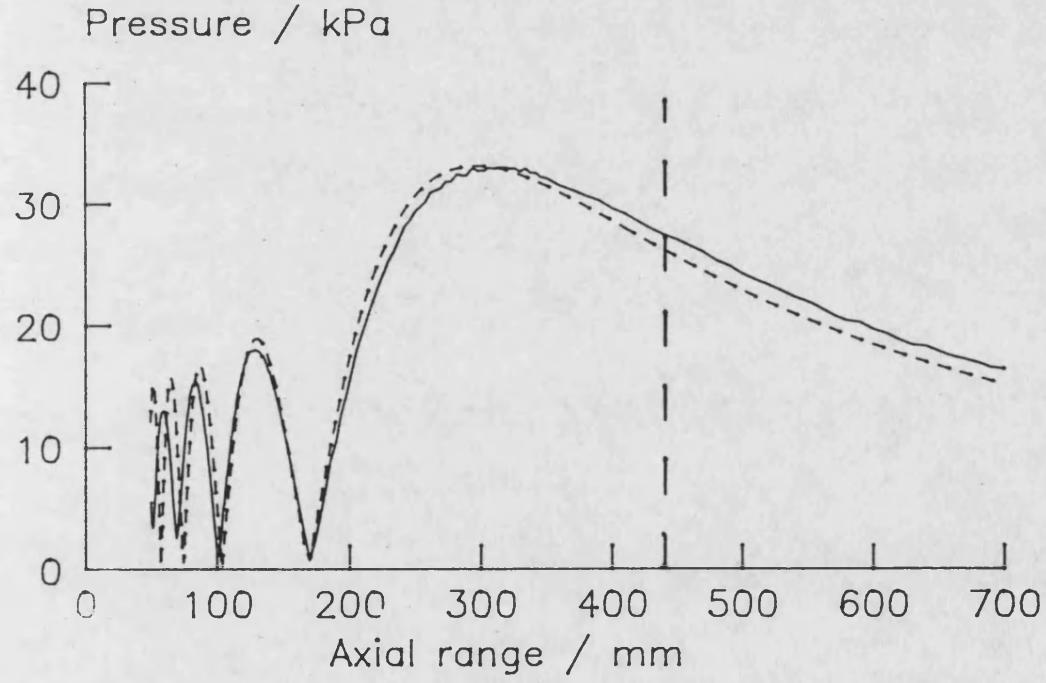

Figure 5.2. Small signal, axial pressure field for G = 3.7, experiment (—) and theory (- -). Focal plane at 440 mm.

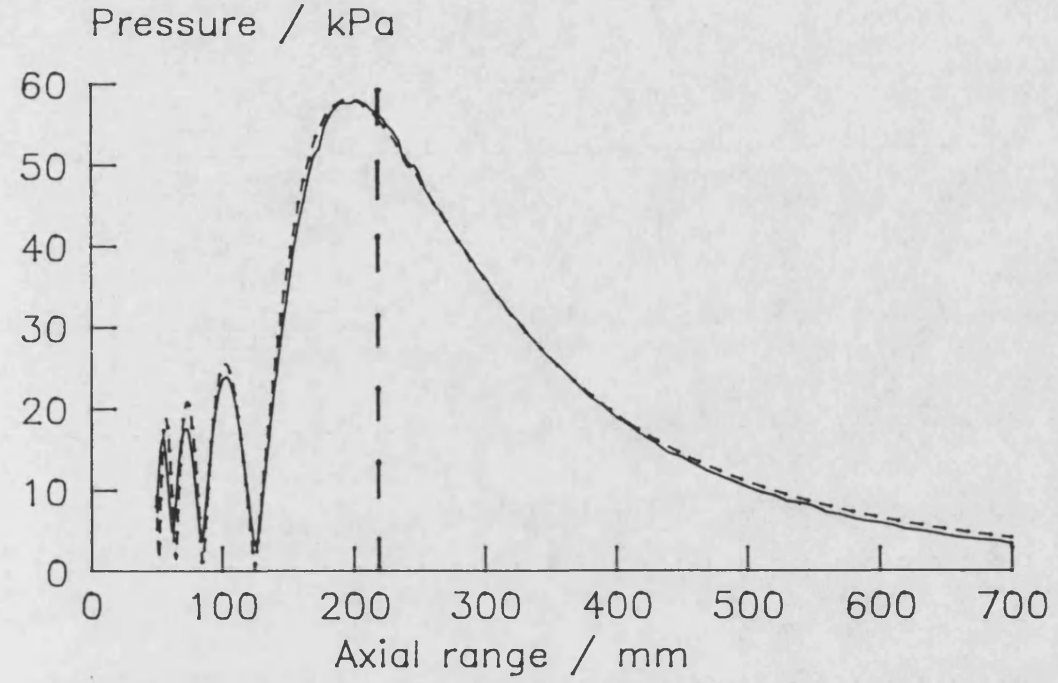

Figure 5.3. Small signal, axial pressure field for G = 7.6, experiment (—) and theory (- -). Focal plane at 216 mm.

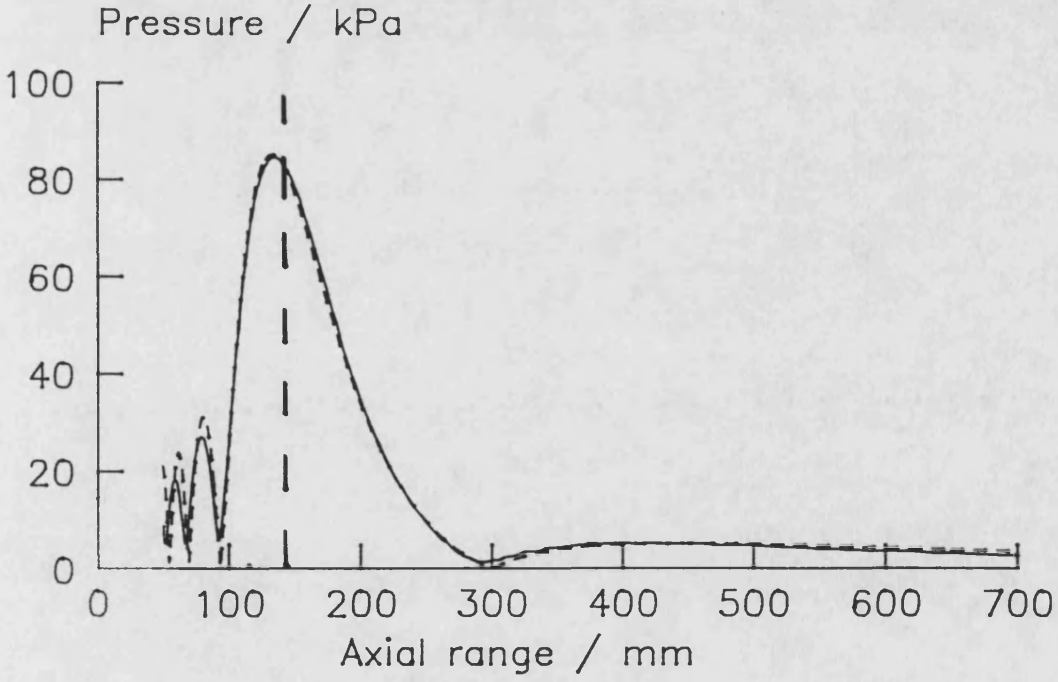

Figure 5.4. Small signal, axial pressure field for G = 11.9, experiment (—) and theory (- -). Focal plane at 147 mm.

5.2 FINITE AMPLITUDE FIELDS

Axial field

The finite amplitude axial results for each of the four basic continuous wave systems are presented in the following format. The experimental measurements for the first five harmonic amplitudes are plotted together on a linear ordinate. (Plotting the harmonics together shows the relative levels at different ranges.) The picture at this stage is too complicated to superimpose the theoretical results so each harmonic from the initial plot is taken in turn and plotted on a logarithmic ordinate (dB re 1 MPa) with the corresponding theoretical predictions. The phase results are added beneath the amplitude plots.

Experimental results are not presented for the fundamental phase since it could not be determined from the measurements made. Harmonic phases are measured relative to the fundamental phase and in radians of the fundamental phase. Experimental results are plotted as continuous lines since the data points are numerous and closely spaced. The theoretical results are plotted as dashed lines.

Comments of a general nature that apply to all four systems are made below. Any exceptions specific to a particular system are noted at the beginning of each set of results.

General Remarks on axial fields

1. At short ranges the harmonic levels are negligibly small, i.e. the harmonic generation observed is occurring in the medium not at the source.

2. The harmonic levels initially increase in amplitude with increasing range, albeit in a rather oscillatory fashion. At longer ranges as the amplitude of the fundamental starts to fall the harmonic levels fall although their ratios to the fundamental are roughly constant and inversely proportional to harmonic number.

3. The second harmonic (and the higher harmonics) are generated from the fundamental in a cumulative manner so a feature such as a minimum in the fundamental does not have an immediate effect on the second harmonic which has its minimum at a greater range. Each single peak in the near-field of the fundamental gives rise to a double peak in the second harmonic but at a greater range.

4. The nonlinear effects are more significant in the main axial lobe than at any other point in the field. In the main axial lobe, at these drive levels, the harmonics fall off roughly as the reciprocal of harmonic number.

5. In general the agreement between experiment and theory is good and would allow accurate predictions of amplitudes and phases up to the fifth harmonic for all four systems.

6. The main deviation shown by all systems is an axial displacement of the minima (and maxima). This is mainly due to the radial step sizes used in the finite difference model. (See Chapter 3).

7. At short ranges the theoretical model tends toward the average pressure level, averaging out the small scale variations in the near-field.

8. At short ranges the measured amplitudes of the higher harmonics become noisy, due to low signal level. (The experimental measurements were from an 8 bit digital oscilloscope with no averaging so assuming the fundamental occupied the full range of the digitiser the noise level will be 48 dB below the maximum level of the fundamental.)

9. Phase measurements are quite sensitive to noise (see point 8 above) and a small random error in a phase angle near $\pm\pi$ will cause an apparent phase jump of 2π, hence at low amplitudes the phase measurements appear very erratic.

10. The theoretical model stores the harmonic amplitudes and phases on a much coarser grid than that which is used to calculate them thus rapid phase jumps may be misrepresented.

11. The harmonic phases are presented relative to the fundamental phase; hence jumps in fundamental phase can cause corresponding discontinuities in the harmonic phases.

Plane piston (G = 0)

The plane piston was chosen as the starting point for this study since it presents a simple geometry and the theoretical model of Aanonsen et al [1984] could be applied directly. Fortunately the Panametrics transducer behaved as a perfect piston at small signal and at finite amplitude drive levels which simplified the analysis and made extension to focused fields viable. The simple axial field of the plane piston shows the diffraction loss at short ranges but also makes it easy to observe loss of energy from the fundamental to the harmonics. Figure 5.5 shows the last axial maximum to be about 10% lower than the penultimate axial maximum. The last axial maximum of the fundamental has also moved closer to the transducer in comparison with the small signal case (about 480 mm instead of 550 mm); this is due to the loss of energy at longer ranges caused by the build up of harmonics. At the longest ranges the harmonic levels relative to the fundamental vary as the reciprocal of harmonic number indicating a shocked waveform.

Figures 5.6 to 5.10 show good agreement between experimental measurements and theoretical predictions from the fundamental to the fifth harmonic; however there is an apparent discrepancy between measured and predicted phase for the second harmonic (Fig. 5.7) at an axial range of 275 mm where the measured phase shows a marked deviation (due to the fundamental phase jump) whereas the theoretical prediction does not due to the coarseness of the output step size. Similar effects are seen in the third harmonic phase (Fig. 5.8) at a range of 140 mm and the fourth and fifth harmonic phases (Figs. 5.9 and 5.10) at 275 mm.

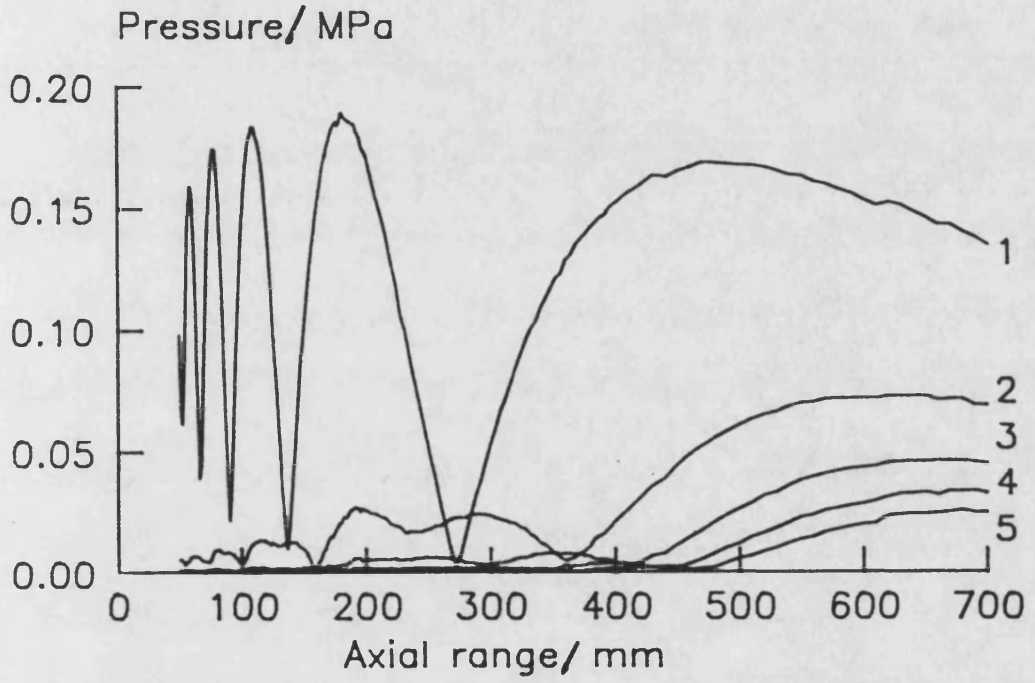

Figure 5.5.
Plane piston, experimental measurements, axial amplitudes of first five harmonics.
p_o = 100 kPa.

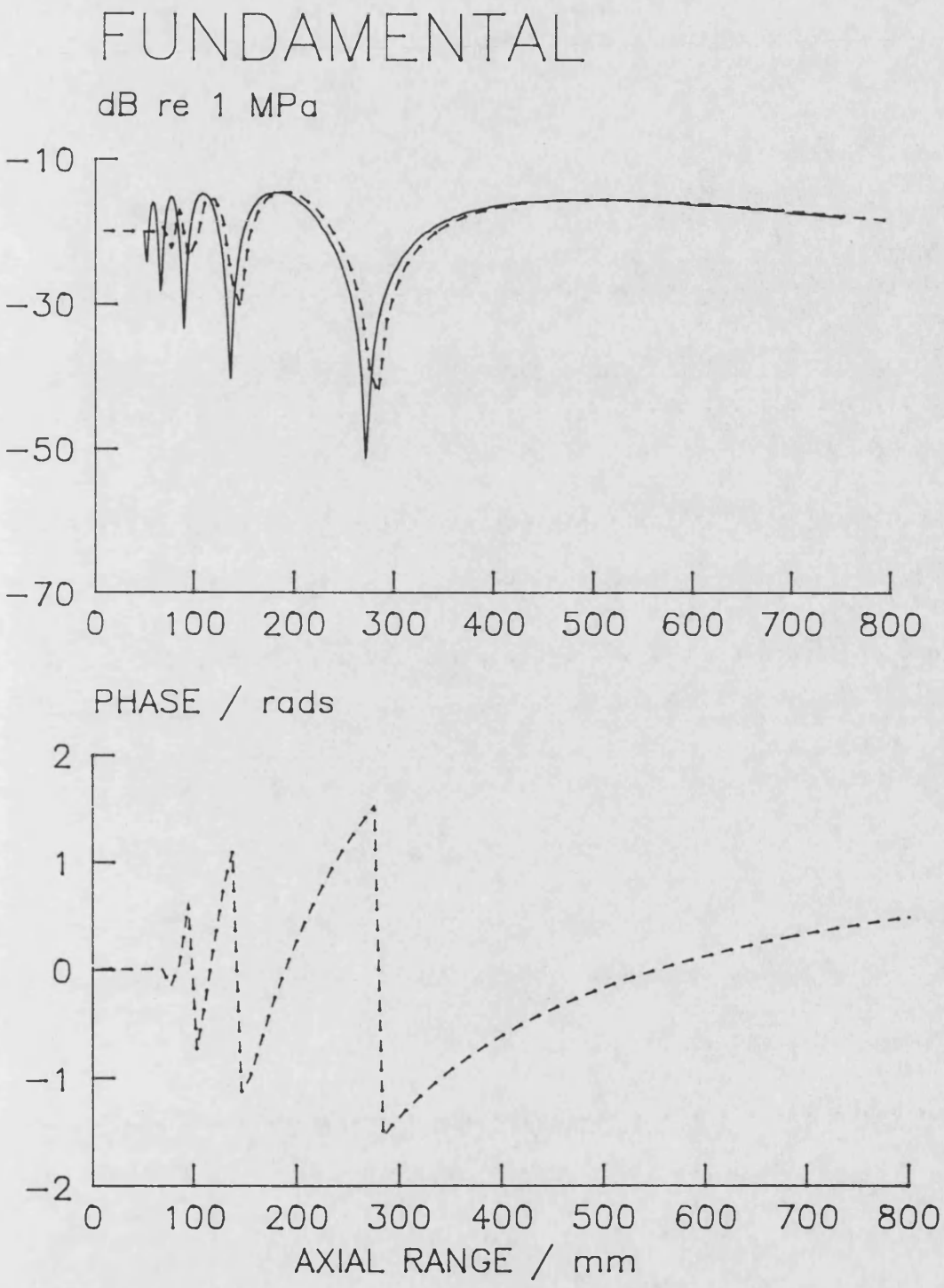

Figure 5.6.
Plane piston, fundamental amplitude and phase on axis.
Experiment —, theoretical model - -. p_o = 100 kPa.

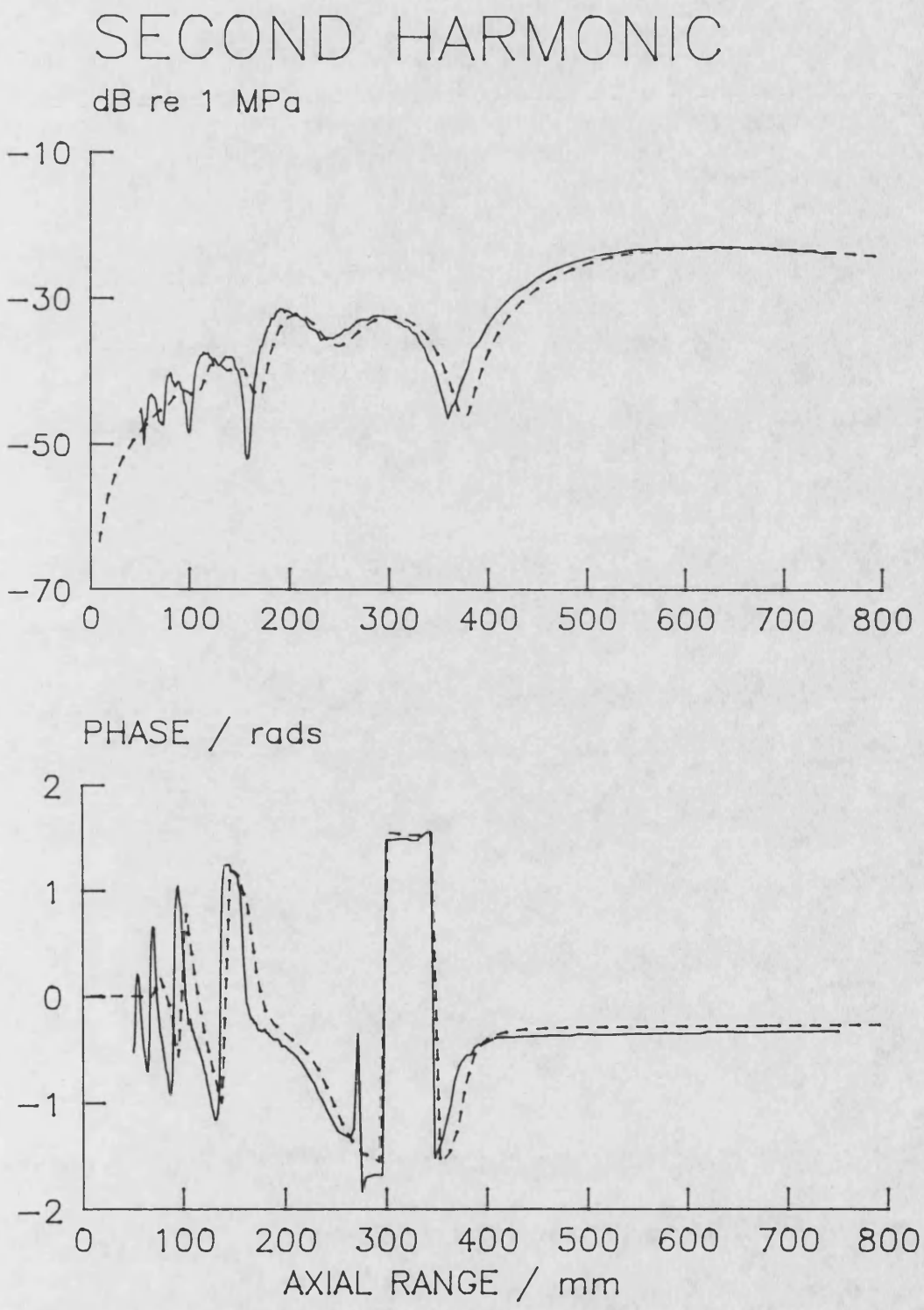

Figure 5.7.
Plane piston, second harmonic amplitude and phase on axis.
Experiment —, theoretical model - -. p_o = 100 kPa.

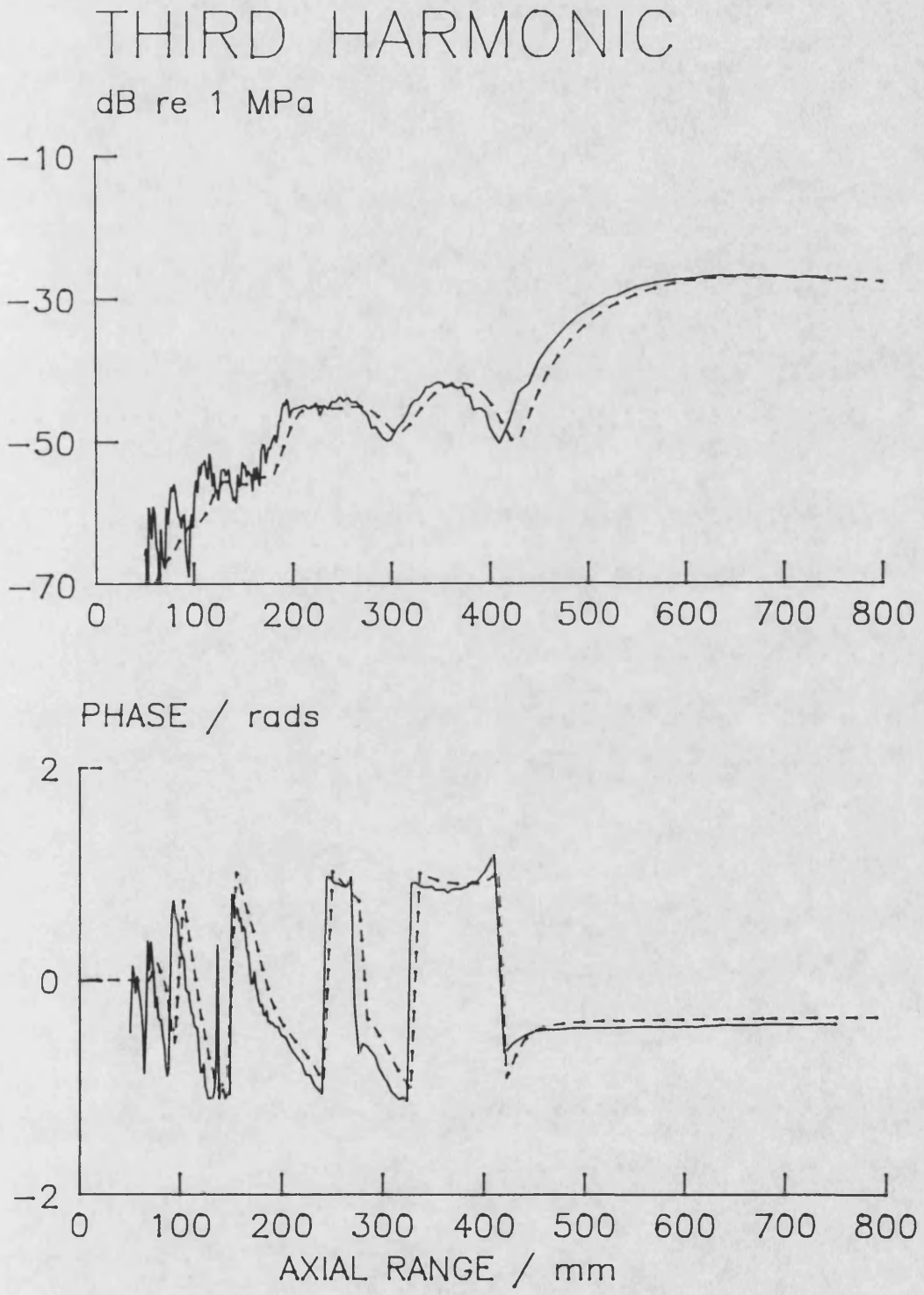

Figure 5.8.
Plane piston, third harmonic amplitude and phase on axis.
Experiment —, theoretical model - -. p_o = 100 kPa.

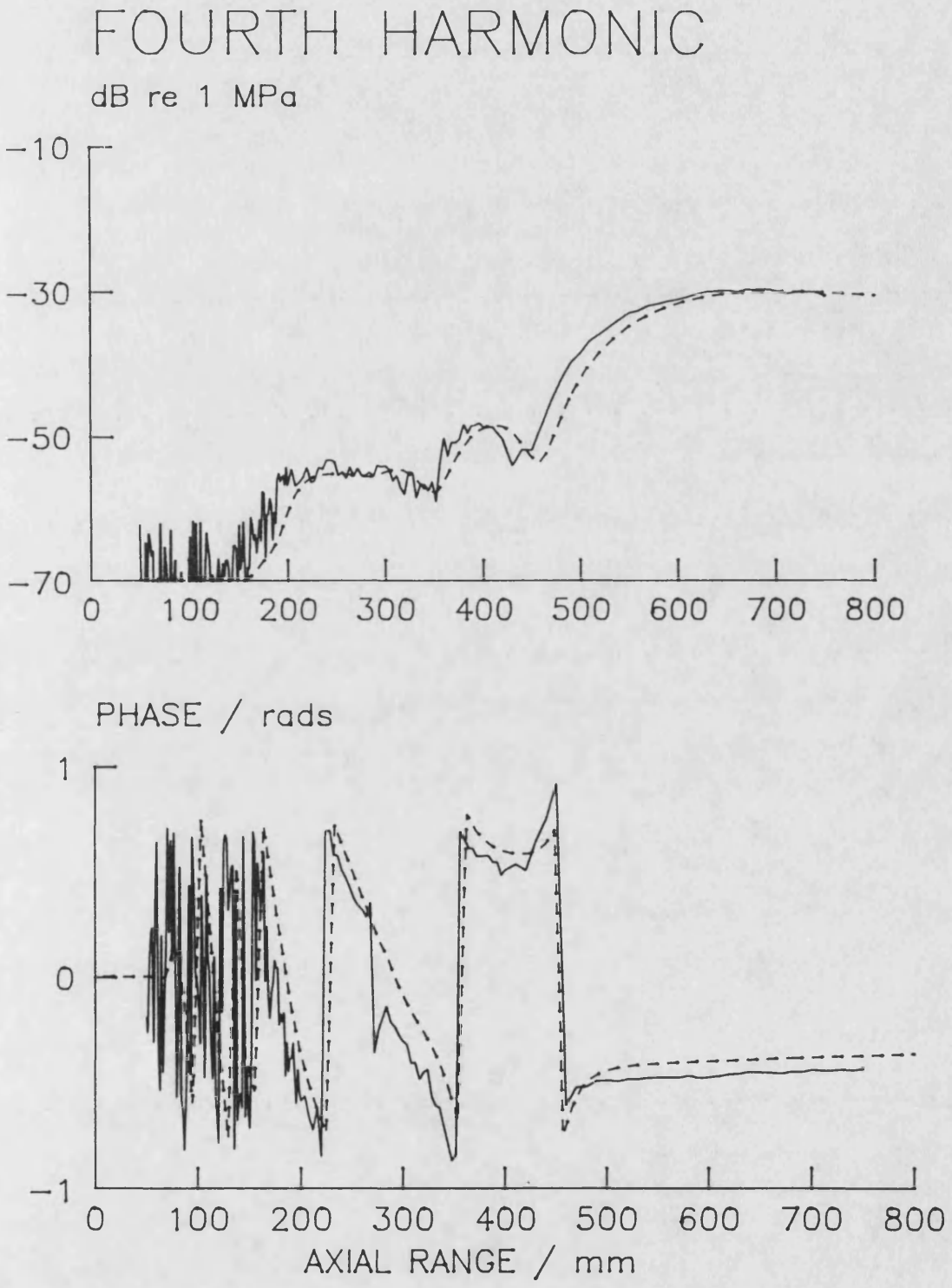

Figure 5.9.
Plane piston, fourth harmonic amplitude and phase on axis.
Experiment —, theoretical model - -. p_o = 100 kPa.

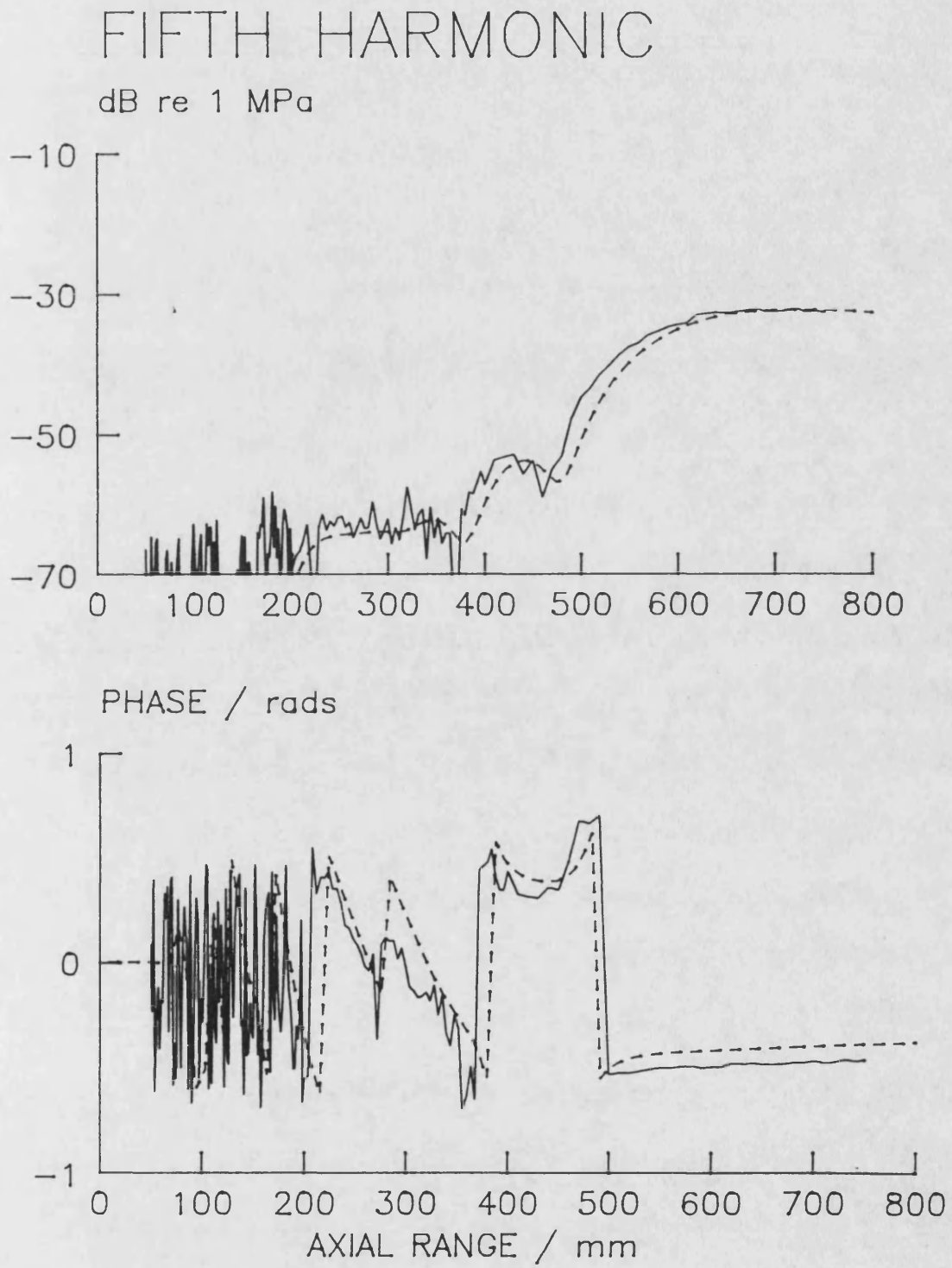

Figure 5.10.
Plane piston, fifth harmonic amplitude and phase on axis.
Experiment —, theoretical model - -. p_o = 100 kPa.

Focused piston (G = 3.7)

This configuration with its relatively low focal gain is typical of many medical imaging systems where an increase in pressure is required to counteract the effects of attenuation but not at the cost of a small depth of field. Apart from the axial pressure peak at about 60% of the focal distance (Figure 5.11) this system shares many features with the plane piston field. In particular the shape and position of the second harmonic curve relative to the fundamental is similar, the oscillations of the fundamental amplitude in the near-field prevent any sizeable build up of harmonics until after the last axial minimum has been passed and the harmonics increase rapidly in the main axial lobe and then assume a typical 1/n fall off for a shocked waveform. In common with the plane piston case good agreement is seen between experiment and theory apart from the progressive displacement of the axial minima as the axial range is reduced. Although the radial step size in the model could be reduced somewhat to reduce this mismatch there is a limit beyond which there would be no advantage because the parabolic approximation would no longer be valid, in this case at ranges much less than about 80 mm. This highlights one of the problems of using the parabolic approximation with focused fields; the higher the focusing gain the closer the region of interest is moved towards the aperture where the parabolic approximation is less valid.

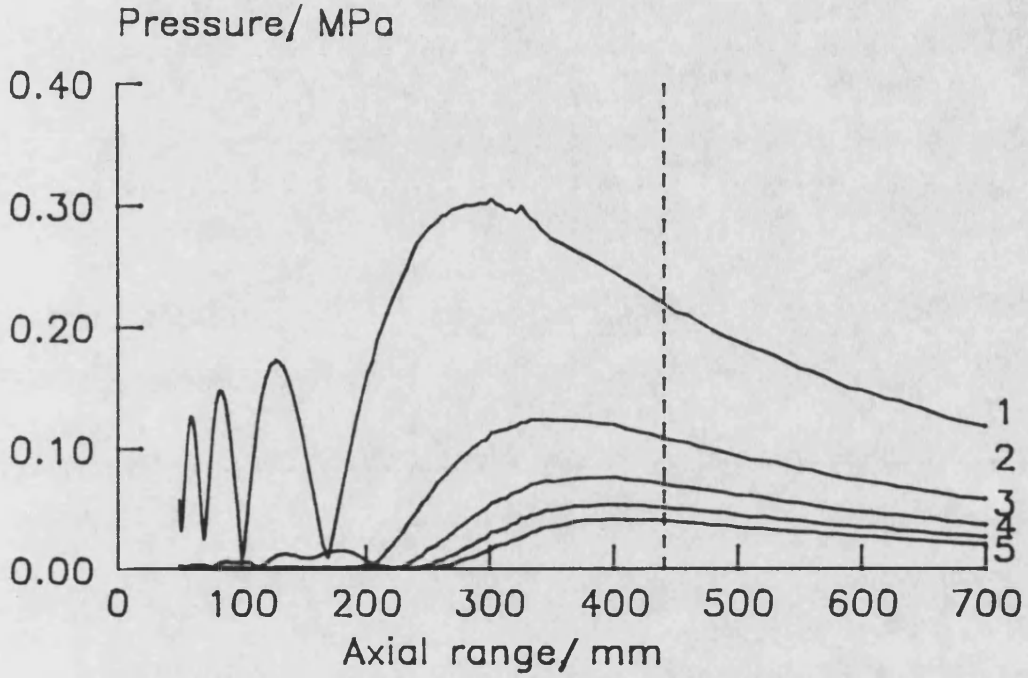

Figure 5.11.
Focused piston (G = 3.7), experimental measurements, axial amplitudes of first five harmonics. p_o = 68 kPa. Focal plane at 440 mm.

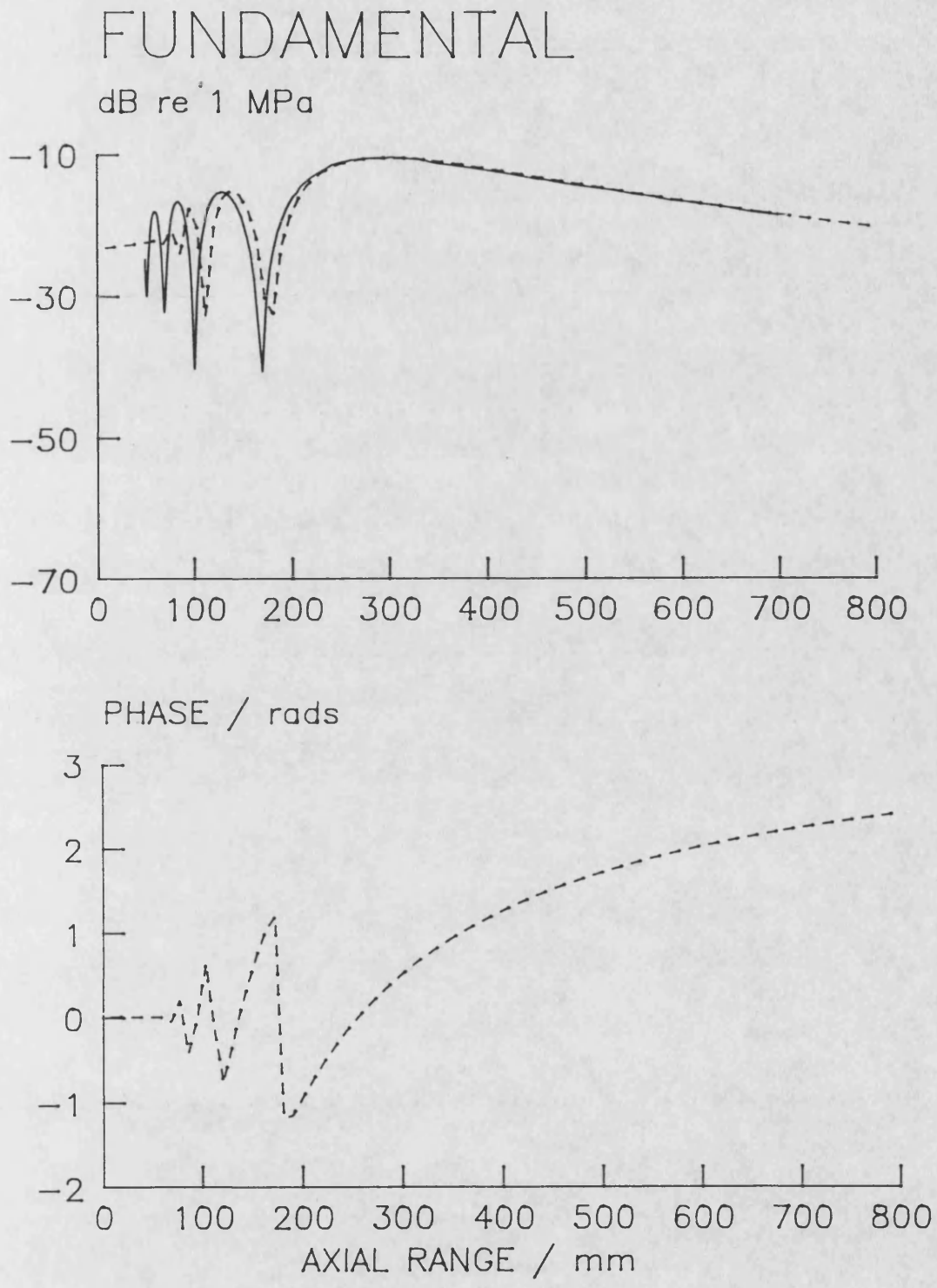

Figure 5.12.
Focused piston (G = 3.7), fundamental amplitude and phase on axis.
Experiment —, theoretical model - -. p_o = 68 kPa.

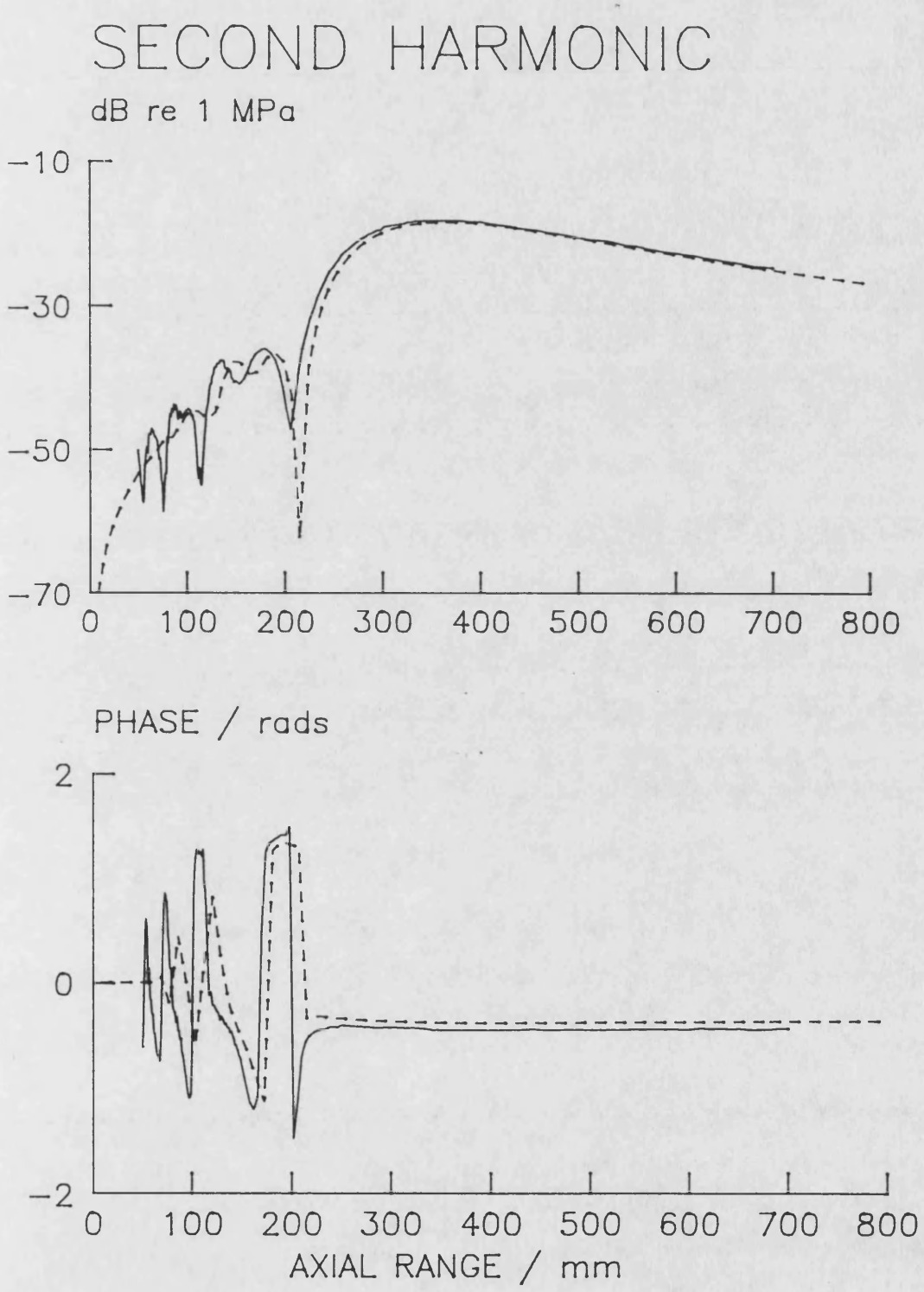

Figure 5.13.
Focused piston (G = 3.7), second harmonic amplitude and phase on axis.
Experiment —, theoretical model - -. p_o = 68 kPa.

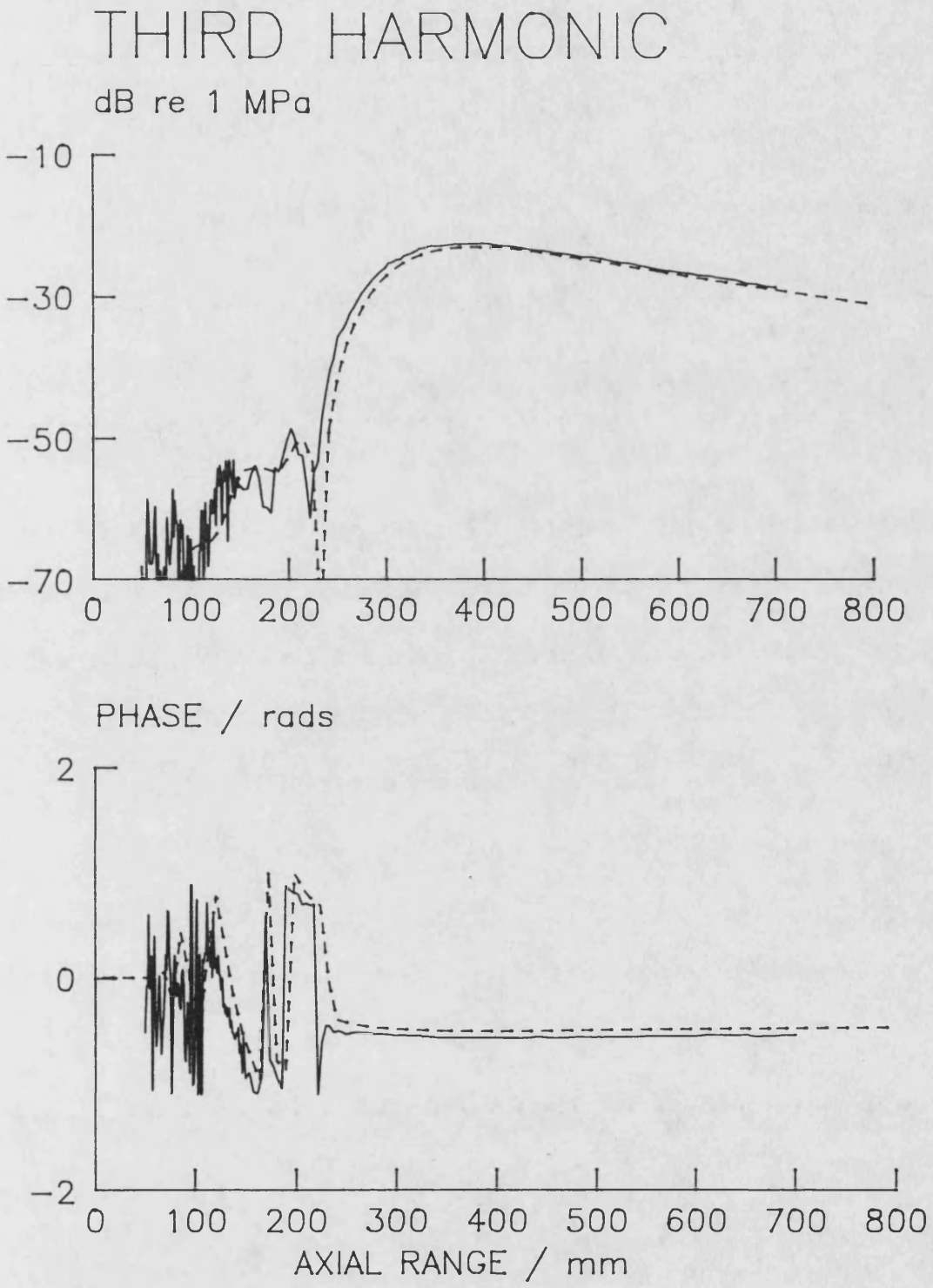

Figure 5.14.
Focused piston (G = 3.7), third harmonic amplitude and phase on axis.
Experiment —, theoretical model - -. p_o = 68 kPa.

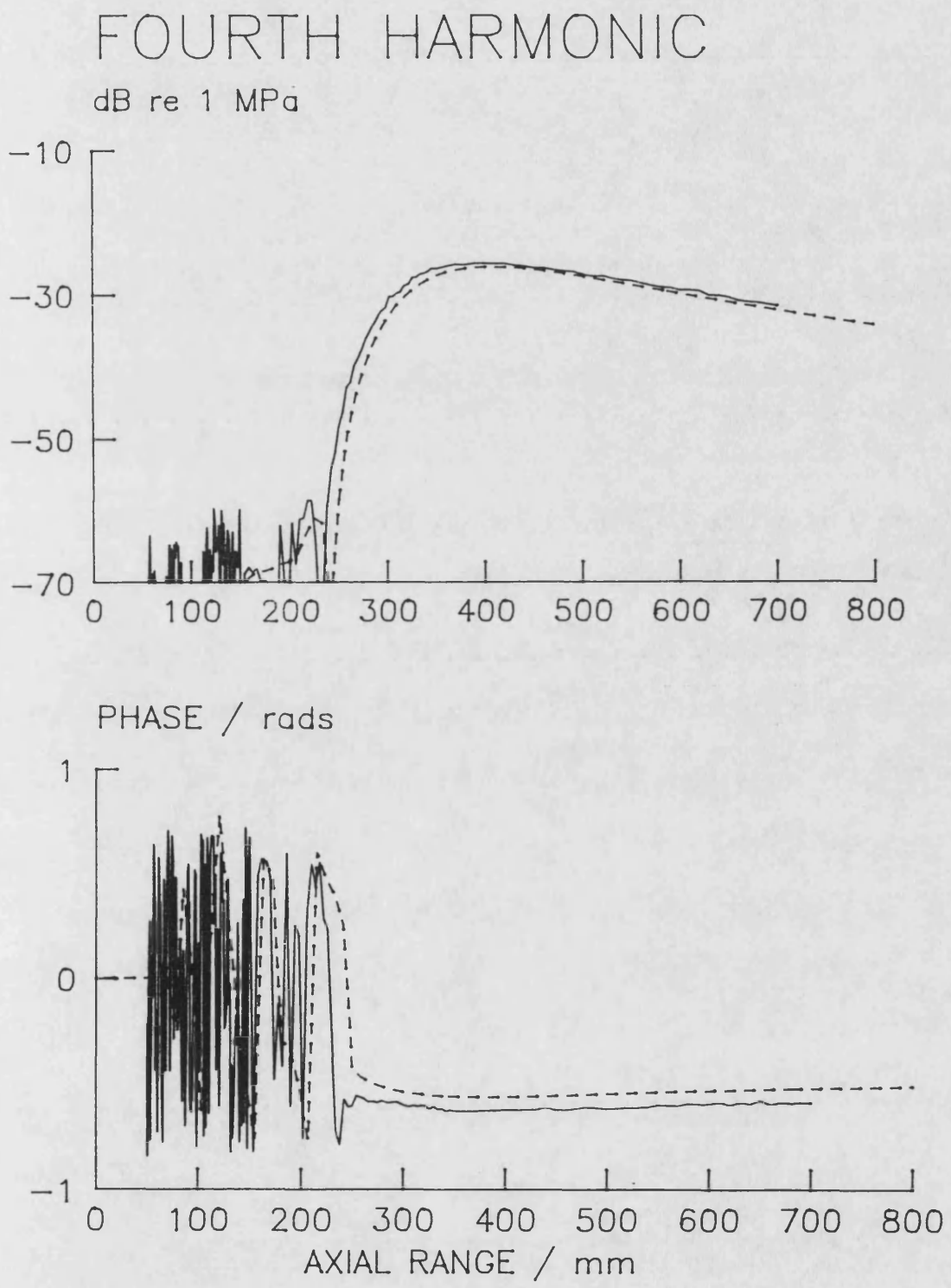

Figure 5.15.
Focused piston (G = 3.7), fourth harmonic amplitude and phase on axis.
Experiment —, theoretical model - -. p_o = 68 kPa.

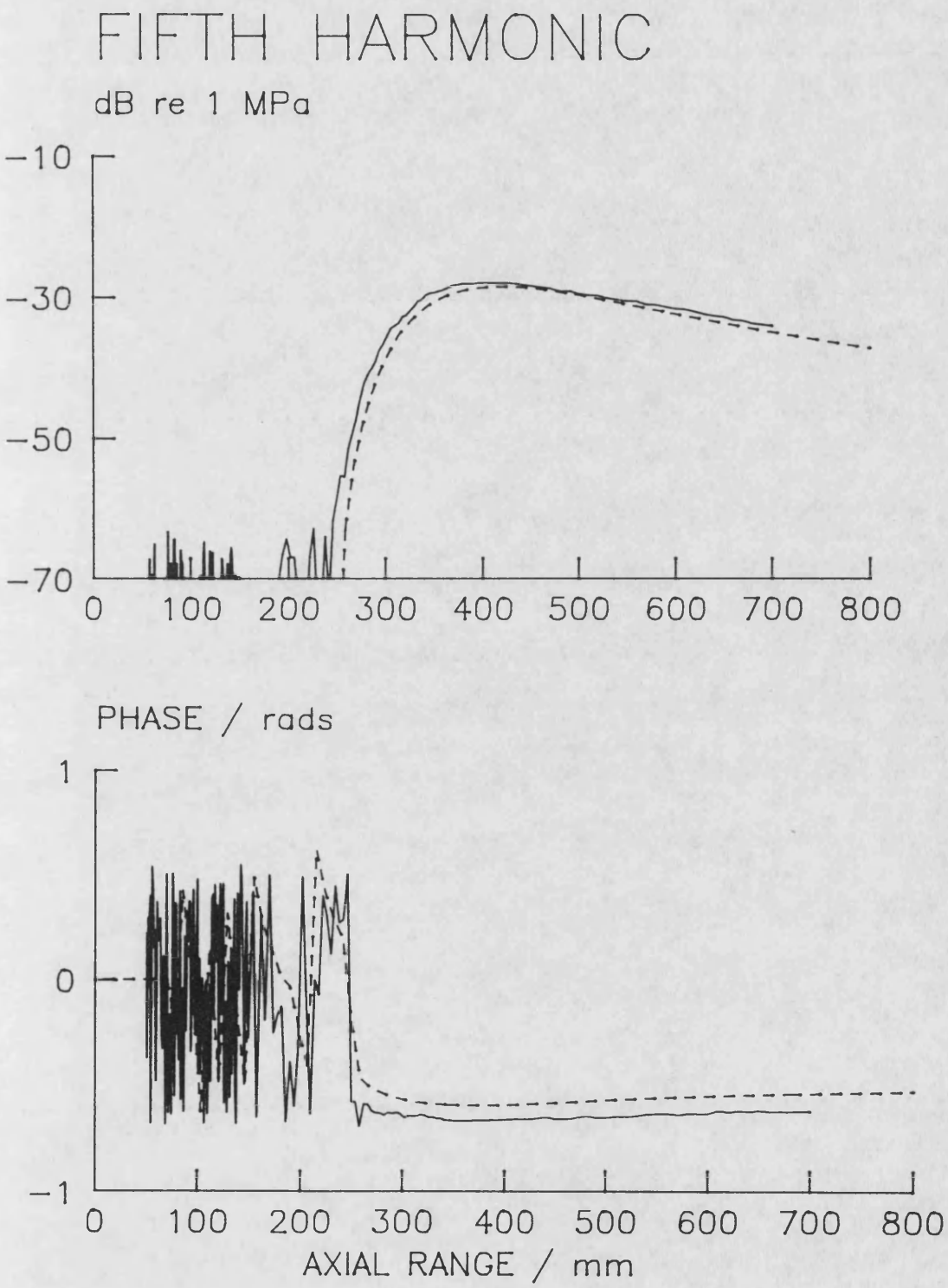

Figure 5.16.
Focused piston (G = 3.7), fifth harmonic amplitude and phase on axis.
Experiment —, theoretical model - -. p_o = 68 kPa.

Focused piston (G = 7.6)

The full comparison for the focused gain of 7.6 has not been included since the results fall somewhere between the other two focused systems. The experimental measurements are shown (Figure 5.17) and it can been seen that they are similar to the gain of 3.7 only more tightly packed near the transducer and the peak pressure occurs closer to the true focal plane. This system should display a minima on axis beyond the focal plane since the gain is greater than 2π but it occurs at a range of 1300 mm and was beyond the reach of the measuring system. The agreement between experiment and theory was comparable to the system with the focal gain of 3.7.

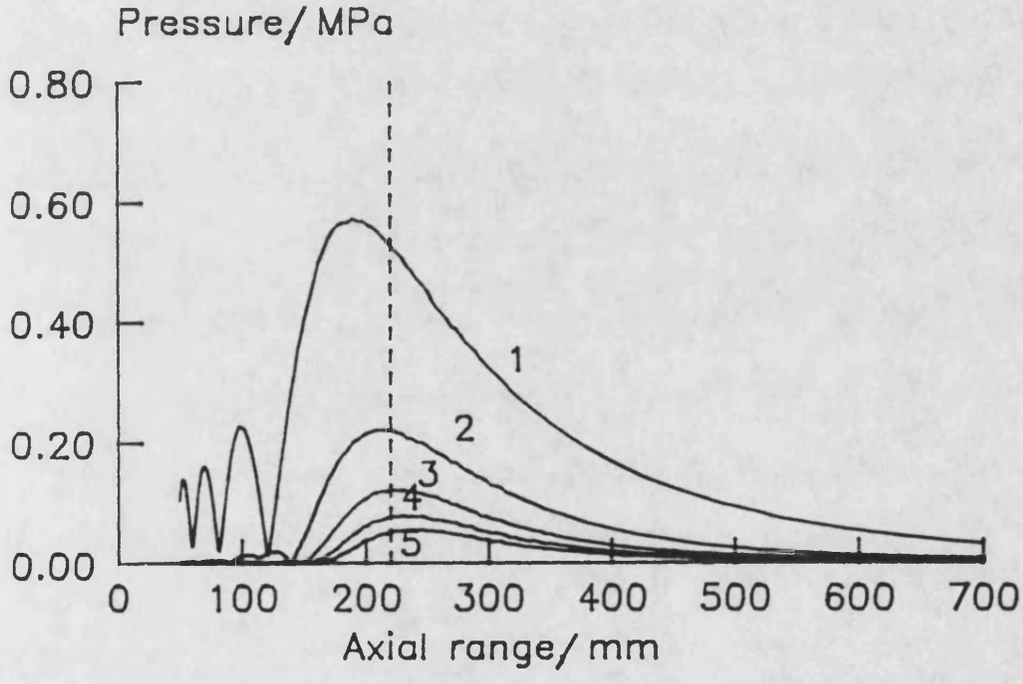

Figure 5.17.
Focused piston (G = 7.6), experimental measurements, axial amplitudes of first five harmonics. p_o = 72 kPa. Focal plane at 216 mm.

Focused piston (G = 11.9)

This configuration with its relatively high focal gain of 11.9 is more typical of lithotripters than of imaging systems and shows (Figure 5.18) a very high pressure gain occurring directly in the focal plane which falls off rapidly either side of the focal plane. The high gain also causes a minimum in the post focal region (at a range of 300 mm). Apart from these differences there are still a number of similarities with the focal gain of 3.7 and the plane piston. Harmonic generation occurs mostly in the main axial pressure lobe since the near-field fluctuations prevent a substantial build up elsewhere. The harmonics again reach a 1/n fall off and then decay away as the fundamental amplitude decreases.

The main discrepancy between the experimental measurements and the theoretical predictions occurs in the post focal region around the last axial minimum. This could be due to the extra attenuation at the edges of the lens shading the aperture. A similar problem was seen by Lucas and Muir [1982 and 1983] and Humphrey et al [1986]; both experiments used a perspex lens. It would be necessary to re-run the theory with an estimate of the shading factor (or to measure the field due to a curved radiator rather than a plane one with a lens attached) in order to resolve this discrepancy.

The pressure gain should be equal to the focal gain (G = 11.9) but the fundamental has lost energy to the harmonics so the apparent gain at this drive level is only 10.5 and at higher drive pressures the apparent gain would be further reduced. Although the focal plane for this system is close to the transducer it is still possible to make predictions for a large proportion of the pressure field without invalidating the parabolic approximation and in general the agreement is good.

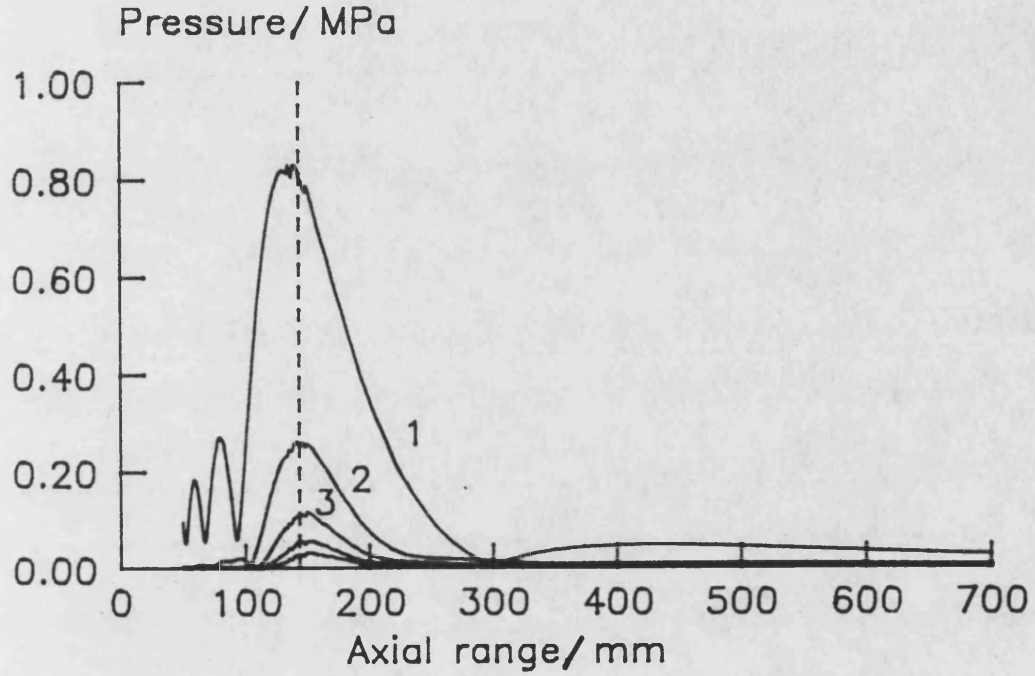

Figure 5.18.
Focused piston (G = 11.9), experimental measurements, axial amplitudes of first five harmonics. p_o = 75 kPa. Focal plane at 147 mm.

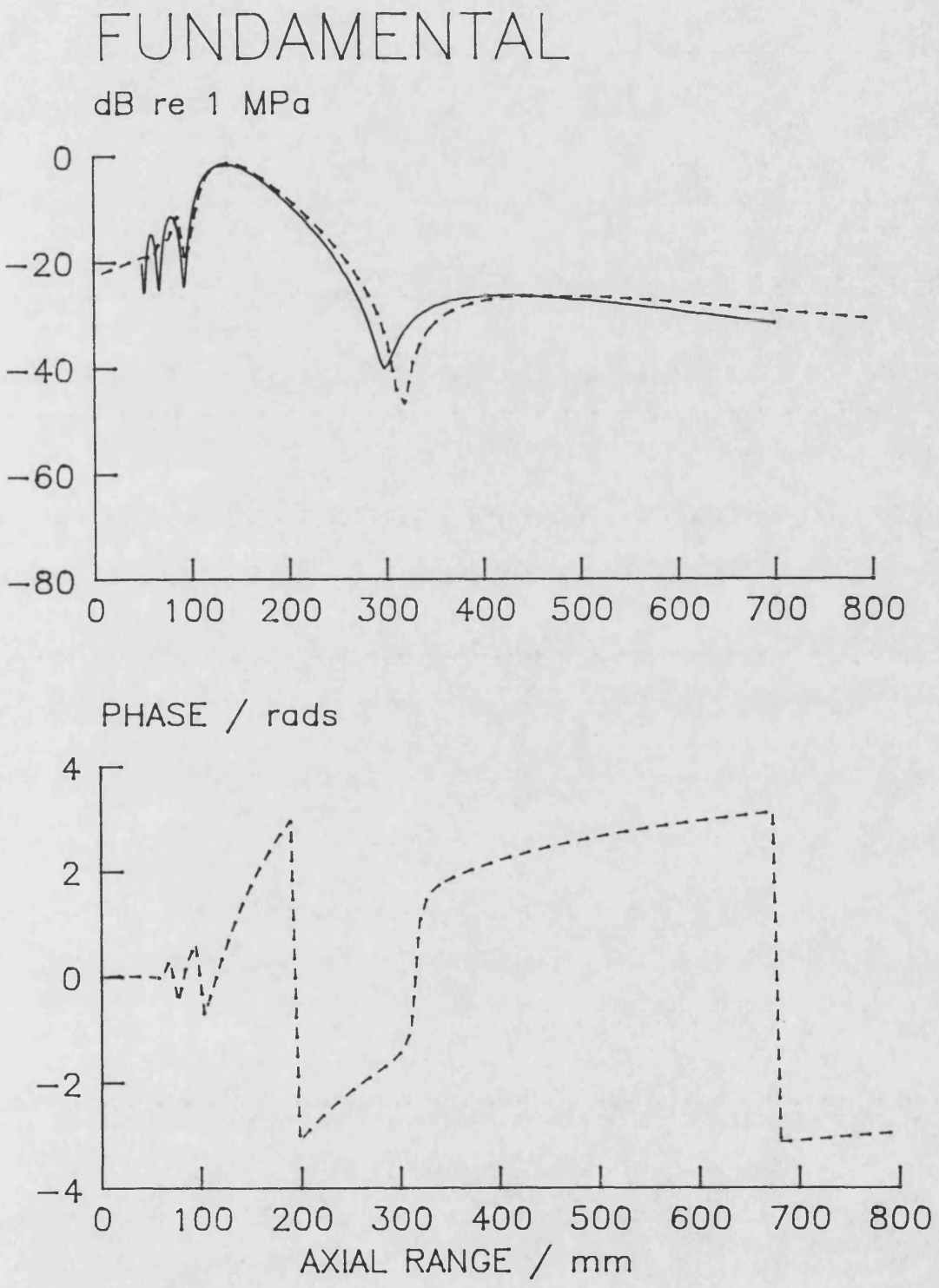

Figure 5 19.
Focused piston (G = 11.9), fundamental amplitude and phase on axis.
Experiment —, theoretical model - -. p_o = 75 kPa.

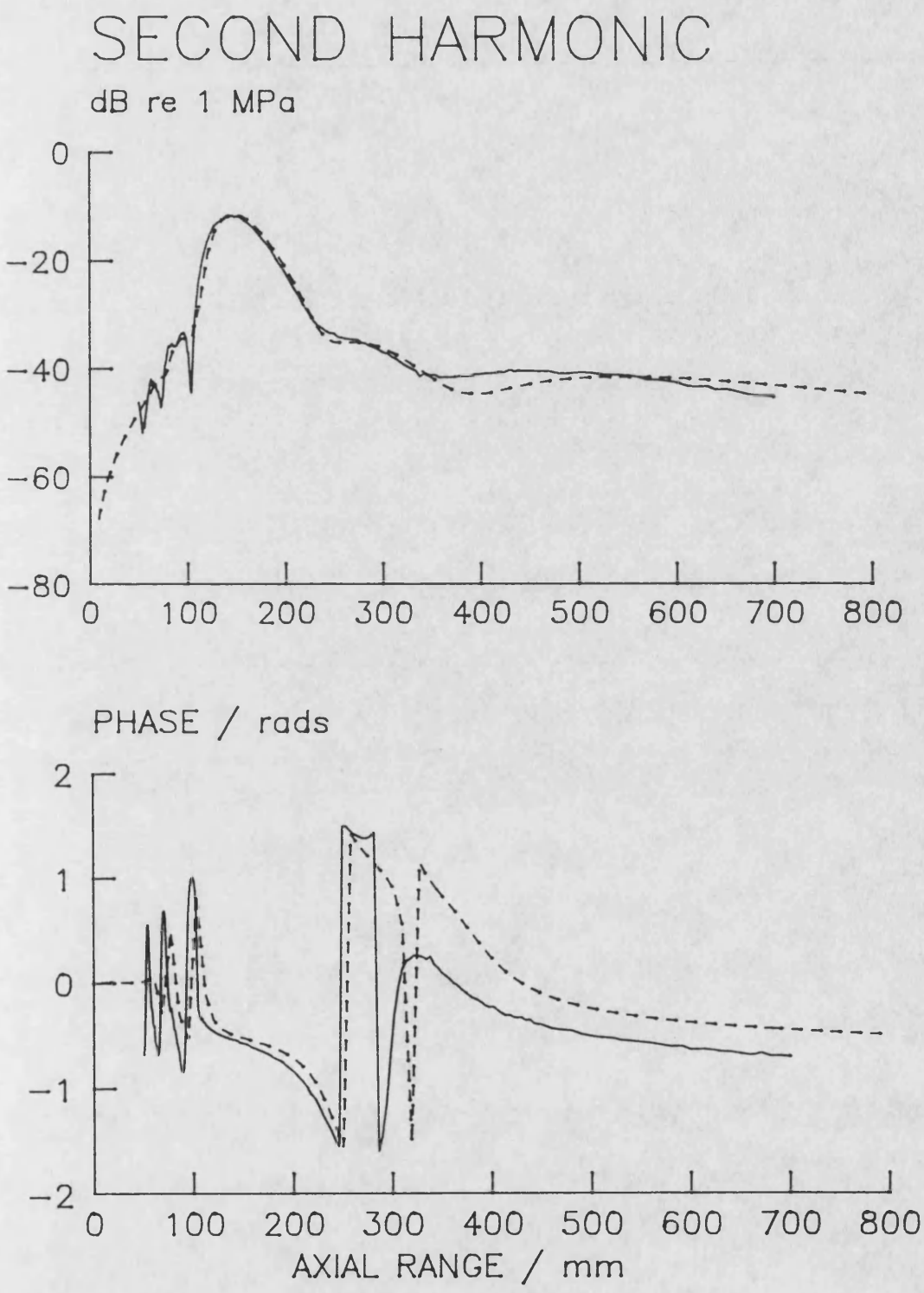

Figure 5.20.
Focused piston (G = 11.9), second harmonic amplitude and phase on axis.
Experiment —, theoretical model - -. p_o = 75 kPa.

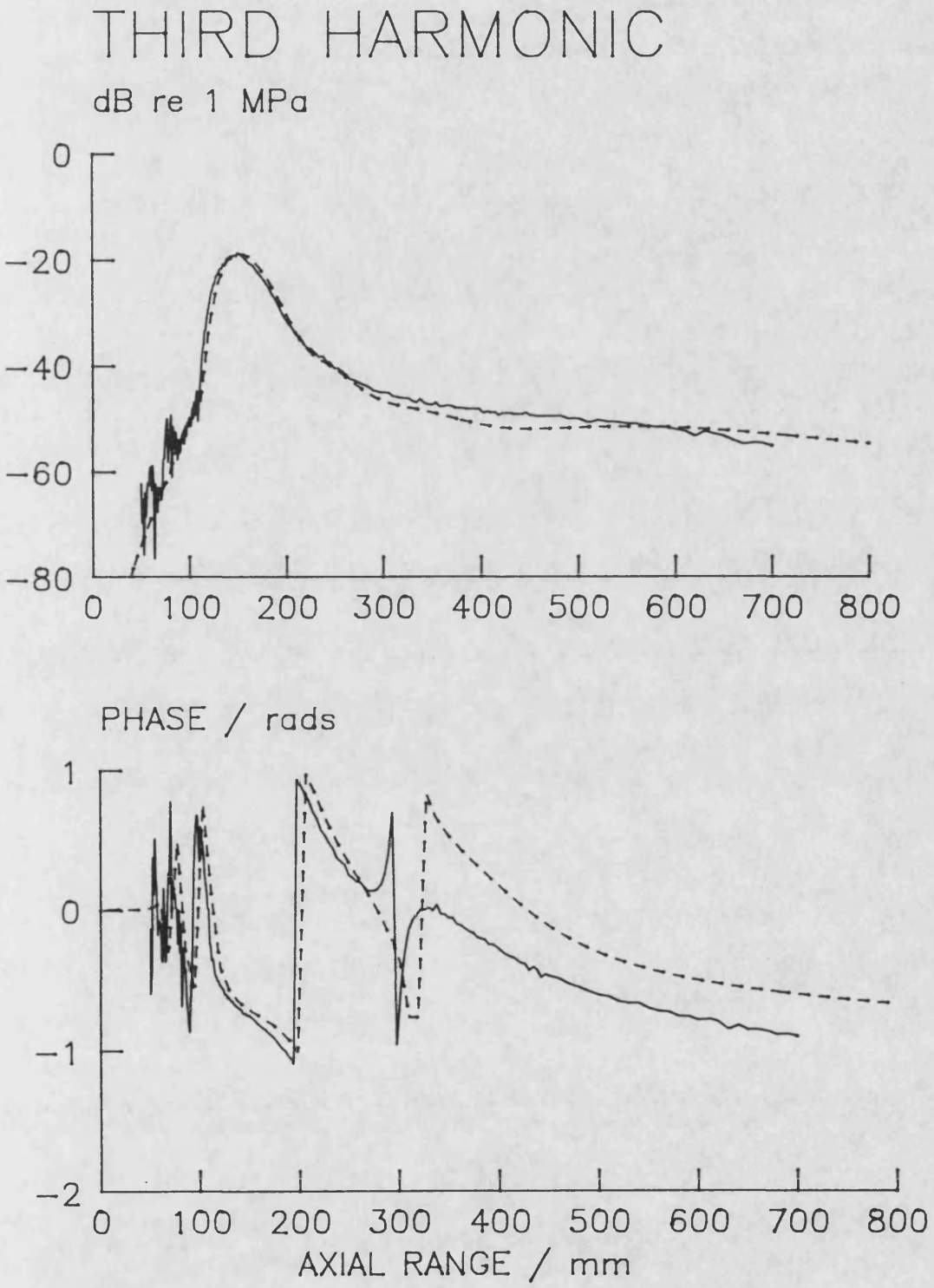

Figure 5.21.
Focused piston (G = 11.9), third harmonic amplitude and phase on axis.
Experiment —, theoretical model - -. p_o = 75 kPa.

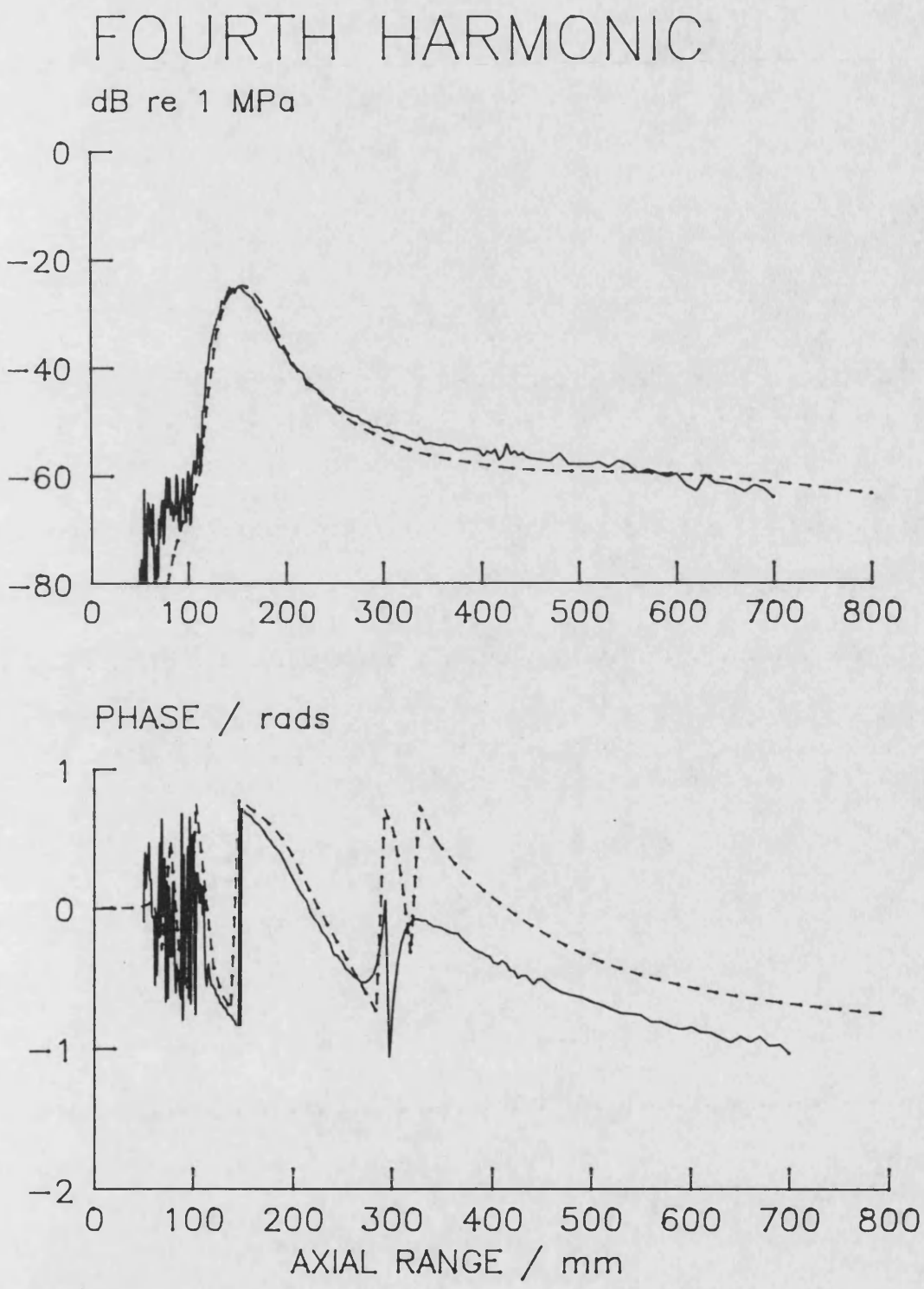

Figure 5.22.
Focused piston (G = 11.9), fourth harmonic amplitude and phase on axis.
Experiment —, theoretical model - -. p_o = 75 kPa.

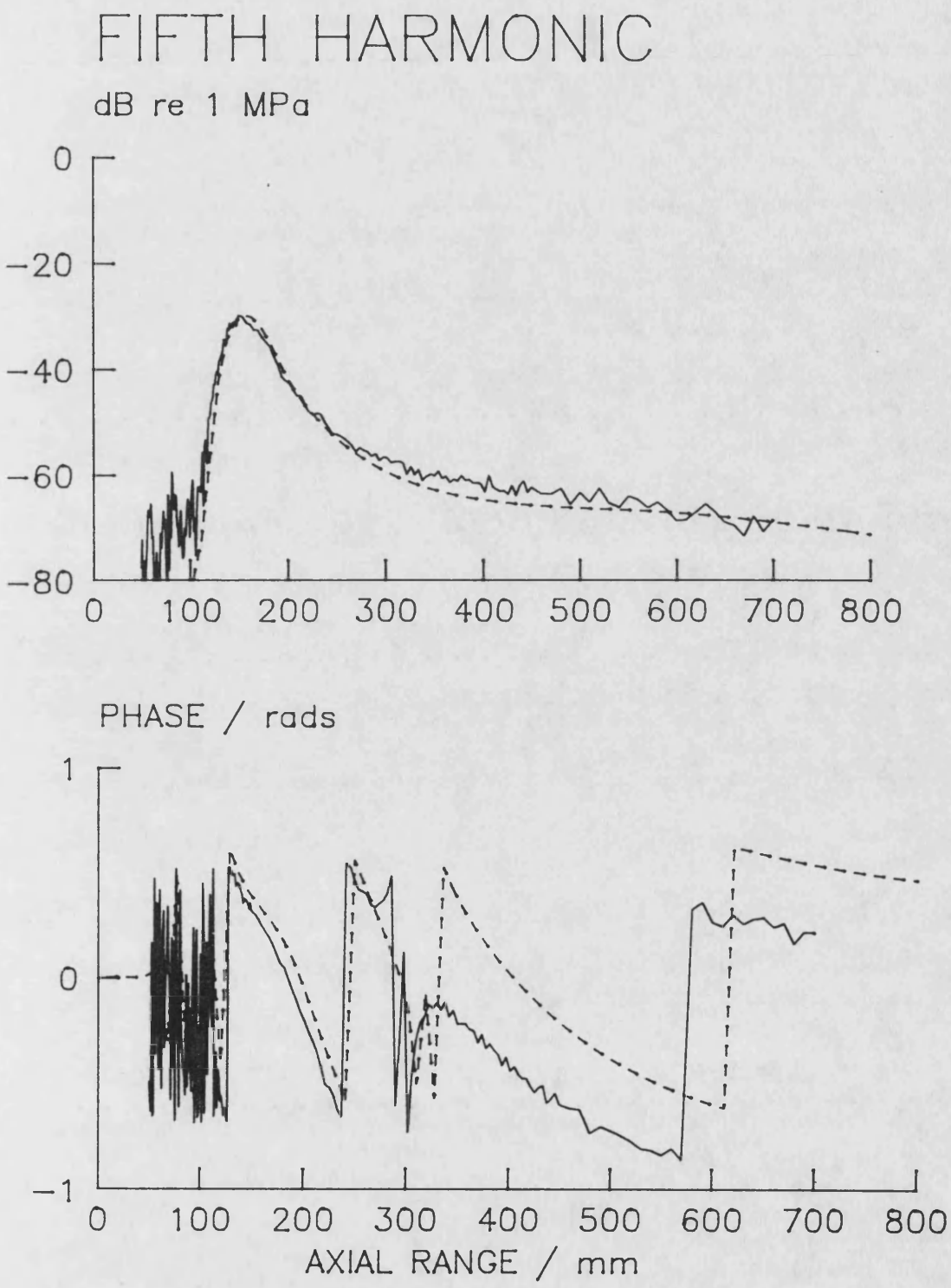

Figure 5.23.
Focused piston (G = 11.9), fifth harmonic amplitude and phase on axis.
Experiment —, theoretical model - -. p_o = 75 kPa.

5.3 RADIAL FIELD

The finite amplitude results for radial sections across the acoustic axis are presented for the low gain system (G = 3.7) at a high drive level (68 kPa). Similar results were obtained for the other systems but these are not included here for the sake of brevity.

Measured radial pressure field

The measured pressure field close to the piston face (z = 30 mm) is shown in Figure 5.24. The fundamental variation is affected by the finite hydrophone size which reduces the rapid oscillations that would expected here. The average pressure at this range is slightly greater than p_o (68 kPa) due to the focusing gain which increases the pressure by a factor of D/(D-z) to give an average pressure of 73 kPa. It can be seen that at this range the beam still has approximately the same radius as the piston (19 mm). The second harmonic is, as expected, almost negligible since the nonlinear distortion has not yet built up.

The measured pressure field through the last axial minimum of the fundamental (z = 160 mm) is shown in figure 5.25. The well pronounced minimum in the fundamental can be seen and the second harmonic has now reached appreciable levels. The second harmonic level is highest off axis at this range due the form of the fundamental pressure field.

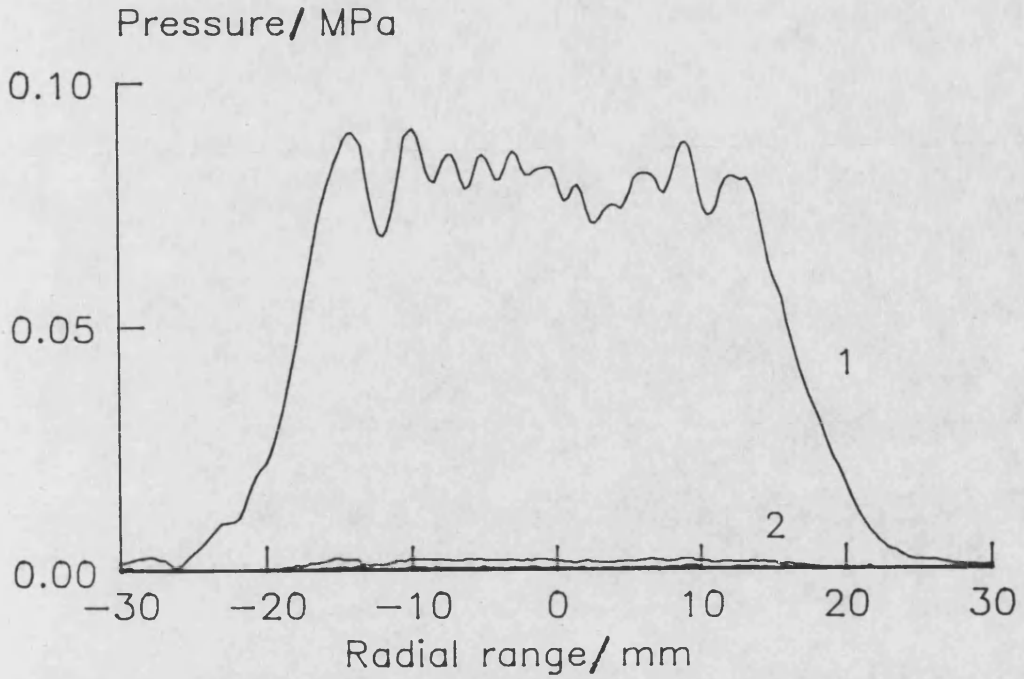

Figure 5.24. Measured radial pressure field close to a focused piston (G = 3.7) First two harmonic amplitudes, axial range (z) = 30 mm.

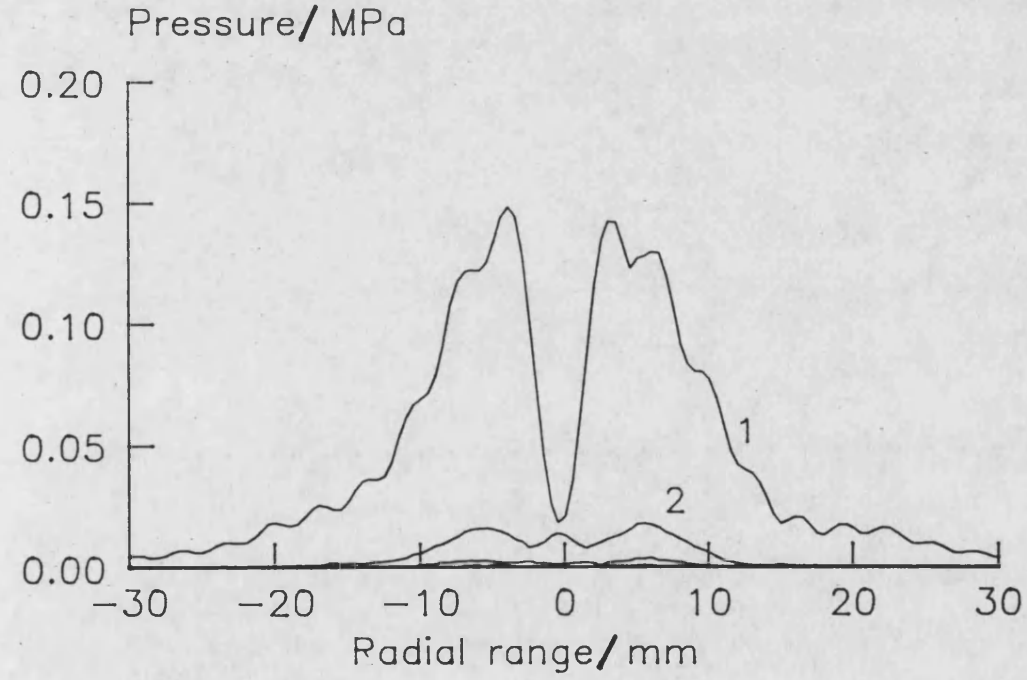

Figure 5.25. Measured radial pressure field through last axial minimum of focused field (G = 3.7) First three harmonic amplitudes, axial range (z) = 160 mm.

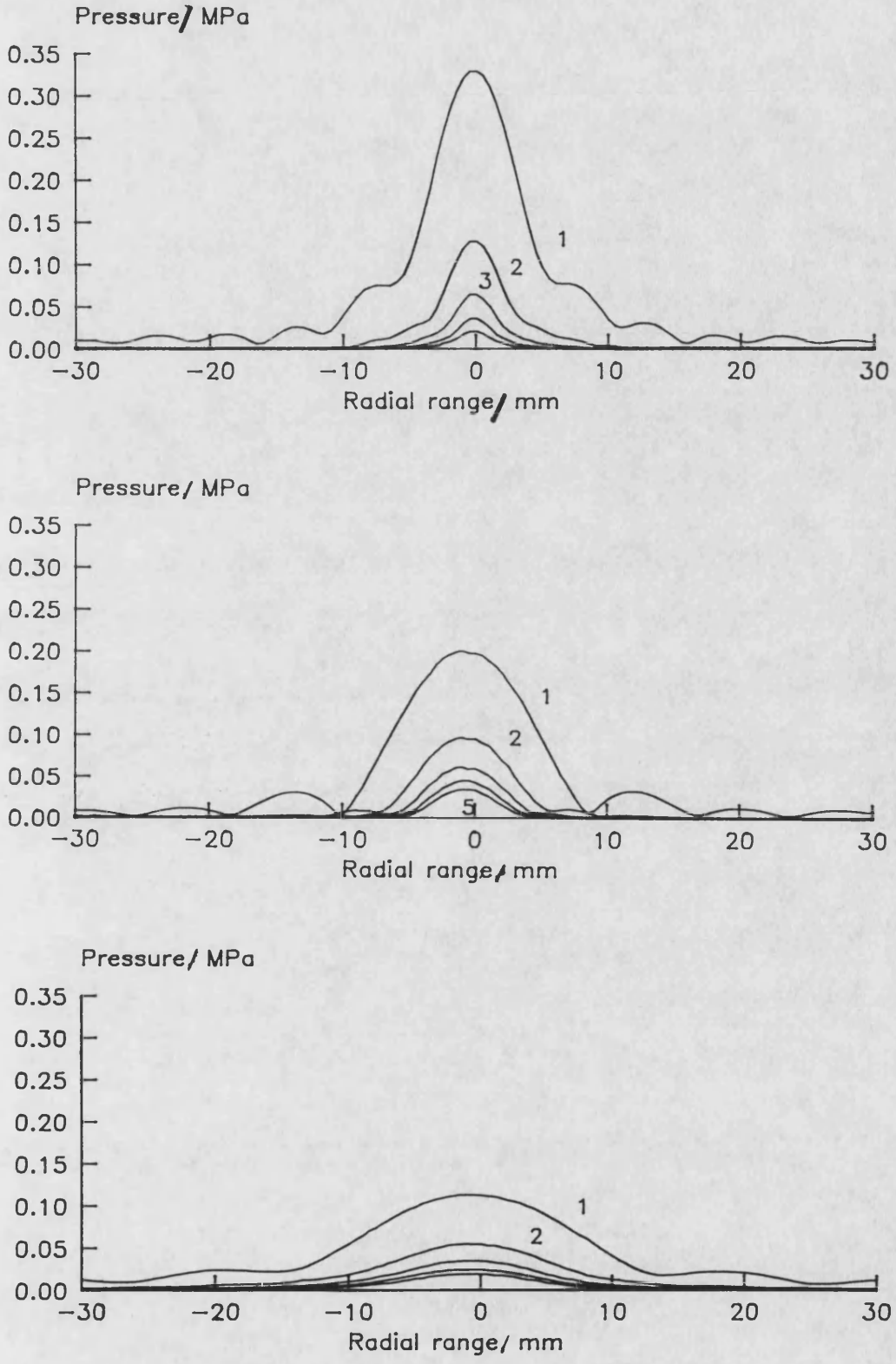

Figure 5.26. Measured radial pressure field of focused piston (G = 3.7, D = 440 mm) first five harmonics. **TOP:** z = 280 mm (Last axial maximum), **MIDDLE:** z = 440 mm (Focal plane), **BOTTOM:** z = 700 mm (Post-focal region).

Figure 5.26 shows the measured radial pressure amplitudes for the first five harmonics in the focal plane (z = D = 440 mm) and on either side of the focal plane (z = 280 and 700 mm). All three plots are plotted with the same vertical scale so it can be seen immediately that the beam is narrower and has greater amplitude on the transducer side of the focal plane (z = 280 mm) and for these reasons many authors mistakenly refer to this position as the focal plane. The notable features of the focal plane are the zeros on either side of the axis (9.5 mm either side). Comparisons with the plots for the maximum axial pressure (z = 280 mm) and in the post-focal region (z = 700 mm) show that out of the focal plane these zeros become minima. All three plots show that at longer ranges the most significant region for harmonic generation is on the acoustic axis within the main lobe.

Comparison with theory

Figures 5.27 to 5.32 compare experimental measurements made across the acoustic axis of the focused system (G = 3.7) with theoretical predictions from the finite difference model, at axial ranges of 280 mm and 440 mm (the last axial maximum and the focal plane respectively). At the shorter range (280 mm) Figure 5.27 shows that the experiment and theory agree well apart from a slight deviation at the extremes of radial range; this is similar to the problem seen at close ranges in the axial plots and is due to the rather large radial step size used in the model. The second harmonic (Figure 5.28) shows good agreement near the axis although the experimental measurements are subject to some noise off axis. The third harmonic level (Figure 5.29) is lower still but again in the central region good predictions are possible for the harmonic amplitude and phase.

In the focal plane the measured fundamental (Figure 5.30) shows good agreement with the theoretical predictions over a much larger range. The agreement is good for the second harmonic amplitude (Figure 5.31) apart from some spatial averaging due to the finite hydrophone size. The agreement in the phase plot does not look so good but this is also partially due to the hydrophone size. The second harmonic amplitude

plot shows a number of minima with each minima having an associated rapid phase shift. Spatial averaging due to the hydrophone will smooth out or displace any rapid phase shifts. This combined with noise in the phase measurements, which causes apparently inappropriate phase shifts in places, may be responsible for the rather poor agreement. The third harmonic (Figure 5.32) suffers from the same problems as the second harmonic but to a greater extent. This problem could be alleviated by using a smaller hydrophone to solve some of the spatial averaging problems but a smaller hydrophone would almost certainly have a lower sensitivity and this would increase the noise problem unless waveform averaging were used.

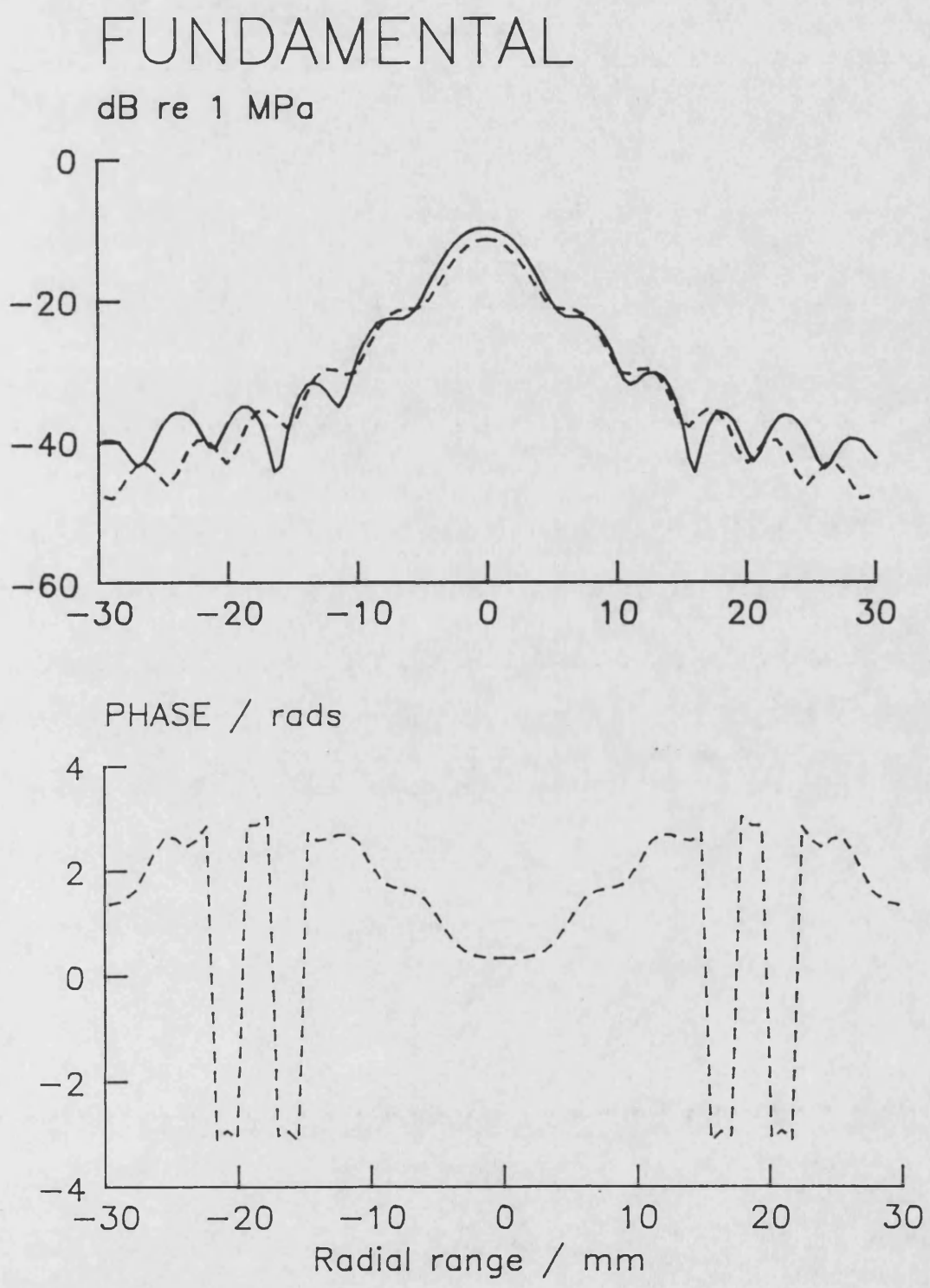

Figure 5.27. Radial pressure field, z = 280 mm.
Focused piston (G = 3.7), fundamental amplitude and phase.
Experiment —, theoretical model - -.

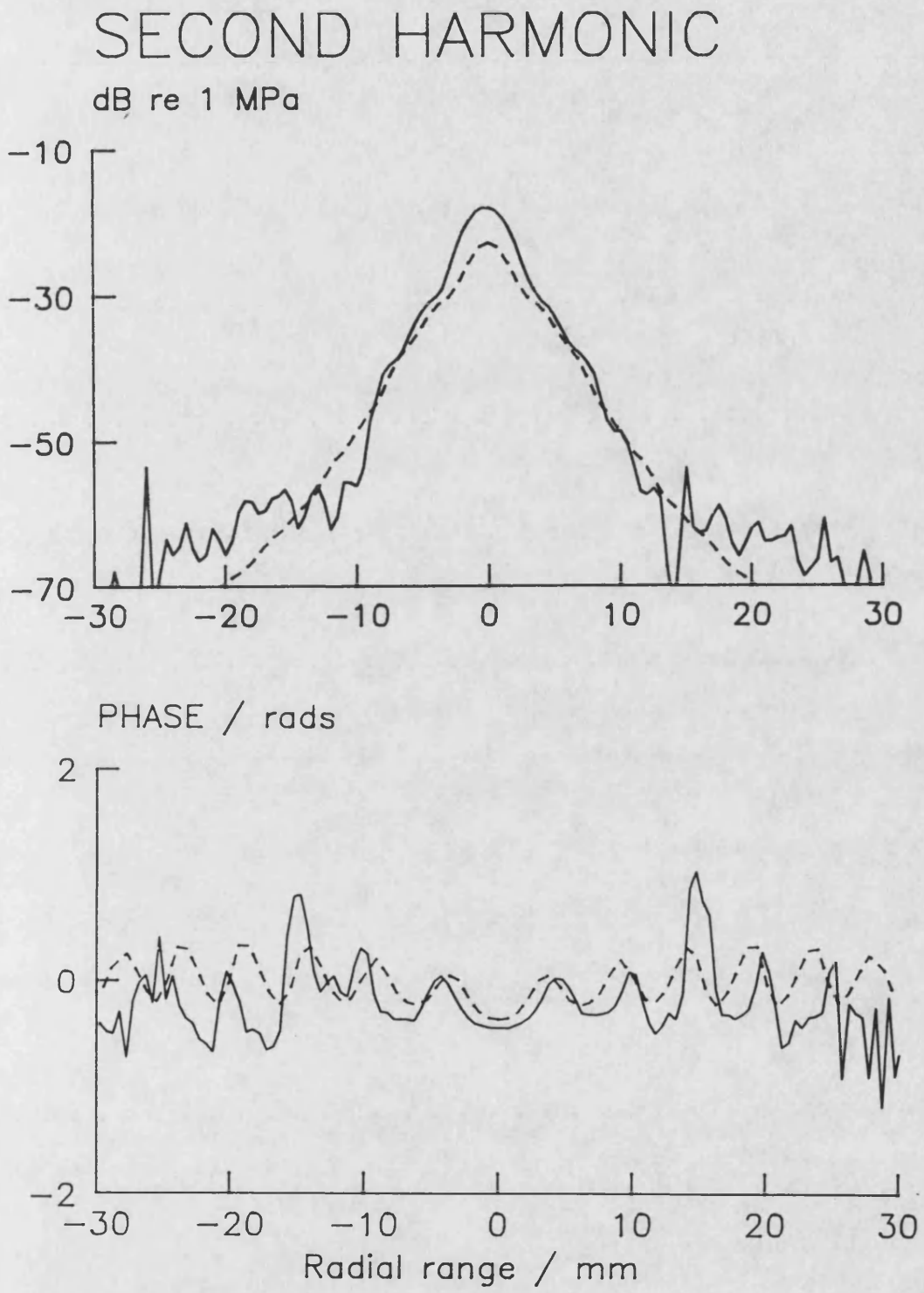

Figure 5.28. Radial pressure field, z = 280 mm.
Focused piston (G = 3.7), second harmonic amplitude and phase.
Experiment —, theoretical model - -.

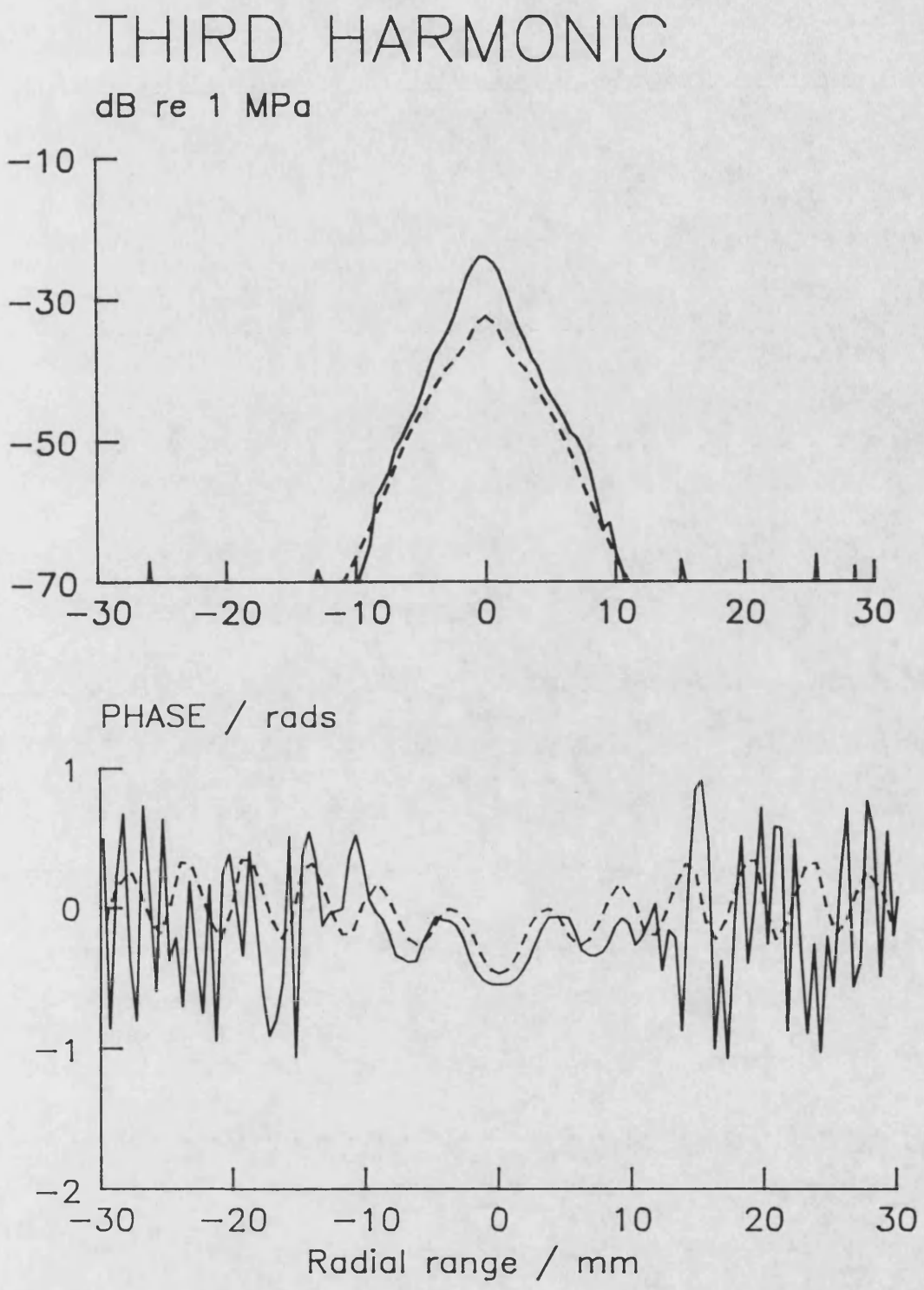

Figure 5.29. Radial pressure field, z = 280 mm.
Focused piston (G = 3.7), third harmonic amplitude and phase.
Experiment —, theoretical model - -.

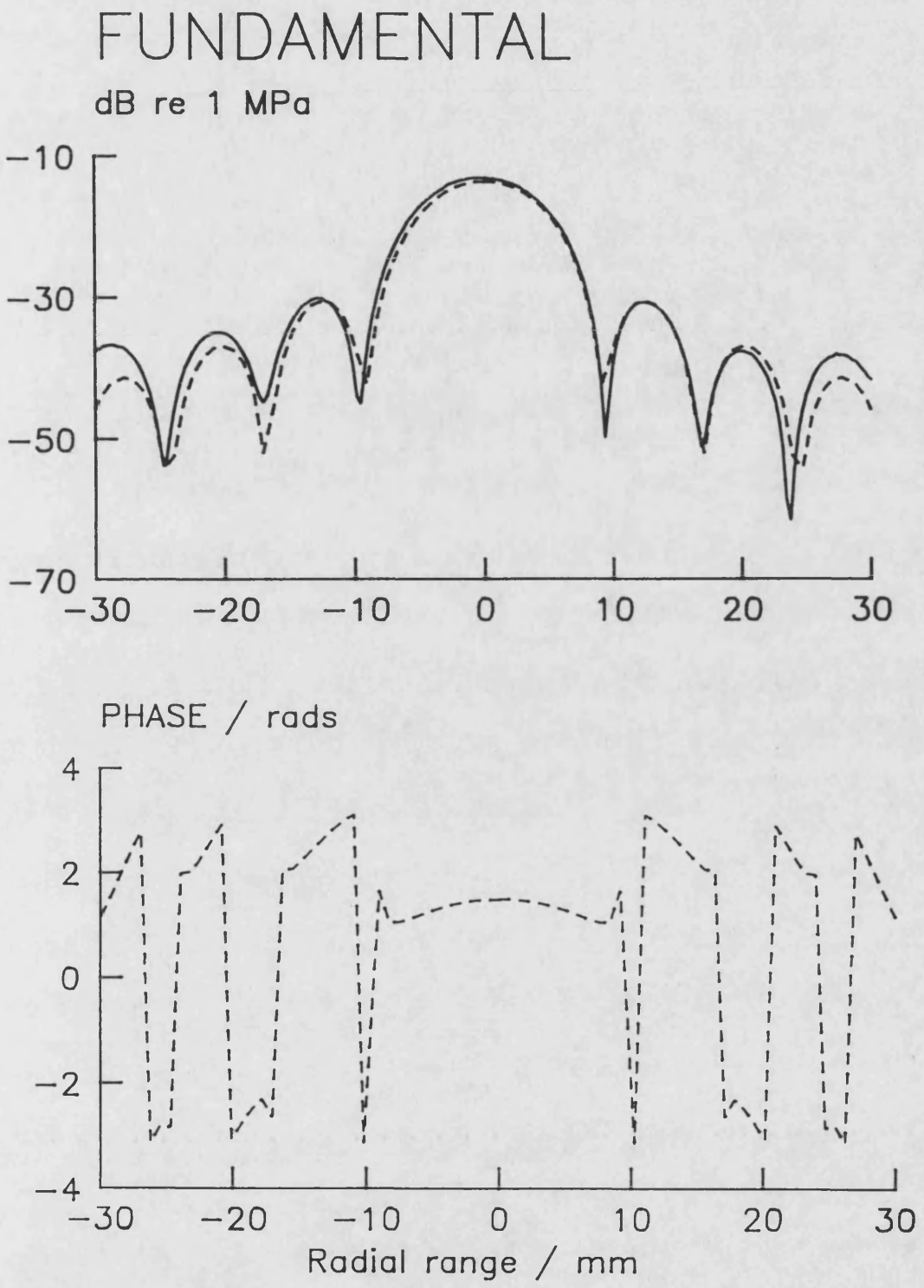

Figure 5.30. Radial pressure field, z = 440 mm.
Focused piston (G = 3.7), fundamental amplitude and phase.
Experiment —, theoretical model - -.

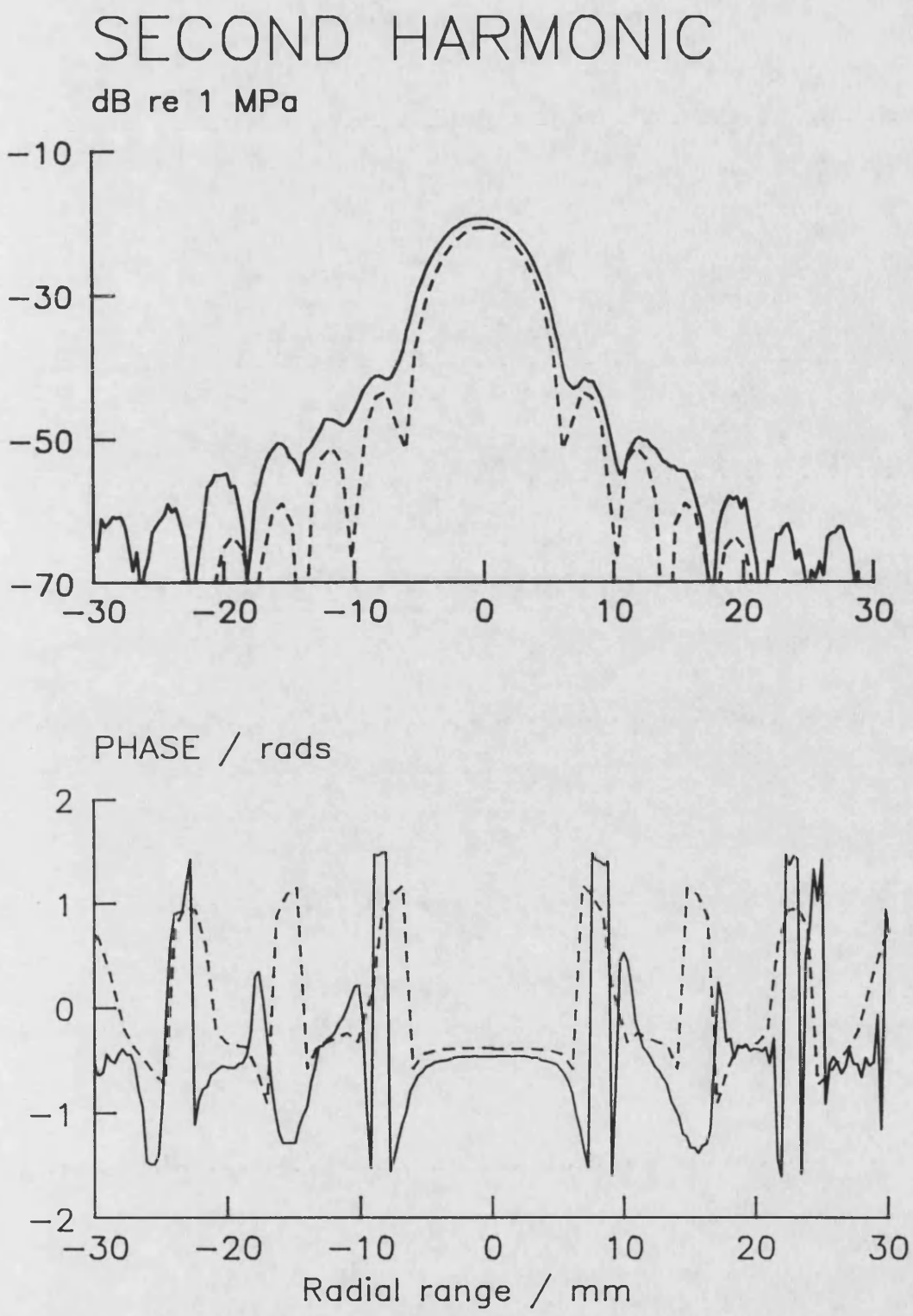

Figure 5.31. Radial pressure field, z = 440 mm.
Focused piston (G = 3.7), second harmonic amplitude and phase.
Experiment —, theoretical model - -.

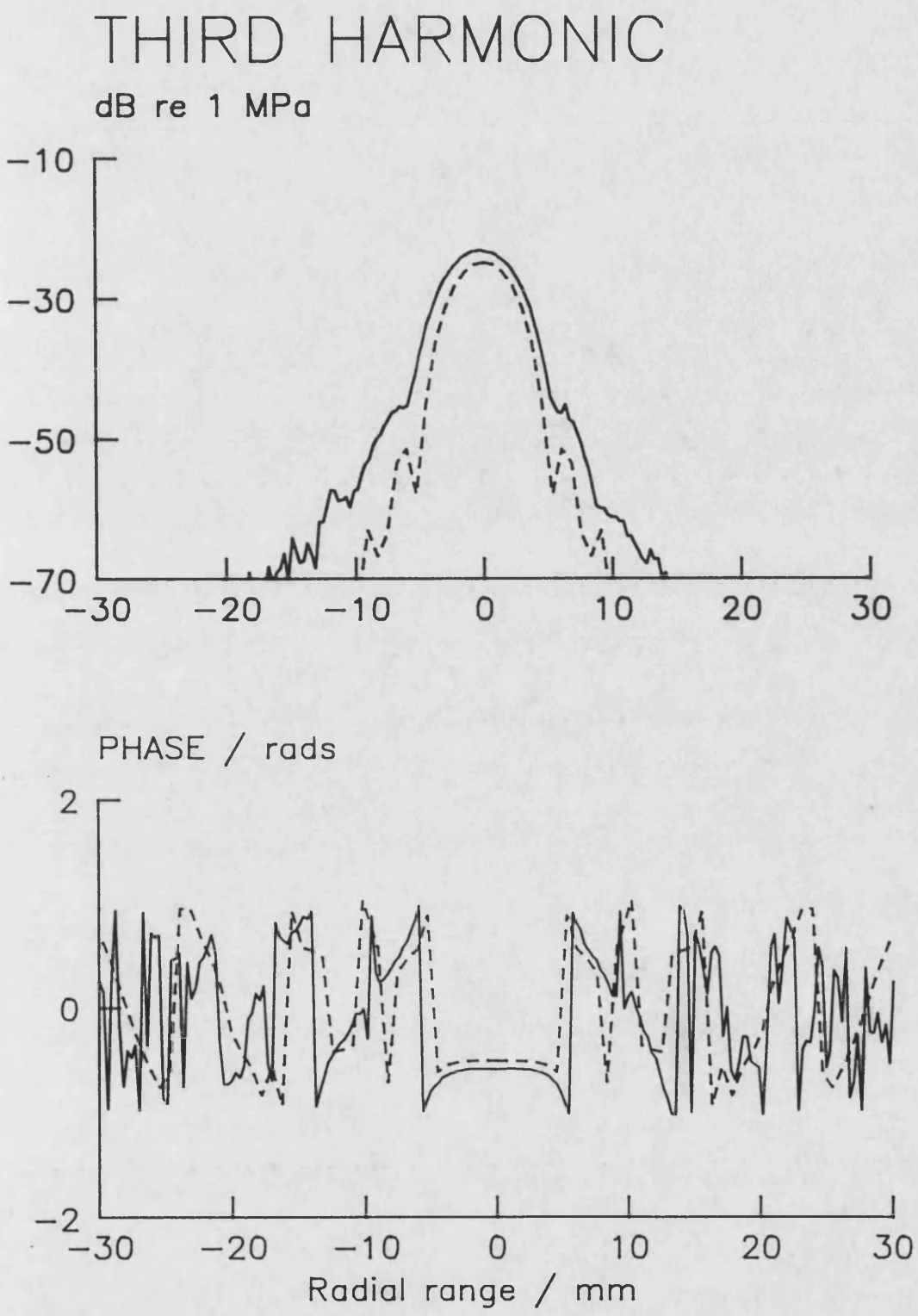

Figure 5.32. Radial pressure field, z = 440 mm.
Focused piston (G = 3.7), third harmonic amplitude and phase.
Experiment —, theoretical model - -.

Approximate analysis for the focal plane

O'Neil [1949] showed that for the small signal case the radial pressure variation in the focal plane follows the far-field directivity function of a plane piston radiator:

$D(\Theta) = 2J_1(ka \sin\Theta)/ka \sin\Theta$.

In addition Lockwood et al [1973] showed that for a plane piston the far-field directivity function for the n^{th} harmonic is approximately:

$D_n(\Theta) \approx [D(\Theta)]^n$.

These approximate results are shown in Figures 5.33 to 5.36, the experimental results having been normalised to give the fundamental a maximum value of unity (0 dB).

The fundamental (Figure 5.33) shows good agreement with $D(\Theta)$ although such good agreement would not be expected at higher drive levels since energy would be lost from the axial direction and this would give the impression of higher side lobes. The finite difference model, however, would still give valid results.

The second harmonic measurements are plotted against two functions, first (Figure 5.34) against $2J_1(2ka \sin\Theta)/2ka \sin\Theta$, i.e. the directivity pattern for direct transmission at the second harmonic frequency and second (Figure 5.35) against $[2J_1(ka \sin\Theta)/ka \sin\Theta]^2$ which is the fundamental directivity squared. It can be seen that compared with direct transmission of the second harmonic (Figure 5.34) the nonlinearly generated levels of second harmonic have a wider beam width although the side-lobe levels are lower. Figure 5.35 shows that $[D(\Theta)]^2$ is a good approximation to the nonlinearly generated second harmonic in the main lobe; similarly Figure 5.36 shows that $[D(\Theta)]^3$ approximates well to the third harmonic in the main lobe.

It can be seen from Figure 5.35 that this approximate analysis does not account for the additional side-lobes (sometimes referred to as fingers) that are observed experimentally in the second harmonic; the first pair occur at about 9 mm on either

side of the axis. Lockwood et al [1973] attributed these fingers to direct transmission of second harmonic from the transducer but the finite difference model shows that they are due to nonlinear generation (cf. Figure 5.31).

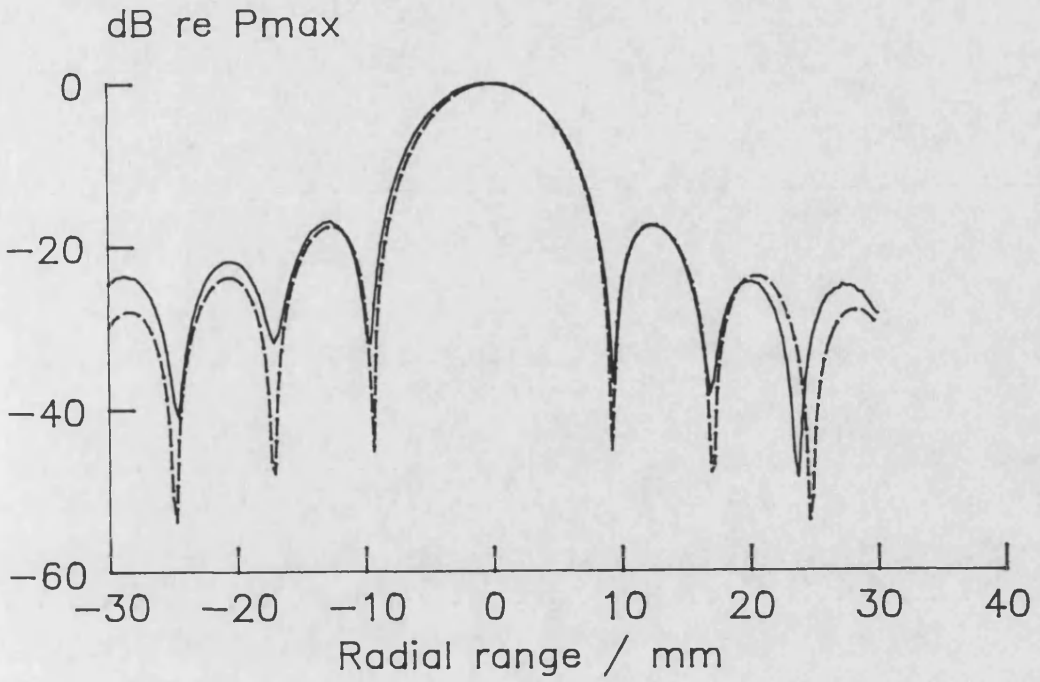

Figure 5.33. Fundamental radial pressure field, z = 440 mm (focal plane) focused piston (G = 3.7). Experiment —, $2J_1(ka \sin\Theta)/ka \sin\Theta$ - -.

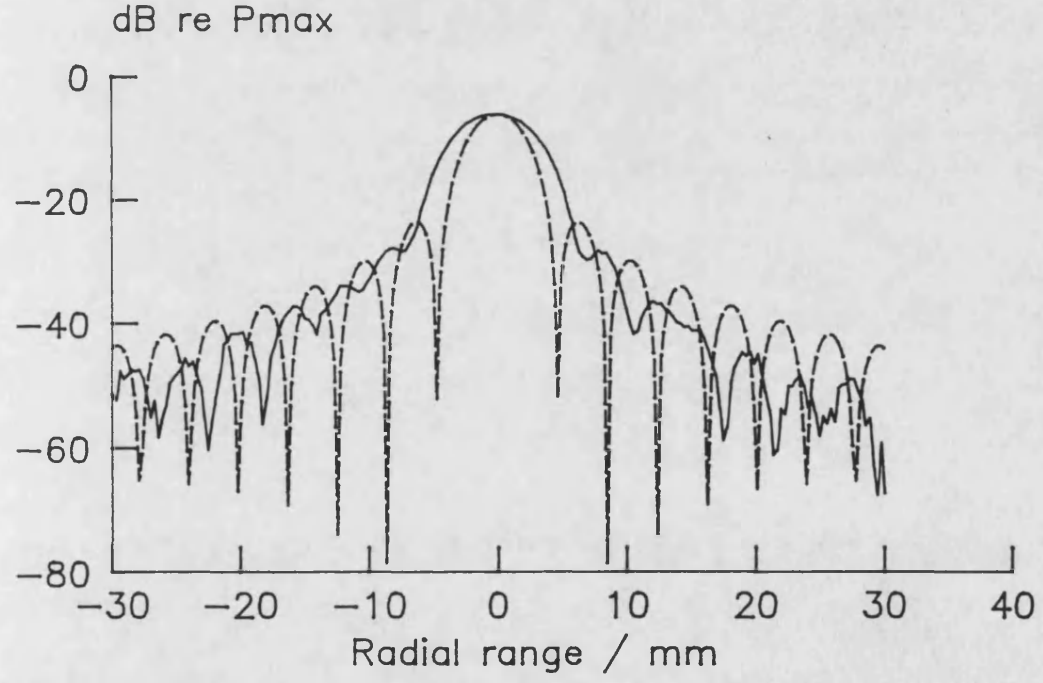

Figure 5.34. Second harmonic radial pressure field, z = 440 mm (focal plane) focused piston (G = 3.7). Experiment —, $2J_1(2ka \sin\Theta)/2ka \sin\Theta$ - -.

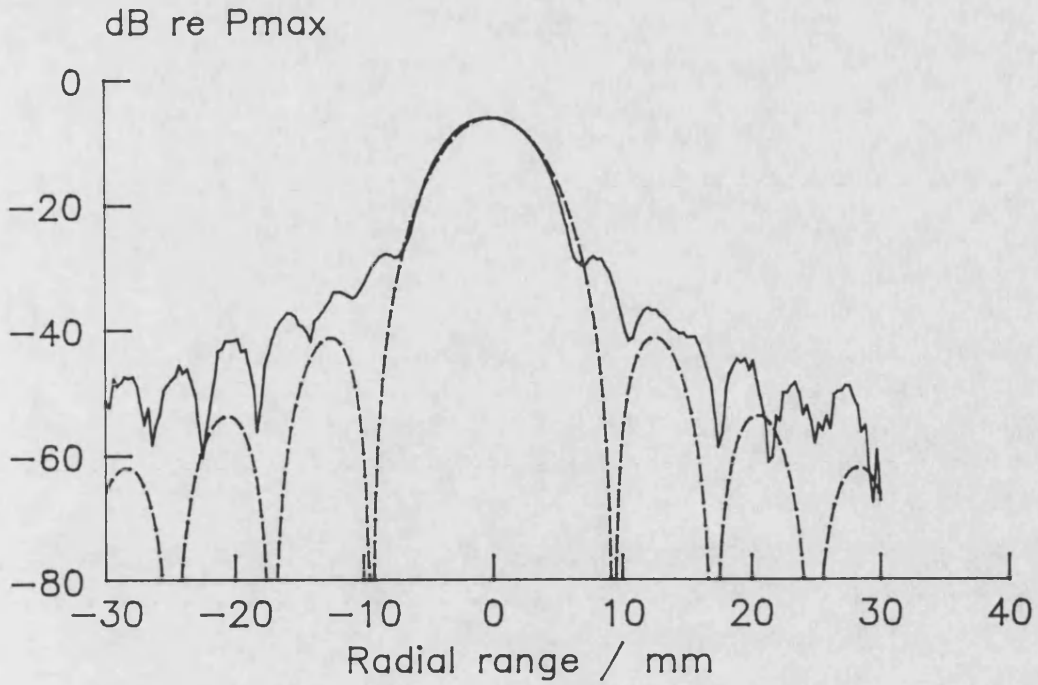

Figure 5.35. Second harmonic radial pressure field, z = 440 mm (focal plane) focused piston (G = 3.7). Experiment —, $[2J_1(ka \sin\Theta)/ka \sin\Theta]^2$ - -.

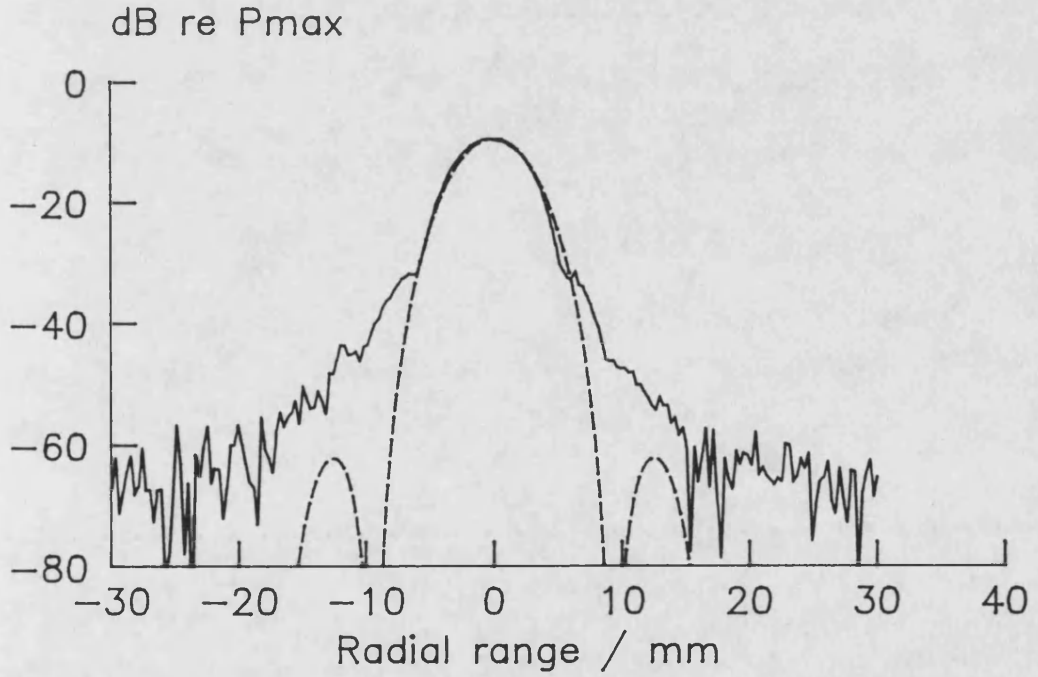

Figure 5.36. Third harmonic radial pressure field, z = 440 mm (focal plane) focused piston (G = 3.7). Experiment —, $[2J_1(ka \sin\Theta)/ka \sin\Theta]^3$ - -.

5.4 EFFECT OF DRIVE LEVEL

The effect of the drive level on the relative harmonic amplitudes and phases is shown in Figure 5.37. The measurements were made on the axis of the plane piston at a range of 700 mm and are compared with theoretical predictions (solid lines). The fundamental amplitude is normalised to the expected level for the small signal case and the other harmonics are multiplied by the same factor. Thus if the system were linear the fundamental would remain constant at unit normalised amplitude. Nonlinear effects (that is, the generation of harmonics) cause energy to be lost from the fundamental into the harmonics, and hence a reduction in amplitude of the fundamental occurring at drive levels above about 50 kPa.

It can be seen that at the lowest drive levels there was no harmonic generation. The harmonics then grow fairly linearly in the region up to 50 kPa. Note that a linear increase in relative levels actually refers to a square law increase in absolute levels because of the normalisation use in these figures. Above 50 kPa the relative fundamental level starts to decrease due to saturation and eventually at drive levels over about 100 kPa the harmonics assume a fairly constant ratio (1/n) with the fundamental, i.e. the second harmonic is about 1/2 of the fundamental, the third is 1/3 of the fundamental. At the highest drive level used here the fundamental amplitude is reduced to half of its expected (small signal) level.

The corresponding phase plot shows the relative harmonic phases for the second to fourth harmonics; from this it appears that there are two limiting cases. At low drive levels the phase shifts appear to remain fairly constant, whereas at higher drive levels the phase shift decreases until a saturation level is reached. Note that the theoretical model does not suffer from random noise at low amplitudes as the experimental measurements do. The fundamental phase (not plotted here) appeared to increase fairly linearly from 0.34 radians at the lowest drive level to 0.38 radians at the highest drive level.

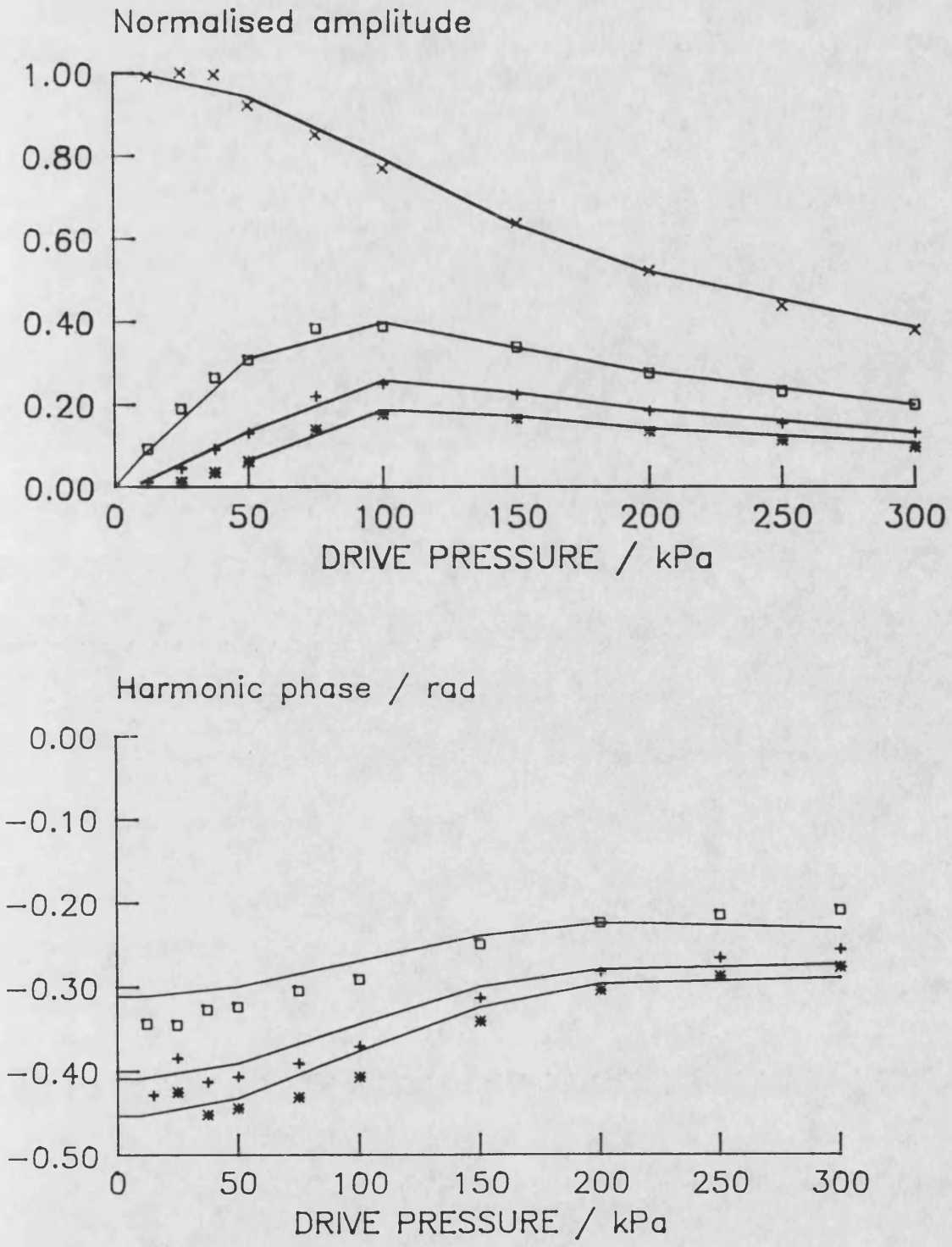

Figure 5.37. Effect of drive level on normalised harmonic amplitudes and phases. Plane piston, on axis, z = 700 mm. Theory —, Experiment; x o + * harmonics 1, 2, 3 and 4 respectively.

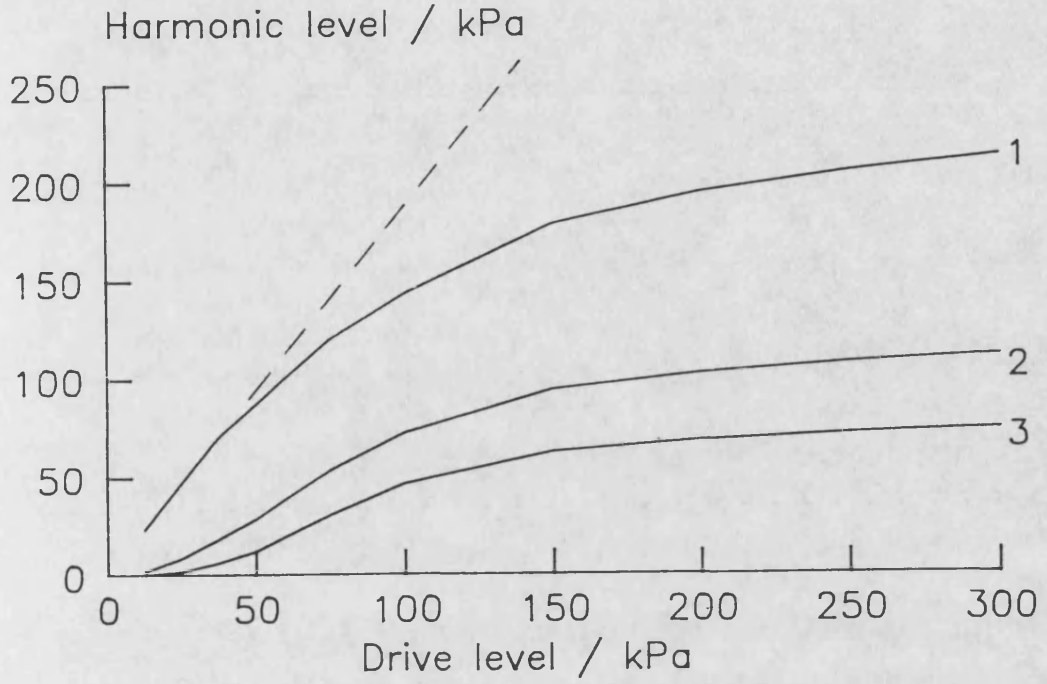

Figure 5.38. Effect of drive level on predicted harmonic amplitudes and phases. Plane piston, on axis, z = 700 mm. (Linear theory fundamental denoted by dashed line.)

An alternative representation of the amplitudes in Figure 5.37 is shown in Figure 5.38, where instead of normalising the amplitude to the pressure expected in the small signal case the amplitudes are plotted in absolute pressure. This has the advantage of showing clearly that the acoustic beam is saturating. In a linear system no harmonics are generated and the fundamental increases in direct proportion to the drive level (denoted by the dashed line). At drive levels up to about 50 kPa the fundamental follows linear theory closely and although low levels of second and third harmonic are generated it is at negligible cost to the fundamental. In this region a perturbation approach could be used successfully to model the nonlinear effects. At drive levels above 50 kPa the fundamental departs from linear theory until at 300 kPa the fundamental is less than half the value predicted by linear theory. At this level the fundamental has also almost ceased to change with drive level, i.e. saturation has occurred, and any further increase in drive level will fail to increase the fundamental

pressure at this point in the field. Instead the extra energy put into the beam is pumped up into the higher harmonics and dissipated as thermal energy. At these drive levels a full nonlinear model must be used to account for energy transfer between the fundamental and the harmonics. It is worth noting that in this particular case saturation is being approached at pressures as low (by medical ultrasound standards) as 300 kPa.

5.5 TIME DOMAIN MEASUREMENTS

There are two problems that arise when using the time domain representation of distorted waveforms:

1. Quantitative comparisons are difficult to make in the time domain whereas in the frequency domain comparisons can be made for the amplitude and phase of each harmonic.

2. In order to get accurate time domain representations of highly distorted waveforms very wide bandwidths are required from the instrumentation, whereas frequency domain comparisons can be made over the limited reliable calibration range of the instrument. In particular, the effects of hydrophone resonances can be removed relatively easily in the frequency domain.

There are occasions however when a time domain representation is useful, especially in qualitative comparisons of pulsed waveforms, and this section presents some time domain results.

Variation of time waveform with drive level

Figure 5.39 shows the effect of increasing drive level on the time waveform on axis at a distance of 700 mm from the plane piston transducer. At the lowest drive level (p_o = 12.5 kPa) the observed waveform is sinusoidal and shows no sign of distortion. At

37.5 kPa the waveform has started to distort and the tops of the waveform have started to "lean" to the left. At 75 kPa the rising edge of the waveform is starting to resemble a step change in pressure and the waveform has taken on a sawtooth appearance. There is a marked top-bottom asymmetry, caused by the phase shifts between the harmonics. This leads to a higher peak positive pressure than peak negative pressure; in this case they are in a ratio of about 2:1. There is also some evidence of the hydrophone resonance just after the peak positive pressure. The hydrophone resonance is clearly visible in the time waveform for the highest drive level (300 kPa). The resonant frequency of the hydrophone membrane was about 22 MHz so it is manifest as ripple at about the tenth harmonic of the driving frequency (2.25 MHz).

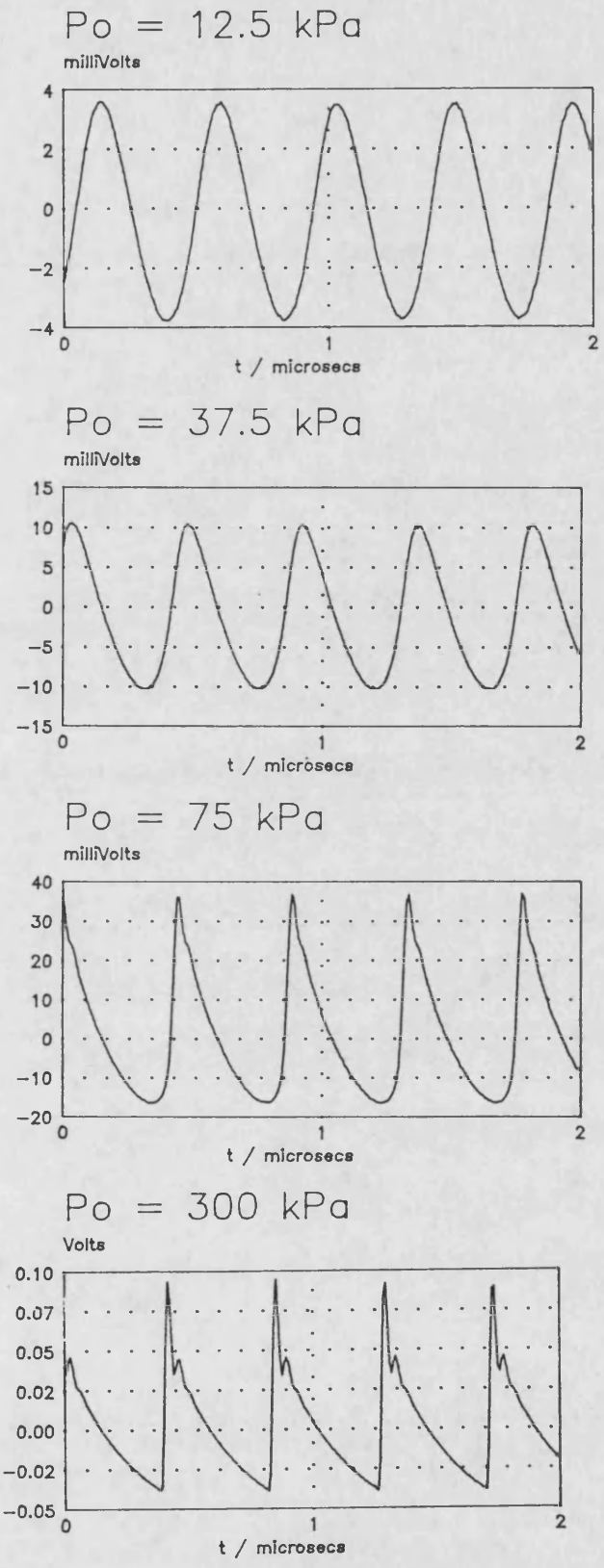

Figure 5.39. Effect of drive level on the observed time waveform, on axis, at 700 mm from the plane piston. Drive at piston face = 12.5 kPa, 37.5 kPa, 75 kPa and 300 kPa.

Variation of time waveform with position

Two transducer configurations were considered, namely the plane piston and the highest focusing gain (G = 11.9). Observed time waveforms from different positions in their pressure fields are presented in figures 5.40 and 5.41 along with corresponding axial plots of the first 5 harmonic levels.

Plane piston

The plane piston case (Figure 5.40) shows the waveform to be sinusoidal at short ranges (z = 105 mm) where the second harmonic level is still low. At the position of the last axial minimum in the fundamental (z = 275 mm) the low level of the fundamental enables the large second harmonic component produced in the region before the minimum to be observed. At an axial range of 430 mm the waveform is starting to resemble a sawtooth wave and by 640 mm the distortion has built up to give marked top-bottom asymmetry, a shock front on the rising edge and the hydrophone resonance are clearly visible. Holding the axial range at 640 mm and moving off axis 10 mm shows a sawtooth waveform of reduced amplitude but with more symmetry (apart from the hydrophone resonance). At this point in the pressure field all of the harmonics are in phase so that the waveform is symmetrical; this appears to occur at the angle at which the first minima will occur in the fundamental far-field directivity pattern.

Focused piston

The focused case (Figure 5.41) shares some common features with the plane case: the waveform is sinusoidal at short axial ranges (z = 77 mm) and there is a high level of second harmonic at the last (pre-focal) axial minimum (z = 92 mm). On axis, in the focal plane (z = 147 mm, r= 0 mm) the waveform shows the usual nonlinear distortion but moving off axis to the first minimum in the radial direction in the focal plane (z = 147 mm, r = 3.3 mm) shows almost pure second harmonic albeit at a low level. Returning to the axial waveforms, at an axial range of 230 mm the waveform is no longer a sawtooth but shows a bowl type of waveform with even symmetry. This

waveform has the same ratios for the harmonic amplitudes (1/n) but the phase angles are all $\pi/2$. At the position of the post focal minimum (z = 320 mm) an even more unusual waveform can be seen which is mostly second harmonic but with the peaks alternating between distorted and undistorted.

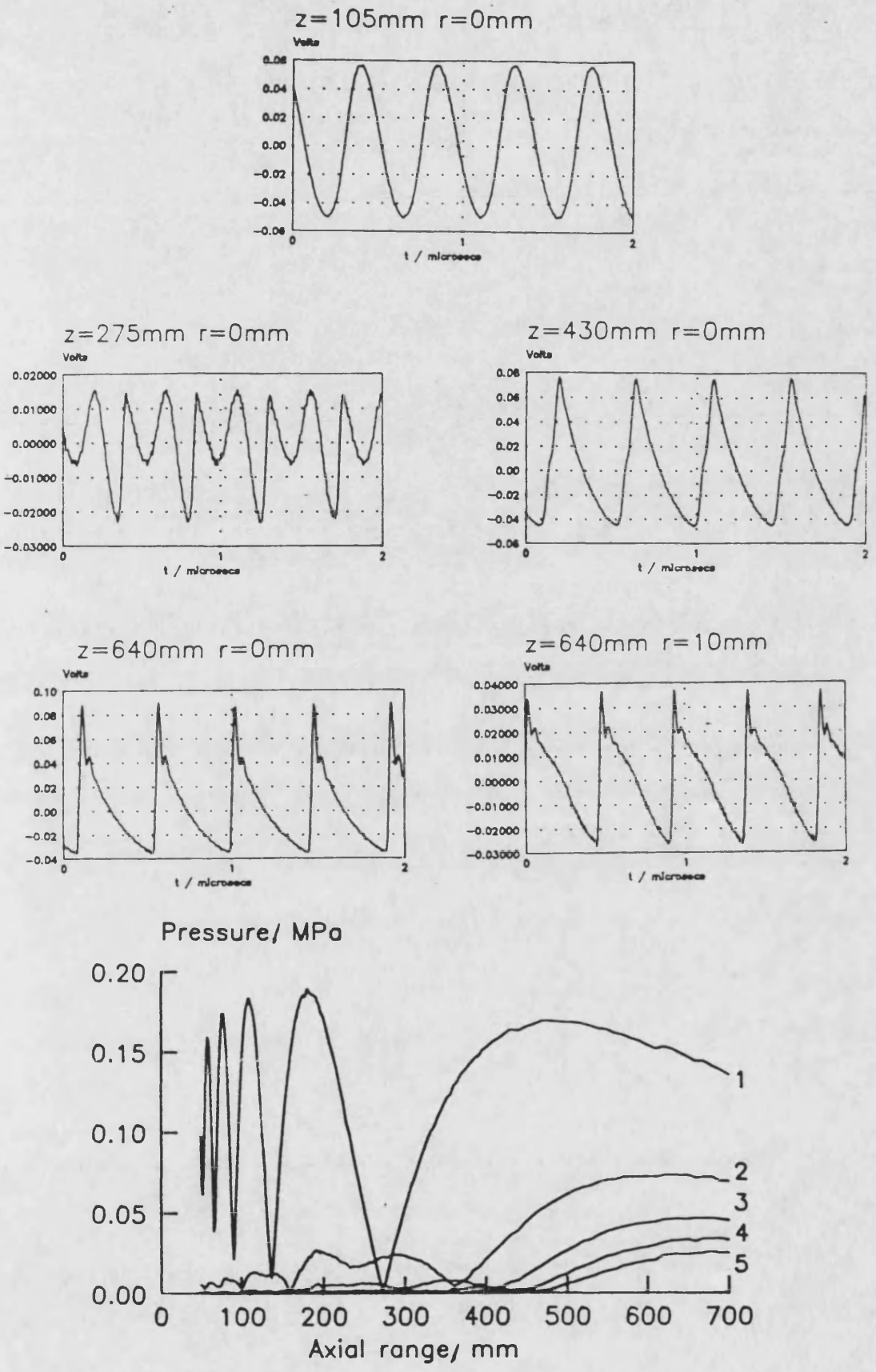

Figure 5.40. Measured variation of time waveform with position in the plane piston field (p_o = 100 kPa) Axial coord. = z, radial coord. = r. (Axial variation in first 5 harmonics shown at bottom.)

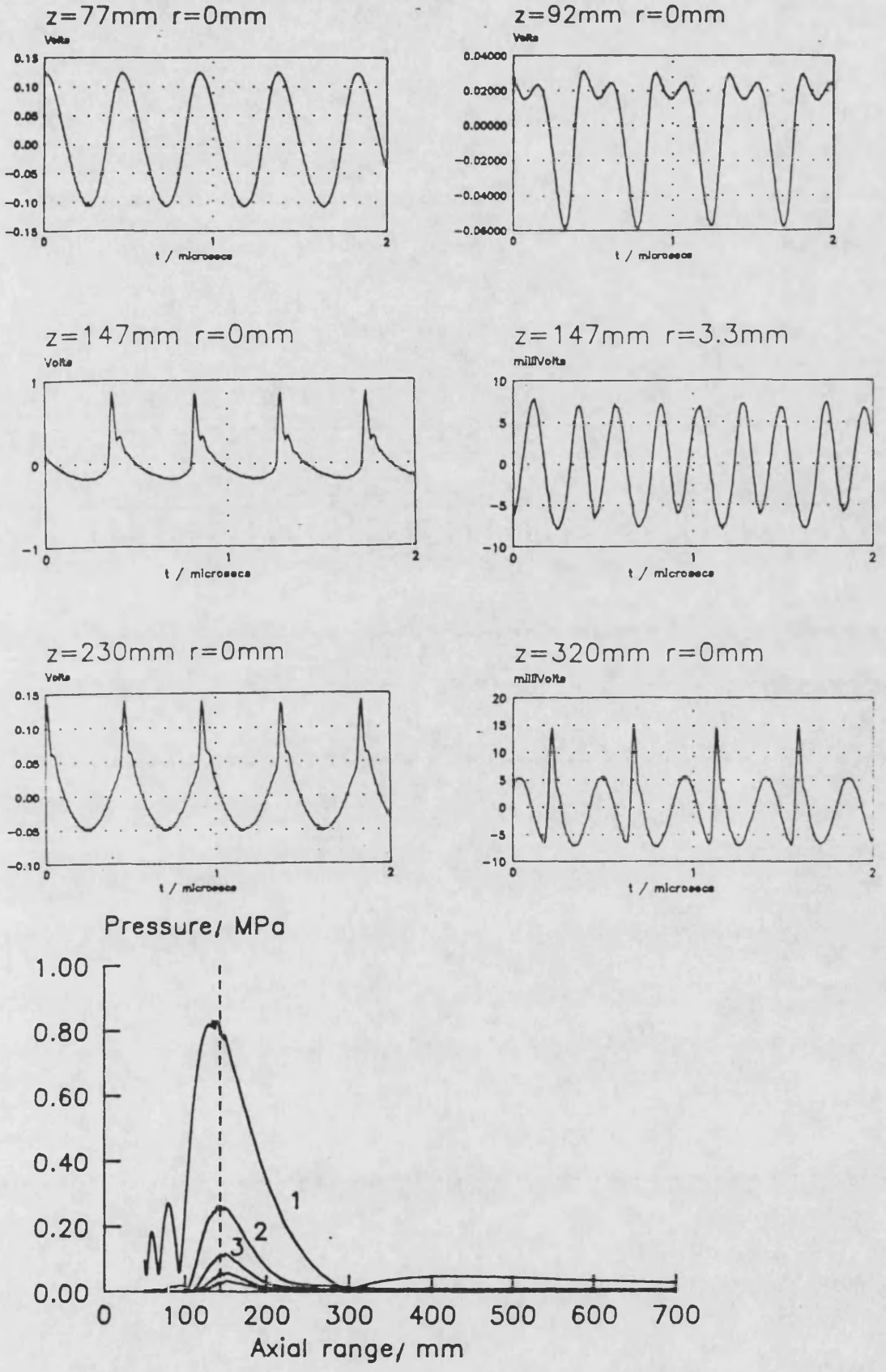

Figure 5.41. Measured variation of time waveform with position in the focused piston field (G = 11.9, p_o = 75 kPa) Axial coord. = z, radial coord. = r. (Axial variation in first 5 harmonics shown at bottom.)

5.6 PULSED FIELDS

Measurements were made on the shock excited plane piston and compared with the finite difference model. The level of nonlinearity was deliberately kept low since the number of frequency components required in the theoretical model is significantly increased for the pulsed case.

The drive waveform (Figure 5.42) was obtained by measuring the pressure field close to the transducer face (z = 15 mm) where the edge wave and central plane wave were separated to such an extent that only the central plane wave was visible. A section (3 microseconds long) including the central plane wave was extracted and Fourier analysed to get the initial amplitudes and phases for the finite difference model. Figure 5.42 also shows the FFT magnitudes of the initial pulse and it can be seen that the initial spectrum has a peak centred at about 2 MHz. The finite difference model was run and harmonic amplitudes and phases for two axial positions (z = 500 mm and z = 700 mm) were retained for comparison with the corresponding experimental measurements. At 500 mm range (Figure 5.43) the Fourier amplitudes show very good agreement as do the time waveforms. At 700 mm range (Figure 5.44) the agreement is still reasonable but there are some discrepancies; the Fourier amplitudes from the theoretical prediction are higher than the measured values particularly towards the top of the spectrum. This is due to a problem with theoretical modelling and the treatment of the highest harmonics in the theoretical spectrum. At 500 mm the model was using only 90 of the harmonics; however by 700 mm the distortion had increased further and the full 200 harmonics were in use. In the basic model once energy starts to reach the highest harmonic there is no mechanism to dissipate energy that should be going above this point in frequency, so the attenuation coefficient of the higher harmonics was increased artificially to remove excess energy at the top of the spectrum. This still does not account for energy that should be lost directly from say the 100^{th} and the 101^{st} harmonics to the 201^{st}. In addition interactions between say

the 201st and the 202nd harmonics which would remove energy from the fundamental are not accounted for. It will be necessary to investigate this problem further if the theoretical model is to be used efficiently for higher levels of nonlinearity.

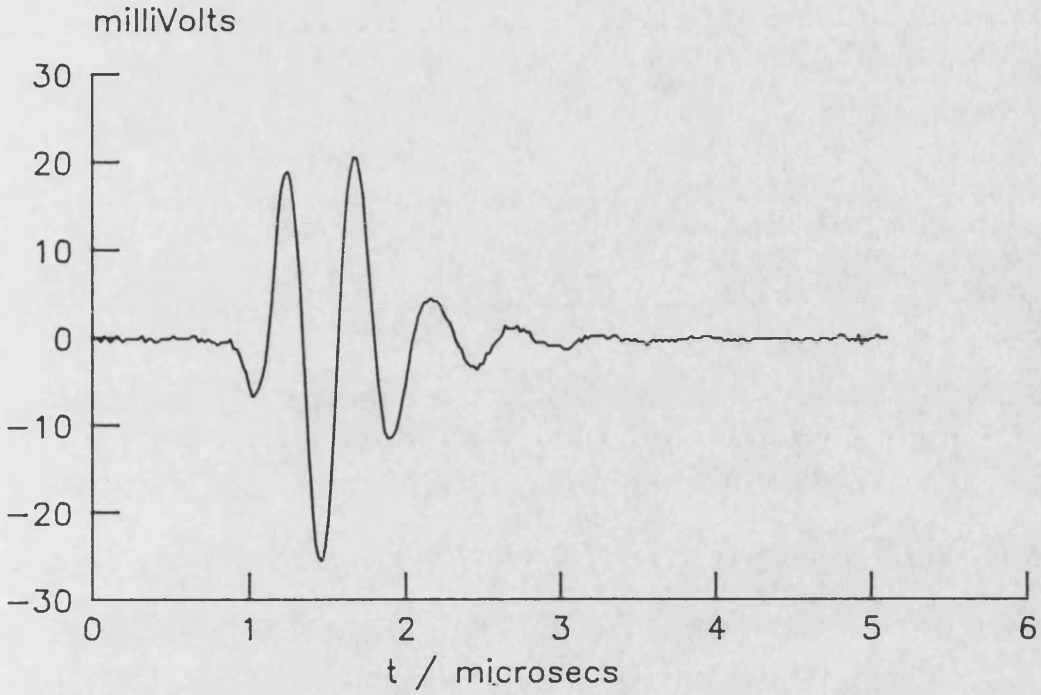

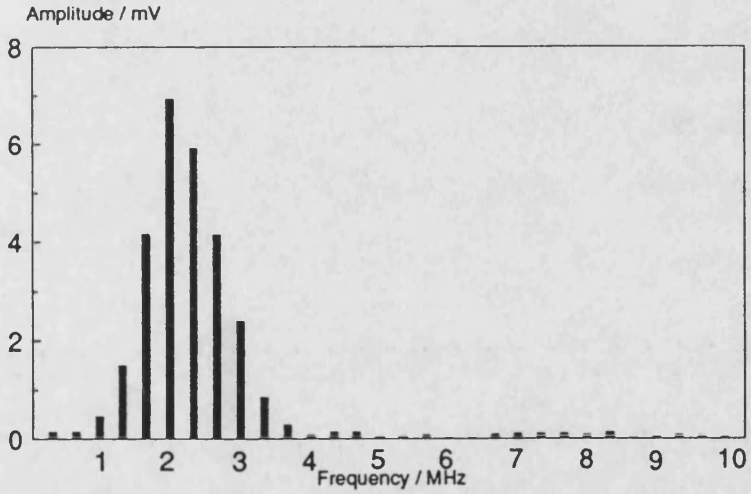

Figure 5.42. Pulse excited plane piston, measured initial waveform and spectral magnitudes at axial range of 15 mm.

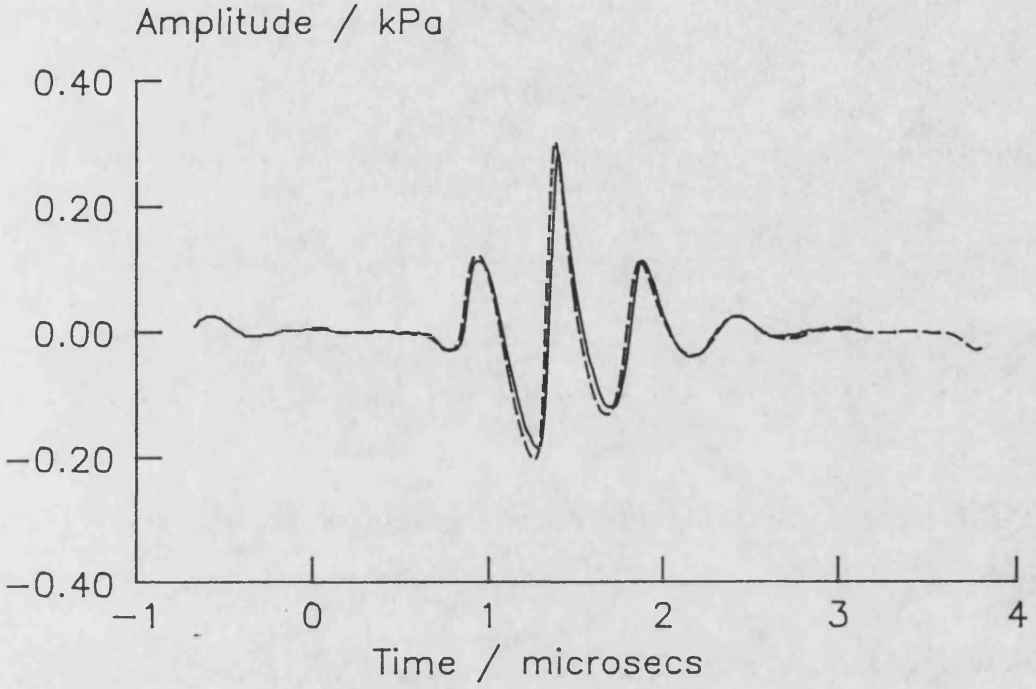

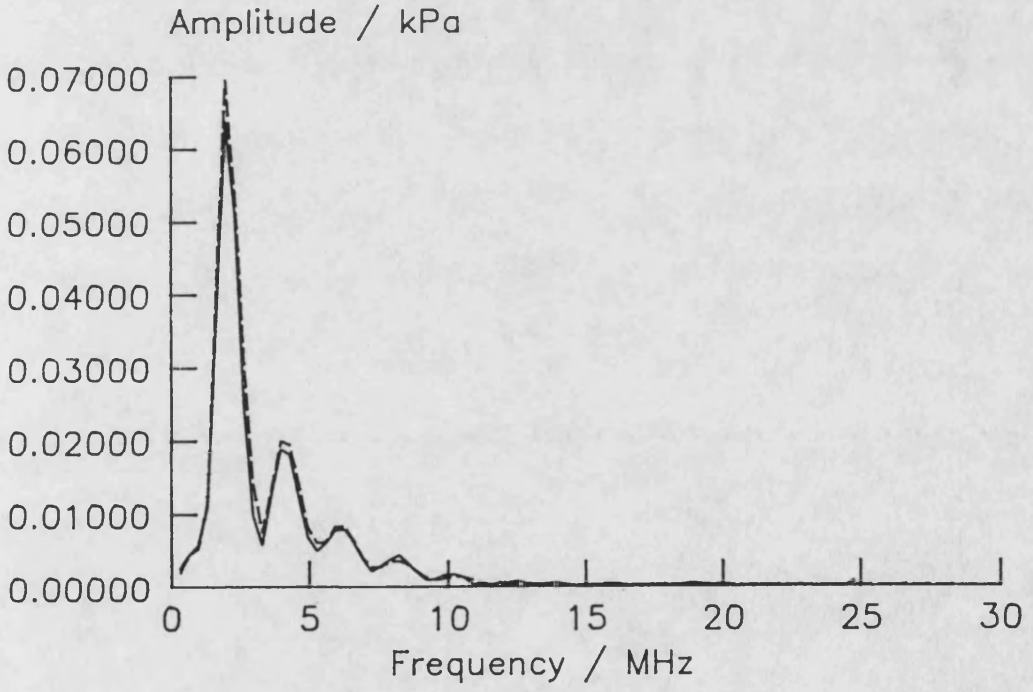

Figure 5.43. Pulse excited plane piston, waveform and spectral magnitudes at axial range of 500 mm. Expt —, theory - -.

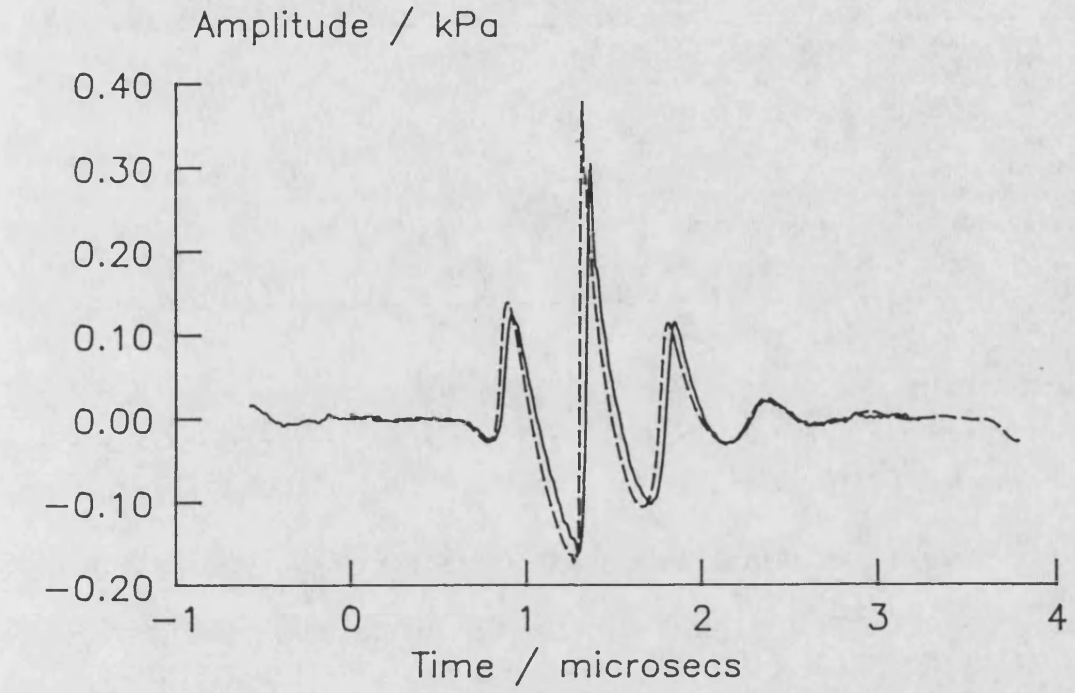

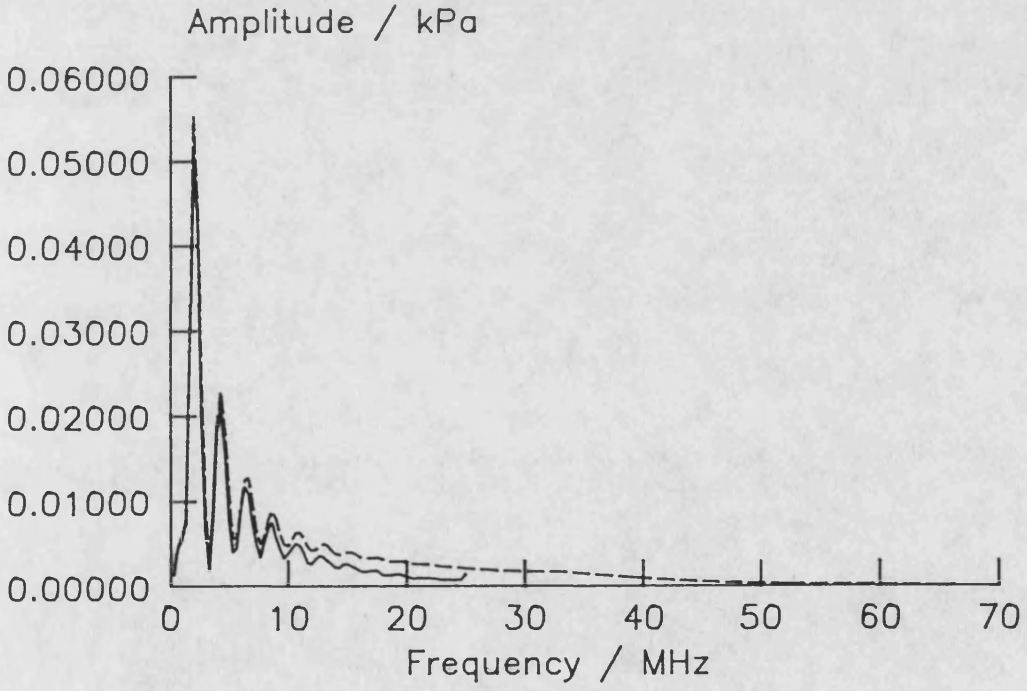

Figure 5.44. Pulse excited plane piston, waveform and spectral magnitudes at axial range of 700 mm. Expt —, theory - -.

Chapter 6: CONCLUSIONS

Extensive experimental measurements have been made on the finite amplitude pressure field generated by a plane circular transducer of 19 mm radius operating in a quasi-continuous wave mode at 2.25 MHz with source pressures ranging between 10 kPa and 300 kPa. These have been compared with theoretical predictions from a finite difference model based on the nonlinear parabolic wave equation. Good agreement has been found for the harmonic amplitudes and phases up to the fifth harmonic within the known limitations of the experimental measurements and the theoretical model.

The study was extended to cover focused finite amplitude pressure fields and similar good agreement has been found between experimental measurements and theoretical predictions for focusing gains of 3.7, 7.6 and 11.9.

The theoretical model has also been extended to model short pulses typical of those used in medical imaging systems and comparisons were made with experimental measurements along the acoustic axis; the initial results show good agreement between experimental measurements and theoretical predictions.

Overall, the finite difference solution of the nonlinear parabolic wave equation has been shown to be an accurate theoretical model for a wide range of real ultrasonic systems similar to those encountered in medical ultrasound.

LIMITATIONS

The main limitations encountered in the study were:

1. The limited frequency range and accuracy of the hydrophone calibration and the lack of information regarding the phase response of the hydrophone.

2. The uncertainty in determining aperture excitation, particularly for the focused cases.

3. The time needed to compute the theoretical solutions could make the finite difference model could be a source of inconvenience.

4. The limited range of validity of the parabolic approximation makes it unsuitable for use with complex geometries and at short ranges particularly with very high gains.

FUTURE WORK

1. The hydrophone calibration needs extending to cover the amplitude and phase response at higher frequencies and a further reduction in uncertainty would be useful. It may be possible to use nonlinear effects to provide the required information. The effect of spatial averaging in finite amplitude sound fields also needs investigation.

2. A method is required for determining transducer parameters and in particular the effective aperture and the excitation across the aperture. This will enable more accurate theoretical predictions since the initial conditions will be more precisely known. It may be possible to use the inverse Hankel transform of the measured pressure field in focal plane to obtain both amplitude shading and phase information.

3. The pulsed measurements and calculations require further work to cover more fully focused systems that are typical of those used in medical ultrasound including lithotripters.

4. The study needs extension to more complicated geometries typical of many real ultrasound systems such as a rectangular aperture with different focal gains along and across the aperture.

5. A more general, and preferably exact, theoretical model is required to cope with high gain systems such as lithotripters and for the solution of more complex geometries such as rectangular apertures.

6. Very high drive levels and pulsed fields require a large number of frequency components in the theoretical model which cause it to run more slowly, some work is required to reduce the computational requirements.

7. In addition to a more general model there is also a need for a simpler theoretical model that would allow "rough and ready" predictions of nonlinear distortion for ultrasound systems that are in clinical use. Such a model would only need to be valid over restricted regions of the pressure field, e.g. the acoustic axis.

8. The propagation of finite amplitude propagation in tissue-like materials needs to be studied, in particular the rate of energy loss from the acoustic beam will enable estimates of in vivo temperature rises to be made. The higher absorption coefficient of tissue should reduce the computational load since fewer harmonics would be needed in the finite difference model. The effect of scattering and reflection of finite amplitude waves also needs considering.

9. It may be possible to extend the theoretical model to estimate streaming forces in fluids by treating the d.c. force as a perturbation of the existing theoretical model.

ACKNOWLEDGEMENTS

This work was performed at the School of Physics at the University of Bath with support from the Science and Engineering Research Council whilst the author was on unpaid leave from the Admiralty Research Establishment, Portland.

The author is pleased to acknowledge the supervision of Dr Victor Humphrey and thanks are also due to Professor Orhan Berktay and Dr Francis Duck for their interest and advice. Thanks also to Kosmas Anastasiadis who undertook much of the early work on the finite difference model and to the Department of Applied Mathematics at Bergen University, Norway for supplying the initial program listing [Aanonsen, 1983], thanks also to Dennis Davis of the Bath University Computing Services for recently optimising the code.

The author also thanks the other members of the School of Physics, too numerous to mention, who aided and abetted him and who contributed to the congenial working atmosphere.

Last and certainly not least the author would like to record his gratitude to Jane Christmas for supporting him in all things during this study.

REFERENCES

Aanonsen, S.I. 1983 "Numerical computation of the near-field of a finite amplitude sound beam," Report No. 73, Dept. of Applied Mathematics, University of Bergen, Norway.

Aanonsen, S.I., Barkve, T., Naze Tjøtta, J. and Tjøtta, S. 1984 "Distortion and harmonic generation in the near-field of a finite amplitude sound beam," J. Acoust. Soc. Am. 75, 749-768.

Anastasiadis, K. 1987 "Numerical investigation of nonlinear effects in acoustical beams," University of Bath, School of Physics Report.

Bacon, D.R. 1982 "Characteristics of a pvdf membrane hydrophone for use in the range 1-100 MHz," IEEE Trans. Sonics and Ultrasonics SU-29, 18-25.

Bacon, D.R. 1986 "Finite amplitude propagation in acoustic beams," University of Bath (Ph. D. thesis).

Bacon, D.R. and Baker, A.C. 1989 "Comparison of two theoretical models for predicting nonlinear propagation in medical ultrasound fields," To be published in Physics in Medicine and Biology as proceedings from the IPSM conference "Physics in Medical Ultrasound", York.

Baker, A.C., Anastasiadis, K. and Humphrey, V.F. 1987 "Nonlinear propagation in focused fields: Experiment and theory," Proceedings of Ultrasonics International 87, Butterworths, 184-189.

Baker, A.C., Anastasiadis, K. and Humphrey, V.F. 1988 "The nonlinear pressure field of a plane circular piston: Theory and experiment," J. Acoust. Soc. Am. 84, 1483-1487.

Baker, A.C. and Humphrey, V.F. 1989 "Nonlinear propagation in pulsed ultrasonic fields," to be published in Proceedings of Ultrasonics International 89, Butterworths.

Beaver, W.L. 1974 "Sonic near-fields of a pulsed piston radiator," J. Acoust. Soc. Am. 56, 1043-1048.

Beissner, K. 1981 "Exact integral expression for the diffraction loss of a circular piston source," Acustica 49, 212-217.

Beyer, R.T. 1974 "Nonlinear acoustics," American Department of the Navy (Naval Sea Systems Command), 101.

Bjørnø, L. 1986 "Characterisation of biological media by means of their nonlinearity," Ultrasonics 24, 254-259.

Blackstock, D.T. 1966 "Connection between the Fay and Fubini solutions for plane sound waves of finite amplitude," J. Acoust. Soc. Am. 39, 1019-1026.

Blackstock, D.T. 1964a "Thermoviscous attenuation of plane, periodic, finite amplitude sound waves," J. Acoust. Soc. Am. 36, 534-542.

Blackstock, D.T. 1964b "On plane, spherical and cylindrical sound waves of finite amplitude in lossless fluids," J. Acoust. Soc. Am. 36, 217-219.

Blackstock D.T. 1962 "Propagation of plane sound waves of finite amplitude in non-dissipative fluids," J. Acoust. Soc. Am. 34, 9-30

Cobb, W.N. 1984 "Frequency domain method for the prediction of the ultrasonic field patterns of pulsed, focused radiators," J. Acoust. Soc. Am. 75, 72-75.

Coleman, A.J., Saunders, J.E., Preston, R.C. and Bacon, D.R. 1987 "Pressure waveforms generated by a Dornier extra-corporeal shock wave lithotripter," Ultrasound in Med. and Biol. 13, 651-657.

Du, G. and Breazeale, M.A. 1985 "The ultrasonic field of a Gaussian transducer," J. Acoust. Soc. Am. 78, 2083-2086.

Du, G. and Breazeale, M.A. 1986 "Harmonic distortion of a finite amplitude Gaussian beam in a fluid," J. Acoust. Soc. Am. 80, 212-216.

Duck, F.A. 1989 "Output data from European studies," Ultrasound in Med. and Biol 15, 61-64.

Duck, F.A. 1987 "The measurement of exposure to ultrasound and its application to estimates of ultrasound dose," Phys. Med. Biol. 32, 303-325.

Duck, F.A. and Starritt H.C. 1984 "Acoustic shock generation by ultrasonic imaging equipment," Brit. J. Radiol. 57, 231-240.

Duck, F.A., Starritt, H.C., Aindow, J.D., Perkins, M.A. and Hawkins, A.J. 1985 "The output of pulse-echo ultrasound equipment: a survey of powers pressures and intensities," Brit. J. Radiol. 58, 989-1001.

Fay, R.D. 1931 "Plane sound waves of finite amplitude," J. Acoust. Soc. Am. 3, 222-241.

FDA 1985 "510(K) Guide for measuring and reporting acoustic output of diagnostic ultrasound medical devices," Center for Devices and Radiological Health, (Final draft).

Fox, F.E. and Wallace, W.A. 1954 "Absorption of finite amplitude sound waves," J. Acoust. Soc. Am. 26, 994-1006.

Fubini, E. 1935 "Anomalies in the propagation of an acoustic wave of large amplitude," Alta. Freq. 4, 173-180.

Galantree, H.R. 1987 "PVDF membrane hydrophones - an ultrasonic characterisation tool," GEC Technical Brief Y/221/369.MQ2.2.

Goodsitt, M.M., Madsen E.L. and Zagzebski, J.A. 1982 "Field patterns of pulsed, focused, ultrasonic radiators in attenuating and non-attenuating media," J. Acoust. Soc. Am. 71, 318-328

Hamilton, M.F., Naze Tjøtta, J. and Tjøtta, S. 1985 "Nonlinear effects in the far-field of a directive sound source," J. Acoust. Soc. Am. 78, 202-216.

Hart, T.S. and Hamilton, M.F. 1987 "Nonlinear effects in focused sound fields," Proc. XI Int. Symposium on Nonlinear Acoustics, Vol. 1, 24-28.

Hasegawa, T., Matsuzawa, K. and Inoue, N. 1986 "A new expansion for the velocity potential of a circular concave piston," J. Acoust. Soc. Am. 79, 927-931.

Hasegawa, T., Inoue, N. and Matsuzawa, K. 1987 "A new theory for the radiation from a concave piston source," J. Acoust. Soc. Am. 82, 706-708.

Humphrey, V.F., Burgess, M. and Sampson, N. 1986 "Harmonic generation due to nonlinear propagation in a focused ultrasonic field," Ultrasound in Medicine Conference, Proc. Inst. Acoust. 8, 47-54.

Hutchins, D.A., Mair, H.D., Puhach, P.A. and Osei, A.J. 1986 "Continuous wave pressure fields of ultrasonic transducers," J. Acoust. Soc. Am. 80, 1-12.

Hutchins, D.A., Mair, H.D. and Taylor, R.G. 1987 "Transient pressure fields of PVDF transducers," J. Acoust. Soc. Am. 82, 183-193.

Ingenito, F. and Williams, A.O. 1971 "Calculation of second harmonic generation in a piston beam," J. Acoust. Soc. Am. 49, 319-328.

International Electrotechnical Commission 1984 "Measurement and characterisation of ultrasonic fields using hydrophones in the frequency range 0.5 MHz to 15 MHz," Draft standard IEC 29D/WG8, 13 and 48.

Kinsler, L.E., Frey, A.R., Coppens, A.B. and Sanders, J.V. 1982 "Fundamentals of acoustics," John Wiley, 3 ed., 107 and 462.

Kuznetsov, V.P. 1971 "Equations of nonlinear acoustics," Sov. Phys. Acoust. 16, 467-470.

Lancaster, M. 1983 "The finite amplitude field of a circular piston," University of Bath (Ph.D. thesis).

Lockwood, J.C., Muir, T.G. and Blackstock, D.T 1973 "Directive harmonic generation in the radiation field of a circular piston," J. Acoust. Soc. Am. 53, 1148-1153.

Lockwood, J.C. and Willette, J.G. 1973 " High speed method for computing the exact solution for pressure variations in the near-field of a baffled piston," J. Acoust. Soc. Am. 53, 735-741.

Lucas, B.G. and Muir, T.G. 1982 "The field of a focusing source," J. Acoust. Soc. Am. 72, 1289-1296.

Lucas, B.G. and Muir, T.G. 1983 "Field of a finite amplitude focusing source," J. Acoust. Soc. Am. 74, 1522-1528.

Madsen, E.L., Goodsitt, M.M. and Zagzebski, J.A. 1981 "Continuous waves generated by focused radiators," J. Acoust. Soc. Am. 70, 1508-1517.

Martin, F.D. and Breazeale M.A. 1971 "A simple way to eliminate diffraction lobes emitted by ultrasonic transducers," J. Acoust. Soc. Am. 49, 1668.

Morse, P.M. and Ingard, K.U. 1968 "Theoretical acoustics," McGraw-Hill, New York, 388.

Muir, T.G. and Carstensen, E.L. 1980 "Prediction of nonlinear acoustic effects at biomedical frequencies and intensities," Ultrasound in Medicine and Biology 6, 345-347.

Naugolnykh, K.A., Soluyan, S.I. and Khokhlov, R.V. 1963 "Spherical waves of finite amplitude in a viscous thermally conducting medium," Sov. Phys. Acoust. 9, 42-46.

Naze Tjøtta, J. and Tjøtta, S. 1980 "An analytical model for the near-field of a baffled piston transducer," J. Acoust. Soc. Am. 68, 334-339.

Naze Tjøtta, J. and Tjøtta, S. 1981 " Nonlinear equations of acoustics, with application to parametric acoustic arrays," J. Acoust. Soc. Am. 69, 1644-1652.

Naze Tjøtta, J. and Tjøtta, S. 1982 "Near-field and far-field of pulsed acoustic radiators", J. Acoust. Soc. Am. 71, 824-834.

O'Neil, H.T. 1949 "Theory of focusing radiators," J. Acoust. Soc. Am. 21, 516-526.

Parker, K.J. 1985 "Observation of nonlinear acoustic effects in B-scan imaging instrument," IEEE Trans. Sonics and Ultrasonics SU-32, 4-8.

Papoulis, A. 1981 "Systems and transforms with applications in optics," R.E. Krieger, 346-347.

Penttinen, A. and Luukkala, M. 1976a "The impulse response and pressure near-field of a curved ultrasonic radiator," J. Phys. D: Appl. Phys. 9, 1547-1557.

Penttinen, A. and Luukkala, M. 1976b "Sound pressure near the focal area of an ultrasonic lens," J. Phys. D: Appl. Phys. 9, 1927-1936.

Philips 1985 Digital storage oscilloscope PM3315, Operating Manual, Philips Scientific and Industrial Equipment.

Poisson, S.D. 1808 "Memoir on the theory of sound," J. L'Ecole Polytech. 7, 364-370.

Rugar, D. 1984 "Resolution beyond the diffraction limit in the acoustic microscope: A nonlinear effect," J. Appl. Phys. 56, 1338-1346.

Saito, S., Kim, B.C. and Muir, T.G. 1987 "Second harmonic component of a nonlinearly distorted wave in a focused field," J. Acoust. Soc. Am. 82, 621-628.

Smith, C.W. and Beyer, R.T. 1968 "Ultrasonic radiation field of a focusing spherical source at finite amplitudes," J. Acoust. Soc. Am. 46, 806-813.

Smith, R.A. 1986 "The importance of the frequency response of a hydrophone when characterising medical ultrasonic fields," Proceedings of Ultrasound in Medicine Conference, Institute of Acoustics, 119-128.

Starritt, H.C., Duck, F.A., Hawkins, A.J. and Humphrey, V.F. 1986 "The development of harmonic distortion in pulsed finite amplitude ultrasound passing through liver," Phys. Med. Biol. 31, 1401-1409.

Starritt, H.C., Perkins, M.A., Duck, F.A. and Humphrey, V.F. 1985 "Evidence for ultrasonic finite amplitude distortion in muscle using medical equipment," J. Acoust. Soc. Am. 77, 302-306.

Stephanishen, P.R. 1971 Transient radiation form pistons in an infinite baffle," J. Acoust. Soc. Am. 49, 1629-1638.

Stokes, G.G. 1848 "On a difficulty in the theory of sound," Philos. Mag. Ser. 3, 33, 349-356.

Thompson, R.B., Gray, T.A., Rose, J.H., Kogan, V.G. and Lopes, E.F. 1987 "The radiation of elliptical and bicylindrically focused piston transducers," J. Acoust. Soc. Am. 82, 1818-1828.

Trivett, D.H. and Van Buren, A.L. 1981 "Propagation of plane, cylindrical and spherical finite amplitude waves," J. Acoust. Soc. Am. 69, 943-949.

Westervelt, P.J. 1963 "Parametric acoustic array," J. Acoust. Soc. Am. 35, 535-537.

Weyns, A. 1980a "Radiation field calculations of pulsed ultrasonic transducers, Part 1: planar circular, square and annular transducers," Ultrasonics 18, 183-188.

Weyns, A. 1980b "Radiation field calculations of pulsed ultrasonic transducers, Part 2: spherical disc- and ring-shaped transducers," Ultrasonics 18, 219-223.

Williams, A.R. 1983 "Ultrasound: Biological effects and potential hazards," Academic Press, London.

Zabolotskaya, E.A. and Khokhlov, R.V. 1969 "Quasi-plane waves in the nonlinear acoustics of confined beams," Sov. Phys. Acoust. 15, 35-40.

Zemanek, J. 1970 "Beam behaviour within the near-field of a vibrating piston," J. Acoust. Soc. Am. 49, 181-191.

Ziskin, M.C. and Petitti, D.B. 1988 "Epidemiology of human exposure to ultrasound: a critical review," Ultrasound in Med. and Biol. 14, 91-96.

Appendix A: SMALL SIGNAL THEORY FOR FOCUSED RADIATORS

This appendix contains a number of results relating to the small signal pressure field of a focused circular radiator. It concentrates mainly on the axial field since this is easily measured and is often used to characterise a radiator. An approximate correction for the finite hydrophone size is also given.

Consider a curved shell, radius of curvature D and shell radius a.

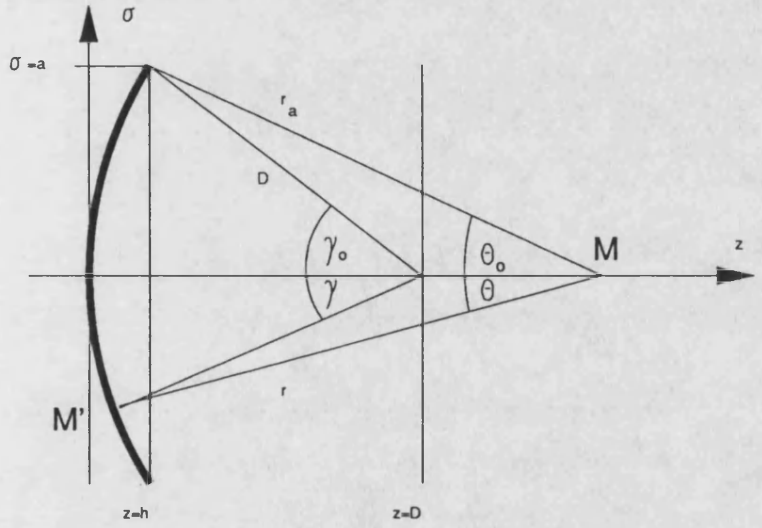

Figure A1.
Geometry of focused radiator.

KEY:

a - radiator radius
D - focal length
h - bowl depth
z - axial co-ordinate
σ - radial co-ordinate
r - distance from arbitrary point on radiator (M') to axial field point (M)

If a sinusoidal excitation with angular frequency ω is assumed the pressure at a point (M) in the field is given by the diffraction integral:

$$p(z,\sigma)=\frac{jkp_0}{2\pi}\int\int_S \frac{\exp(-jkr)}{r}dS.$$

Here k is the wavenumber (k = ω/c), p_o is the average pressure across the radiating face and dS is an elemental area on the radiating face. The above expression assumes that elemental point sources radiate freely into half space which is not strictly true for high focal gains.

1.1 AXIAL FIELD

In order to calculate the axial field we first express dS in terms of the angle γ, i.e.

$$dS = 2\pi D^2 \sin(\gamma) d\gamma$$

the diffraction integral then becomes:

$$p(z,0) = jkp_0 D^2 \int_{\gamma=0}^{\gamma_0} \frac{\exp(-jkr)\sin(\gamma)d\gamma}{r}, \qquad A1$$

where $\sin(\gamma_0) = a/D$.

The integral can now be simplified by using r as the variable of integration since:

$$r = \sqrt{z^2 + 2D(D-z)(1-\cos(\gamma))} \quad \text{and} \quad \frac{dr}{d\gamma} = \frac{D(D-z)\sin(\gamma)}{r}.$$

Then we can write:

$$p(z,0) = \frac{jkp_0 D}{(D-z)} \int_{r=z}^{r_a} \exp(-jkr) dr$$

with: $r_a = \sqrt{((z-h)^2 + a^2)}$

where h is the bowl depth, given by:

$$h = D - \sqrt{D^2 - a^2}.$$

Alternatively we can write $h = D(1-\cos(\gamma_0))$, then:

$$p(z,0) = p_0 \left(\frac{D}{D-z}\right)(\exp(-jkz) - \exp(-jkr_a)) \qquad A2$$

Examination of equation A2 shows that the term D/(D-z) is the "geometrical gain" envelope obtained from a ray approach to focusing, with a singularity in the focal plane. The term involving the two exponentials is essentially the interference pattern for two plane waves, one emanating from the edge of the radiator and one from the centre. In the focal plane z=D=r_a and the difference of these two exponentials is zero which counters the singularity introduced by the geometrical gain term (See Figure A2). The pressure at this point can be found by re-writing equation A1 with z=D, i.e.

$$p(D,0) = jkp_0 D^2 \int_{\gamma=0}^{\gamma_0} \frac{\exp(-jkD)}{D} \sin(\gamma) d\gamma$$

therefore

$$p(D,0) = jkp_0 \exp(-jkD)D(1-\cos(\gamma_0));$$

but $D(1-\cos(\gamma_0)) = h = D - \sqrt{D^2 - a^2}$

thus if $D \gg a$ then $h \approx \frac{a^2}{2D}$ and

$$p(D,0) \approx \frac{jka^2}{2D} p_0 \exp(-jkD)$$

Therefore on axis, in the focal plane the pressure amplitude is simply Gp_0 since $G = R_0/D = ka^2/2D$.

Returning to equation A2 it is often convenient to extract the term exp(-jkz) which is a plane wave phase term to give:

$$p(z,0) = p_o \exp(-jkz)\left(\frac{D}{D-z}\right)[1-\exp(-jk(r_a - z))]. \qquad A3$$

The plane wave term exp(-jkz) is known as the fast phase term and the remaining phase variation is known as the slow phase. The phase plot of Figure A2 shows the phase variation due to the ray term and the slow phase of the interference term. It can be seen that the π radians phase jump caused by the change in sign of the ray term in the focal plane adds to the π radians phase jump due to the interference term to give a smooth phase variation through the focal plane.

Examination of the focusing geometry (Figure A1) shows that the term $(r_a - z)$ of equation A3 is actually the path difference between waves travelling from the edge of the radiator and from the centre and we can write:

$\Gamma = r_a - z$ then:

$$p(z,0) = p_0 \exp(-jkz)\left(\frac{D}{D-z}\right)[1-\exp(-jk\Gamma)]. \qquad A4$$

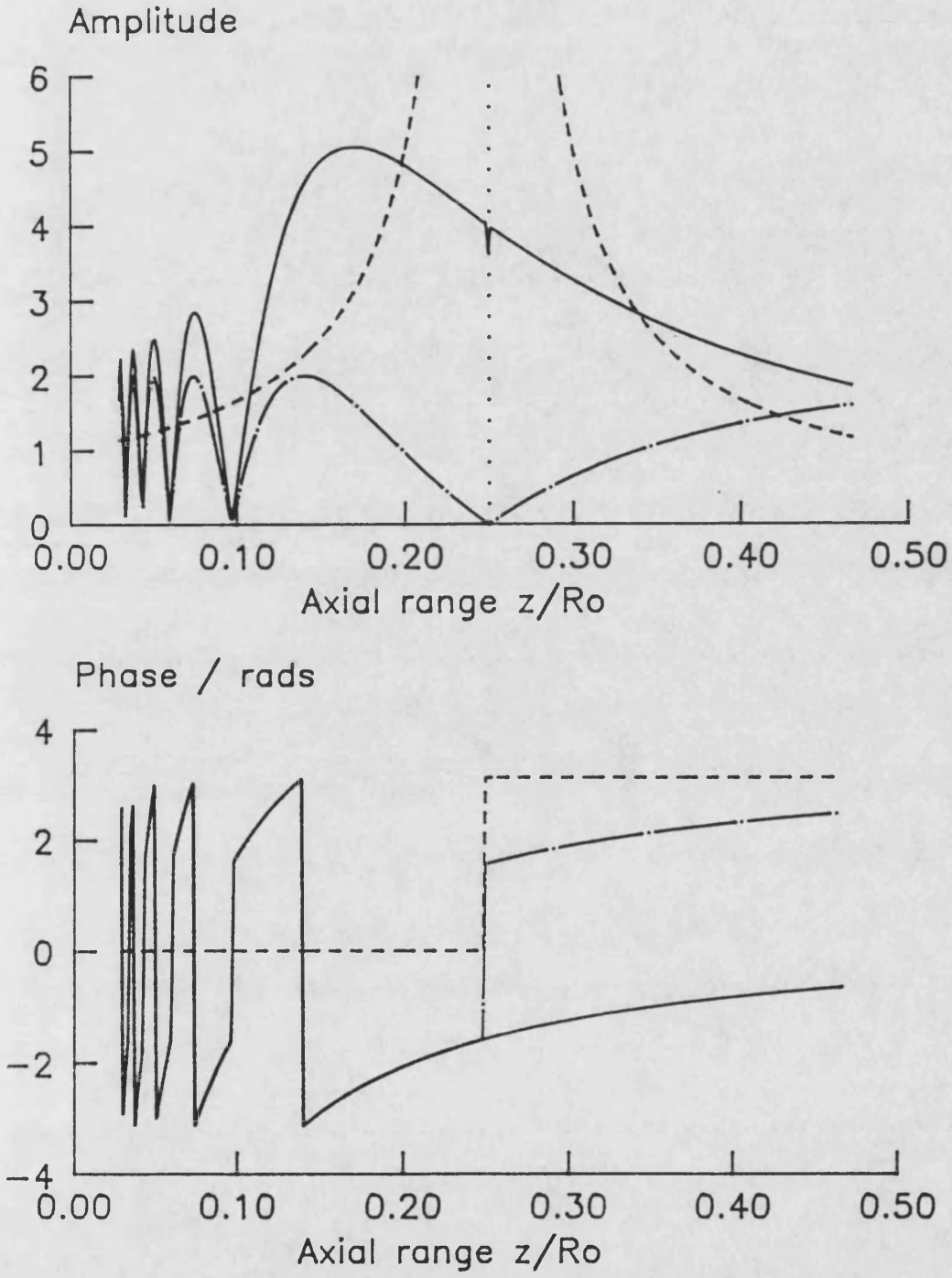

Figure A2. Components of the axial field of a focused piston. G = 4, ka = 180. Ray focusing envelope (- -), interference effects (-.-), resultant field (—).

As the focal plane is approached the path difference (Γ) gets smaller, hence if the radiator is driven with a pulse described by f(t) then the observed time waveform on axis will be $f(t)-f(t+\Delta t)$, where $\Delta t = \Gamma c$. Thus in the focal plane where Δt tends to zero the observed time waveform is proportional to the derivative of the driving function f(t).

The interference term has zeros whenever $k\Gamma = 2n\pi$ or $\Gamma = n\lambda$ in other words, zeros occur for path differences that are integer multiples of the wavelength.

1.1.1 Fresnel approximation

Equation A4 can be simplified if the observation distance (z) and the focal distance (D) are much greater than the aperture radius (a) and the bowl depth (h). This is done by expanding r_a.

$$r_a = \sqrt{(z-h)^2 + a^2}$$

$$= z\left(1 + \frac{h^2}{z^2} - \frac{2h}{z} + \frac{a^2}{z^2}\right)^{1/2}$$

Ignoring the term h^2/z^2 as small compared with 2h/z and using the binomial expansion gives

$$r_a \approx z + \frac{a^2}{2z} - h,$$

then using the approximate expression for h gives:

$$r_a \approx z + \frac{a^2}{2z} - \frac{a^2}{2D}.$$

Thus we can write $$\Gamma = r_a - z \approx \frac{a^2}{2z} - \frac{a^2}{2D}$$

and equation A4 becomes:

$$p(z,0) \approx p_0 \exp(-jkz)\left(\frac{D}{D-z}\right)\left[1 - \exp\left(-j\left(\frac{R_0}{z} - G\right)\right)\right], \qquad A5$$

since $\frac{ka^2}{2} = R_0$ and $\frac{ka^2}{2D} = \frac{R_0}{D} = G.$

Equation A5 has zeros whenever

$$R_0\left(\frac{1}{z}-\frac{1}{D}\right)=2n\pi.$$

Thus for positive n, z must be less than D, i.e. the minima occur in the pre-focal region, for n=0 we have the zero in the focal plane although this is never seen due to the singularity in the ray term. When n is negative we get minima in the post-focal region but only if the gain (R_0/D) is greater than 2π.

1.1.2 Plane piston

The plane piston results can be obtained from the focused results by allowing the gain (G) to tend to zero, i.e. the focal distance (D) tends to infinity, thus equation A2 becomes:

$$p(z,0)=p_0(\exp(-jkz)-\exp(-jkr_a))$$

where $r_a=\sqrt{z^2+a^2}$.

The Fresnel approximation gives:

$$\Gamma \approx a^2/2z \qquad A6$$

and equation A5 becomes:

$$p(z,0)\approx p_0\exp(-jkz)\left[1-\exp\left(\frac{-jR_0}{z}\right)\right]$$

1.1.3 Validity of Fresnel approximation

Since the Fresnel approximation is equivalent to the parabolic approximation it is useful to examine the range of validity of the Fresnel approximation for a simple geometry such as the plane piston. The exact expression for r_a in the case of the plane piston is:

$$r_a=\sqrt{z^2+a^2}$$

whereas the Fresnel approximation uses the binomial expansion to expand the square root, i.e. $r_a \approx a^2/2z$. If we include the next term of the binomial expansion, the expression for the axial pressure field becomes:

$$p(z,0) \approx p_0 \exp(-jkz)\left[1 - \exp\left(-jk\left(\frac{a^2}{2z} - \frac{a^4}{8z^3}\right)\right)\right]$$

Thus if we are to ignore the term in a^4/z^3 its effect on the phase term must be small, i.e.

$$\frac{ka^4}{8z^3} \ll 2\pi.$$

Noting from Figure A1 that $a/z = \tan(\theta_0)$, where θ_0 is the half-angle of the aperture as seen from the field point, we can write:

$$\frac{ka}{8}\tan^3(\theta_0) \ll 2\pi \quad \text{or} \quad \tan(\theta_0) \ll \left(\frac{16\pi}{ka}\right)^{1/3}.$$

Thus for the geometry used in this study (ka = 180) the aperture half-angle must be much less than 33°, which for an aperture radius of 19 mm implies that axial observation distance must be much greater than 30 mm.

1.2 RADIAL FIELD

A useful result due to O'Neil [1949] is that the relative pressure field across the focal plane can be approximated by the far field directivity function of a plane piston, i.e.

$$\frac{p(D,\sigma)}{p(D,0)} = \frac{2J_1(ka\sin\beta)}{ka\sin\beta}$$

where J_1 is a Bessel function of the first kind, order one and β is the angle of the field point off axis which can be expressed as:

$$\sin(\beta) = \frac{\sigma}{\sqrt{D^2+\sigma^2}}$$

1.3 APPROXIMATE CORRECTION FOR HYDROPHONE SIZE

The effect of finite hydrophone size on the measured axial acoustic pressure can be accounted for approximately by considering the directional response of the hydrophone. The hydrophone was relatively small (for the membrane hydrophones used here the kb values were about unity) hence the measurements were always made in the far-field of the hydrophone. Thus the edge wave from the transducer could be

weighted with the hydrophone far-field directivity pattern to give the pressure measured by the hydrophone. Modifying equation A4 in this way gives the axial pressure field of the focused transducer, as measured by a hydrophone of radius b as:

$$p(z,0) \approx p_o \exp(-jkz)\left(\frac{D}{D-z}\right)[1 - D(\theta_0)\exp(-jk\Gamma)]$$

where $D(\theta_0) = \dfrac{2J_1(kb\sin(\theta_0))}{kb\sin(\theta_0)}$, noting that $\sin(\theta_0) = a/r_a$, we get :

$$p(z,0) \approx p_o \exp(-jkz)\left(1 - \left(\frac{2J_1\left(\frac{kab}{r_a}\right)}{\frac{kab}{r_a}}\right)\exp(-jk\Gamma)\right). \qquad A6$$

1.4 DISCUSSION

Figure A3 shows the theoretical small signal axial pressure fields for a circular aperture different focusing gains, the pressure amplitudes have been normalised by p_o and the axial ranges by the Rayleigh distance. The plane case shows the axial pressure varying between 0 and $2p_o$, the oscillations become more rapid nearer the aperture because the path difference Γ, which governs the interference effect, varies to a first approximation as 1/z (Equation A6).

The focused fields shown in Figure A3 were calculated for the same aperture radius as the plane piston case but have focal gains of 4, 8 and 12. The position of the focal planes are denoted by the vertical dashed lines; the plane piston can be considered as having its focal plane at infinity. It can be seen that the effect of increasing the gain is to increase the peak pressure and move the point at which peak pressure occurs closer to the aperture, causing the near-field oscillations between the aperture and the focal plane to become more compressed. As O'Neil [1949] observed the peak pressure always occurs on the aperture side of the focal plane and gets nearer to the focal plane with increasing gain.

The variation of the position of the axial peak pressure with gain is shown in Figure A4. The vertical scale is the position of the peak axial pressure normalised with respect to the focal plane, thus at high gains it can be seen that the peak pressure occurs at a normalised distance of almost unity, i.e. nearly in the focal plane. At low gains the peak pressure moves nearer the aperture, e.g. at a gain of 4 (typical of medical imaging systems) the peak pressure occurs at 60% of the focal distance (cf. Figure A3). Thus it would be incorrect to assume that the focal plane is always at the position of peak axial pressure. As the gain tends to zero, i.e. a plane piston, the graph becomes linear with a slope of $1/\pi$ since the peak pressure occurs at R_o/π for a plane piston.

REFERENCE

O'Neil, H.T. 1949 "Theory of focusing radiators," J. Acoust. Soc. Am. 21, 516-526.

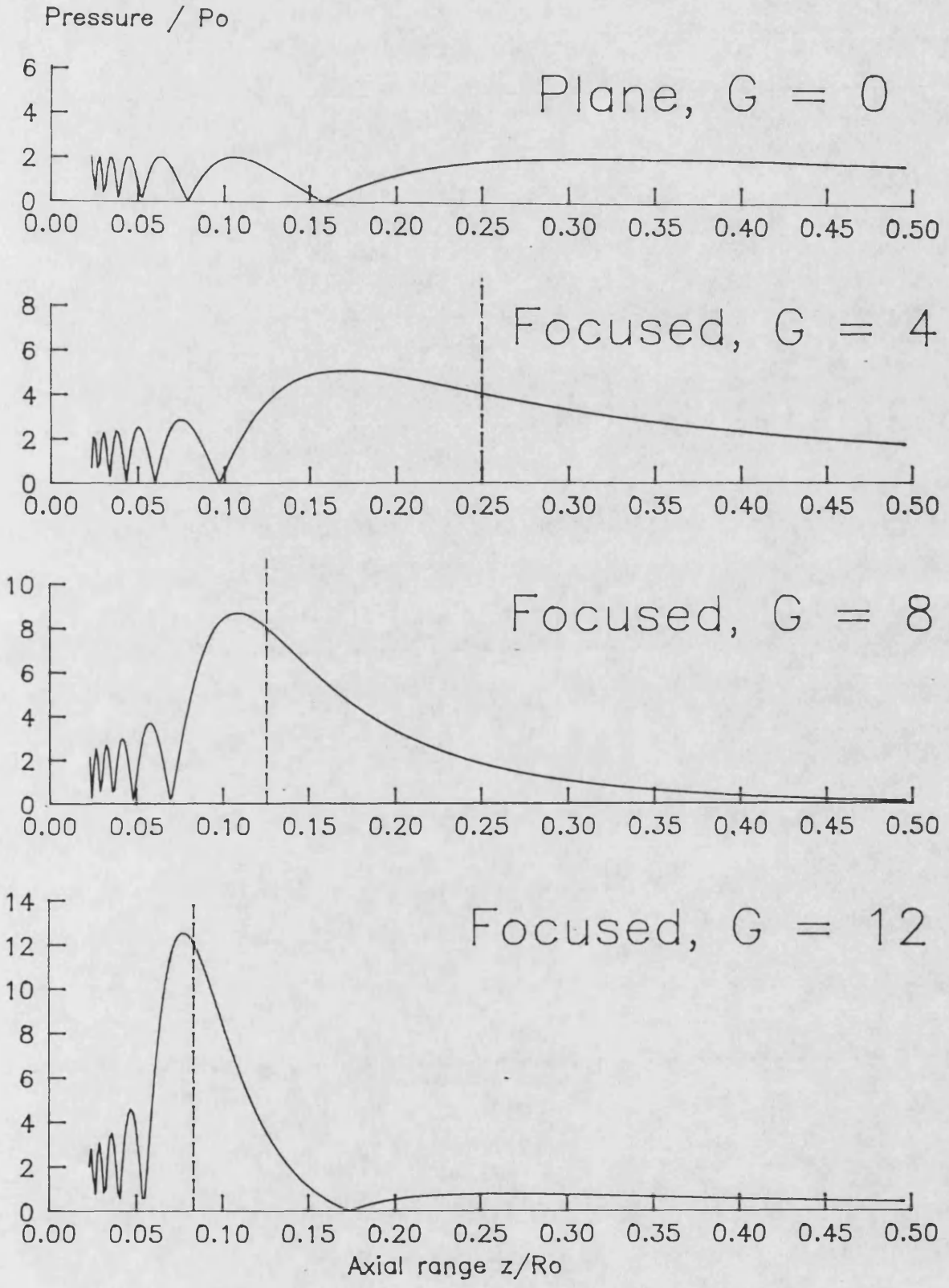

Figure A3. Small signal axial pressure fields of focused circular apertures (ka = 180). Gain ($G = R_o/D$) = 0, 4, 8 and 12.

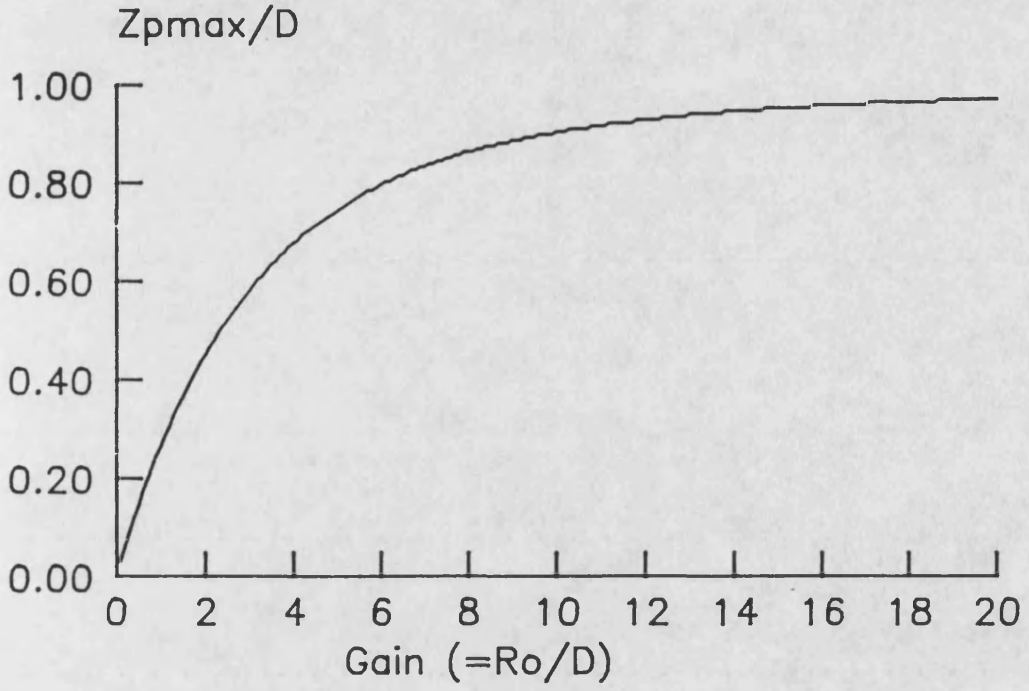

Figure A4. Variation of the position of the axial pressure peak with gain.

Appendix B: USER GUIDE FOR PROGRAM pulse.f

1.1 GENERAL

Notation

The names of files on the Gould computer (uk.ac.bath.gdr) are italicised.

INTRODUCTION

pulse.f is a FORTRAN program that calculates the pressure field of a circular aperture under finite amplitude conditions. *pulse.f* is a modified version of a program (called FOCAB) from Bergen University in Norway [Aanonsen, 1983]. The original program, FOCAB, was implemented on the Honeywell Multics main-frame at the University of Bath by Anastasiadis [1987] and was later transferred, slightly modified, onto the author's IBM PC-AT. Most recently, the program was modified to use a pulsed time waveform as an initial condition and renamed *pulse.f*, before being transferred to the new main-frame at the University of Bath, a Gould NP1 (uk.ac.bath.gdr). During this time the program was used to predict the pressure field of plane and focused circular apertures resembling medical ultrasound fields, in this role the program was found to be an accurate predictor of experimentally measured fields. The main limitation being the computer run-time required for high drive levels and pulsed fields.

INPUT

Three data files are used by *pulse.f* namely:

FILENAME	DESCRIPTION
param.dat	Contains the parameters for the run, e.g. focusing gain, number of harmonics etc.

init.dat	Contains the initial pulse spectrum for the run, i.e. the harmonic magnitudes and phases at the piston face.
pgrid.dat	Contains the grid co-ordinates for which output is required.

OUTPUT

The results from *pulse.f* are stored in four files (two other files contain diagnostic output).

FILENAME	DESCRIPTION
ax.out	Holds the calculated harmonic magnitudes and phases for the axial points specified in *pgrid.dat.*
rad1.out *rad2.out* *rad3.out*	Hold the calculated harmonic magnitudes and phases for the three radial sections specified in *pgrid.dat.*
pulse.log	Is used for any error messages from the program.
pulse.count	Holds the current step number, axial range and number of harmonics and can be read during the run to find out what stage the program is at.

1.2 INPUT FILES IN DETAIL

1.2.1 *param.dat*

This file contains the main parameters for the run as a simple list of 10 real numbers which are read into the program under the following variable names:

Variable Description

GAMMA is the ratio of nonlinearity to absorption given by:

$$\Gamma = \frac{\beta \varepsilon k}{\alpha}.$$

Here α is the absorption coefficient = $0.025f^2$

(f is the first frequency component of the model in MHz)

and $\beta\varepsilon k$ is the reciprocal of the plane wave shock distance, i.e. $\frac{1}{l_D}$.

Here β is the parameter of nonlinearity (3.5 for water), and

ε is the Mach number $\left(=\frac{u_o}{c_o}=\frac{p_o}{\rho_o c_o^2}\right)$. In turn

p_o is the acoustic pressure amplitude at the piston face,

c_o is the speed of sound (1486 m/s for water),

ρ_o is the mean density($1000 kg/m^3$ for water),

and k is the wavenumber $\left(=\frac{2\pi}{\lambda}\right)$.

Using the values for freshwater, at 20°C, the above reduces to:

$$\Gamma = \frac{268 p_o}{f},$$

where p_o is the acoustic pressure at the piston face in MPa and f is the first frequency component in the model in MHz.

A is the ratio of diffraction to nonlinearity given by:

$A = \frac{2R_o}{l_D}$ where l_D is defined as above

and R_o is the Rayleigh distance given by $\frac{ka^2}{2}$

where a is the aperture radius.

Again using the values for freshwater, at 20°C, the above reduces to:

$A = 0.028335a^2f^2p_o$

with a in mm, f in MHz and p_o in MPa.

ZMAX is the maximum axial distance for the run, normalised by the Rayleigh distance, i.e. z/R_o

RMAX is the initial radial boundary, normalised by the aperture radius, i.e. r/a

MRMAX is the maximum radial boundary, normalised by the aperture radius.

KSTEP is the axial step size for the calculating grid, normalised by R_o.

HSTEP is the radial step size for the calculating grid, normalised by a.

M is the initial number of frequency components in the model.

MMAX is the maximum number of frequency components in the model.

GAIN is the focusing gain, defined as the Rayleigh distance divided by the distance to the geometrical focal plane.

NOTES:

(i) In general, as GAMMA and A are made larger the maximum number of frequency components (MMAX) will need to be increased since more energy is lost to higher frequencies.

(ii) The maximum number of harmonics allowed is currently 100 and is determined by array sizes in *pulse.f*.

(iii) The total number of axial calculation steps is given by ZMAX/KSTEP. There is no real limit to the maximum number of axial calculation steps since only the previous step is required to calculate the next step. In practice the computer run-time will limit the number of axial steps used.

(iv) The number of radial points in the grid is given by MRMAX/HSTEP and currently has an upper limit of 1000 due to array sizes in *pulse.f*.

(v) KSTEP and HSTEP must satisfy the condition:

$$\frac{KSTEP}{HSTEP^2} < 0.5$$

An example of a typical *param.dat* is shown below.

```
11.91
5.45
0.51
2.0
4.0
0.00015
0.02
2
5
0.0
```

1.2.2 *init.dat*

This file contains the initial pulse spectrum for the run as a list of 30 magnitude-phase pairs. The first pair corresponding to the frequency of the first component as determined for GAMMA and A in *param.dat* and successive pairs represent harmonics of that component. The magnitudes are normalised such that the maximum amplitude becomes unity and the scale factor required is used as p_o in the calculation of GAMMA and A. The phases are in radians of the harmonics.

In the case of a continuous wave source the first component, the fundamental for the CW case, would normally have unit magnitude and zero phase and all higher components zero magnitude and phase. Such a case is shown in the example below, which only shows the first few values in *init.dat.*

Part of *init.dat* for a CW case. Column 1 = magnitudes, Column 2 = phases.

```
1.0     0.0
0.0     0.0
0.0     0.0
0.0     0.0
0.0     0.0
0.0     0.0
0.0     0.0
0.0     0.0
0.0     0.0
0.0     0.0
0.0     0.0
0.0     0.0
0.0     0.0
0.0     0.0
0.0     0.0
0.0     0.0
0.0     0.0
```

1.2.3 *pgrid.dat*

pgrid.dat contains the co-ordinates for printout form *pulse.f.* The format of the file is as follows. The first line holds three real numbers {ZRPRINT(I), I=1,3)} which are the axial distance, normalised by R_o, at which radial cross sections are required. The next line holds two integers {ZNUM and RNUM} which specify the number of axial printout points and the number of radial printout points respectively. Maximum values for these two numbers are currently 100 and 50 respectively. On the third line a column of ZNUM real numbers {ZPRINT(I), I=1,ZNUM} form the normalised axial co-ordinates for printout, followed by RNUM real numbers {RPRINT(I), I=1,RNUM} for the normalised radial co-ordinate for the cross section printout.

A separate program (*wcoords.f* and *wcoords.e*) exists to generate the required file format. *wcoords.e* puts the grid into a file called *coords.dat* which can then be copied into *pgrid.dat.*

An example of part of a typical *pgrid.dat* is shown below.

```
 0.01    0.3  0.5
        100          50
  5.000003E-03
  1.000001E-02
  1.500001E-02
  2.000001E-02
  2.500001E-02
  3.000002E-02
  3.500002E-02
  4.000002E-02
  4.500002E-02
  5.000003E-02
  5.500003E-02
  6.000003E-02
  6.500006E-02
  7.000005E-02
  7.500005E-02
  8.000004E-02
  8.500004E-02
  9.000003E-02
  9.500003E-02
 0.1000000
```

1.3 OUTPUT FILES IN DETAIL

1.3.1 *ax.out*

On completion of a run this file should hold the harmonic amplitudes and phases for each axial printout point specified in *pgrid.dat*. At the top of the file the run parameters are shown, this part of the output is a simple re-statement of *param.dat*. The rest of the file comprises ZNUM sections of the form: axial distance, radial boundary, number of harmonics, number, amplitude and phase of each harmonic. Each section has a few explanatory lines of text. See example:

Part of typical *ax.out* showing run parameters and harmonic magnitudes and phases for first axial printout point.

```
 GAMMA =    11.91000             A =    5.450000
 MAX AXIAL DISTANCE =   0.5100000
 INITIAL & MAX DISTANCE FROM AXIS =    2.000000        4.000000
 AXIAL & RADIAL STEP SIZE =    1.500000E-04    2.000000E-02
 INITIAL & MAX NO. OF HARMONICS =            2           5
 FOCUSING GAIN =    0.000000E+00

Z/Ro =
 0.0050
 RAD. BOUND =
 100
 HARMONICS =
  5
     N          AMPL             PHASE
          1  0.9988447      -4.472930E-07
          2   6.720394E-03  -5.293221E-07
          3   6.969173E-05  -8.850128E-07
          4   8.713687E-07  -9.972537E-07
          5   0.000000E+00   0.000000E+00
Z/Ro =
 0.0100
 RAD. BOUND =
```

1.3.2 *rad1.out, rad2.out* and *rad3.out*

The radial printout files follow the same format as the axial file except that the magnitudes and phases are printed out for each of RNUM radial distances. See below.

```
 GAMMA =    11.91000             A =    5.450000
 MAX AXIAL DISTANCE =   0.5100000
 INITIAL & MAX DISTANCE FROM AXIS =    2.000000        4.000000
 AXIAL & RADIAL STEP SIZE =    1.500000E-04    2.000000E-02
 INITIAL & MAX NO. OF HARMONICS =            5           5
 FOCUSING GAIN =    0.000000E+00
 Z/Ro =    1.020000E-02
 r/a  =
  0.000000E+00

0
 HARMONICS =
          5
     N          AMPL             PHASE
          1  0.9975740      -1.879897E-06
          2   1.379557E-02  -1.521639E-06
          3   2.897580E-04  -1.181600E-06
          4   7.267267E-06  -2.526528E-06
          5   2.013999E-07  -3.401180E-06
 r/a  =
  4.000000E-02
```

Part of typical radial output file showing run parameters and harmonic magnitudes and phases for the first radial printout point.

1.3.3 GRAPHICAL OUTPUT

A FORTRAN program, *pl_pulse.f*, exists to display the harmonics from *ax.out* and *rad1.out* etc on a graphics terminal. Running *pl_pulse.e* creates a graphics file which can then be displayed using the 'draw' command. The data from the above example is shown in graphical form below.

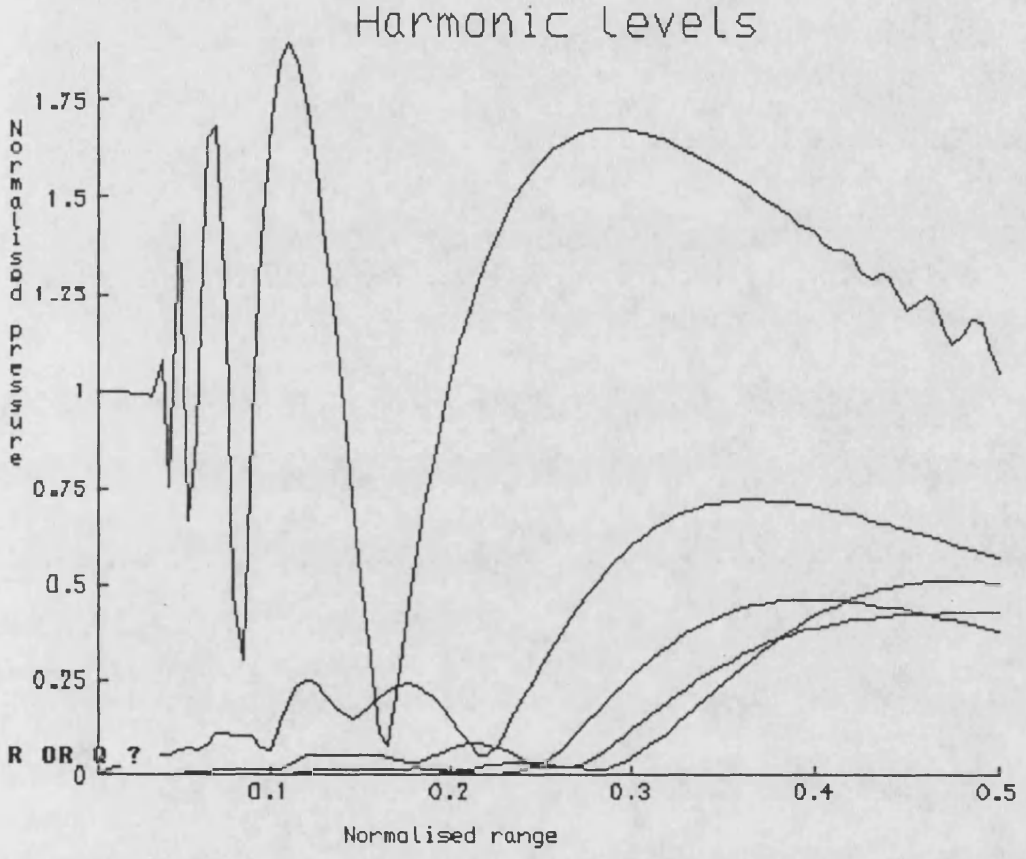

Graphics screen showing first five harmonics on axis of plane piston.

1.4 REFERENCES

Aanonsen, S.I. 1983 "Numerical computation of the near-field of a finite amplitude sound beam," Report No. 73, Department of Mathematics, University of Bergen, Bergen, Norway.

Anastasiadis, K. 1987 "Numerical investigation of nonlinear effects in acoustical beams," University of Bath, School of Physics Report.

Appendix C: PUBLISHED PAPERS

Copies of three published papers arising from this study are attached, the titles are:

1. NONLINEAR PROPAGATION IN FOCUSED FIELDS: EXPERIMENT AND THEORY

2. THE NONLINEAR PRESSURE FIELD OF A PLANE CIRCULAR PISTON: THEORY AND EXPERIMENT

3. NONLINEAR PROPAGATION IN PULSED ULTRASONIC FIELDS

1 FOCUSED FIELDS

TITLE: NONLINEAR PROPAGATION IN FOCUSED FIELDS: EXPERIMENT AND THEORY

AUTHORS: A.C. Baker, K. Anastasiadis and V.F. Humphrey

SOURCE: Proceedings of Ultrasonics International 87, Butterworths

DATE: 1987

PAGES: 184-189

NONLINEAR PROPAGATION IN FOCUSED FIELDS: EXPERIMENT AND THEORY

A. C. Baker, K. Anastasiadis and V.F. Humphrey

School of Physics, University of Bath, Bath BA2 7AY, UK

This paper presents some results of an extensive experimental study of finite amplitude effects in focused ultrasound fields at 2.25 MHz. A plane transducer and focused systems with gain factors of 3.7 and 11.9 are compared. The results for a gain of 3.7 are also compared with a numerical solution of the parabolic approximation to the nonlinear wave equation. The results show that the model accurately predicts the amplitudes of the fundamental and the second and third harmonics and the phase of the second harmonic.

INTRODUCTION

The prediction of the pressure wavefield in the nearfield of an acoustic source at high intensities must take into account nonlinear propagation in the medium as well as diffraction effects. At moderate drive levels the problem can be treated by assuming that only the second harmonic is generated and that this does not affect the fundamental pressure field. At higher pressure levels, such as those routinely encountered in medical ultrasound systems, it is necessary to take into account the interactions that produce higher harmonics,so that a simple perturbation approach will no longer suffice. The method adopted here is the use of a numerical solution to the parabolic approximation to the wave equation. The solution, described by Aanonsen et al [1] for plane piston, can include any number of harmonics and can be used to demonstrate effects such as saturation in the fundamental. Here we compare results obtained with this model, adapted to take account of focusing, with measurements made on a plane circular transducer fitted with a perspex lens to create a focused pressure field.

THEORY

Zabolotskaya and Khokhlov [2] derived a parabolic (or paraxial) approximation for the nonlinear wave equation that accounted for diffraction and nonlinearity. Kuznetsov [3] subsequently accounted for absorption. Aanonsen et al [1] used a numerical finite difference technique to solve this equation for the harmonic amplitudes and phases in the frequency domain. The technique solves the equations for any number of harmonics and can show interactions between the fundamental and the harmonics. The approximation requires that the aperture is large compared with the wavelength, ie. $ka \gg 1$, and is not valid for field points that are far off the acoustic axis or close to the source. These restrictions do not pose any serious difficulties for many geometries of practical importance. For this work, the model was modified to include the effect of focusing by the introduction of phase shifts in the initial conditions. The main limitation of the model is that it assumes a continuous wave excitation therefore it is not possible to model a pulsed field. The program was run on an IBM PC AT.

EXPERIMENTAL MEASUREMENTS

The experimental measurements were made using a 2.25 MHz, 19mm radius, Panametrics plane transducer as an acoustic source. The transducer was driven at its nominal centre frequency with a tone burst of about 80 cycles. The electrical signal applied to the transducer was a sine wave signal of up to 100 volts peak to peak. Various degrees of focusing were achieved by placing a plano-concave perspex lenses in front of the transducer. Three different lenses were used, with focal lengths (D) of 143mm, 216mm and 440mm, corresponding to gain factors (G) of 11.9, 7.6 and 3.7 respectively. The plane, unfocused, transducer has a gain factor of zero. The gain factor is simply the ratio of the Rayleigh distance ($Ro = ka^2/2$) to the focal length (D).

The detector used was a 1mm diameter polyvinylidene fluoride (PVdF) membrane hydrophone of the bilaminar type. These hydrophones have a fairly flat response below their resonant frequency of about 20 MHz. The hydrophone was mounted on a two dimensional translation stage that allowed movement, under the control of an IBM PC AT, in the horizontal plane. The output of the hydrophone was fed directly into a 125 MHz digital sampling oscilloscope (DSO) then to the computer via an IEEE interface. The time waveform at each sampling point in the pressure field was Fourier analysed and the first five harmonic amplitudes and phases were stored for comparison with the theoretical solution. The whole system could be placed under software control to allow a series of "move/sample/analyse" cycles to be carried out.

EXPERIMENTAL RESULTS

Figure 3 shows the measured axial pressure field on the acoustic axis of three different systems. These are the 'bare' plane transducer, a low gain (G = 3.7) focused system and a high gain (G = 11.9) focused system. The drive level for the plane transducer corresponds to a pressure at the transducer face of 100 kPa. The focused systems have a pressure at the lens face of 75 kPa.

The plane transducer shows the usual nearfield oscillations in the fundamental component. However there are two points to note: firstly the oscillations taper towards the transducer. This is due to the finite size of the hydrophone integrating over the rapid spatial variations in the pressure field near the transducer. The magnitude of the tapering is consistent with Beissner's theory [4]. Secondly the last axial maximum is about 10% lower that the penultimate maximum. At lower drive levels the last maximum would be of the same amplitude as the penultimate maximum. This nonlinear loss is a result of energy being pumped into the harmonics at the expense of the fundamental.

The second harmonic shows similar oscillations to the fundamental near the transducer but there is an underlying growth superimposed on the oscillations. It builds up steadily after the last axial minimum and finally attains a level of about half the fundamental. At this stage the time waveform is strongly shocked. The third harmonic shows similar behaviour to the second harmonic but at a lower level; at the extreme ranges the third harmonic is about a third of the fundamental.

The effect of weak focusing (G = 3.7) on the axial pressure field is to draw the oscillations in the pressure field closer to the transducer and to cause an increase in the maximum pressure attained. The weakly focused system has a focal length of 440mm, (denoted by the vertical dashed line); however, it can be seen that the peak pressure occurs at a shorter range, about 300mm. Thus, in the case of weak focusing, it is erroneous to assume that the focal plane is located at the position of peak pressure. The second and third harmonics show similar behaviour to the plane case given the change in the fundamental envelope.

A higher gain (G = 11.9) draws the nearfield oscillations still closer to the transducer and increases further the peak pressure. An interesting effect of strong focusing of the axial pressure field is the production of zeros in the post-focal region; in this case there is a zero at around 300mm. Minima occur in the post-focal region for systems with gains greater that 2π. Another effect of strong focusing gains is that the peak pressure now occurs very near to the focal plane.

Figure 1 shows the measured axial pressure field for the weakly focused case on a logarithmic ordinate; this shows the detail in the second and third harmonics to greater advantage. It can be seen that the second harmonic peaks in the near-field are "double humped" and lag those in the fundamental field. These features also occur in the plane transducer field and for the high gain case, the principal difference being that the build-up is more rapid in the high gain cases.

Figure 2 shows the measured pressure field across the axis of the weakly focused system, in the focal plane. The fundamental follows the farfield directivity pattern for a plane transducer. This provides a useful method for locating the focal plane, since the first minimum either side of the maximum is sharpest in the focal plane. The harmonics are confined to a narrower region that the fundamental and show much lower sidelobes.

COMPARISON WITH THEORY

Figure 4 compares measured results for the weak gain system with theoretical results from the solution to the parabolic approximation. In each part of the figure the solid lines represent measured data and the dashed lines theoretical predictions. There are three main parameters required to fit the theory to the measured data; the Rayleigh distance, the focal length and the pressure at the transducer face (Po). The focal length was found by locating the range at which the off-axis minima were deepest, while the Rayleigh distance was obtained from the range at which the axial minima occurred. The pressure at the transducer face was determined from axial pressure measurements made close to the transducer where nonlinearity had little effect on the fundamental level. These parameters were also checked by comparison of measured data at low-drive levels with small signal solutions for the pressure field.

The fundamental magnitude shows good agreement at ranges greater than about 100mm, but gets progressively worse towards the transducer. This mainly because the parabolic approximation is not valid for large aperture angles, ie. close to the transducer or at large distances off axis. The theoretical solution, because it is a finite difference scheme, does not show any oscillations close to the transducer since the edge effects take a number of steps to propagate towards the axis. The second harmonic magnitude and phase also shows very good agreement, subject to the limitations outlined above. The third harmonic shows good agreement beyond about 200mm. At shorter ranges the noise in the experimental measurements becomes a problem although this will be reduced by averaging.

The agreement shown for the weakly focused system here is typical of the results obtained for other cases such as the plane piston and focused systems with higher gain factors. Space limitations do not allow analysis of these systems here.

CONCLUSIONS

The results show that the numerical solution of the parabolic approximation is a powerful tool for predicting accurately the harmonic build-up in focused wave-fields from circular apertures. The solution provides detail of the entire wave field, not just the on-axis results shown here. The model is not valid for short axial ranges. The model may also be amended to include the effects of attenuation in media such as tissue.

ACKNOWLEDGEMENTS

The authors gratefully acknowledge the cooperation of the Department of Applied Mathematics at the University of Bergen, Norway.

REFERENCES

1. S. I. Aanonsen, T. Barkve, J. Naze Tjotta and S. Tjotta, J. Acoust. Soc. Am. 75, 749-768 (1984).

2. E.A. Zabolotskaya and R.V. Khokhlov, Sov. Phys-Acoust. 15, 35-40 (1969).

3. V.P. Kuznetsov, Sov. Phys-Acoust. 16, 467-470 (1971).

4. K. Beissner, Acustica 49, 212-217 (1981).

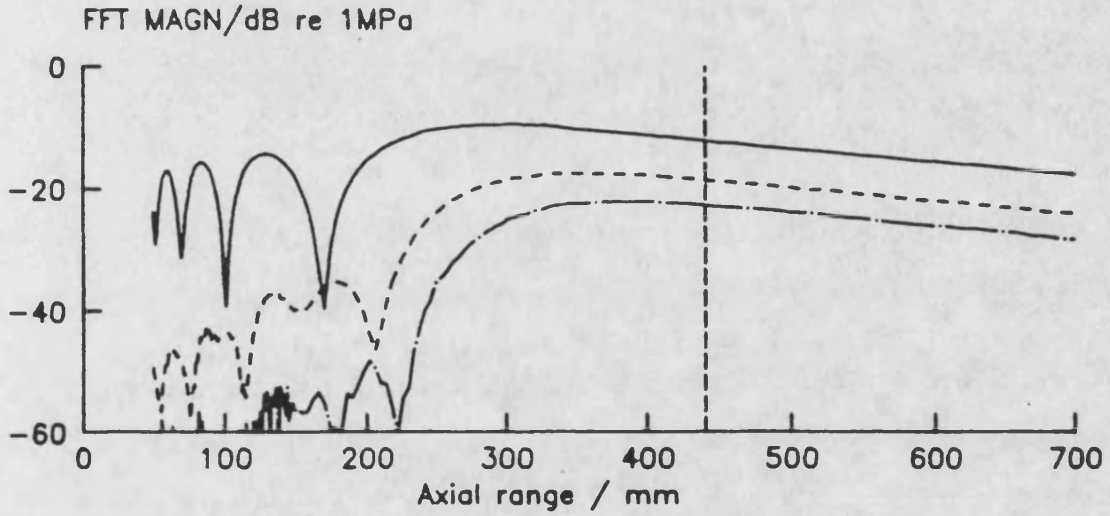

Fig 1. Measured axial pressure variation for focused transducer (G = 3.7) —— Fundamental, --- Second harmonic, -·- Third harmonic

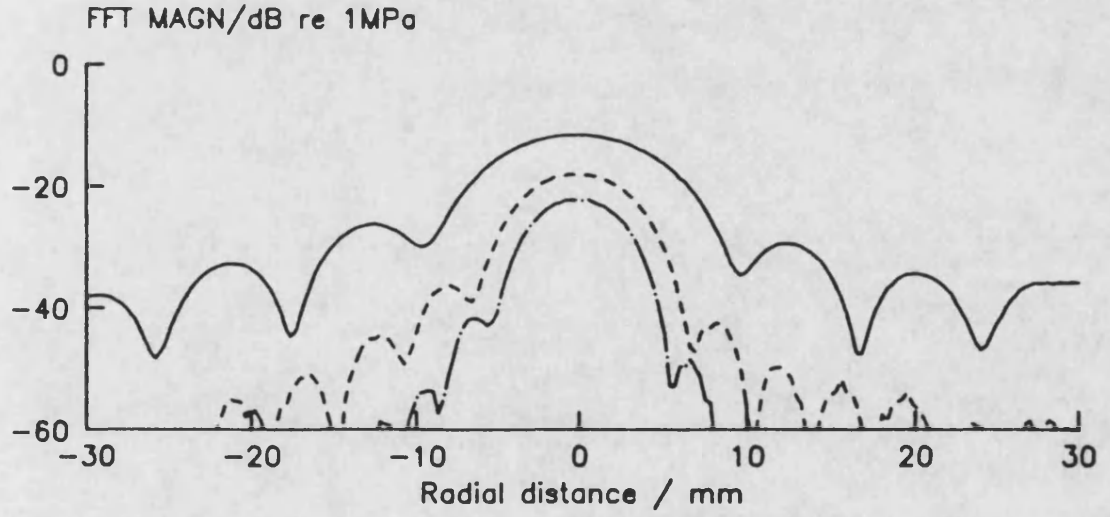

Fig. 2. Measured pressure variation across the focal plane of a focused transducer (G = 3.7) —— Fundamental, --- Second harmonic, -·- Third harmonic

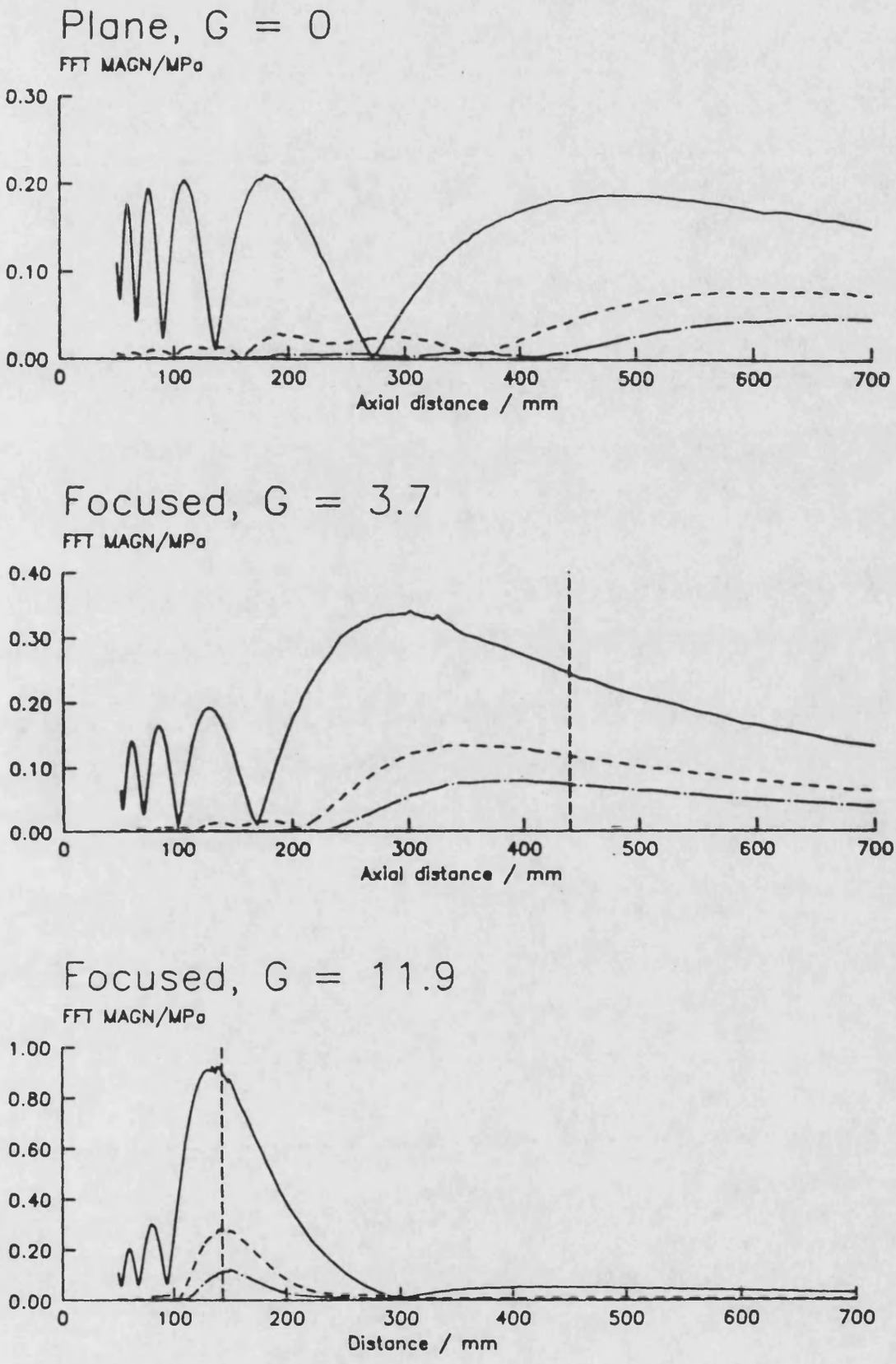

Fig.3. Measured axial pressure variation for plane and focused tranducers.
— Fundamental, --- Second harmonic, -·- Third harmonic

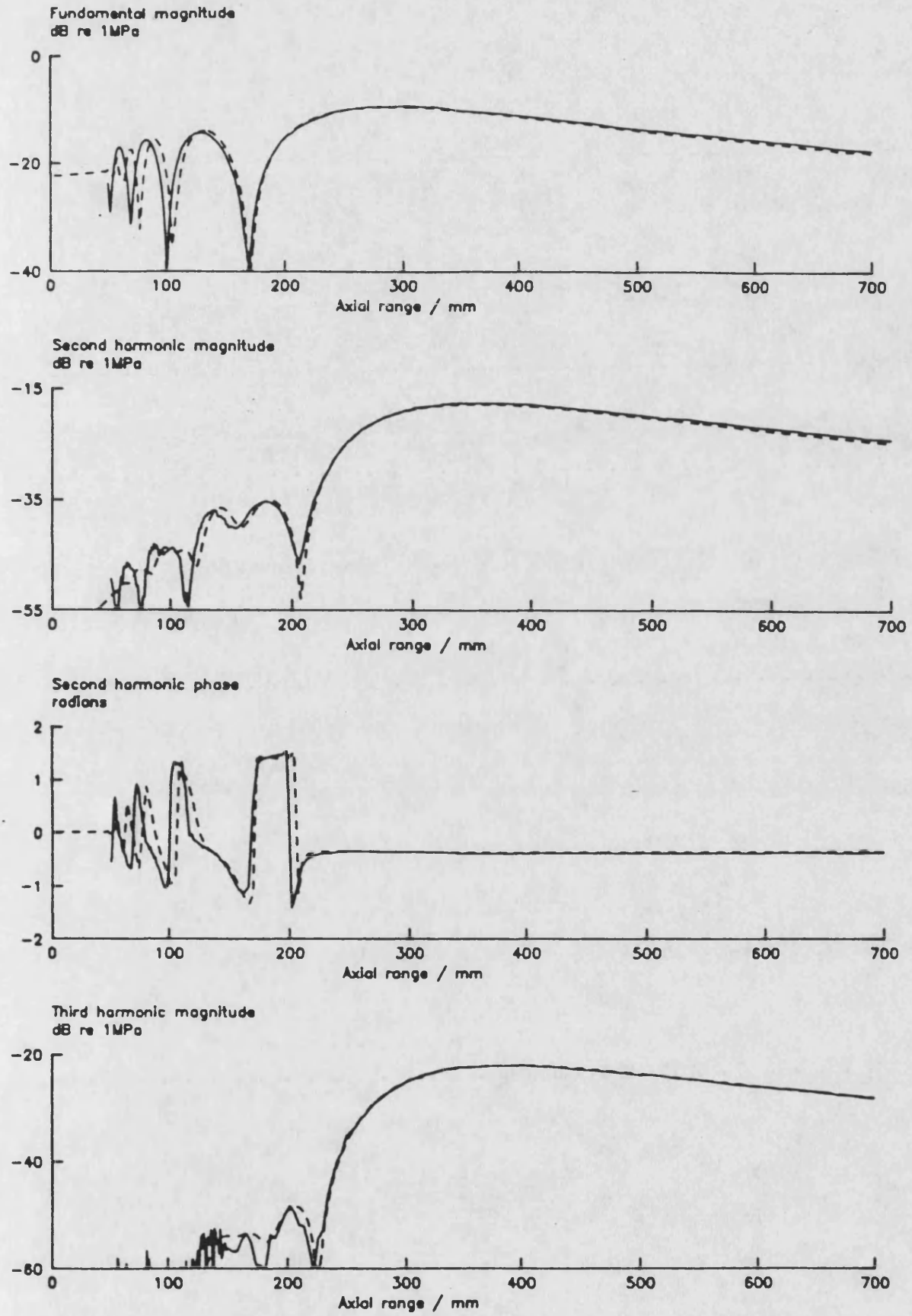

Fig. 4. Comparison of measured axial pressure field (——) with parabolic approximation (---), (G = 3.7).

2 PLANE PISTON

TITLE: THE NONLINEAR PRESSURE FIELD OF A PLANE CIRCULAR PISTON: THEORY AND EXPERIMENT

AUTHORS: A.C. Baker, K. Anastasiadis and V.F. Humphrey

SOURCE: Journal of the Acoustical Society of America, Vol. 84

DATE: 1988

PAGES: 1483-1487

The nonlinear pressure field of a plane circular piston: Theory and experiment

Andrew C. Baker, Kosmas Anastasiadis, and Victor F. Humphrey
School of Physics, University of Bath, Bath, BA2 7AY, United Kingdom

(Received 28 March 1988; accepted for publication 16 June 1988)

The measured nearfield pressure levels of a plane circular piston are compared with a numerical solution of the parabolic approximation to the nonlinear wave equation under conditions of high nonlinearity (100 kPa at the piston face). The solution allows for nonlinearity, diffraction, and absorption in continuous wave pressure fields. The measurements were made in water, using a transducer (38-mm diameter) driven at 2.25 MHz and a 1-mm-diam membrane hydrophone. Comparisons are made along and across the acoustic axis for the amplitudes of the fundamental, second, and third harmonics and the phases of the second and third harmonics. Good agreement is shown between experiment and theory within the known limitations of both.

PACS numbers: 43.25.Cb, 43.30.Yj

INTRODUCTION

Aanonsen *et al.*[1] examined harmonic generation in the nearfield of a finite amplitude sound beam. The study was based on a numerical solution of the parabolic approximation to the nonlinear wave equation. Hamilton *et al.*[2] in a later article extended the study to the farfield of the transducer and included some comparisons with experimental results. The purpose of this article is to present some experimental results for the nearfield case and compare them with values computed using the solution shown in Ref. 1.

I. EXPERIMENT

The experimental measurements were made with a plane transducer (38-mm-diam Panametrics) mounted at one end of water tank 1.3 m long by 0.3 m wide and 0.3 m deep. The transducer was driven at its nominal center frequency of 2.25 MHz corresponding to a ka value of 181 (k is the wavenumber, a is the transducer radius). It was driven with a tone burst, approximately 80 cycles long at a pulse repetition frequency of about 1 kHz. This gave a quasicontinuous wave field without producing standing waves and enabled spurious reflections to be eliminated by using a time gate on the received pulse. The measurement of the acoustic drive level was complicated by the presence of nonlinear propagation. It was necessary, therefore, to measure the acoustic pressure at low amplitude by inserting a calibrated attenuator on the input side of the power amplifier. This reduced the drive, by a known amount, to a level at which nonlinear propagation was not significant so that the fundamental pressure level could be measured directly. The above procedure was repeated with the hydrophone positioned close to the transducer to ensure that the power amplifier and transducer were linear over the range of interest. The average peak pressure across the transducer face was set at 100 kPa and all the results presented here are for this pressure.

The pressure field generated by the transducer was sampled using a 1-mm-diam bilaminar polyvinylidene fluoride hydrophone. The hydrophone was mounted on a two-dimensional translation stage which allowed the hydrophone to be positioned anywhere in a horizontal plane through the acoustic axis of the transducer. The hydrophone was calibrated by intercomparison with a similar device that had been calibrated at the National Physical Laboratory. The output from the hydrophone was fed directly into an eight-bit digital storage oscilloscope (DSO) with a sampling rate of 125 MHz. The DSO was used to capture a portion of the time waveform from the middle of the tone burst. The time waveform was then transferred to the controlling computer and single cycles were Fourier analyzed to extract the harmonic amplitudes and phases. The results presented here are based on single captures, i.e., no averaging has been performed on the measured waveforms.

The translation stage and the DSO were both controlled by an IBM personal computer (PC-AT) via an IEEE interface. The controlling program executed a "capture/analyze/move" cycle, allowing large numbers of measurements to be made at relatively high spatial frequencies. A typical run along the axis of the transducer described here comprised 200 measurements made at 1-mm intervals near the transducer and 10-mm intervals at greater distances.

II. IMPLEMENTATION OF THEORY

The theoretical investigation was conducted through the numerical solution of the parabolic wave equation. The formal derivation of this equation is described in Refs. 1, 3, and 4. The main limitations of the parabolic approximation are that it is only valid for sources with $ka \gg 1$, the angle off axis must be small, and the distance from the source must not be small. The model includes diffraction, attenuation, and nonlinearity. It will work for almost any level of nonlinearity but the greater the nonlinearity, the more harmonics have to be included. The numerical solution is based on a computer model developed by Aanonsen.[5] The harmonic content of an acoustical beam, with axial symmetry, is calculated using a finite difference method, which solves the parabolic wave equation in the frequency domain.

 0001-4966/88/101483-05$00.80

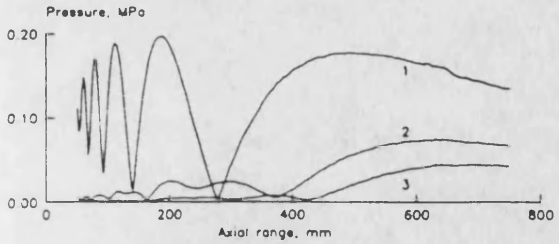

FIG. 1. Measured pressure levels of fundamental, second, and third harmonics along the acoustic axis.

The computer program was initially implemented by the authors on a Honeywell Multics mainframe and later, after some modification, on an IBM personal computer (PC-AT). The execution time of the program varied from several minutes to several hours and depended on many factors such as the initial conditions, the number of harmonics retained in the calculation, the extent of the finite difference grid, and the size of the steps used to construct it. These factors also affect the overall accuracy of the model, especially for large radial distances and small axial ranges, and it is necessary to trade accuracy against run time. The actual parameters used in this study are given in the Appendix.

III. RESULTS AND DISCUSSION

Figure 1 shows the measured harmonic amplitudes along the acoustic axis for the fundamental, second, and third harmonics. The fourth and fifth harmonics were also recorded but these have been omitted here for the sake of clarity. The measurements are shown as lines rather than individual points since the spatial separation of adjacent measurements is small. The high relative levels of the second and third harmonics (0.5 and 0.3, respectively) at the maximum range (750 mm) indicate a highly distorted waveform. It can also be seen that the level of the fundamental at the last axial maximum (500 mm) is reduced compared to the previous maximum at 200 mm. This is caused by the energy loss from the fundamental into the higher harmonics.

The progressive reduction of the nearfield oscillations toward the transducer is not related to the nonlinear effects but is a consequence of the hydrophone size. The pressure field close to the transducer contains rapid spatial variations on a length scale smaller than the hydrophone diameter, so the hydrophone output is the integrated pressure field over its area (or over the volume if the finite hydrophone thickness is also considered). The pressure seen by the hydrophone, close to the transducer, will tend toward the average pressure (P_0). The extent of this tapering off (or diffraction loss) is consistent with the expressions derived by Beissner.[6] The effect can be reduced by using a smaller hydrophone; however, this would lead to a reduction in hydrophone output due to the reduced sensitivity.

Figures 2–4 compare the experimental measurements for the axial pressure field (solid lines) with theoretical predictions from the numerical solution (dashed lines). The harmonic phases are relative to the fundamental and are expressed in radians of the fundamental. The fundamental phase shown is the slow phase variation from the model; there are no experimental measurements to compare with the predicted fundamental phase. It can be seen that, in general, the agreement between theory and experiment is very good for the magnitudes and phases. It should be noted that the reference hydrophone is subject to an overall uncertainty of 5% and thus the input pressure level to the theoretical model could not be determined to greater accuracy.

The agreement is not so good near the transducer and there are a number of reasons for this. First, the experimental results are showing the diffraction loss discussed above. Second, the limitations of the theoretical model are becoming apparent. The radial pressure field is represented in the model by arrays of coefficients. The spacing between these radial points leads to a quantization error in the size of the aperture. The effect of this error on the axial pressure field is more significant at short ranges and causes the positions of the axial maxima and minima to become progressively worse as the transducer is approached. The errors in the positions of the axial minima are consistent with the quantization of the aperture in the radial direction. The finite step size along the axis causes the rapid oscillations that occur close to the transducer to be undersampled. This makes the nearfield oscillations appear to reduce in amplitude as the transducer is approached. This effect is similar to the diffraction loss experienced experimentally and occurs because the length scale of the oscillations is small compared with the step size in the model. The pressure calculated by the model will also be an integrated value for the small volume enclosed by the cell in the finite difference grid. The radial and axial step sizes can be reduced to minimize these effects. There is, however, a limit to the improvement that can be thus gained since the model contains the parabolic approximation that will ultimately govern its performance at short ranges.

Figures 5–7 show comparisons between measurements on the radial pressure field and corresponding theoretical predictions at axial ranges of 275 and 500 mm. These correspond to sections through the last axial minimum and maximum, respectively. It can be seen that the radial extent of the second and third harmonics is considerably reduced in comparison with the fundamental. In general, the higher the harmonic, the more closely it is confined to the axis of the transducer. The rate at which the higher harmonics fall off with radial distance is also considerably greater than that of the fundamental. The overall agreement between experiment and theory is good and much of the fine detail is accurately predicted by the model. Agreement is particularly good near the axis but the theoretical model would be expected to become progressively less accurate with increasing radial distance; further, the experimental measurements, especially phase, are affected by the reduced signal levels off axis.

IV. CONCLUSIONS

In general, the parabolic model described provides a good representation of a nonlinear continuous wave pressure field for an aperture that is many wavelengths across. The trade-off in using the model is between run time and the accuracy required close to the aperture and at large angles off axis. The accuracy can only be improved up to the limita-

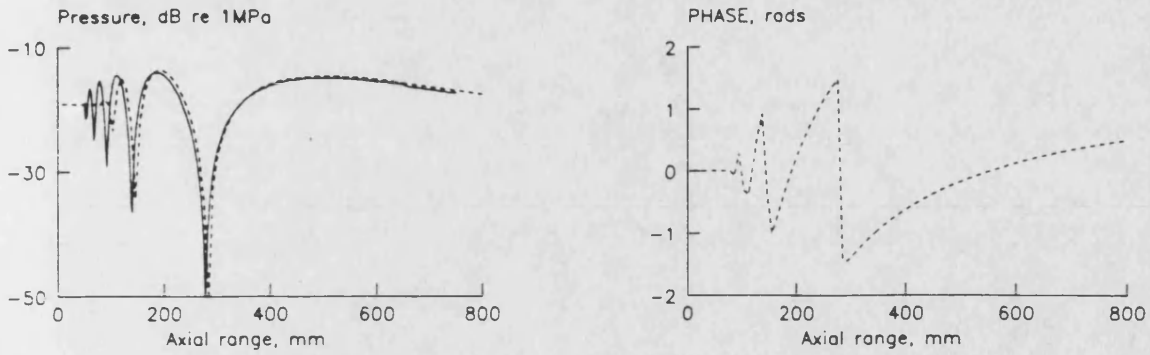

FIG. 2. Comparison of measured fundamental (—) and theoretical levels (- - -) along the acoustic axis.

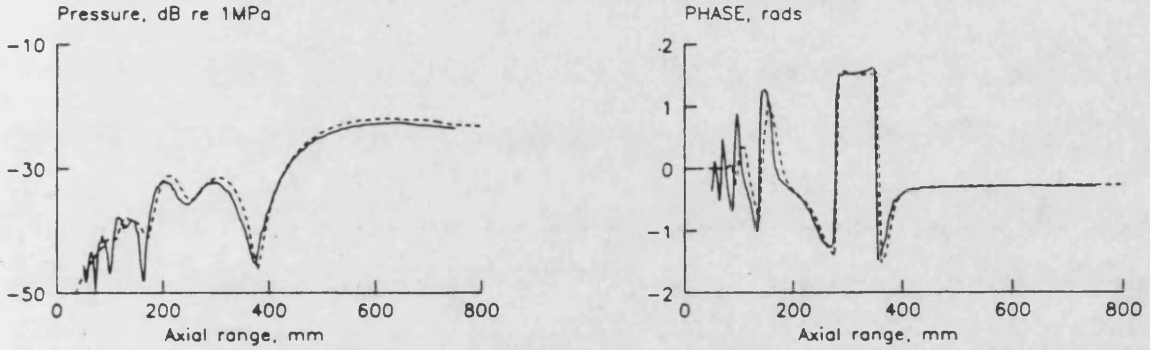

FIG. 3. Comparison of measured second harmonic (—) and theoretical levels (- - -) along the acoustic axis.

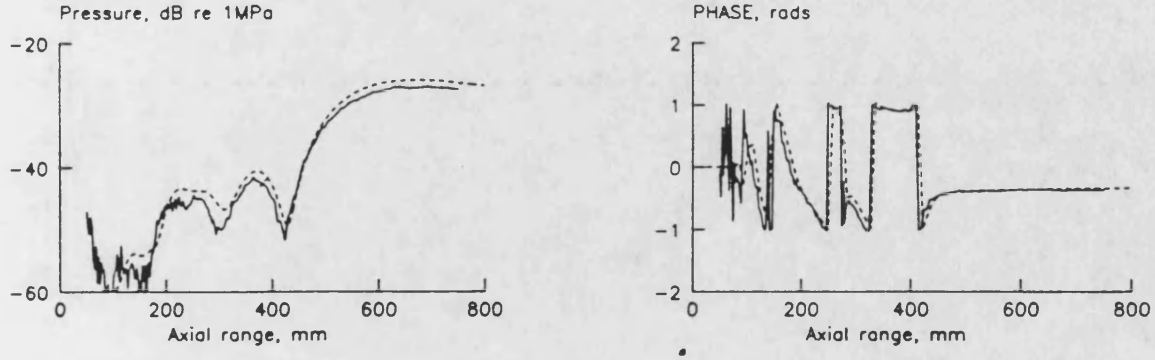

FIG. 4. Comparison of measured third harmonic (—) and theoretical levels (- - -) along the acoustic axis.

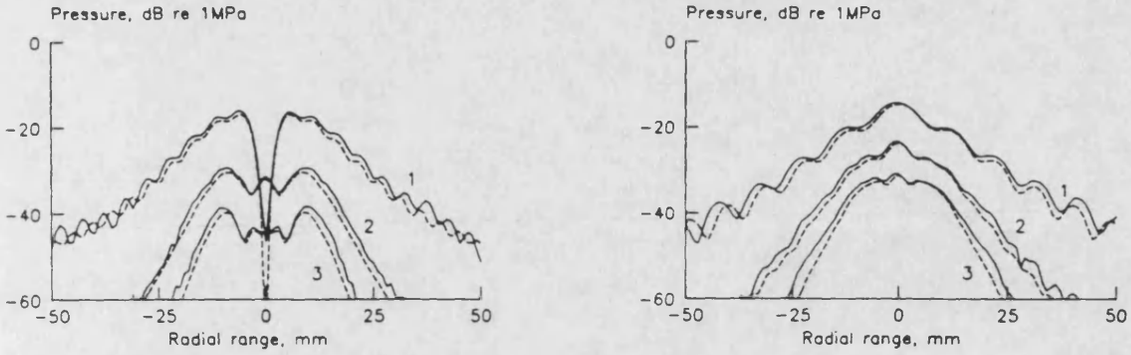

FIG. 5. Comparison of measured (—) fundamental, second, and third harmonics with theoretical values (- - -) across the axis, $z = 275$ and 500 mm.

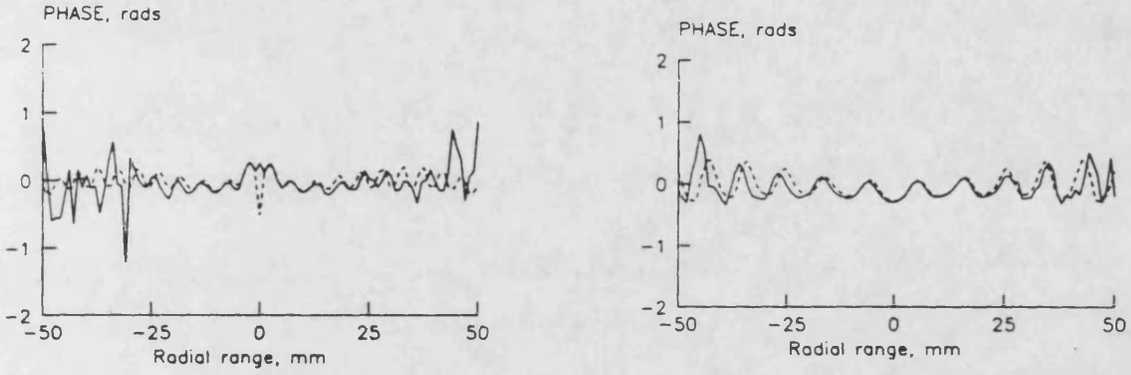

FIG. 6. Comparison of measured phase (—) with theoretical values (- - -) for the second harmonic across the axis, $z = 275$ and 500 mm.

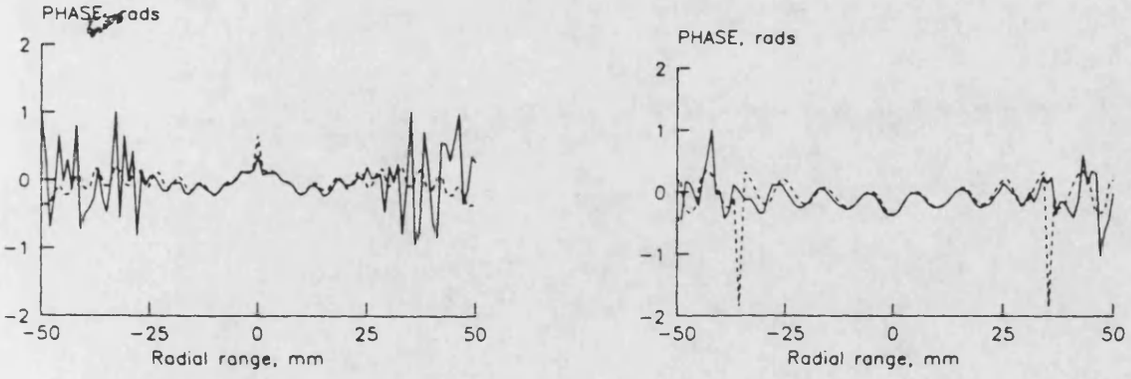

FIG. 7. Comparison of measured phase (—) with theoretical values (- - -) for the third harmonic across the axis, $z = 275$ and 500 mm.

tion of the parabolic approximation that will provide an ultimate limit on closeness to the aperture and distance of axis. In practice, this limitation is not too severe for many sources of practical importance and useful predictions can be obtained (with a minimal number of underlying assumptions) for pressure fields with high levels of nonlinearity. The model has also been adopted to consider focused fields.[7]

APPENDIX

Parameters used in finite difference model:
Average pressure across transducer face: 100 kPa
Transducer radius (a): 19 mm
Fundamental frequency: 2.25 MHz
Speed of sound: 1486 m/s
Parameter of nonlinearity (β): 3.5
Density: 1000 kg/m^3
Attenuation coefficient (α/f^2): 25×10^{-15} Np/m/Hz^2
Axial grid step size: 0.000 25 R_0 ($R_0 = ka^2/2$)
Radial grid step size: 0.025 a
Maximum number of harmonics: 10

Initial radial boundary: two piston radii (80 grid points)

Final radial boundary: four piston radii

[1] S. I. Aanonsen, T. Barkve, J. Naze Tjøtta, and S. Tjøtta, "Distortion and harmonic generation in the nearfield of a finite amplitude sound beam," J. Acoust. Soc. Am. **75**, 749–768 (1984).

[2] M. F. Hamilton, J. Naze Tjøtta, and S. Tjøtta, "Nonlinear effects in the farfield of a directive sound source," J. Acoust. Soc. Am. **78**, 202–216 (1985).

[3] J. Naze Tjøtta and S. Tjøtta, "Nonlinear equations of acoustics, with application to parametric acoustic arrays," J. Acoust. Soc. Am. **69**, 1644–1652 (1981).

[4] V. P. Kuznetsov, "Equations of nonlinear acoustics," Sov. Phys.-Acoust. **16**, 467–470 (1971) [Akust. Zh. **16**, 548–553 (1970)].

[5] S. I. Aanonsen, "Numerical computation of the nearfield of a finite amplitude sound beam," Rep. No. 73, Department of Mathematics, University of Bergen, Bergen, Norway (1983). (The authors are grateful to the Department of Mathematics at Bergen for supplying a copy of this reference.)

[6] K. Beissner, "Exact integral expression for the diffraction loss of a circular piston source," Acustica **49**, 212–217 (1981).

[7] A. C. Baker, K. Anastasiadis, and V. F. Humphrey, "Nonlinear propagation in focused fields: Experiment and theory," in *Proceedings of Ultrasonics International 87* (Butterworths, London, 1987), pp. 184–189.

3 PULSED FIELDS

TITLE: NONLINEAR PROPAGATION IN PULSED ULTRASONIC FIELDS

AUTHORS: A.C. Baker and V.F. Humphrey

SOURCE: Proceedings of Ultrasonics International 89, Butterworths

DATE: 1989

PAGES: To be published, camera ready copy attached.

NONLINEAR PROPAGATION IN PULSED ULTRASONIC FIELDS

A.C. Baker and V.F. Humphrey

School of Physics, University of Bath, Bath BA2 7AY, UK.

The numerical solution of the Khokhlov-Zabolotskaya-Kuznetsov parabolic wave equation by the finite difference method is extended to the case of pulsed wavefields by means of Fourier analysis of the initial waveform. The method, which accounts for nonlinearity, diffraction and absorption in the sound beam, enables the propagation of short pulses typical of those used in diagnostic medical ultrasound to be modelled. The theory is applied to plane and low gain focused transducers and the results are compared with experimental observations. The factors limiting the accuracy of the numerical solution are considered and the problem of obtaining the starting parameters for the pulsed wavefield are discussed.

INTRODUCTION

Medical ultrasound systems make wide use of focused transducers and operate at high frequencies and pressures. Under these conditions finite amplitude propagation effects need to be considered if accurate measurements and predictions of the ultrasound field are to be made. Some medical systems, such as those used in physiotherapy, transmit relatively long tone bursts that may be modelled by considering the equivalent continuous wave (CW) case. Accurate predictions of the nonlinear pressure fields produced by such systems in water can now be made using numerical finite difference techniques [1,2]. However, many systems, such as diagnostic scanners and lithotripters, generate short pulses for which the CW approximation is not valid. This paper considers the extension of the numerical modelling technique to these pulsed pressure fields.

THEORY

A numerical solution of the parabolic approximation to the nonlinear wave equation has been developed by Aanonsen *et al* [3]. This frequency domain solution takes into account nonlinearity, diffraction and absorption and is based on an equation derived by Kuznetsov [4] and Zabolotskaya and Khokhlov [5] which is sometimes referred to as the KZK equation. The resulting continuous wave solutions are valid for circular apertures that are many wavelengths in diameter and for field points that are not too close to the source or too far off axis.

The numerical model represents the wavefield at each point on a finite difference grid by a series of Fourier frequency components, each with its own complex amplitude. The model is initialised by assigning appropriate values to the frequency components on the grid points in the plane of the transducer. The model then calculates the level of each frequency component as the wave propagates through the medium using finite difference techniques with the effects of nonlinearity, diffraction and absorption being calculated for each step.

In the case of a CW excitation the model is initialised by setting the first frequency component to unity across the transducer aperture and to zero outside the aperture. All the other frequency components are initially set to zero. In this case the first frequency component represents the fundamental frequency of the waveform and the other components are harmonics of this frequency.

In order to model a pulsed pressure field the initial waveform (Figure 1(a)) is Fourier analysed and the amplitudes (Figure 1(b)) and phases of the resulting Fourier components are used as the initial conditions for the numerical model. In this case the first frequency in the model is determined by the length of the time waveform that is analysed. For the example shown the waveform was analysed between 0.5 μs and 3.5 μs to give a first frequency component of 333 kHz. Consequently the most significant frequencies in the initial conditions were the 6^{th} and 7^{th} components since the pulse was centred on about 2.1 MHz. By representing the pulse in this way by a Fourier series there is an implicit assumption that the waveform repeats outside the chosen interval, in this case every 3 μs. This gives an unrealistically high pulse repetition frequency and means that at short axial ranges, where the extra delay of the edge wave is comparable with 3 μs, it is possible for successive pulses to interact in the numerical model. However, this is not considered to be too great a restriction as the build up of nonlinear distortion in the immediate vicinity of the transducer is not great. The time interval between pulses can be increased by using a lower frequency for the first component but this increases the number of components required to represent the initial pulse and places unacceptable demands on the number of frequencies required once the wave becomes distorted.

The limitations on computer run time place restrictions on both the number of steps that can be used for the finite element grid and also on the number of frequencies that can be retained in the calculation. The use of too large a step size in the radial direction can give rise to errors in the location of the axial maxima and minima while the limited number of frequencies used prevents very high pressures being considered. In the current calculations the number of frequencies used was increased automatically as the waveform became more distorted, with an upper limit of 199. In a similar way the number of radial steps was increased automatically with range, starting with 66. The calculations and measurements were all performed for a pulse with a peak pressure of 150 kPa at the transducer.

EXPERIMENTAL MEASUREMENTS

The measurements were made using a 2.25 MHz, 19 mm radius Panametrics plane transducer as an acoustic source. A perspex lens with a focal length of 440 mm was used to produce a focused pressure field of known characteristics. The transducer was driven from the B scan output of a Philips "sono DIAGNOST B" imaging system to produce an acoustic output typical of diagnostic systems.

A Marconi bilaminar polyvilidene difluoride (PVdF) membrane hydrophone with an active area 1 mm in diameter was used as the receiver. This had a reasonably flat frequency response below its resonance at about 24 MHz. The hydrophone was mounted on a computer controlled translation stage and connected directly to the input of a 125 MHz digital storage oscilloscope. Time waveforms were then captured and transferred to the controlling computer (IBM PC-AT) for analysis. The waveforms were then deconvolved to allow for the frequency response of the hydrophone, using a theoretical model of the hydrophone's complex sensitivity that was matched at low frequencies (<15 MHz) to the available calibration data.

The initial waveform (Figure 1(a)) was measured at a distance of 15 mm from the transducer where the edge wave could be clearly separated from the direct signal. This enabled the waveform to be measured at the same drive level as that used for the propagation measurements. An alternative method of obtaining the starting waveform was also tried and gave similar results. This involved measuring the pressure waveform in the focal plane (or in the farfield in the plane transducer case) and then integrating this waveform numerically to obtain the initial conditions. The disadvantage of this approach was that it required the input signal to be electrically attenuated to prevent nonlinear propagation occuring. Both approaches assume that the transducer acts as a perfect piston transducer; CW measurements of the axial field at low drive levels indicated that this was a reasonable assumption.

RESULTS AND DISCUSSION

Plane piston transducer

Figure 2(a) compares the experimentally measured time signal with the output of the numerical model for a plane piston transducer at an axial range of 500 mm. At this range (approximately the position of the last axial maximum for the "centre" frequency of the pulse) the central cycle of the pulse is starting to show significant nonlinear distortion. The agreement between experimental and theoretical waveforms is good, with the central cycle showing the positive-negative asymmetry produced by phase shifts due to nearfield diffraction. This agreement is confirmed by Figure 2(b) which shows the corresponding spectral amplitudes of the measured and calculated waveforms. The clear periodicity in the spectrum resulting from the distorted central cycle of the waveform should be noted, as should the fact that little energy has been transferred to frequencies above 15 MHz.

Figures 3(a) and 3(b) show similar results for an axial range of 700 mm at the same drive level. Here the central cycle is clearly much more distorted and the other, lower amplitude, cycles are starting to distort. In this case the agreement is again good but the peak pressure predicted is significantly higher than that measured. Figure 3(b) indicates the reason for this difference. As the wave propagates the nonlinear interaction results in a steady net transfer of energy upwards to higher frequencies. In the numerical model this transfer is limited by the finite number of frequencies used and has to stop at the maximum frequency considered. As a result of this effect the level of the highest harmonics can become artificially high and, in turn, distort the amplitude of the lower frequencies. This process can be seen to be occuring in Figure 3(b) which shows that the agreement at lower frequencies is good but that the predicted amplitudes above 20 MHz are at least twice those measured. A number of techniques of overcoming this limitation are currently being considered.

The theoretical axial variation of four of the frequency components of the pulsed waveform, namely the 7^{th}, 14^{th}, 21^{st} and 28^{th} components, are shown in Figure 4. These correspond, approximately, to the fundamental, second, third and fourth harmonics for the CW case. The similarity of Figure 4 to the CW result for an initial pressure of 100 kPa shown in Figure 1 of reference [1] should be noted. The amplitude of the 7^{th} component is flat up to a range of 130 mm due to the rather large step size used in the finite difference grid for this calculation.

Focused transducer

Similar results for a weakly focused field were obtained by using a perspex lens to modify the plane transducer and produce a system with a pressure gain of 3.7 at the centre frequency of the pulse. The experimentally observed waveform in the focal plane at an

axial range of 440 mm is shown in Figure 5(a). The agreement is again good but the theoretical result shows more distortion of the second and third cycles. The corresponding spectra are shown in Figure 5(b). These again show very good agreement at low frequencies but a significant enhancement of the predicted levels of the higher harmonics due truncation of the number of harmonics in the frequency domain.

CONCLUSIONS

The results presented show that this technique may be used to predict accurately the finite amplitude wavefields of plane and low gain focused transducers. The solution provides detail of the entire wavefield, not just the axial behaviour shown here. At the present time the model is limited to moderate pressure levels by the limitations on the number of harmonics that can be retained in the calculations. This is not expected to be such a significant limitation for the modelling of propagation through more attenuating media such as tissue.

ACKNOWLEDGEMENT

The authors gratefully acknowledge the assistance of the Department of Applied Mathematics at the University of Bergen, Norway.

REFERENCES

1. Baker, A.C., Anastasiadis, K. and Humphrey, V.F., The nonlinear pressure field of a plane circular piston: theory and experiment J Acoust Soc Am (1988) 84 1483-1487

2. Baker, A.C., Anastasiadis, K. and Humphrey, V.F., Nonlinear propagation in focused fields: experiment and theory, In: Ultrasonics International 87 Conference Proceedings Butterworths, Guildford, UK (1987) 184-189

3. Aanonsen, S.I., Barkve, T., Naze Tjøtta, J. and Tjøtta, S., Distortion and harmonic generation in the nearfield of a finite amplitude sound beam J Acoust Soc Am (1984) 75 749-768

4. Kuznetsov, V.P., Equations of nonlinear acoustics Sov Phys Acoust (1970) 16 467-470

5. Zabolotskaya, E.A. and Khokhlov, R.V., Quasi-plane waves in the nonlinear acoustics of confined beams Sov Phys Acoust (1969) 15 35-40

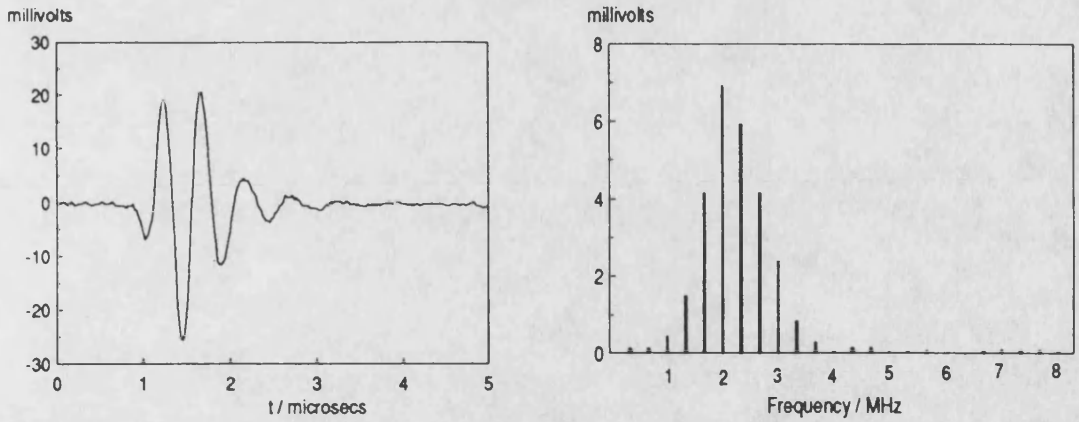

Figure 1: (a) Initial pulse and (b) spectral magnitudes.

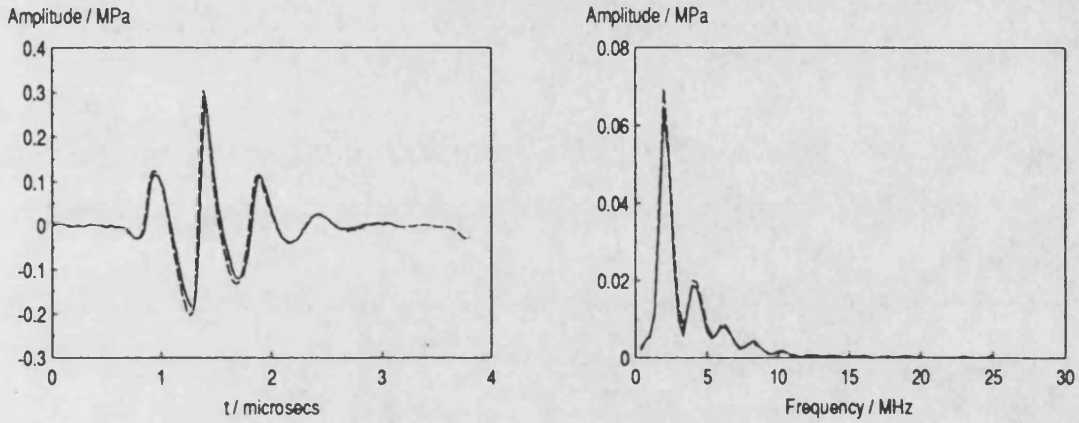

Figure 2: (a) Waveform and (b) spectral magnitudes for plane piston transducer at axial range z = 500 mm. Expt —, theory - -.

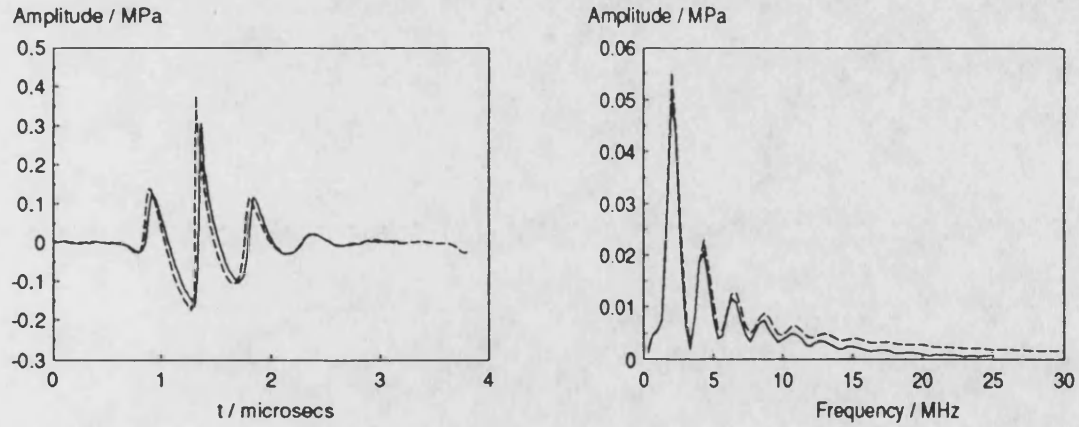

Figure 3: (a) Waveform and (b) spectral magnitudes for plane piston transducer at axial range z = 700 mm. Expt —, theory - -.

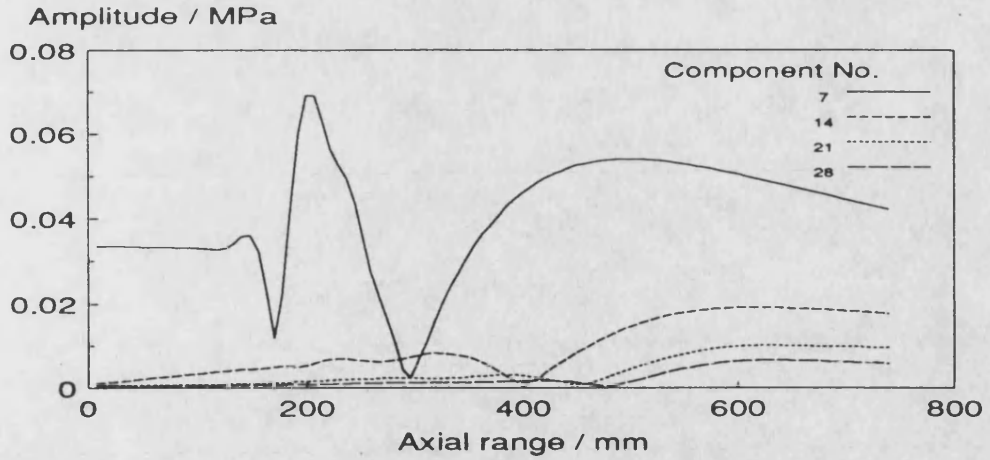

Figure 4: Axial variation of selected frequency components.

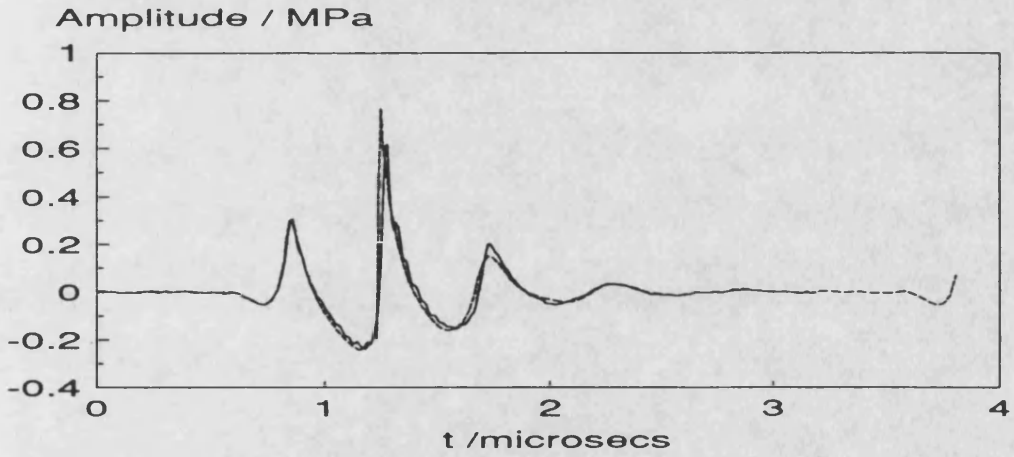

Figure 5: (a) Waveform for focused transducer at axial range z = 440 mm (Focal plane). Expt —, theory - -.

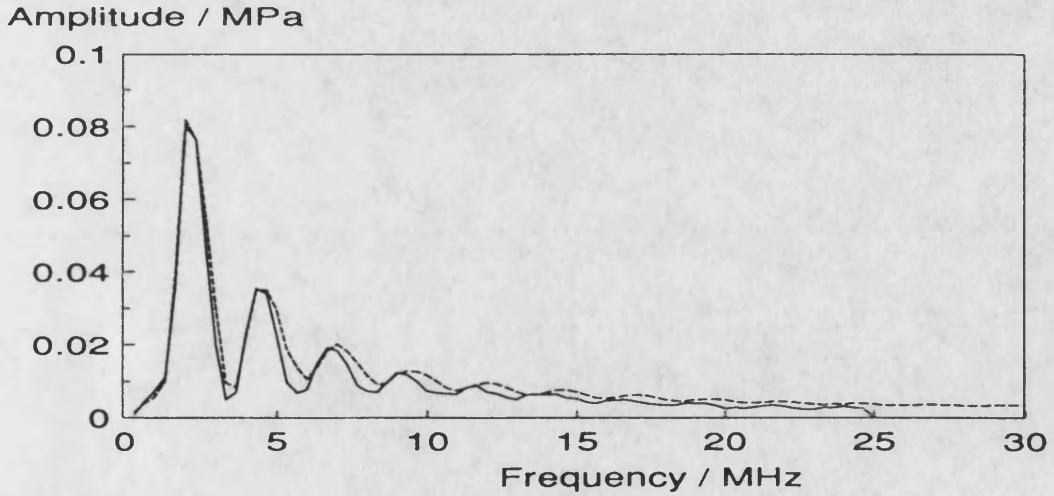

Figure 5: (b) Spectral magnitudes of pulse in Figure 5. Expt —, theory - -.